COLOSSAL MAGNETORESISTANT MATERIALS: THE KEY ROLE OF PHASE SEPARATION

Elbio DAGOTTO[a], Takashi HOTTA[b], Adriana MOREO[a]

[a]*National High Magnetic Field Laboratory and Department of Physics, Florida State University, Tallahassee, FL 32306, USA*

[b]*Institute for Solid State Physics, University of Tokyo, 5-1-5 Kashiwa-no-ha, Kashiwa, Chiba 277-8581, Japan*

ELSEVIER

AMSTERDAM – LONDON – NEW YORK – OXFORD – PARIS – SHANNON – TOKYO

ELSEVIER

Physics Reports 344 (2001) 1–153

PHYSICS REPORTS

www.elsevier.com/locate/physrep

Colossal magnetoresistant materials: the key role of phase separation

Elbio Dagotto[a,*], Takashi Hotta[b], Adriana Moreo[a]

[a]*National High Magnetic Field Laboratory and Department of Physics, Florida State University, Tallahassee, FL 32306, USA*
[b]*Institute for Solid State Physics, University of Tokyo, 5-1-5 Kashiwa-no-ha, Kashiwa, Chiba 277-8581, Japan*

Received October 2000; editor: D.L. Mills

Contents

* Corresponding author. Fax: +18506445038.
E-mail address: dagotto@magnet.fsu.edu (E. Dagotto).

0370-1573/01/$ - see front matter
PII: S0370-1573(00)00121-6

Abstract

The study of the manganese oxides, widely known as manganites, that exhibit the "colossal" magnetoresistance effect is among the main areas of research within the area of strongly correlated electrons. After considerable theoretical effort in recent years, mainly guided by computational and mean-field studies of realistic models, considerable progress has been achieved in understanding the curious properties of these compounds. These recent studies suggest that the ground states of manganite models tend to be intrinsically inhomogeneous due to the presence of strong tendencies toward phase separation, typically involving ferromagnetic metallic and antiferromagnetic charge and orbital ordered insulating domains. Calculations of the resistivity versus temperature using mixed states lead to a good agreement with experiments. The mixed-phase tendencies have two origins: (i) electronic phase separation between phases with different densities that lead to nanometer scale coexisting clusters, and (ii) disorder-induced phase separation with percolative characteristics between equal-density phases, driven by disorder near first-order metal–insulator transitions. The coexisting clusters in the latter can be as large as a micrometer in size. It is argued that a large variety of experiments reviewed in detail here contain results compatible with the theoretical predictions. The main phenomenology of mixed-phase states appears to be independent of the fine details of the model employed, since the microscopic origin of the competing phases does not influence the results at the phenomenological level. However, it is quite important to clarify the electronic properties of the various manganite phases based on microscopic Hamiltonians, including strong electron–phonon Jahn–Teller and/or Coulomb interactions. Thus, several issues are discussed here from the microscopic viewpoint as well, including the phase diagrams of manganite models, the stabilization of the charge/orbital/spin ordered half-doped correlated electronics (CE)-states, the importance of the naively small Heisenberg coupling among localized spins, the setup of accurate mean-field approximations, the existence of a new temperature scale T^* where clusters start forming above the Curie temperature, the presence of stripes in the system, and many others. However, much work remains to be carried out, and a list of open questions is included here. It is also argued that the mixed-phase phenomenology of manganites may appear in a large variety of compounds as well, including ruthenates, diluted magnetic semiconductors, and others. It is concluded that manganites reveal such a wide variety of interesting physical phenomena that their detailed study is quite important for progress in the field of correlated electrons.

PACS: 71.70.Ej; 71.15.-m; 71.38. + i; 71.45.Lr

Keywords: Manganites; Colossal magnetoresistance; Computational physics; Inhomogeneities; Phase separation

1. Introduction

This is a review of theoretical and experimental work in the context of the manganese oxides widely known as manganites. These materials are currently being investigated by a sizable fraction of the condensed matter community, and their popularity is reaching levels comparable to that of the high-temperature superconducting cuprates. From this review hopefully the reader will be able to understand the reasons behind this wide interest in manganites, the problems that have been solved in this context, and those that remain to be investigated. The authors have made a considerable effort in trying to include in this review the majority of what they consider to be the most relevant literature on the subject. However, clearly it is not possible to cover all aspects of the problem in a single manuscript. Here the main focus has been directed into recent theoretical calculations that address the complex spin, charge, and/or orbital ordered phases of manganites, which have important and prominent intrinsic inhomogeneities, and also on the recent experimental results against which those calculations can be compared. Due to the complexity of the models needed to address manganites, it is natural that the most robust results have been obtained with computational tools, and those are the calculations that will be emphasized in the text. The continuous growth of available computer power has allowed simulations that were simply impossible not long ago. In addition, the physics of manganites appears dominated by intrinsic inhomogeneities and its description is quite difficult in purely analytic frameworks that usually assume uniform states. However, several calculations, notably some mean-field approximations, have also reached a high-accuracy level and they are important in deciding which are the phases of relevance in manganites. These calculations are also discussed in detail below. Finally, it is reassuring for the success of manganite investigations that a variety of experiments, reviewed here, appear to be in qualitatively good agreement with the most recent theoretical calculations. Even quantitative agreement is slowly starting to emerge, although there are still many aspects of the problem that require further investigation. At a more general level, from this review it is expected that the readers will understand the richness of manganite physics and how it challenges aspects of our present understanding of condensed matter systems. The effort to fully unveil the behavior of electrons in manganites should continue at its current fast pace in the near future.

The field of manganites started with the seminal paper of Jonker and Van Santen (1950) where the existence of ferromagnetism in mixed crystals of $LaMnO_3$–$CaMnO_3$, $LaMnO_3$–$SrMnO_3$, and $LaMnO_3$–$BaMnO_3$ was reported. The general chemical formula for the manganese oxides described in Jonker and van Santen's paper (1950), and many other compounds investigated later on, is $T_{1-x}D_xMnO_3$, with T a trivalent rare earth or Bi^{3+} cation, and D a divalent alkaline or Pb^{2+} cation. Oxygen is in a O^{2-} state, and the relative fraction of Mn^{4+} and Mn^{3+} is regulated by "x". The perovskite lattice structure of these materials is illustrated in Fig. 1.1a. Jonker and Van Santen (1950) adopted the terminology "manganites" to refer to these mixed compounds, although it is not strictly correct, as they emphasized in a footnote, since the term manganite should in principle apply only to the 100% Mn^{4+} compound.

More detailed information about $La_{1-x}Ca_xMnO_3$ using neutron scattering techniques was obtained later by Wollan and Koehler (1955). In their study the antiferromagnetic (AF or AFM) and ferromagnetic (FM) phases were characterized, and the former was found to contain nontrivial arrangements of charge at particular hole densities. Wollan and Koehler (1955) noticed the mixture of C- and E-type magnetic unit cells in the structure at $x = 0.5$, and labeled the insulating state at this density as a "CE-state" (the seven possible arrangements A, B, C, D, E, F, and G for the spin in

the unit cell are shown in Fig. 1.1b, with the spins of relevance being those located in the manganese ions). Theoretical work at approximately the same time, to be reviewed below, explained the ferromagnetic phase as caused by an effect called "double exchange" (DE), and thus one of the most interesting properties of these materials appeared to have found a good rationalization in the early studies of these compounds. Perhaps as a consequence of the apparent initial theoretical success, studies of the manganites continued in subsequent years at a slow pace.

The renewed surge of interest in manganites in the 1990s started with the experimental observation of large magnetoresistance (MR) effects in $Nd_{0.5}Pb_{0.5}MnO_3$ by Kusters et al. (1989) and in $La_{2/3}Ba_{1/3}MnO_x$ by von Helmolt et al. (1993) (actually Searle and Wang (1969) were the first to report MR studies in manganites, which were carried out using $La_{1-x}Pb_xMnO_3$ single crystals). Resistivity vs. temperature results for the (La,Ba) compound are shown in Fig. 1.2a, reproduced from von Helmolt et al. (1993). The MR effect was found to be as high as 60% at room temperature using thin films, and it was exciting to observe that this value was higher than found in artificial magnetic/nonmagnetic multilayers, allowing for potential applications in magnetic

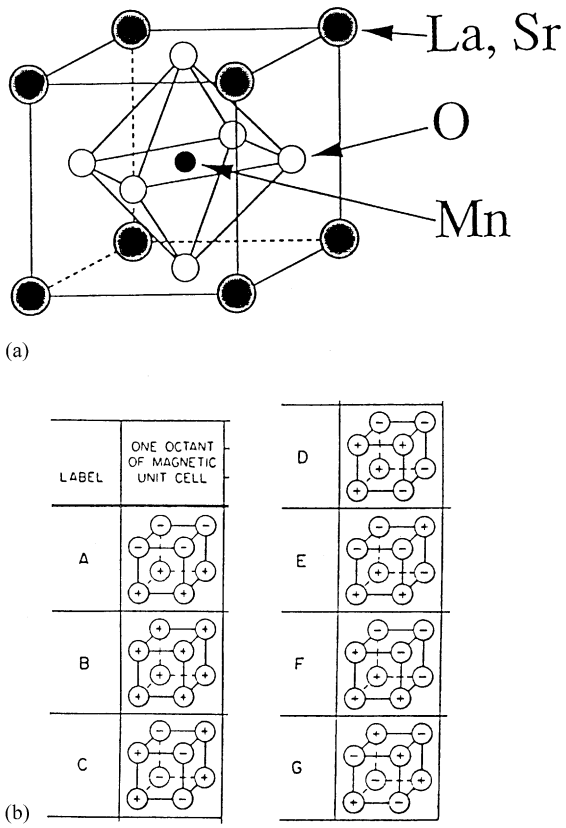

Fig. 1.1. (a) Arrangement of ions in the perovskite structure of manganites (from Tokura, 1999). (b) Possible magnetic structures and their labels. The circles represent the position of Mn ions, and the sign that of their spin projections along the z-axis. The G-type is the familiar antiferromagnetic arrangement in the three directions, while B is the familiar ferromagnetic arrangement. Taken from Wollan and Koehler (1955).

recording. However, as discussed extensively below, while a large body of subsequent experimental work has shown that the MR factor can actually be made very close to 100% (for a definition of the MR ratio see below), this occurs unfortunately at the cost of reducing the Curie temperature T_C, which jeopardizes those possible technological applications. Consider for instance in Fig. 1.2b the results for $Nd_{0.5}Pb_{0.5}MnO_3$ reproduced from Kusters et al. (1989). In this case the change in resistivity is larger than for the (La,Ba) compound, however its Curie temperature is reduced to 184 K. Also complicating possible applications, it is known that giant MR multilayer structures

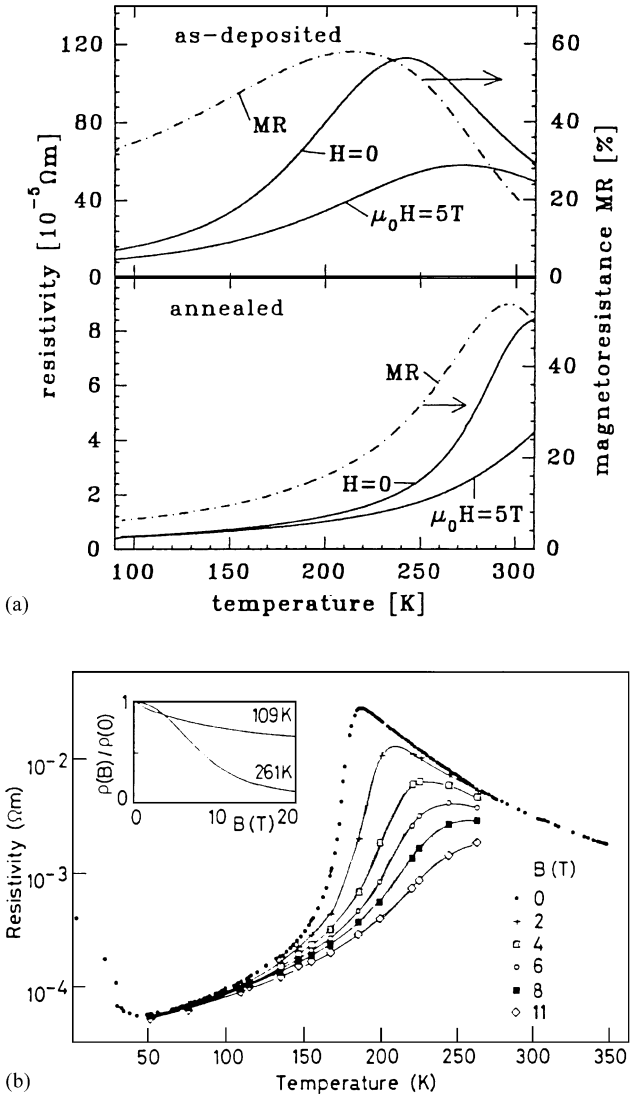

Fig. 1.2. (a) Temperature dependence of the resistivity of a $La_{2/3}Ba_{1/3}MnO_x$ thin film at 0 and 5 T, taken from von Helmolt et al. (1993). The two panels are results as-deposited and after a subsequent annealing, respectively. For more details see von Helmolt et al. (1993). (b) Resistivity of $Nd_{0.5}Pb_{0.5}MnO_3$ as a function of temperature and magnetic fields taken from Kusters et al. (1989). The inset is the magnetoresistance at the indicated temperatures.

present their appreciable changes in resistivity with fields as small as 0.01 T (Helman and Abeles, 1976; Fert and Campbell, 1976), while manganites typically need larger fields of about 1 T or more for equivalent resistivity changes, which appear too large for potential use in magnetic recording. Although progress in the development of applications is frequently reported (for recent references see Chen et al., 2000; Venimadhav et al., 2000; Kida and Tonouchi, 2000b), in this review the manganites will be mainly considered as an interesting basic-physics problem, with emphasis focused on understanding the microscopic origin of the large MR effect which challenges our current knowledge of strongly correlated electron systems. The discussion of possible applications of manganites is left for future reviews.

The big boost to the field of manganites that led to the present explosion of interest in the subject was produced by the discovery of the so-called "colossal" magnetoresistance (CMR) effect. In studies of thin films of $La_{0.67}Ca_{0.33}MnO_x$, a MR effect three orders of magnitude larger than the typical "giant" MR of superlattice films was observed (the name colossal was coined mainly to distinguish the effect from this previously found giant MR effect). Defining the MR ratio as $\Delta R/R(H) = (R(0) - R(H))/R(H)$, where $R(0)$ and $R(H)$ are the resistances without and with a magnetic field H, respectively, and expressing the result as a percentage (i.e., multiplying by an additional factor 100) it has been shown that MR ratios as large as 127,000% near 77 K can be obtained (Jin et al., 1994). This corresponds to more than a 1000-fold change in resistivity. Alternatively, expressed in terms of $\Delta R/R(0) = (R(0) - R(H))/R(0)$ the MR ratio in this case is as large as 99.92%. Xiong et al. (1995) reported thin-films studies of $Nd_{0.7}Sr_{0.3}MnO_\delta$ and in this case $\Delta R/R(H)$ was as high as 10^6%, a truly colossal factor. Triggered by such huge numbers, the experimental and theoretical study of manganites reignited, and is presently carried out by dozens of groups around the world. Early work tended to focus on the $x = 0.3$ doping due to its large T_C. However, more recently the attention has shifted towards other densities such as $x < 0.2$ or $x > 0.5$, where the competition between the various states of manganites can be better analyzed. In fact, one of the main results of recent investigations is that in order to understand the CMR effect, knowledge of the ferromagnetic metallic phase is not sufficient. The competing phases must be understood as well. This issue will be discussed extensively below.

Previous reviews on manganites are already available, but they have mainly focused on experiments. For instance, the reader can consult the reviews of Ramirez (1997), Coey et al. (1998), as well as the books recently edited by Rao and Raveau (1998), Kaplan and Mahanti (1999) and Tokura (1999). See also Loktev and Pogorelov (2000). The present review differs from previous ones in several aspects: (i) It addresses theoretical work in detail, especially regarding the stabilization in a variety of calculations of the many nontrivial charge/spin/orbital phases found in experiments; (ii) it highlights the importance of *phase separation* tendencies in models for manganites and the potential considerable influence of disorder on transitions that would be first order in the clean limit, leading to percolative processes; and (iii) it emphasizes the experimental results that have recently reported the presence of intrinsic inhomogeneities in manganites, results that appear in excellent agreement with the theoretical developments. If the review could be summarized in just a few words, the overall conclusion would be that theoretical and experimental work is rapidly converging to a unified picture pointing toward a physics of manganites in the CMR regimes clearly dominated by *inhomogeneities* in the form of coexisting competing phases. This is an *intrinsic* feature of single crystals, unrelated to grain boundary effects of polycrystals, and its theoretical understanding and experimental control is a challenge that should be strongly pursued. In fact, in spite of the considerably progress in recent years reviewed here, it is

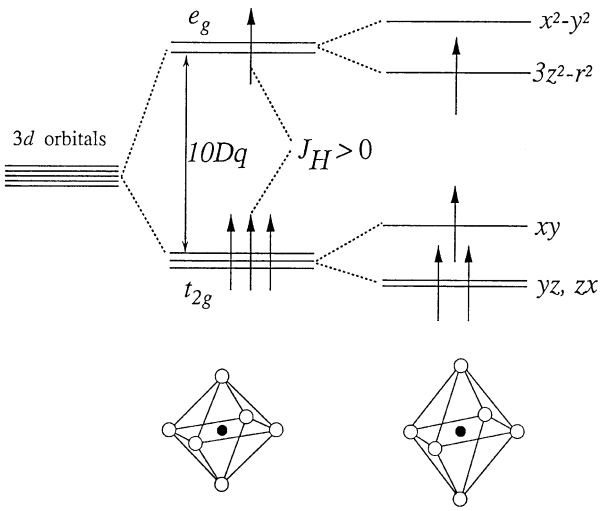

Fig. 1.3. Field splitting of the five-fold degenerate atomic 3d levels into lower t_{2g} and higher e_g levels. The particular Jahn–Teller distortion sketched in the figure further lifts each degeneracy as shown. Figure taken from Tokura (1999).

clear that the analysis of mixed-phase systems is at its early stages, and considerable more work should be devoted to the detailed study of manganese oxides and related compounds in such a regime.

In this review, it is assumed that the reader is familiar with some basic phenomenology involving the d-orbitals of relevance in manganese oxides. In the cubic lattice environment, the five-fold degenerate 3d-orbitals of an isolated atom or ion are split into a manifold of three lower energy levels (d_{xy}, d_{yz}, and d_{zx}), usually referred to as "t_{2g}" once mixing with the surrounding oxygens is included, and two higher energy states ($d_{x^2-y^2}$ and $d_{3z^2-r^2}$) called "e_g". The valence of the Mn-ions in this context is either four (Mn^{3+}) or three (Mn^{4+}), and their relative fraction is controlled through chemical doping. The large Hund coupling favors the population of the t_{2g} levels with three electrons forming a spin 3/2 state, and the e_g level either contains one electron or none. A sketch with these results is shown in Fig. 1.3. Considerable more detail about all the theoretical and experimental issues reported in this review can be found in a book in preparation by one of the authors (E.D., Springer Verlag).

The organization is the following. In Section 2, the most basic properties of manganites will be reviewed from the experimental viewpoint. Emphasis will be given to the phase diagrams and magnitude of the CMR effect in various manganites. For this section, the manganites will be divided into large, intermediate, and small bandwidth W compounds, a slightly unorthodox classification since previous work simply labeled them as either large or small W. In Section 3, the theoretical aspects are presented, starting with the early developments in the subject. Models and approximations will be discussed in detail, and results will be described. Especially, the key importance of the recently found phase separation tendencies will be remarked. In Section 4, the experimental work that have reported evidence of intrinsic inhomogeneities in manganites compatible with the theoretical calculations will be reviewed. Finally, conclusions are presented in Section 5 including the problems still open.

2. Basic properties, phase diagrams, and CMR effect in manganites

2.1. Large-bandwidth manganites: the case of $La_{1-x}Sr_xMnO_3$

In the renaissance of the study of manganites during the 1990s, a considerable emphasis has been given to the analysis of $La_{1-x}Sr_xMnO_3$, a material considered to be representative of the "large" bandwidth subset of manganese oxides. It is believed that in this compound the hopping amplitude for electrons in the e_g-band is larger than in other manganites, as a consequence of the sizes of the ions involved in the chemical composition, as discussed below. Its Curie temperature T_C as a function of hole doping is relatively high, increasing its chances for future practical applications. It has also been found that $La_{1-x}Sr_xMnO_3$ presents a complex behavior in the vicinity of $x = 1/8$ (see below), with a potential phenomenology as rich as found in the low-bandwidth manganites described later in this section. Resistivities vs. temperature for this compound at several densities are shown in Fig. 2.1.1a (taken from Urushibara et al., 1995). From these transport measurements, the phase diagram of this compound can be determined and it is shown in Fig. 2.1.1b (Y. Tokura and Y. Tomioka, prepared with data from Urushibara et al. (1995) and Fujishiro et al. (1998). See also Moritomo et al. (1998)). At hole concentrations such as $x = 0.4$, the system is metallic (defined straightforwardly as regions where $d\rho_{dc}/dT > 0$) even above T_C. At densities above $x = 0.5$ an interesting A-type antiferromagnetic metallic state is stabilized, with ferromagnetism in planes and antiferromagnetism between those planes. This phase was actually first observed in another compound $Nd_{1-x}Sr_xMnO_3$ (Kawano et al., 1997) and is believed to have $d_{x^2-y^2}$-type uniform orbital order within the ferromagnetic planes (for a visual representation of this state see Fig. 4 of Kajimoto et al., 1999). Considering now lower hole densities, at concentrations slightly below $x = 0.30$ the state above T_C becomes an insulator, which is an unexpected property of a paramagnetic state that transforms into a metal upon reducing the temperature. This curious effect is present in all the intermediate and low-bandwidth manganites, and it is a key property of this family of compounds. At densities $x \lesssim 0.17$, an insulating state is found even at low temperatures. As reviewed in more detail below, currently considerable work in the context of $La_{1-x}Sr_xMn\,O_3$ is being focused on the $x \sim 0.12$ region, simply labeled "ferromagnetic insulator" in Fig. 2.1.1b. In this region, indications of charge ordering have been found even in this putative large-bandwidth material, establishing an interesting connection with intermediate- and low-bandwidth manganites where charge-ordering tendencies are very prominent. A revised phase diagram of $La_{1-x}Sr_xMnO_3$ will be presented later when the experimental evidence of inhomogeneous states in this compound is discussed.

Studies by Tokura et al. (1994) showed that the MR effect is maximized in the density region separating the insulating from metallic states at low temperature, namely $x = 0.175$. The MR effect here is shown in Fig. 2.1.2a, taken from Tokura et al. (1994). The Curie temperature is still substantially large in this regime, which makes it attractive from the viewpoint of potential applications. A very important qualitative aspect of the results shown in Fig. 2.1.2a is that the MR effect is maximized at the smallest T_C which leads to a metallic ferromagnetic state; this observation let the authors to conclude that the large MR regime can only be clearly understood when the various effects which are in competition with DE are considered. This point will be a recurrent conclusion emerging from the theoretical calculations reviewed below, namely in order to achieve a large MR effect the insulating phase is at least as important as the metallic phase, and the region of the most interest should be the *boundary* between the metal and the insulator (Moreo et al.,

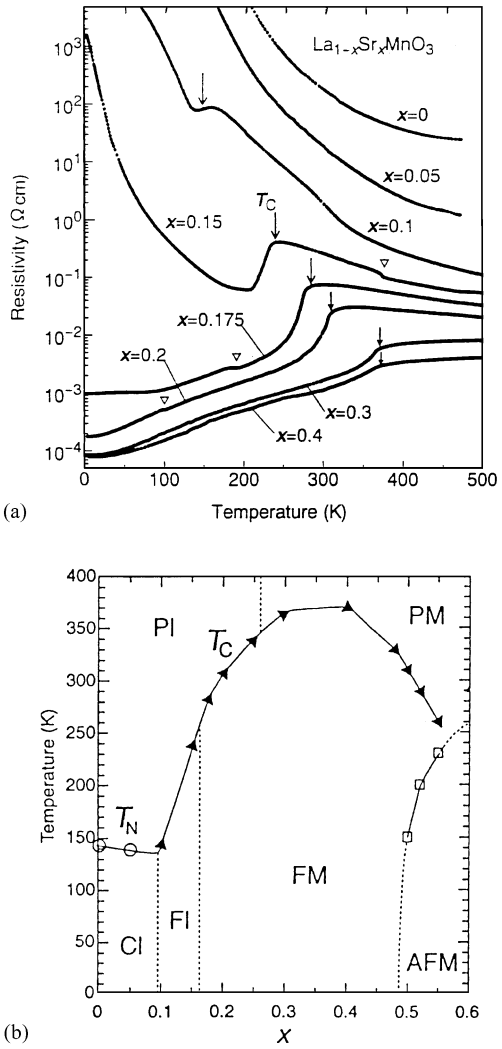

Fig. 2.1.1. (a) Temperature dependence of resistivity for various single crystals of $La_{1-x}Sr_xMnO_3$. Arrows indicate the Curie temperature. The open triangles indicate anomalies due to structural transitions. For more details see Urushibara et al. (1995) from where this figure is reproduced. (b) Phase diagram of $La_{1-x}Sr_xMnO_3$ (courtesy of Y. Tokura and Y. Tomioka) prepared with data from Urushibara et al. (1995) and Fujishiro et al. (1998). The AFM phase at large x is an A-type AF metal with uniform orbital order. PM, PI, FM, FI, and CI denote paramagnetic metal, paramagnetic insulator, FM metal, FM insulator, and spin-canted insulator states, respectively. T_C is the Curie temperature and T_N is the Néel temperature. A more detailed version of this phase diagram is shown below in Fig. 4.4.1, with emphasis on the small hole-density region which presents tendencies to charge-ordering and mixed-phase states.

1999a; Moreo et al., 2000). These insulating properties occur at low temperature by changing the density, or, at fixed density, by increasing the temperature, at least in some density windows. It is at the metal–insulator boundary where the tendencies to form coexisting clusters and percolative transitions are the most important. This point of view is qualitatively different from the approach followed in previous theories based on polaronic formation, Anderson localization, or on

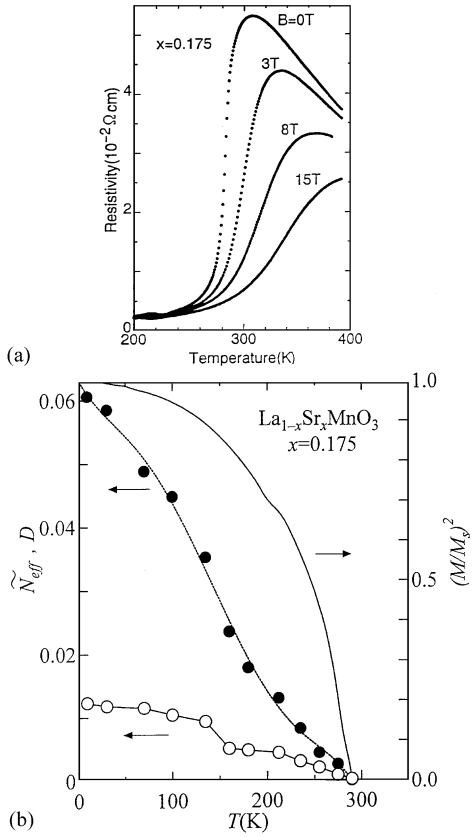

Fig. 2.1.2. (a) Temperature dependence of the resistivity in magnetic fields corresponding to $La_{1-x}Sr_xMnO_3$ at $x = 0.175$ (from Tokura et al., 1994). (b) Temperature dependence of the total infrared-absorption spectral weight N_{eff} (open circles) and Drude weight D (closed circles) for a single crystal of $La_{1-x}Sr_xMnO_3$ ($x = 0.175$). The solid line is the square of the normalized ferromagnetic magnetization $(M/M_s)^2$, with M_s the saturated magnetization. Results reproduced from Tokura (1999).

modifications of the double-exchange ideas, but it is crucial in the phase-separation-based approaches described here. Note, however, that the metallic phase of $La_{1-x}Sr_xMnO_3$ at sufficiently large hole density seems quite properly described by double-exchange approaches, namely there is a simple relation between the resistivity and the magnetization in the metallic ferromagnetic phase (Tokura et al., 1994; Furukawa et al., 1998). Then, it is important to distinguish the theoretical understanding of the individual phases, far from others in parameter space, from the understanding of the *competition* among them. It is the latest issue that is the most important for the explanation of the MR effect according to recent calculations (Moreo et al., 1999a, 2000).

It is also interesting to point out that the low-temperature ferromagnetic metallic state that appears prominently in Fig. 2.1.1b is actually "unconventional" in many respects. For instance, in Fig. 2.1.2b, taken from Tokura (1999), it is shown that the total low-energy spectral weight of the optical conductivity N_{eff} is still changing even in the low-temperature region, where the spin is already almost fully polarized. Clearly, there is another scattering mechanism in the system besides the spin. Actually, even within the FM-state the carrier motion is mostly incoherent since the

Drude weight is only 1/5 of the total low-energy weight. The conventional Drude model is not applicable to the FM-state of manganites. Probably the orbital degrees of freedom are important to account for this effect.

2.2. *Intermediate-bandwidth manganites*: the case of $La_{1-x}Ca_xMnO_3$

Currently, a large fraction of the work in manganites focuses on intermediate- to low-bandwidth materials since these are the ones that present the largest CMR effects, which are associated with the presence of charge ordering tendencies. Unfortunately, as discussed in the Introduction, this comes at a price: the Curie temperature decreases as the magnitude of the MR effects increases. In this section, the properties of $La_{1-x}Ca_xMnO_3$ will be discussed in detail. This compound presents some characteristics of large bandwidth manganites, such as the presence of a robust ferromagnetic metallic phase. However, it also has features that indicate strong deviations from double-exchange behavior, including the existence of charge/orbital-ordered phases. For this reason, the authors consider that this compound should be labeled as of "intermediate bandwidth", to distinguish it from the truly low-bandwidth compound $Pr_{1-x}Ca_xMnO_3$ where a metallic ferromagnetic phase can only be stabilized by the application of magnetic fields.

$La_{1-x}Ca_xMnO_3$ has been analyzed since the early days of manganite studies (Jonker and Van Santen, 1950; Wollan and Koehler, 1955; Matsumoto, 1970b), but it is only recently that it has been systematically scrutinized as a function of density and temperature. In particular, it has been

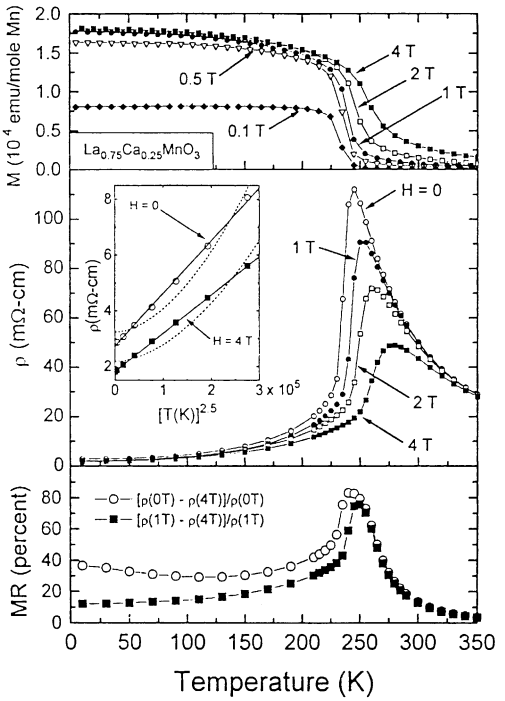

Fig. 2.2.1. The magnetization, resistivity, and magnetoresistance of $La_{1-x}Ca_xMnO_3$ ($x = 0.25$), as a function of temperature at various fields. The inset is ρ at low temperatures. Reproduced from Schiffer et al. (1995).

observed that $La_{1-x}Ca_xMnO_3$ has a large MR effect. For example, Fig. 2.2.1 reproduces results from Schiffer et al. (1995) at $x = 0.25$ showing the magnetization and resistivity as a function of temperature, and the existence of a robust MR, larger than 80%. The drop in $\rho_{dc}(T)$ with decreasing temperature and the peak in MR are correlated with the ferromagnetic transition in the magnetization. The insulating behavior above the Curie temperature is very prominent and the explanation of its origin is among the most important issues to be addressed in theories of manganites, as already discussed in the previous subsection. Below T_C the presence of ferromagnetism was tentatively attributed to the double-exchange mechanism, but further work reviewed in Section 4 has actually revealed a far more complex structure with coexisting phases even in this metallic regime. In fact, hints of this behavior may already be present in Fig. 2.2.1 which already reveals a MR effect as large as 30% well below T_C. In addition, it is also interesting to observe that hydrostatic pressure leads to large changes in resistivity comparable to those found using magnetic fields [see for instance Fig. 2.2.2 where $\rho_{dc}(T)$ is shown parametric with pressure at $x = 0.21$, taken from Neumeier et al. (1995). See also Hwang et al. (1995b)].

The qualitative features of Fig. 2.2.1 contribute to the understanding, at least in part, of the CMR effect found in thin films of this same compound (Jin et al., 1994). For references on thin film work in manganites, see Ramirez (1997, p. 8182). See also Kanki et al. (2000). In the work of Jin et al. (1994), T_C was suppressed by substrate-induced strain, and, as a consequence, the ρ_{dc} was much higher immediately above the transition than in crystals since the system was still in the insulating state, inducing an enormous change in resistivity. Thus, it appears that to understand the large MR values the insulating state is actually *more* important than the metallic state, and the relevance of the DE ideas is limited to the partial explanation of the low-temperature phase in a narrow density window, as explained in more detail later. Clearly, the DE framework is insufficient for describing the physics of the manganites.

The complete phase diagram of $La_{1-x}Ca_xMnO_3$, based on magnetization and resistivity measurements, is reproduced in Fig. 2.2.3, taken from Cheong and Hwang (1999). Note that the

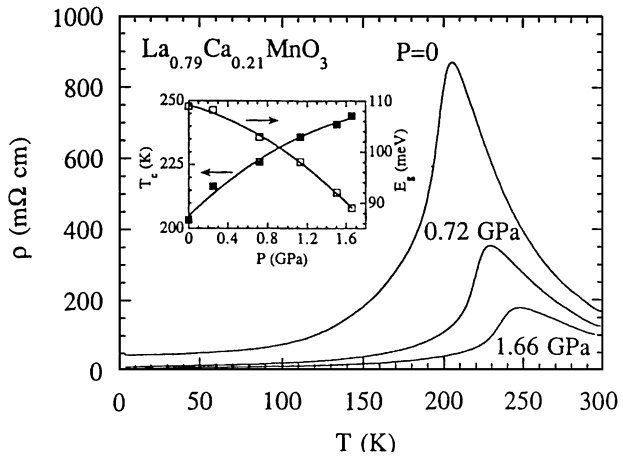

Fig. 2.2.2. Resistivity vs. temperature at three hydrostatic pressures for $La_{1-x}Ca_xMnO_3$ ($x = 0.21$). In the inset the pressure dependence of T_C and the activation energy e_g are plotted. For details see Neumeier et al. (1995), from where these results have been reproduced.

FM phase actually occupies just a fraction of the whole diagram, illustrating once again that DE does not provide a full understanding of the manganites. For instance, equally prominent are the charge ordered (CO) states between $x = 0.50$ and 0.87. The CO state at $x = 0.50$ was already described by Wollan and Koehler (1955) as a CE-state, and the characteristics at other densities are discussed below. In the regime of CO-states, studies by Ramirez et al. (1996) of the sound velocity, specific heat, and electron diffraction were attributed to strong electron–phonon coupling, in agreement with the predictions of Millis et al. (1995). The "canted" state at x close to 1 could be a mixed-phase state with coexisting FM–AF characteristics based on recent theoretical calculations (see below Section 3), but the issue is still under discussion. The low hole-density regime is quite unusual and nontrivial, and it appears to involve a charge-ordered phase, and a curious ferromagnetic insulator. Actually at $x = 0.10$, there is no large MR effect using fields of 12 T, according to Fig. 6 of Ibarra and De Teresa (1998c). Fig. 25 of the same reference shows that at $x = 0.65$, well inside the charge-ordered state, a 12 T field is also not sufficient to destabilize the insulating state into a metallic one. Thus, to search for a large MR effect, the density must be closer to that leading to the FM metallic regime, as emphasized before.

In Fig. 2.2.3 note also the presence of well-defined features at commensurate carrier concentrations $x = N/8$ ($N = 1,3,4,5$ and 7). The Curie temperature is maximized at $x = 3/8$ according to Cheong and Hwang (1999), contrary to the $x = 0.30$ believed by many to be the most optimal density for ferromagnetism. Cheong and Hwang (1999) also remarked that in the large-bandwidth compound $La_{1-x}Sr_xMnO_3$, T_C is also maximized at the same $x = 3/8$ concentration, implying that this phenomenon is universal. It is important to realize that within a simple one-orbital double-exchange model, as described later, the optimal density for ferromagnetism should be $x = 0.50$. The fact that this is not observed is already indicative of the problems faced by a double-exchange description of manganites. Note also that Zhao et al. (1996, 1999) found a giant

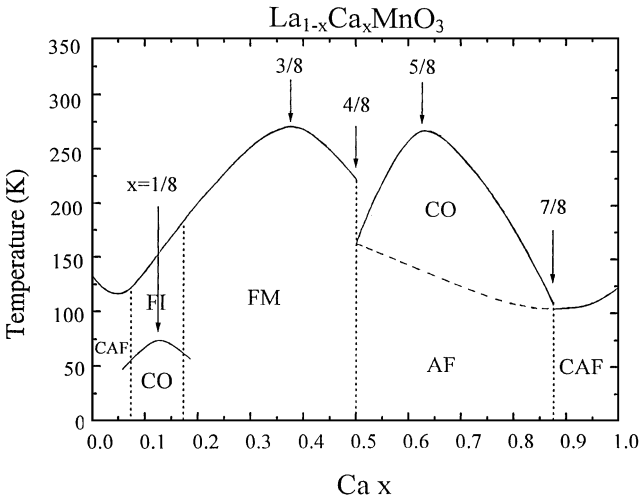

Fig. 2.2.3. Phase diagram of $La_{1-x}Ca_xMnO_3$, constructed from measurements of macroscopic quantities such as the resistivity and magnetic susceptibility, reproduced from Cheong and Hwang (1999). FM: Ferromagnetic Metal, FI: Ferromagnetic Insulator, AF: Antiferromagnetism, CAF: Canted AF, and CO: Charge/Orbital Ordering. FI and/or CAF could be a spatially inhomogeneous states with FM and AF coexistence.

oxygen isotope shift in T_C of about 20 K at $x = 0.2$, showing the relevance of electron–phonon couplings in manganites, a recurrent result of many papers in this context.

The charge-ordering temperature T_{CO} peaks at $x = 5/8$ (the same occurs in (Bi, Ca)-based compounds), while at $x = 4/8 = 1/2$ there is a sharp change from ferromagnetic to antiferromagnetic ground states. The whole phase diagram has a pronounced electron–hole *asymmetry*, showing again that simple double-exchange models with only one orbital are not realistic. At $x = 1/8$ the low-density charge-ordered state appears to have the largest strength, while on the other side at $x = 7/8$ charge ordering disappears into a mixed FM–AF state. Finally, at $x = 0$ the ground state is an A-type antiferromagnet (see also Matsumoto, 1970a) with ferromagnetic spin correlations on a plane and antiferromagnetism between planes, while at $x = 1$ it is a G-type antiferromagnet (AF in all directions), both of them insulating.

The pattern of charge- and orbital order in the CO states of Fig. 2.2.3 is highly nontrivial and at several densities still under discussion (for early work in the context of orbital ordering see Kugel and Khomskii, 1974; Eremin and Kalinenkov, 1978, 1981). Some of the arrangements that have been identified are those shown in Fig. 2.2.4, reproduced from Cheong and Hwang (1999). At $x = 0$, the A-type spin state is orbitally ordered as it appears in Fig. 2.2.4a. At $x = 0.5$ the famous CE-type arrangement (Fig. 2.2.4b) already found in early studies of manganites is certainly stabilized. This state has been recently observed experimentally using resonant X-ray scattering (Zimmermann et al., 1999, see also Zimmermann et al., 2000). At $x = 2/3$, and also $x = 3/4$, a novel "bi-stripe" arrangement is found (Mori et al., 1998a). The $x = 0.65$ state is very stable upon the application of a magnetic field (Fig. 25 of Ibarra and De Teresa, 1998c). The origin of the term bi-stripe is obvious from Fig. 2.2.4c. However, theoretical work (Hotta et al., 2000a and references therein) has shown that it is more appropriate to visualize this arrangement as formed by FM zigzag chains running in the direction *perpendicular* to those of the charge stripes of Fig. 2.2.4c. This issue will be discussed in more detail later in the review when the theoretical aspects are addressed. Based on electron microscopy techniques Cheong and Hwang (1999) believe that at the, e.g., $x = 5/8$ concentration

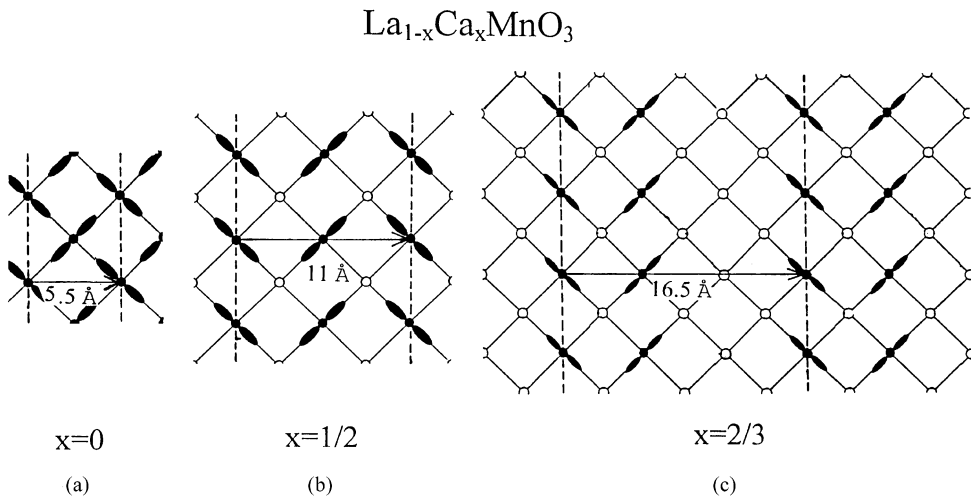

Fig. 2.2.4. The charge and orbital ordering configurations for $La_{1-x}Ca_xMnO_3$ with $x = 0$, 1/2, and 2/3. Open circles are Mn^{4+} and the lobes show the orbital ordering of the e_g-electrons of Mn^{3+}. Figure reproduced from Cheong and Hwang (1999).

a mixture of the $x = 1/2$ and $2/3$ configurations forms the ground state. The size of the coexisting clusters is approximately 100 Å. Once again, it appears that phase separation tendencies are at work in manganese oxides.

However, note that studies by Radaelli et al. (1999) on the $x = 2/3$ compound arrived to the conclusion that a "Wigner crystal" charge arrangement is stable at this density, with the charge ordered but spread as far from each other as possible. It appears that bi-stripes and Wigner crystal states must be very close in energy. While the results at $x = 0.0$ and 0.5 have been reproduced in recent theoretical studies of manganite models, the more complex arrangements at other densities are still under analysis (Hotta et al., 2000b) and will be discussed in more detail below.

Finally, there is an interesting observation that is related with some theoretical developments to be presented later in the review. In Fig. 2.2.5, the resistivity at 300 K and 100 K vs. hole density is shown, reproduced from Cheong and Hwang (1999). Note at 300 K the smooth behavior as x grows from 0, only interrupted close to $x = 1$ when the G-type AF insulating state is reached. Then, at 300 K there is no *precursor* of the drastically different physics found at, e.g., 100 K where for $x < 0.5$ a FM-state is found while for $x > 0.5$ the state is CO and AF. This lack of precursors is also in agreement with neutron scattering results that reported FM fluctuations above the CO and Néel temperatures in the large x regime (Dai et al., 1996), similar to those observed at lower hole densities. These results are consistent with an *abrupt* first-order-like transition from the state with FM fluctuations to the

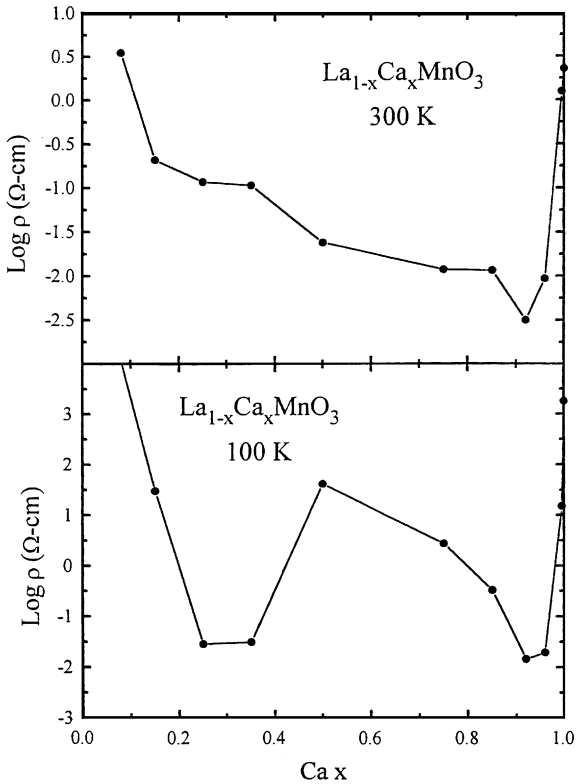

Fig. 2.2.5. Resistivity at 300 and 100 K vs. Ca concentration for $La_{1-x}Ca_xMnO_3$ reproduced from Cheong and Hwang (1999).

CO/AF-state, as observed in other experiments detailed in later sections (for very recent work see Ramos et al., 2000). These two states are so different that a smooth transition between them is not possible. In addition, recent theoretical developments assign considerable importance to the influence of disorder on this type of first-order transitions to explain the large MR effect in manganites (Moreo et al., 2000), as shown elsewhere in this review. Then, the sudden character of the transition from ferromagnetism to charge-ordered antiferromagnetism appears to play a *key* role in the physics of manganites, and its importance is emphasized in many places in the text that follows.

2.3. *Low-bandwidth manganites*: the case of $Pr_{1-x}Ca_xMnO_3$

As explained before, in perovskite manganites, such as $La_{1-x}Ca_xMnO_3$ and the compound $Pr_{1-x}Ca_xMnO_3$ described here, the bandwidth W is smaller than in other compounds that have a behavior more in line with the standard double-exchange ideas. In the low-bandwidth compounds, a charge-order state is stabilized in the vicinity of $x = 0.5$, while manganites with a large W ($La_{1-x}Sr_xMnO_3$ as example) present a metallic phase at this hole density. Let us focus in this subsection on $Pr_{1-x}Ca_xMnO_3$ which presents a particularly stable CO-state in a broad density region between $x = 0.30$ and 0.75, as Jirak et al. (1985) showed. Part of the phase diagram of this compound is in Fig. 2.3.1, reproduced from Tomioka et al. (1996) (see also Tomioka and Tokura, 1999). Note that a metallic ferromagnetic phase is *not* stabilized at zero magnetic field and ambient pressure in this low-bandwidth compound. Instead, a ferromagnetic insulating (FI) state exists in the range from $x = 0.15$ to 0.30. This FI state has not been fully explored to the best of our knowledge, and it may itself present charge ordering as some recent theoretical studies have suggested (Hotta and Dagotto, 2000). For $x \geq 0.30$, an antiferromagnetic CO-state is stabilized. Neutron diffraction studies (Jirak et al., 1985) showed that at *all* densities between 0.30 and 0.75, the arrangement of charge/spin/orbital order of this state is similar to the CE-state (see Fig. 2.2.4b) already discussed in the context of $x = 0.5$ (La, Ca)-based manganites. However, certainly the hole density is changing with x, and as a consequence the CE-state cannot be "perfect" at all densities but electrons have to be added or removed from the structure. Jirak et al. (1985) discussed a "pseudo"-CE-type structure for $x = 0.4$ that has the proper density. Other authors simply refer to the $x \neq 0.5$ CO-states as made out of the $x = 0.5$ structure plus "defects". Hotta and Dagotto (2000) proposed an ordered state for $x = 3/8$ based on mean-field and numerical approximations. Neutron diffraction studies have shown that the coupling along the c-axis changes from AF at $x = 0.5$ to FM at $x = 0.3$ (Yoshizawa et al., 1995) and a canted state has also been proposed to model this behavior. Certainly more work is needed to fully understand the distribution of charge in the ground-state away from $x = 0.5$.

The effect of magnetic fields on the CO-state of $Pr_{1-x}Ca_xMnO_3$ is remarkable. In Fig. 2.3.2 the resistivity vs. temperature is shown parametric with magnetic fields of a few Teslas, which are small in typical electronic units. At low temperatures, changes in ρ_{dc} by several orders of magnitude can be observed. Note the stabilization of a metallic state upon the application of the field. This state is ferromagnetic according to magnetization measurements, and thus it is curious to observe that a state not present at zero field in the phase diagram, is nevertheless stabilized at finite fields, a puzzling result that is certainly difficult to understand. The shapes of the curves in Fig. 2.3.2 resemble similar measurements carried out in other manganites which also present a large MR effect, and a possible origin based on percolation between the CO- and FM-phase will be discussed later in the review. First-order characteristics of the metal–insulator transitions in this context are

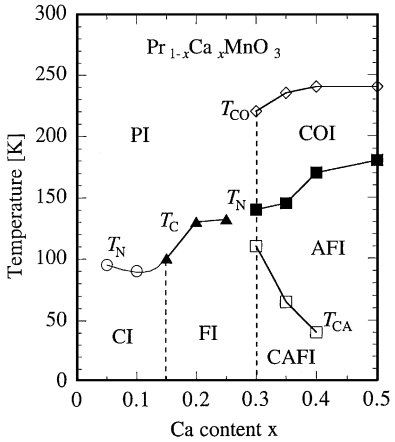

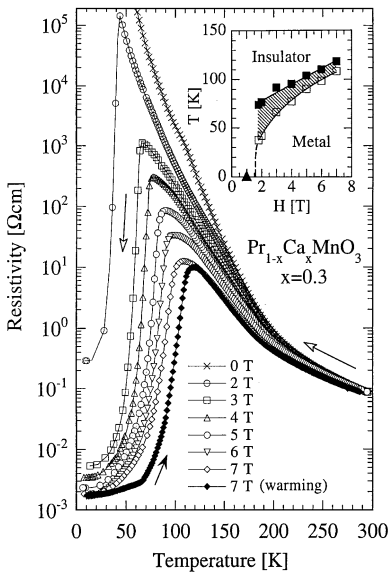

Fig. 2.3.1. Phase diagram of $Pr_{1-x}Ca_xMnO_3$. PI and FI denote the paramagnetic insulating and ferromagnetic insulating states, respectively. For hole density between 0.3 and 0.5, the antiferromagnetic insulating (AFI) state exists in the charge/orbital-ordered insulating (COI) phase. The canted antiferromagnetic insulating (CAFI) state, which may be a mixed FM–AF state, also has been identified between $x = 0.3$ and 0.4. Reproduced from Tomioka and Tokura (1999).

Fig. 2.3.2. Temperature dependence of the resistivity of $Pr_{1-x}Ca_xMnO_3$ with $x = 0.3$ at various magnetic fields. The inset is the phase diagram in the temperature–magnetic field plane. The hatched region has hysteresis. Results reproduced from Tomioka and Tokura (1999).

very prominent, and they have been reviewed by Tomioka and Tokura (1999). It is interesting to observe that pressure leads to a colossal MR effect quite similar to that found upon the application of magnetic fields (see for example Fig. 2.3.3, where results at $x = 0.30$ from Moritomo et al. (1997) are reproduced).

The abrupt metal–insulator transition at small magnetic fields found in $Pr_{1-x}Ca_xMnO_3$ at $x = 0.30$ appears at other densities as well, as exemplified in Fig. 2.3.4, which shows the resistivity vs. temperature at $x = 0.35$, 0.4 and 0.5, reproduced from Tomioka et al. (1996). Fig. 2.3.5 (from Tomioka and Tokura, 1999) shows that as x grows away from $x = 0.30$, larger fields are needed to destabilize the charge-ordered state at low temperatures (e.g., 27 T at $x = 0.50$ compared with 4 T at $x = 0.30$). It is also interesting to observe that the replacement of Ca by Sr at $x = 0.35$ also leads to a metal-insulator transition, as shown in Fig. 2.3.6 taken from Tomioka et al. (1997). Clearly $Pr_{1-x}Ca_xMnO_3$ presents a highly nontrivial behavior that challenges our theoretical understanding of the manganese oxide materials. The raw huge magnitude of the CMR effect in this compound highlights the relevance of the CO–FM competition.

2.4. Other perovskite manganite compounds

Another interesting perovskite manganite compound is $Nd_{1-x}Sr_xMnO_3$, and its phase diagram is reproduced in Fig. 2.4.1 (from Kajimoto et al., 1999). This material could be labeled as

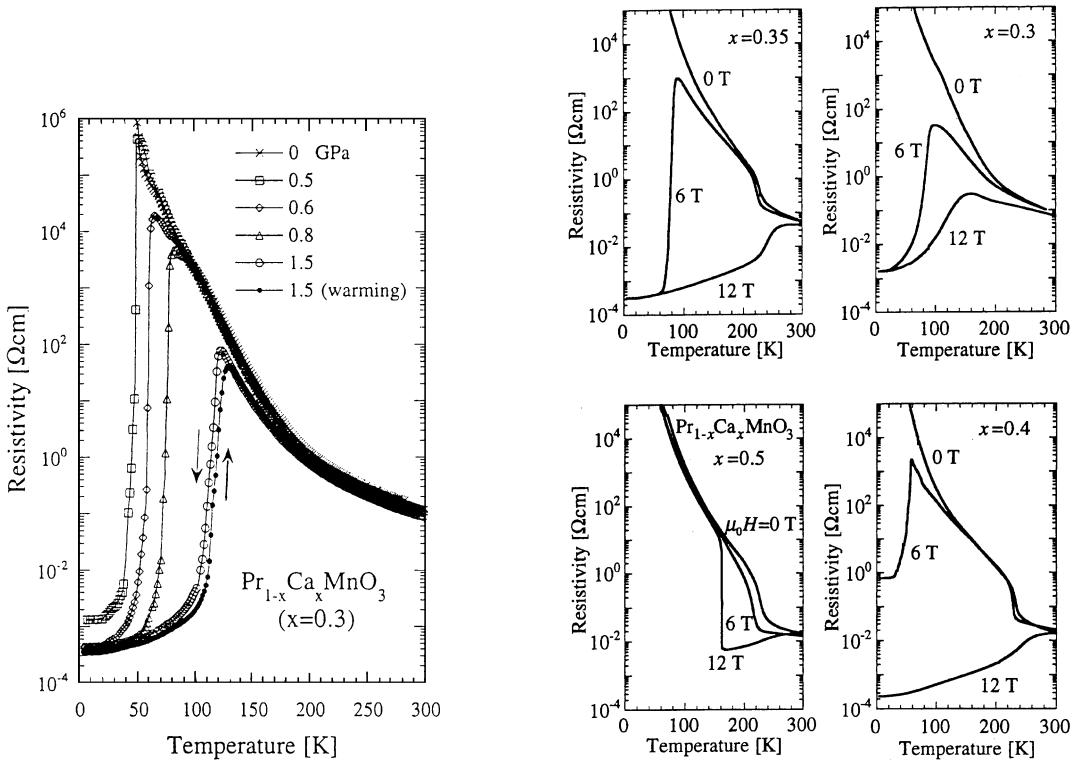

Fig. 2.3.3. Temperature dependence of resistivity for $Pr_{1-x}Ca_xMnO_3$ at $x = 0.3$ under the various pressures indicated. Reproduced from Moritomo et al. (1997).

Fig. 2.3.4. Temperature dependence of the resistivity corresponding to $Pr_{1-x}Ca_xMnO_3$ at the hole concentrations and magnetic fields indicated. Reproduced from Tomioka et al. (1996).

"intermediate bandwidth" due to the presence of a stable CO-phase at $x = 0.50$, state which can be easily destroyed by a magnetic field in a first-order transition (Kuwahara et al., 1995). However, this phase appears only in a tiny range of densities and at low temperature. In fact, aside from this CO-phase, the rest of the phase diagram is very similar to the one of $La_{1-x}Sr_xMnO_3$. In particular, it is interesting to observe the presence of an A-type antiferromagnetic metallic structure which is believed to have ferromagnetic planes with *uniform* $d_{x^2-y^2}$-type orbital order (Kawano et al., 1997), making the system effectively anisotropic (Yoshizawa et al., 1998). A compound that behaves similarly to $Nd_{1-x}Sr_xMnO_3$ is $Pr_{1-x}Sr_xMnO_3$, with the exception of $x = 0.5$: In $Pr_{1-x}Sr_xMnO_3(x = 0.5)$ the CO-state is not stable. Actually, Tokura clarified to the authors (private communication) that the polycrystal results that appeared in Tomioka et al. (1995) showing a CO-phase in this compound were later proven incorrect after the preparation of single crystals. Nevertheless, such a result illustrates the fragile stability of the CO-phase in materials where the bandwidth is not sufficiently small. Results for this compound reporting mixed-phase tendencies were recently presented by Zvyagin et al. (2000). The corresponding phase diagram for a mixture $(La_{1-z}Nd_z)_{1-x}Sr_xMnO_3$ can be found in Akimoto et al. (1998) and it shows that the CO-phase at $x = 0.5$ of the pure (Nd,Sr) compound disappears for z smaller than ~ 0.5. The phase

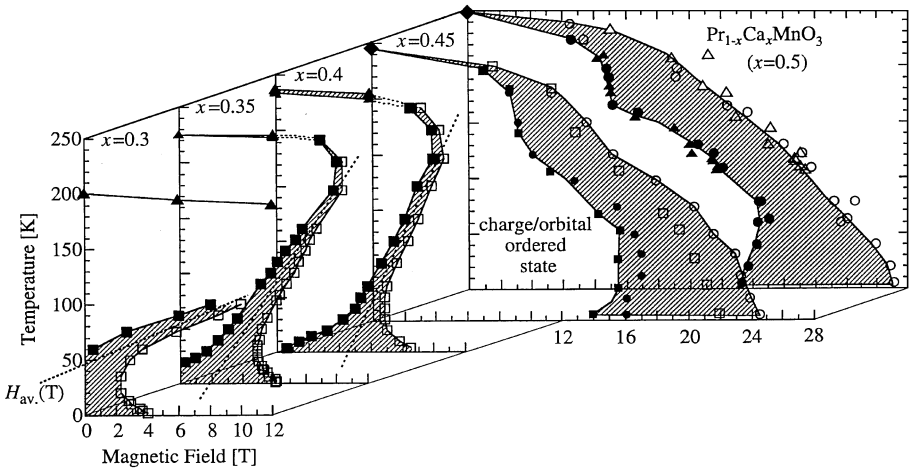

Fig. 2.3.5. The charge/orbital-ordered state of $Pr_{1-x}Ca_xMnO_3$ at several hole concentrations, plotted on the magnetic field-temperature plane. The hatched area indicates the hysteresis region. For more details see Tomioka and Tokura (1999).

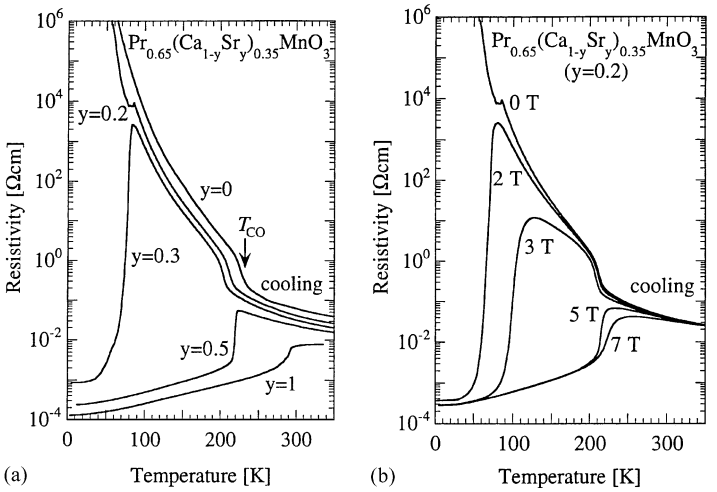

Fig. 2.3.6. (a) Temperature dependence of the resistivity for $Pr_{0.65}(Ca_{1-y}Sr_y)_{0.35}MnO_3$ crystals with varying y. (b) Resistivity vs. temperature of $Pr_{0.65}(Ca_{1-y}Sr_y)_{0.35}MnO_3$ ($y = 0.2$) for several magnetic fields. Reproduced from Tomioka and Tokura (1999).

diagram of $(La_{1-z}Nd_z)_{1-x}Ca_xMnO_3$ investigated by Moritomo (1999b) also shows a competition between FM and CO, with phase separation characteristics in between.

Other manganites present CO-phases at $x = 0.5$ as well, and the compound where this phase seems to be the strongest is $Sm_{0.5}Ca_{0.5}MnO_3$, as exemplified in Fig. 2.4.2, where the effect of magnetic fields on several low-bandwidth manganites is shown. An interesting way to visualize the relative tendencies of manganite compounds to form a CO-state at $x = 0.5$ can be found in Fig. 2.4.3, taken from Tomioka and Tokura (1999). As discussed in more detail at the end of this

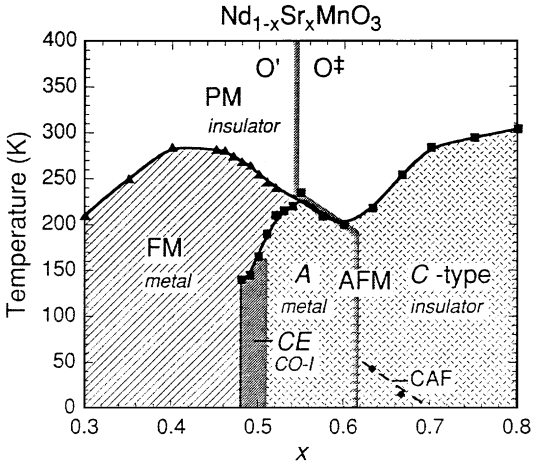

Fig. 2.4.1. Phase diagram of $Nd_{1-x}Sr_xMnO_3$, reproduced from Kajimoto et al. (1999). The notation is standard.

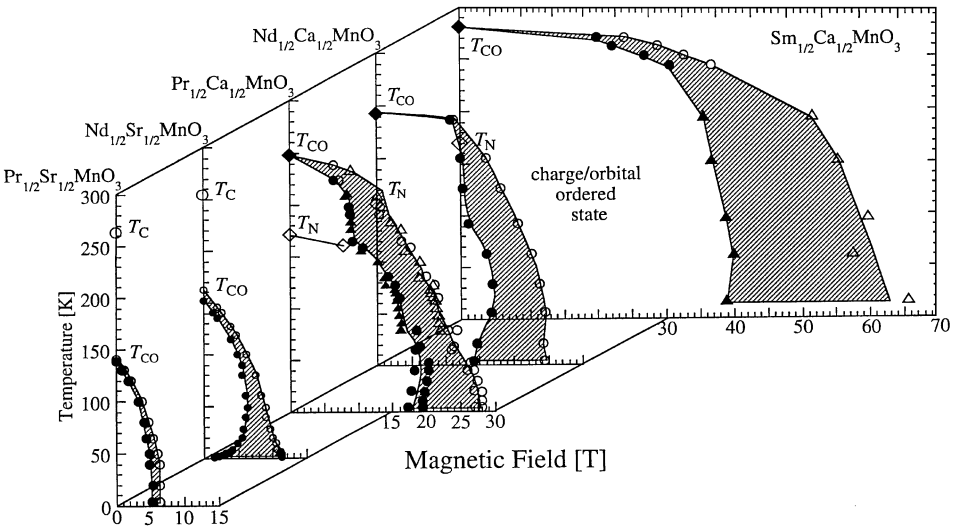

Fig. 2.4.2. The charge-ordered phase of various compounds $(RE)_{1/2}(AE)_{1/2}MnO_3$ plotted on the magnetic field-temperature plane. The hatched area indicates the hysteresis region. Reproduced from Tomioka and Tokura (1999).

section, the key ingredient determining the FM vs. CO character of a state at a fixed density is the size of the ions involved in the chemical composition. In Fig. 2.4.3 the radius of the trivalent and divalent ions, as well as their average radius at $x = 0.5$, appear in the horizontal axes. The Curie and CO temperature are shown below in part (b). As an example, for the extreme case of (La,Sr) based manganites, a metallic ferromagnetic state is observed at $x = 0.5$, while (Pr,Ca) compounds are charge-ordered. As a byproduct of Fig. 2.4.2, Fig. 2.4.3 it is quite interesting to note the similarities between the actual values of the critical temperatures T_C and T_{CO}. Being two rather different states, there is no obvious reason why their critical temperatures are similar. A successful theory must certainly address this curious fact.

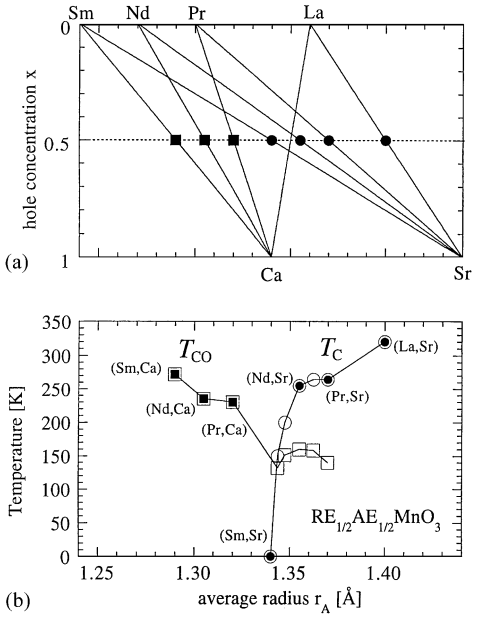

Fig. 2.4.3. (a) Average ionic radius at $x = 0.5$ corresponding to a mixture of a trivalent ion (upper abscissa) and a divalent ion (lower abscissa). (b) Critical Curie temperature T_C and charge/orbital ordering transition T_{CO} for various trivalent-divalent ion combinations. Reproduced from Tomioka and Tokura (1999).

2.5. Double-layer compound

Not only three-dimensional perovskite-type structures are present in the family of manganite compounds, but layered ones as well. In fact, Moritomo et al. (1996) showed that it is possible to prepare double-layer compounds with a composition $La_{2-2x}Sr_{1+2x}Mn_2O_7$. Single-layer manganites can also be synthesized, as will be discussed in the next subsection. In fact, these are just special cases of the Ruddlesden–Popper series $(T_{1-x}D_x)_{n+1}Mn_nO_{3n+1}$, with T a trivalent cation, D a divalent cation, and $n = 1$ corresponding to the single layer, $n = 2$ to the double layer, and $n = \infty$ to the cubic perovskite structure (see Fig. 2.5.1 for the actual structure). The temperature dependence of the resistivity in representative multilayer structures is shown in Fig. 2.5.2 for the $n = 1$, 2, and ∞ (3D perovskite) compounds at a hole concentration of $x = 0.4$. In the regime where the single layer is insulating and the $n = \infty$ layer is metallic, the double layer has an intermediate behavior, with insulating properties above a critical temperature and metallic below. A large MR effect is observed in this double-layer system as shown in Fig. 2.5.3, larger than the one found for $La_{1-x}Sr_xMnO_3$. The full phase diagram of this compound will be discussed later in this review (Section 4) in connection with the presence of inhomogeneities and clustering tendencies.

2.6. Single-layer compound

As mentioned in the previous subsection, the single-layer manganite has also been synthesized (see Rao et al., 1988). Its chemical formula is $La_{1-x}Sr_{1+x}MnO_4$. This compound does not have a ferromagnetic phase in the range from $x = 0.0$ to 0.7, which is curious. Note that other

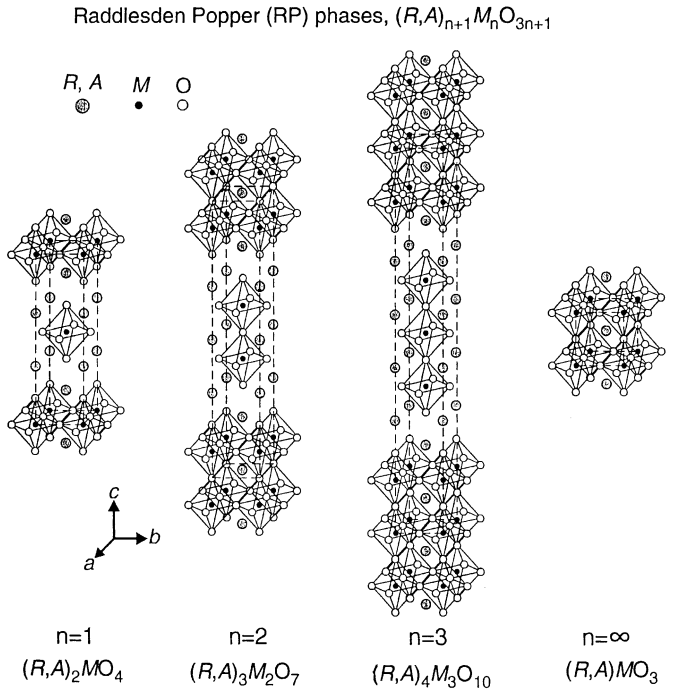

Fig. 2.5.1. Schematic crystal structure of four representatives of the Ruddlesden–Popper series of manganese oxides (taken from Tokura, 1999).

manganites have not presented a ferromagnetic metallic phase also, but they had at least a ferro-insulating regime (e.g., $Pr_{1-x}Ca_xMnO_3$). A schematic phase diagram of the one-layer compound is given in Fig. 2.6.1, reproduced from Moritomo et al. (1995). For more recent results, see Larochelle et al. (2000). At all the densities shown, insulating behavior has been found. Note the prominent CO-phase near $x = 0.5$, and especially the "spin-glass" phase in a wide range of densities between $x = 0.2$ and $x \sim 0.5$. The $x = 0.5$ charge-ordered phase is of the CE-type (Sternlieb et al., 1996; Murakami et al., 1998a). The large x regime has phase separation according to Bao et al. (1996), as discussed in more detail below. The actual microscopic arrangement of charge and spin in the intermediate spin-glass regime has not been experimentally studied in detail, to the best of our knowledge, but it certainly deserves more attention since the two dimensionality of the system makes possible reliable theoretical studies and simulations.

2.7. Importance of tolerance factor

It has been clearly shown experimentally that working at a fixed hole density the properties of manganites strongly depend on a geometrical quantity called the "tolerance factor", defined as $\Gamma = d_{A\text{-}O}/(\sqrt{2}d_{Mn\text{-}O})$. Here $d_{A\text{-}O}$ is the distance between the A site, where the trivalent or divalent non-Mn ions are located, to the nearest oxygen. Remember that the A ion is at the center of a cube with Mn in the vertices and O in between the Mn's. $d_{Mn\text{-}O}$ is the Mn–O shortest distance. Since for an undistorted cube with a straight Mn–O–Mn link, $d_{A\text{-}O} = \sqrt{2}$ and $d_{Mn\text{-}O} = 1$ in units of the Mn–O distance, then $\Gamma = 1$ in this perfect system. However, sometimes the A ions are too small to

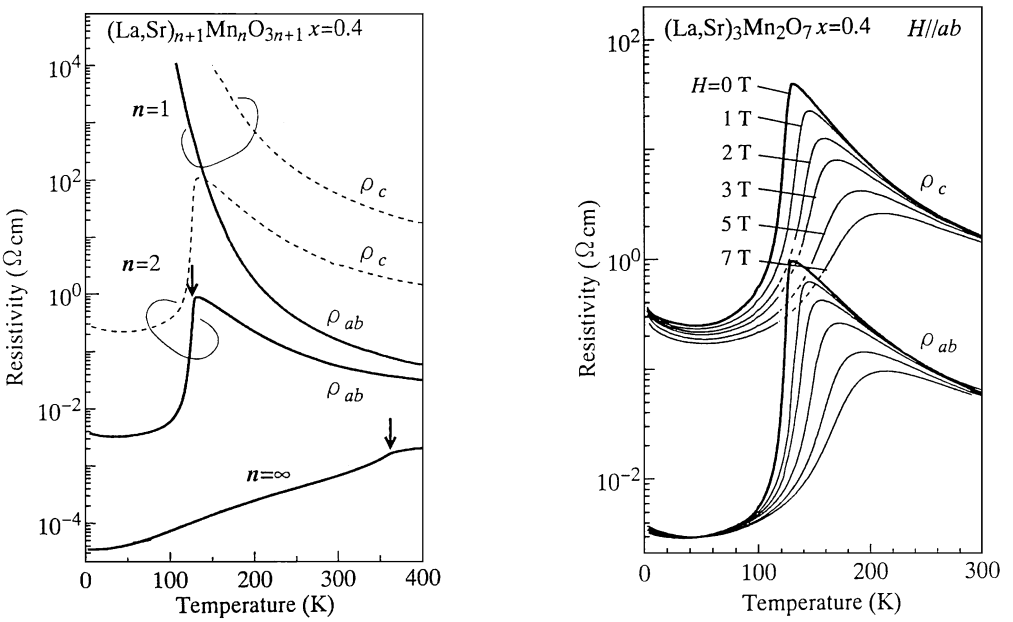

Fig. 2.5.2. Temperature dependence of the resistivity in the $n = 1$ (single layer), $n = 2$ (double layer) and $n = \infty$ (cubic) representatives of the Ruddlesden–Popper series of manganese oxides. The hole concentration is $x = 0.4$. Results along the layers and perpendicular to them are shown for $n = 1$ and 2. Reproduced from Moritomo et al. (1996).

Fig. 2.5.3. Temperature dependence of the resistivity for single crystals of the $n = 2$ compound at $x = 0.4$ (from Moritomo et al., 1996), with an external field parallel to the layer.

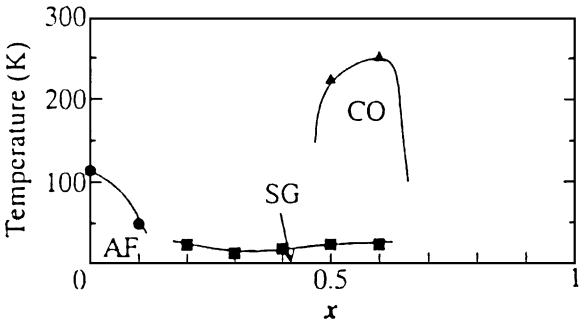

Fig. 2.6.1. Phase diagram corresponding to the single layer compound $La_{1-x}Sr_{1+x}MnO_4$. AF, SG, and CO stand for the antiferromagnetic, spin-glass, and charge-ordering phases, respectively. Solid lines are a guide to the eye. Reproduced from Moritomo et al. (1995).

fill the space in the cube centers and for this reason the oxygens tend to move toward that center, reducing $d_{A\text{–}O}$. In general $d_{Mn\text{–}O}$ also changes at the same time. For these reasons, the tolerance factor becomes less than unity, $\Gamma < 1$, as the A radius is reduced, and the Mn–O–Mn angle θ becomes smaller than 180°. The hopping amplitude for carriers to move from Mn to Mn naturally decreases as θ becomes smaller than 180° (remember that for a 90° bond the hopping

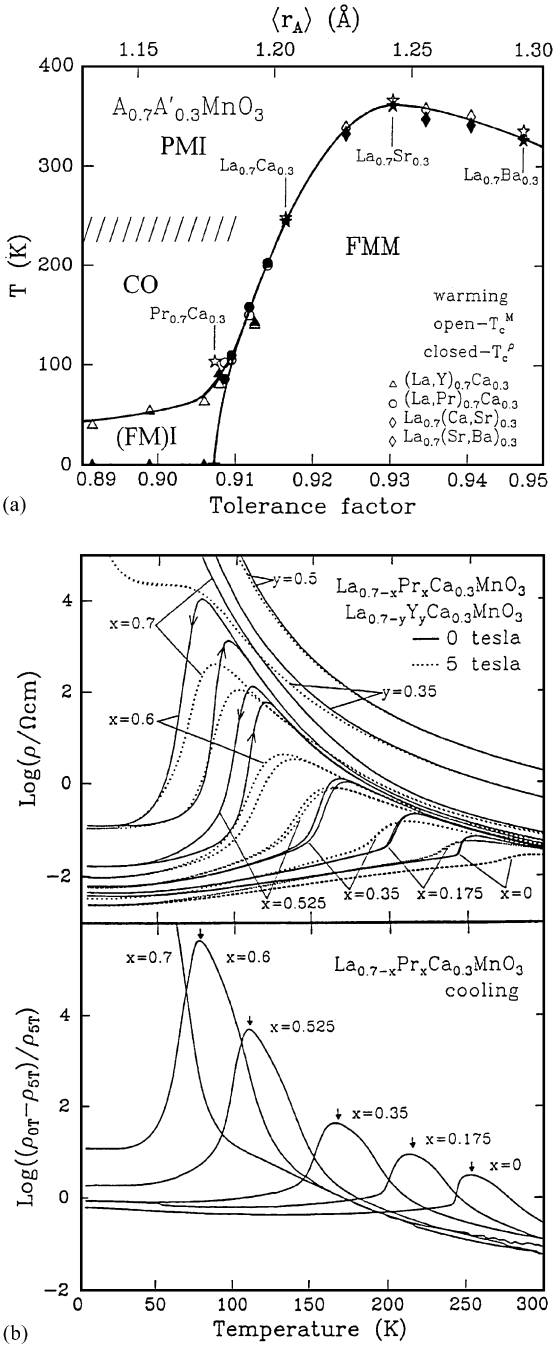

Fig. 2.7.1. (a) Phase diagram of temperature vs. tolerance factor for the system $A_{0.7}A'_{0.3}MnO_3$, where A is a trivalent rare earth ion and A′ is a divalent alkali earth ion. Open and closed symbols denote T_C measured from the magnetization and resistivity, respectively. For more details see Cheong and Hwang (1999), from where this figure is reproduced. A very similar figure appeared in Hwang et al. (1995a). (b) Top panel: $\log\rho(T)$ in 0 and 5 T for a series of samples of $La_{0.7-y}A'_yCa_{0.3}MnO_3$, with A′ mainly Pr but also Y. Bottom panel: MR factor. For details see Hwang et al. (1995a).

involving a *p*-orbital at the oxygen simply cancels, as explained in more detail below). As a consequence, as the tolerance factor decreases, the tendencies to charge localization increase due to the reduction in the mobility of the carriers. Since in the general chemical composition for perovskite manganites $A_{1-x}A'_xMnO_3$ there are two possible ions at the "A" site, then the tolerance factor for a given compound can be defined as a density-weighted average of the individual tolerance factors. In Fig. 2.4.3 the reader can find some of the ionic radius in Å, for some of the most important elements in the manganite composition.

Note that the distance Mn–Mn is actually reduced in the situation described so far ($\Gamma < 1$), while the tolerance factor (monotonically related with the hopping amplitude) is also reduced, which is somewhat counterintuitive since it would be expected that having closer Mn-ions would increase the electron hopping between them. However, the hopping amplitude is not only proportional to $1/(d_{Mn-O})^{\alpha}$, where $\alpha > 1$ (see Harrison, 1989) but also to $\cos\theta$ due to the fact that it is the *p*-orbital of oxygen that is involved in the process and if this orbital points toward one of the manganese ions, it cannot point toward the other one simultaneously for $\theta \neq 180^{\circ}$.

Hwang et al. (1995a) carried out a detailed study of the $A_{0.7}A'_{0.3}MnO_3$ compound for a variety of A and A′ ions. Fig. 2.7.1a summarizes this effort, and it shows the presence of three dominant regimes: a paramagnetic insulator at high-temperature, a low-temperature ferromagnetic metal at large tolerance factor, and a low-temperature charge-ordered ferromagnetic insulator at small tolerance factor. This figure clearly illustrates the drastic dependence with the tolerance factor of the properties of doped manganites. These same results will be discussed in more detail below in this review, when issues related with the presence of coexisting phases are addressed. In particular, experimental work have shown that the "FMI" regime may actually correspond to coexisting CO and FM large clusters. The CO-phase has both charge and orbital order.

An example upon which Fig. 2.7.1a has been constructed is shown in Fig. 2.7.1b that mainly corresponds to results obtained for $La_{0.7-x}Pr_xCa_{0.3}MnO_3$. The temperature dependence of $\rho_{dc}(T)$ presents hysteresis effects, suggesting that the PMI–FMM transition has some *first*-order characteristics, a feature that is of crucial importance in recent theoretical developments to be discussed later (Yunoki et al., 2000; Moreo et al., 2000). Note the huge MR ratios found in these compounds and the general trend that this ratio dramatically increases as T_C is reduced, mainly as a consequence of the rapid increase of the resistivity of the PM insulating state as the temperature is reduced. Certainly, the state above T_C is not a simple metal where ferromagnetic correlations slowly build up with decreasing temperature as in a second order transition, and as expected in the DE mechanism. A new theory is needed to explain these results.

3. Theory of manganites

3.1. Early studies

3.1.1. Double exchange

Most of the early theoretical work on manganites focused on the qualitative aspects of the experimentally discovered relation between transport and magnetic properties, namely the increase in conductivity upon the polarization of the spins. Not much work was devoted to the magnitude of the magnetoresistance effect itself. The formation of coexisting clusters of competing phases was

not included in the early considerations. The states of manganites were assumed to be uniform, and "double exchange" (DE) was proposed by Zener (1951b) as a way to allow for charge to move in manganites by the generation of a spin polarized state. The DE process has been historically explained in two somewhat different ways. Originally, Zener (1951b) considered the explicit movement of electrons schematically written (Cieplak, 1978) as $Mn^{3+}_{1\uparrow}O_{2\uparrow,3\downarrow}Mn^{4+} \rightarrow Mn^{4+}O_{1\uparrow,3\downarrow}Mn^{3+}_{2\uparrow}$ where 1, 2, and 3 label electrons that belong either to the oxygen between manganese, or to the e_g-level of the Mn-ions. In this process there are two *simultaneous* motions (thus the name double exchange) involving electron 2 moving from the oxygen to the right Mn-ion, and electron 1 from the left Mn-ion to the oxygen (see Fig. 3.1.1a). The second way to visualize DE processes was presented in detail by Anderson and Hasegawa (1955) and it involves a second-order process in which the two states described above go from one to the other using an intermediate state $Mn^{3+}_{1\uparrow}O_{3\downarrow}Mn^{3+}_{2\uparrow}$. In this context the effective hopping for the electron to move from one Mn-site to the next is proportional to the square of the hopping involving the *p*-oxygen and *d*-manganese orbitals (t_{pd}). In addition, if the localized spins are considered classical and with an angle θ between nearest-neighbor ones, the effective hopping becomes proportional to $\cos(\theta/2)$, as shown by Anderson and Hasegawa (1955). If $\theta = 0$ the hopping is the largest, while if $\theta = \pi$, corresponding to an antiferromagnetic background, then the hopping cancels. The quantum version of this process has been described by Kubo and Ohata (1972).

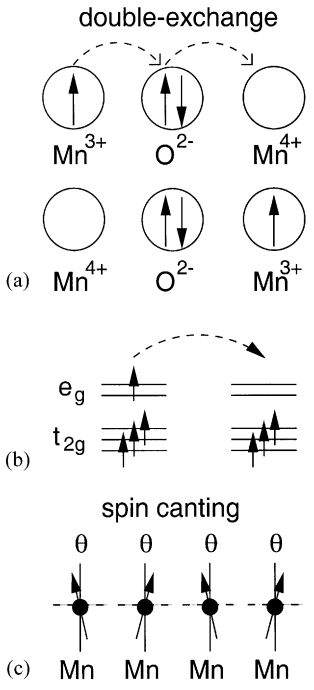

Fig. 3.1.1. (a) Sketch of the Double Exchange mechanism which involves two Mn ions and one O ion. (b) The mobility of e_g-electrons improves if the localized spins are polarized. (c) Spin-canted state which appears as the interpolation between FM and AF states in some mean-field approximations. For more details see the text.

Note that the oxygen linking the Mn-ions is crucial to understand the origin of the word "double" in this process. Nevertheless, the majority of the theoretical work carried out in the context of manganites simply forgets the presence of the oxygen and uses a manganese-only Hamiltonian. It is interesting to observe that ferromagnetic states appear in this context even *without* the oxygen. It is clear that the electrons simply need a polarized background to improve their kinetic energy, in similar ways as the Nagaoka phase is generated in the one-band Hubbard model at large U/t (for a high-T_c review, see Dagotto, 1994). This tendency to optimize the kinetic energy is at work in a variety of models and the term double exchange appears unnecessary. However, in spite of this fact it has become customary to refer to virtually any ferromagnetic phase found in manganese models as "DE induced" or "DE generated", forgetting the historical origin of the term. In this review a similar convention will be followed, namely the credit for the appearance of FM phases will be given to the DE mechanism, although a more general and simple kinetic-energy optimization is certainly at work.

3.1.2. Ferromagnetism due to a large Hund coupling

Regarding the stabilization of ferromagnetism, computer simulations (Yunoki et al., 1998a) and a variety of other approximations have clearly shown that models *without* the oxygen degrees of freedom (to be reviewed below) can also produce FM-phases, as long as the Hund coupling is large enough. In this situation, when the e_g electrons directly jump from Mn to Mn their kinetic energy is minimized if all spins are aligned (see Fig. 3.1.1b). As explained in the previous subsection, this procedure to obtain ferromagnetism is usually also called double-exchange and even the models from where it emerges are called double-exchange models. However, there is little resemble of these models and physical process with the original DE ideas (Zener, 1951b) where two electrons were involved in the actual hopping. Actually, the FM phases recently generated in computer simulations and a variety of mean-field approximations resemble more closely the predictions of another work of Zener (1951a), where indeed a large Hund coupling is invoked as the main reason for ferromagnetism in some compounds.

In addition, it has been questioned whether double-exchange or the large J_H mechanism are sufficient to indeed produce the ferromagnetic phase of manganites. An alternative idea (Zhao, 2000) relies on the fact that holes are located mostly in the oxygens due to the charge-transfer character of manganites and these holes are linked antiferromagnetically with the spins in the adjacent Mn-ions due to the standard exchange coupling, leading to an effective Mn–Mn ferromagnetic interaction. In this context the movement of holes would be improved if all Mn spins are aligned leading to a FM-phase, although many-body calculations are needed to prove that this is indeed the case for realistic couplings. A comment about this idea: in the context of the cuprates a similar concept was discussed time ago (for references see Dagotto, 1994) and after considerable discussion it was concluded that this process has to be contrasted against the so-called Zhang–Rice singlet formation where the spin of the hole at the oxygen couples in a singlet state with the spin at the Cu. As explained in Riera et al. (1997) the analogous process in manganites would lead to the formation of effective $S = 3/2$ "hole" states, between the $S = 2$ of manganese (3+) and the $S = 1/2$ of the oxygen hole. Thus, the competition between these two tendencies should be addressed in detail, similarly as done for the cuprates to clarify the proposal of Zhao (2000).

3.1.3. Spin-canted state

At this point it is useful to discuss the well-known proposed "spin-canted" state for manganites. Work by de Gennes (1960) using mean-field approximations suggested that the interpolation between the antiferromagnetic state of the undoped limit and the ferromagnetic state at finite hole density, where the DE mechanism works, occurs through a "canted state", similar as the state produced by a magnetic field acting over an antiferromagnet (Fig. 3.1.1c). In this state the spins develop a moment in one direction, while being mostly antiparallel within the plane perpendicular to that moment. The coexistence of FM and AF features in several experiments carried out at low hole doping (some of them reviewed below) led to the widely spread belief until recently that this spin-canted state was indeed found in real materials. However, a plethora of recent theoretical work (also discussed below) has shown that the canted state is actually *not* realized in the model of manganites studied by de Gennes (i.e., the simple one-orbital model). Instead phase separation occurs between the AF- and FM-states, as extensively reviewed below. Nevertheless, a spin-canted state is certainly still a possibility in real low-doped manganites but its origin, if their presence is confirmed, needs to be revised. It may occur that substantial Dzyaloshinskii–Moriya (DM) interactions appear in manganese oxides, but the authors are not aware of experimental papers confirming or denying their relevance, although some estimations (Solovyev et al., 1996; Lyanda-Geller et al., 1999; Chun et al., 1999a) appear to indicate that the DM couplings are small. However, even if the DM coupling were large there are still subtle issues to be addressed. For instance, it is widely believed that DM interactions lead to canting. However, Coffey et al. (1990) showed that in the simple case where the D_{ij} factor for the DM interaction is a constant, as in most early work on the subject, the DM term leads to a spiral state rather than a truly canted state. In addition, the authors of this review are not aware of reliable calculations showing that a canted state can indeed be stabilized in a model without terms added that break explicitly the invariance under rotations of the system in such a way that a given direction, along which the moment develops, is made by hand different from the others. For all these reasons and from the discussion below it may appear that the simplest way to explain the experimental data at low doping is to assume an AF–FM-phase coexistence instead of a canted state. However, the issue is still open and more experimental work should be devoted to its clarification.

3.1.4. Charge-ordered state at $x = 0.5$

Early theoretical work on manganites carried out by Goodenough (1955) (see also Goodenough, 1963) explained many of the features observed in the neutron scattering $La_{1-x}Ca_xMnO_3$ experiments by Wollan and Koehler (1955), notably the appearance of the A-type AF phase at $x = 0$ and the CE-type phase at $x = 0.5$. The approach of Goodenough (1955) was based on the notion of "semicovalent exchange" and the main idea can be roughly explained as follows. Suppose one considers a Mn–O bond directed, say, along the x-axis, and let us assume that the Mn-cation has an occupied orbital pointing along y or z instead of x (in other words, there is an empty orbital along x). The oxygen, being in a $(2-)$ state, will try to move towards this Mn site since it does not have a negative cloud of Mn electrons to fight against. This process shortens the distance Mn–O and makes this bond quite stable. This is a semicovalent bond. Suppose now the occupied Mn-orbital has an electron with an up spin. Of the two relevant electrons of oxygen, the one with spin up will feel the exchange force toward the Mn electron, i.e., if both electrons involved have the same spin, the space part of their common wave function has nodes which reduce the

electron–electron repulsion (as in the Hund's rules). Then, effectively the considered Mn–O bond becomes ferromagnetic between the Mn electron and one of the oxygen electrons.

Consider now the left-side O–Mn portion of the Mn–O–Mn bond. In the example under consideration, the second electron of oxygen must be down and it spends most of the time away from the left Mn-ion (rather than close to it as the oxygen spin-up electron does). If the Mn-ion on the right of the link Mn–O–Mn also has an occupied orbital pointing perpendicular to the x-axis, then O–Mn and Mn–O behave similarly (individually FM) but with pairs of spins pointing in opposite directions. As a consequence an effective *antiferromagnetic* Mn–Mn interaction has been generated (see Fig. 3.1.2a), and both Mn–O and O–Mn are shorten in length. However, if the right Mn has an electron in an orbital pointing along x, namely along the relevant p-orbital of the oxygen, the Hund-rule-like argument does not apply anymore since now a simple direct exchange is more important, leading to an AF O–Mn bond. In this case, the overall Mn–Mn interaction is *ferromagnetic*, as sketched in Fig. 3.1.2b. Then, simple arguments lead to the notion that both AF and FM couplings among the Mn-ions can be effectively generated, depending on the orientation of the orbitals involved.

Analyzing the various possibilities for the orbital directions and generalizing to the case where Mn^{4+} ions are also present, Goodenough (1955) arrived to the A- and CE-type phases of manganites very early in the theoretical study of these compounds (the shape of these states was shown in Fig. 2.2.4). In this line of reasoning, note that the Coulomb interactions are important to generate Hund-like rules and the oxygen is also important to produce the covalent bonds. The lattice distortions are also quite relevant in deciding which of the many possible states minimizes the energy. However, it is interesting to observe that in more recent theoretical work described below in this review, both the A- and CE-type phases can be generated *without* the explicit appearance of oxygens in the models and also without including long-range Coulombic terms.

Summarizing, there appears to be three mechanisms to produce effective FM interactions: (i) double exchange, where electrons are mobile, which is valid for noncharge-ordered states and where the oxygen plays a key role, (ii) Goodenough's approach where covalent bonds are

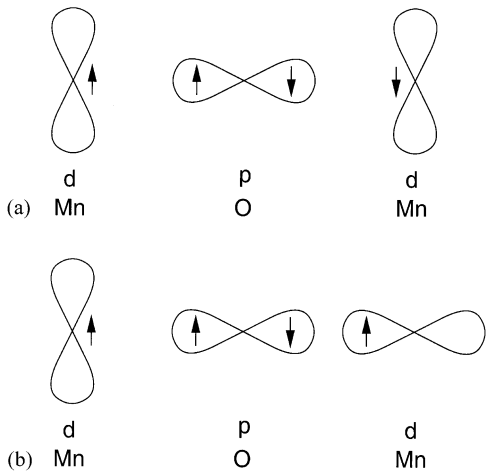

Fig. 3.1.2. Generation of antiferromagnetic (a) or ferromagnetic (b) effective interactions between the spins of Mn ions mediated by oxygen, depending on the orientation of the Mn orbitals. For details see text.

important (here the electrons do not have mobility in spite of the FM effective coupling), and it mainly applies to charge-ordered states, and (iii) the approach already described in this subsection based on purely Mn models (no oxygens) which leads to FM interactions mainly as a consequence of the large Hund coupling in the system. If phonons are introduced in the model it can be shown that the A- and CE-type states are generated, as reviewed later in this section. In the remaining theoretical part of the review most of the emphasis will be given to approach (iii) to induce FM bonds since a large number of experimental results can be reproduced by this procedure, but it is important to keep in mind the historical path followed in the understanding of manganites.

Based on all this discussion, it is clear that reasonable proposals to understand the stabilization of AF- and FM-phase in manganites have been around since the early theoretical studies of manganese oxides. However, these approaches (double exchange, ferromagnetic covalent bonds, and large Hund coupling) are still *not* sufficient to handle the very complex phase diagram of manganites. For instance, there are compounds such as $La_{1-x}Sr_xMnO_3$ that actually do not have the CE-phase at $x = 0.5$, while others do. There are compounds that are never metallic, while others have a paramagnetic state with standard metallic characteristics. And even more important, in the early studies of manganites there was no proper rationalization for the large MR effect. It is only with the use of state-of-the-art many-body tools that the large magnetotransport effects are starting to be understood, owing to theoretical developments in recent years that can address the competition among the different phases of manganites, their clustering and mixed-phase tendencies, and dynamical Jahn–Teller polaron formation.

3.2. More recent theories

The prevailing ideas to explain the curious magnetotransport behavior of manganites changed in the mid-1990s from the simple double-exchange scenario to a more elaborated picture where a large Jahn–Teller (JT) effect, which occurs in the Mn^{3+} ions, produces a strong electron–phonon coupling that persists even at densities where a ferromagnetic ground state is observed. In fact, in the undoped limit $x = 0$, and even at finite but small x, it is well known that a robust static structural distortion is present in the manganites (see Goodenough, 1955; Elemans et al., 1971). In this context it is natural to imagine the existence of small lattice polarons in the paramagnetic phase above T_C, and it was believed that these polarons lead to the insulating behavior of this regime. Actually, the term polaron (see Holstein, 1959) is somewhat ambiguous. In the context of manganites it is usually associated with a local distortion of the lattice around the charge, sometimes together with a magnetic cloud or region with ferromagnetic correlations (magneto polaron or lattice-magneto polaron).

3.2.1. Double-exchange is not enough

The fact that double exchange cannot be enough to understand the physics of manganites is clear from several different points of view. For instance, Millis et al. (1995) arrived at this conclusion by presenting estimations of the critical Curie temperature and of the resistivity using the DE framework. Regarding ferromagnetism, their calculations for a model having as an interaction only a large Hund coupling between e_g- and t_{2g}-electron led to a T_C prediction between 0.1 and 0.3 eV, namely of the order of the bare hopping amplitude and considerably higher than the experimental results. Thus, it was argued that DE produces the wrong T_C by a large factor. However, note that

computational work led to a much smaller estimation of the Curie temperature of the order of $0.1t$ for the double-exchange model (t is the e_g-electron hopping amplitude), and compatible with experiments (Yunoki et al., 1998a; Calderon and Brey, 1998; Yi et al., 1999a; Motome and Furukawa, 1999; Motome and Furukawa, 2000b; some of which will be reviewed in more detail later. Results for $S = 1/2$ localized spins can be found in Röder et al., 1997). For this reason arguments based on the value of T_C are *not* sufficient to exclude the double-exchange model. Regarding the resistance, using the memory function method (in principle valid at large frequency) to estimate the dc component, Millis et al. (1995) found a resistivity that grows with reducing temperature (insulating behavior) even below T_C. For this reason Millis et al. (1995) concluded that the model based only on a large J_H is not adequate for the manganites, and instead the relevance of the Jahn–Teller phonons was invoked. These results have to be contrasted with computer-based calculations of the resistivity for the one-orbital model at $J_H = \infty$ by Calderon et al. (1999) that reported instead a metallic behavior for the double-exchange model, actually both above and below T_C. Paradoxically, this behavior also leads to the same conclusion, namely that double exchange is not sufficient to explain the manganite behavior of, e.g., $La_{1-x}Ca_xMnO_3$ which has insulating characteristics above T_C but it is metallic below. However, both lines of attack to the DE model may need further revision, since the computational work of Yunoki et al. (1998a) at a large but not infinite Hund coupling has established that the simple one-orbital double-exchange model has regions with mixed-phase tendencies presenting an insulating resistivity (Moreo et al., 1999a) at and near $n = 1$ (n is the e_g electron number per site), which becomes metallic as the electronic density is further reduced. The existence of a metal–insulator transition in this model opens the possibility that the one-orbital system may still present physics *qualitatively* similar to that found experimentally, where such a transition is crucial in manganites. For this reason, using the one-orbital model as a toy model for manganites is still quite acceptable, as long as the region of study is close to the metal–insulator regime. In fact, recent work reporting percolative effects in this context use both the one- and two-orbital models with or without a strong JT coupling (Moreo et al., 2000). However, it is clear that the one-orbital model is incomplete for quantitative studies since it cannot describe, e.g., the key orbital ordering of manganites and the proper charge-order states at x near 0.5, which are so important for the truly CMR effect found in low-bandwidth manganites. Then, the authors of this review fully agree with the conclusions of Millis et al. (1995), although the arguments leading to such conclusion are different. It is clear that not even a fully disordered set of classical spins can scatter electrons as much as needed to reproduce the experiments (again, unless large antiferromagnetic regions appear in a mixed-phase regime).

3.2.2. Jahn–Teller phonons and polarons

Millis et al. (1996) (see also Millis et al., 1996a; Millis, 1998) argued that the physics of manganites is dominated by the interplay between a strong electron–phonon coupling and the large Hund coupling effect that optimizes the electronic kinetic energy by the generation of a FM-phase. The large value of the electron–phonon coupling is clear in the regime of manganites below $x = 0.20$ where a static JT distortion plays a key role in the physics of the material. Millis et al. (1996b) argued that a dynamical JT effect may persist at higher hole densities, without leading to long-range order but producing important fluctuations that localize electrons by splitting the degenerate e_g levels at a given MnO_6 octahedron. The calculations were carried out using the infinite-dimensional approximation that corresponds to a *local* mean-field technique where the

polarons can have only a one site extension, and the classical limit for the phonons and spins was used. The latter approximation is not expected to be severe unless the temperatures are very low (for a discussion see Millis et al., 1996b). The Coulomb interactions were neglected, but further work reviewed below showed that JT and Coulombic interactions lead to very similar results (Hotta et al., 2000c), and, as a consequence, this approximation is not severe either. Orbital or charge ordering were not considered in the formalism of Millis et al. (1996). Following the work of Millis et al. (1995), phonons were also argued to be of much importance in manganites by Röder et al. (1996), who found a tendency toward the formation of polarons in a single-orbital DE model with quantum phonons, treating the localized spins in the mean-field approximation and the polaron formation with the Lang–Firsov variational approximation. Coulomb interactions were later incorporated using the Gutzwiller approximation (Zang et al., 1996).

Millis et al. (1996) argued that the ratio $\lambda_{\rm eff} = E_{\rm JT}/t_{\rm eff}$ dominates the physics of the problem. Here $E_{\rm JT}$ is the static trapping energy at a given octahedron, and $t_{\rm eff}$ is an effective hopping that is temperature dependent following the standard DE discussion. In this context it was conjectured that when the temperature is larger than $T_{\rm C}$ the effective coupling $\lambda_{\rm eff}$ could be above the critical value that leads to insulating behavior due to electron localization, while it becomes smaller than the critical value below $T_{\rm C}$, thus inducing metallic behavior. The calculations were carried out using classical phonons and t_{2g} spins. The results of Millis et al. (1996) for $T_{\rm C}$ and the resistivity at a fixed density $n = 1$ when plotted as a function of $\lambda_{\rm eff}$ had formal similarities with experimental results (which are produced as a function of density). In particular, if $\lambda_{\rm eff}$ is tuned to be very close to the metal–insulator transition, the resistivity naturally strongly depends on even small external magnetic fields. However, in order to describe the percolative nature of the transition found experimentally and the notorious phase separation tendencies, calculations beyond mean-field approximations are needed, as reviewed later in this paper.

The existence of a critical value of the electron–phonon coupling constant λ of order unity at $n = 1$ leading to a metal–insulator transition is natural and it was also obtained in Monte Carlo (MC) simulations by Yunoki et al. (1998b). However, computational studies of the conductivity led to either insulating or metallic behavior at all temperatures, for values of λ above or below the critical temperature, respectively. A mixture of metal/insulator behavior in the resistivity at a fixed λ was not observed at $n = 1$.

3.3. Models and parameters

In the previous subsections, the theoretical work on manganites has been reviewed mainly in a historical order. In this section, the first steps toward a description of the latest theoretical developments in this context are taken. First, it is important to clearly write down the model Hamiltonian for manganites. For complex material such as the Mn-oxides, unfortunately, the full Hamiltonian includes several competing tendencies and couplings. However, as shown below, the essential physics can be obtained using relatively simple models, deduced from the complicated full Hamiltonian.

3.3.1. Effect of crystal field

In order to construct the model Hamiltonian for manganites, let us start our discussion at the level of the atomic problem, in which just one electron occupies a certain orbital in the 3*d* shell of

a manganese ion. Although for an isolated ion a five-fold degeneracy exists for the occupation of the 3*d*-orbitals, this degeneracy is partially lifted by the crystal field due to the six oxygen ions surrounding the manganese forming an octahedron. This is analyzed by the ligand field theory that shows that the five-fold degeneracy is lifted into doubly degenerate e_g-orbitals ($d_{x^2-y^2}$ and $d_{3z^2-r^2}$) and triply degenerate t_{2g}-orbitals (d_{xy}, d_{yz}, and d_{zx}). The energy difference between those two levels is usually expressed as 10 Dq, by following the traditional notation in the ligand field theory (see, for instance, Gerloch and Slade, 1973).

Here note that the energy level for the t_{2g}-orbitals is lower than that for e_g-orbitals. Qualitatively, this can be understood as follows: The energy difference originates in the Coulomb interaction between the 3*d* electrons and the oxygen ions surrounding manganese. While the wave functions of the e_g-orbitals is extended along the direction of the bond between manganese and oxygen ions, those in the t_{2g}-orbitals avoid this direction. Thus, an electron in t_{2g}-orbitals is not heavily influenced by the Coulomb repulsion due to the negatively charged oxygen ions, and the energy level for t_{2g}-orbitals is lower than that for e_g-orbitals.

As for the value of 10 Dq, it is explicitly written as (see Gerloch and Slade, 1973)

$$10\ \mathrm{Dq} = \frac{5}{3}\frac{Ze^2}{a}\frac{\langle r^4\rangle}{a^4}\ , \tag{1}$$

where Z is the atomic number of the ligand ion, e is the electron charge, a is the distance between manganese and oxygen ions, r is the coordinate of the 3*d*-orbital, and $\langle\cdots\rangle$ denotes the average value by using the radial wave function of the 3*d*-orbital. Estimations by Yoshida (1998, p. 29) suggest that 10 Dq is about 10,000–15,000 cm^{-1} (remember that 1 eV = 8063 cm^{-1}).

3.3.2. Coulomb interactions

Consider now a Mn^{4+} ion, in which three electrons exist in the 3*d* shells. Although those electrons will occupy t_{2g}-orbitals due to the crystalline field splitting, the configuration is not uniquely determined. To configure three electrons appropriately, it is necessary to take into account the effect of the Coulomb interactions. In the localized ion system, the Coulomb interaction term among *d*-electrons is generally given by

$$H_i^{\mathrm{C}} = (1/2)\sum_{\gamma_1\gamma_2\gamma_1'\gamma_2'}\sum_{\sigma_1\sigma_2\sigma_1'\sigma_2'}\langle\gamma_1\sigma_1,\gamma_2\sigma_2\|\gamma_1'\sigma_1',\gamma_2'\sigma_2'\rangle\, d^{\dagger}_{i\gamma_1\sigma_1}d^{\dagger}_{i\gamma_2\sigma_2}d_{i\gamma_2'\sigma_2'}d_{i\gamma_1'\sigma_1'}\ , \tag{2}$$

where $d_{i\gamma\sigma}$ is the annihilation operator for a *d*-electron with spin σ in the γ-orbital at site $\boldsymbol{i}$, and the Coulomb matrix element is given by

$$\langle\gamma_1\sigma_1,\gamma_2\sigma_2\|\gamma_1'\sigma_1',\gamma_2'\sigma_2'\rangle = \iint \mathrm{d}\boldsymbol{r}\,\mathrm{d}\boldsymbol{r}'\phi^*_{\gamma_1\sigma_1}(\boldsymbol{r})\phi^*_{\gamma_2\sigma_2}(\boldsymbol{r}')g_{r-r'}\phi_{\gamma_1'\sigma_1'}(\boldsymbol{r})\phi_{\gamma_2'\sigma_2'}(\boldsymbol{r}')\ . \tag{3}$$

Here $g_{r-r'}$ is the screened Coulomb potential, and $\phi_{\gamma\sigma}(\boldsymbol{r})$ is the Wannier function for an electron with spin σ in the γ-orbital at position $\boldsymbol{r}$. By using the Coulomb matrix element, the so-called "Kanamori parameters", U, U', J, and J', are defined as follows (see Kanamori, 1963; Dworin and Narath, 1970; Castellani et al., 1978). U is the intraband Coulomb interaction, given by

$$U = \langle\gamma\sigma,\gamma\sigma'\|\gamma\sigma,\gamma\sigma'\rangle \tag{4}$$

with $\sigma \neq \sigma'$. U' is the interband Coulomb interaction, expressed by

$$U' = \langle \gamma\sigma, \gamma'\sigma' || \gamma\sigma, \gamma'\sigma' \rangle \tag{5}$$

with $\gamma \neq \gamma'$. J is the interband exchange interaction, written as

$$J = \langle \gamma\sigma, \gamma'\sigma' || \gamma'\sigma, \gamma\sigma' \rangle \tag{6}$$

with $\gamma \neq \gamma'$. Finally, J' is the pair-hopping amplitude between different orbitals, given by

$$J' = \langle \gamma\sigma, \gamma\sigma' || \gamma'\sigma, \gamma'\sigma' \rangle \tag{7}$$

with $\gamma \neq \gamma'$ and $\sigma \neq \sigma'$.

Note the relation $J = J'$, which is simply due to the fact that each of the parameters above is given by an integral of the Coulomb interaction sandwiched with appropriate orbital wave functions. Analyzing the form of those integrals the equality between J and J' can be deduced [see equation Eq. (2.6) of Castellani et al. (1978); See also the appendix of Frésard and Kotliar (1997)].

Using the above parameters, it is convenient to rewrite the Coulomb interaction term in the following form:

$$\begin{aligned} H_i^{\mathrm{C}} = {} & (U/2) \sum_{\gamma,\sigma \neq \sigma'} n_{i\gamma\sigma} n_{i\gamma\sigma'} + (U'/2) \sum_{\sigma,\sigma',\gamma \neq \gamma'} n_{i\gamma\sigma} n_{i\gamma'\sigma'} \\ & + (J/2) \sum_{\sigma,\sigma',\gamma \neq \gamma'} d^{\dagger}_{i\gamma\sigma} d^{\dagger}_{i\gamma'\sigma'} d_{i\gamma\sigma'} d_{i\gamma'\sigma} + (J'/2) \sum_{\sigma \neq \sigma',\gamma \neq \gamma'} d^{\dagger}_{i\gamma\sigma} d^{\dagger}_{i\gamma\sigma'} d_{i\gamma'\sigma'} d_{i\gamma'\sigma} \ , \end{aligned} \tag{8}$$

where $n_{i\gamma\sigma} = d^{\dagger}_{i\gamma\sigma} d_{i\gamma\sigma}$. Here it is important to clarify that the parameters U, U', and J in Eq. (8) are not independent (here $J = J'$ is used). The relation among them in the localized ion problem has been clarified by group theory arguments, showing that all the above Coulomb interactions can be expressed by the so-called "Racah parameters" A, B, and C (for more details, see Griffith, 1961. See also Tang et al., 1998). Here only the main results are summarized in Table 1, following Tang et al. (1998). Note that the values of U' and J depend on the combination of orbitals, namely they take different values depending on the orbitals used (Table 1), while $U = A + 4B + 3C$ is independent of the orbital choice. Thus, it is easily checked that the relation

$$U = U' + 2J \tag{9}$$

holds in any combination of orbitals.

Table 1
Expressions for U' and J by using Racah parameters A, B, and C. Note that $U = A + 4B + 3C$ for each orbital. For more information, see Tang et al. (1998)

γ	γ'	U'	J
xy, yz, zx	xy, yz, zx	$A - 2B + C$	$3B + C$
$x^2 - y^2$, $3z^2 - r^2$	$x^2 - y^2$, $3z^2 - r^2$	$A - 4B + C$	$4B + C$
xy	$x^2 - y^2$	$A + 4B + C$	C
xy	$3z^2 - r^2$	$A - 4B + C$	$4B + C$
yz, zx	$x^2 - y^2$	$A - 2B + C$	$3B + C$
yz, zx	$3z^2 - r^2$	$A + 2B + C$	$B + C$

Although Eq. (9) has been clearly shown to be valid using the Racah parameters, the discussions in the current literature regarding this issue are somewhat confusing, probably since the arguments usually rely directly on Hamiltonian Eq. (8), rather than Eqs. (2) and (3). Thus, it is instructive to discuss the above-mentioned relation among the several couplings using arguments directly based on the model (8), without using the Racah parameters. First note that even using $J = J'$, the electron–electron interaction is still not invariant under rotations in orbital space. This can be easily understood simply using two orbitals as an example, and two particles. In the absence of hopping terms, the problem involves just one site and it can be easily diagonalized, leading to four eigenenergies. The lowest one is $U' - J$, has degeneracy three, and it corresponds to a spin-triplet and orbital-singlet state. In order to verify that indeed this state is a singlet in orbital space, the operators

$$T_i^x = (1/2)\sum_\sigma (d_{ia\sigma}^\dagger d_{ib\sigma} + d_{ib\sigma}^\dagger d_{ia\sigma}) , \qquad T_i^y = -(i/2)\sum_\sigma (d_{ia\sigma}^\dagger d_{ib\sigma} - d_{ib\sigma}^\dagger d_{ia\sigma}) ,$$
$$T_i^z = (1/2)\sum_\sigma (d_{ia\sigma}^\dagger d_{ia\sigma} - d_{ib\sigma}^\dagger d_{ib\sigma}) \tag{10}$$

are needed. The next state is nondegenerate, it has energy $U' + J$ and it is a spin singlet. Regarding the orbital component, it corresponds to the $T_i^z = 0$ part of an orbital triplet. This result already suggests us that orbital invariance is not respected in the system unless restrictions are imposed on the couplings, since a state of an orbital triplet is energetically separated from another state of the same triplet. The next two states have energies $U + J'$ and $U - J'$, each is nondegenerate and spin singlet, and they are combinations of orbital triplets with $T_i^z = +1$ and -1. Note that the state characterized by $U + J'$ is invariant under rotations in orbital space (using a real rotation matrix parametrized by only one angle), while the other one with $U - J'$ is not. Then, it is clear now how to proceed to restore rotational invariance. It should be demanded that $U - J' = U' + J$, namely, $U = U' + J + J'$ (see, for instance, Kuei and Scalettar, 1997). In addition, following Castellani et al. (1978), it is known that $J = J'$, as already discussed. Then, Eq. (9) is again obtained as a condition for the rotational invariance in orbital space. It should be noted that spin rotational invariance does not impose any constraints on the parameters. Also it should be noted that the orbital rotational invariance achieved here is not a full SU (2) one, but a subgroup, similarly as it occurs in the anisotropic Heisenberg model that has invariance under rotation in the xy plane only. For this reason the states are either singlets or doublets, but not triplets, in orbital space.

For the case of three orbitals, a similar study can be carried out, although it is more tedious. For two particles, the energy levels now are at $U' - J$ (degeneracy nine, spin triplet and orbital triplet), $U' + J$ (degeneracy three, spin singlet, contains parts of an orbital quintuplet), $U - J'$ (degeneracy two, spin singlet, contains portions of an orbital quintuplet), and $U + 2J'$ (nondegenerate, spin singlet and orbital singlet). In order to have the proper orbital multiplets that are characteristic of a rotational orbital invariant system, it is necessary to require that $U' + J = U - J'$. If the relation $J = J'$ is further used, then the condition again becomes $U = U' + 2J$. A better proof of this condition can be carried out by rewriting the H amiltonian in terms of spin and orbital rotational invariant operators such as $N_i = \sum_{\gamma,\sigma} n_{i\gamma\sigma}$, $\boldsymbol{S}_i^2 = \sum_{\gamma,\gamma'} \boldsymbol{S}_{i\gamma} \cdot \boldsymbol{S}_{i\gamma'}$, and $\boldsymbol{L}_i^2 = \sum_{\sigma,\sigma'} \boldsymbol{L}_{i\sigma} \cdot \boldsymbol{L}_{i\sigma'}$, where $\boldsymbol{S}_i$ and $\boldsymbol{L}_i$ are the spin and orbital operators, respectively. By this somewhat tedious procedure, a final expression is reached in which only one term is not in the form of explicitly invariant operators. To cancel that term, the condition mentioned above is needed.

Now let us move to the discussion of the configuration of three electrons for the Mn^{4+} ion. Since the largest energy scale among the several Coulombic interactions is U, the orbitals are not doubly occupied by both up- and down-spin electrons. Thus, only one electron can exist in each orbital of the triply degenerate t_{2g} sector. Furthermore, in order to take advantage of J, the spins of those three electrons point along the same direction. This is the so-called "Hund's rule".

By adding one more electron to Mn^{4+} with three up-spin t_{2g}-electrons, let us consider the configuration for the Mn^{3+} ion. Note here that there are two possibilities due to the balance between the crystalline-field splitting and the Hund coupling: One is the "high-spin state" in which an electron occupies the e_g-orbital with up spin if the Hund coupling is dominant. In this case, the energy level appears at $U' - J + 10$ Dq. Another is the "low-spin state" in which one of the t_{2g}-orbitals is occupied with a down-spin electron, when the crystalline-field splitting is much larger than the Hund coupling. In this case, the energy level occurs at $U + 2J$. Thus, the high-spin state appears if $10\ \mathrm{Dq} < 5J$ holds. Since J is a few eV and 10 Dq is about 1 eV in the manganese oxide, the inequality $10\ \mathrm{Dq} < 5J$ is considered to hold. Namely, in the Mn^{3+} ion, the high-spin state is realized.

In order to simplify the model without loss of essential physics, it is reasonable to treat the three spin-polarized t_{2g}-electrons as a localized "core-spin" expressed by $\boldsymbol{S}_i$ at site $\boldsymbol{i}$, since the overlap integral between t_{2g} and oxygen $p\sigma$ orbital is small compared to that between e_g and $p\sigma$ orbitals. Moreover, due to the large value of the total spin $S = 3/2$, it is usually approximated by a classical spin (this approximation will be tested later using computational techniques). Thus, the effect of the strong Hund coupling between the e_g-electron spin and localized t_{2g}-spins is considered by introducing

$$H_{\mathrm{Hund}} = -J_{\mathrm{H}} \sum_{i} \boldsymbol{s}_i \cdot \boldsymbol{S}_j \ , \tag{11}$$

where $\boldsymbol{s}_i = \sum_{\gamma\alpha\beta} d^{\dagger}_{i\gamma\alpha} \sigma_{\alpha\beta} d_{i\gamma\beta}$, $J_{\mathrm{H}}(>0)$ is the Hund coupling between localized t_{2g}-spin and mobile e_g-electron, and $\sigma = (\sigma_x, \sigma_y, \sigma_z)$ are the Pauli matrices. The magnitude of J_{H} is of the order of J. Here note that $\boldsymbol{S}_i$ is normalized as $|\boldsymbol{S}_i| = 1$. Thus, the direction of the classical t_{2g}-spin at site $\boldsymbol{i}$ is defined as

$$\boldsymbol{S}_i = (\sin\theta_i \cos\phi_i, \sin\theta_i \sin\phi_i, \cos\theta_i), \tag{12}$$

by using the polar angle θ_i and the azimuthal angle ϕ_i.

Unfortunately, the effect of the Coulomb interaction is not fully taken into account only by H_{Hund} since there remains the direct electrostatic repulsion between e_g-electrons, which will be referred to as the "Coulomb interaction" hereafter. Then, the following term should be added to the Hamiltonian

$$H_{\mathrm{el\text{-}el}} = \sum_{i} H_i^{\mathrm{C}} + V \sum_{\langle i,j \rangle} \rho_i \rho_j \ , \tag{13}$$

where $\rho_i = \sum_{\gamma\sigma} n_{i\gamma\sigma}$. Note here that in this expression, the index γ for the orbital degree of freedom runs only in the e_g-sector. Note also that in order to consider the effect of the long-range Coulomb repulsion between e_g-electrons, the term including V is added, where V is the nearest-neighbor Coulomb interaction.

3.3.3. Electron–phonon coupling

Another important ingredient in manganites is the lattice distortion coupled to the e_g-electrons. In particular, the double degeneracy in the e_g-orbitals is lifted by the Jahn–Teller distortion of the

MnO_6 octahedron (Jahn and Teller, 1937). The basic formalism for the study of electrons coupled to Jahn–Teller modes has been set up by Kanamori (1960). He focused on cases where the electronic orbitals are degenerate in the undistorted crystal structure, as in the case of Mn in an octahedron of oxygens. As explained by Kanamori (1960), the Jahn–Teller effect (Jahn and Teller, 1937) in this context can be simply stated as follows: when a given electronic level of a cluster is degenerate in a structure of high symmetry, this structure is generally unstable, and the cluster will present a distortion toward a lower symmetry ionic arrangement. In the case of Mn^{3+}, which is doubly degenerate when the crystal is undistorted, a splitting will occur when the crystal is distorted. The distortion of the MnO_6 octahedron is "cooperative" since once it occurs in a particular octahedron, it will affect the neighbors. The basic Hamiltonian to describe the interaction between electrons and Jahn–Teller modes was written by Kanamori (1960) and it is of the form

$$H_i^{\mathrm{JT}} = 2g(Q_{2i}T_i^x + Q_{3i}T_i^z) + (k_{\mathrm{JT}}/2)(Q_{2i}^2 + Q_{3i}^2)\,, \tag{14}$$

where g is the coupling constant between the e_g-electrons and distortions of the MnO_6 octahedron, Q_{2i} and Q_{3i} are normal modes of vibration of the oxygen octahedron that remove the degeneracy between the electronic levels, and k_{JT} is the spring constant for the Jahn–Teller mode distortions. In the expression of H_i^{JT}, a T_i^y-term does not appear for symmetry reasons, since it belongs to the A_{2u} representation. The nonzero terms should correspond to the irreducible representations included in $E_g \times E_g$, namely, E_g and A_{1g}. The former representation is expressed by using the pseudo-spin operators T_i^x and T_i^z as discussed here, while the latter, corresponding to the breathing mode, is discussed later in this subsection. For more details the reader should consult Yoshida (1998, p. 40) and the book in preparation by one of the authors (E.D.).

Following Kanamori, Q_{2i} and Q_{3i} are explicitly given by

$$Q_{2i} = \frac{1}{\sqrt{2}}(X_{1i} - X_{4i} - Y_{2i} + Y_{5i}) \tag{15}$$

and

$$Q_{3i} = \frac{1}{\sqrt{6}}(2Z_{3i} - 2Z_{6i} - X_{1i} + X_{4i} - Y_{2i} + Y_{5i})\,, \tag{16}$$

where $X_{\mu j}$, $Y_{\mu j}$, and $Z_{\mu j}$ are the displacement of oxygen ions from the equilibrium positions along the x- , y- , and z-direction, respectively. The convention for the labeling μ of coordinates is shown in Fig. 3.3.1. To solve this Hamiltonian, it is convenient to scale the phononic degrees of freedom as

$$Q_{2i} = (g/k_{\mathrm{JT}})q_{2i}, \quad Q_{3i} = (g/k_{\mathrm{JT}})q_{3i}\,, \tag{17}$$

where g/k_{JT} is the typical energy scale for the Jahn–Teller distortion, which is of the order of 0.1 Å, namely, 2.5% of the lattice constant. When the JT distortion is expressed in the polar coordinate as

$$q_{2i} = q_i \sin\xi_i, \quad q_{3i} = q_i \cos\xi_i\,, \tag{18}$$

the ground state is easily obtained as $(-\sin[\xi_i/2]d_{ia\sigma}^{\dagger} + \cos[\xi_i/2]d_{ib\sigma}^{\dagger})|0\rangle$ with the use of the phase ξ_i. The corresponding eigenenergy is given by $-E_{\mathrm{JT}}$, where E_{JT} is the static Jahn–Teller energy, defined by

$$E_{\mathrm{JT}} = g^2/(2k_{\mathrm{JT}})\,. \tag{19}$$

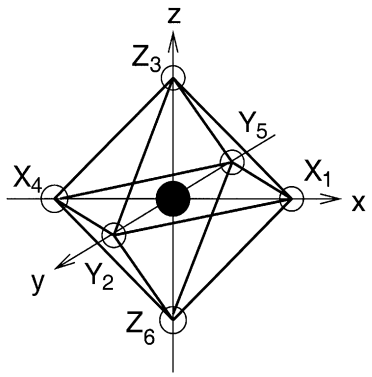

Fig. 3.3.1. MnO_6 octahedron at site ***i***. The labeling for oxygen ions is shown.

Note that the ground state energy is independent of the phase ξ_i. Namely, the shape of the deformed isolated octahedron is not uniquely determined in this discussion. In the Jahn–Teller crystal, the kinetic motion of e_g electrons, as well as the cooperative effect between adjacent distortions, play a crucial role in lifting the degeneracy and fixing the shape of the local distortion. This point will be discussed later in detail.

To complete the electron–phonon coupling term, it is necessary to consider the breathing-mode distortion, coupled to the local electron density as

$$H_i^{\mathrm{br}} = gQ_{1i}\rho_i + (1/2)k_{\mathrm{br}}Q_{1i}^2 \,, \tag{20}$$

where the breathing-mode distortion Q_{1i} is given by

$$Q_{1i} = \frac{1}{\sqrt{3}}(X_{1i} - X_{4i} + Y_{2i} - Y_{5i} + Z_{3i} - Z_{6i}) \tag{21}$$

and k_{br} is the associated spring constant. Note that, in principle, the coupling constants of the e_g electrons with the Q_1, Q_2, and Q_3 modes could be different from one another. For simplicity, here it is assumed that those coupling constants take the same value. On the other hand, for the spring constants, a different notation for the breathing mode is introduced, since the frequency for the breathing-mode distortion has been found experimentally to be different from that for the Jahn–Teller mode. This point will be briefly discussed later. Note also that the Jahn–Teller and breathing modes are competing with each other. As it was shown above, the energy gain due to the Jahn–Teller distortion is maximized when one electron exists per site. On the other hand, the breathing-mode distortion energy is proportional to the total number of e_g electrons per site, since this distortion gives rise to an effective on-site attraction between electrons.

By combining the JT mode and breathing-mode distortions, the electron–phonon term is summarized as

$$H_{\mathrm{el-ph}} = \sum_i (H_i^{\mathrm{JT}} + H_i^{\mathrm{br}}) \,. \tag{22}$$

This expression depends on the parameter $\beta = k_{\mathrm{br}}/k_{\mathrm{JT}}$, which regulates which distortion, the Jahn–Teller or breathing mode, play a more important role. This point will be discussed in a separate subsection.

Note again that the distortions at each site are not independent, since all oxygens are shared by neighboring MnO_6 octahedra, as easily understood by the explicit expressions of Q_{1i}, Q_{2i}, and Q_{3i} presented before. A direct and simple way to consider this cooperative effect is to determine the oxygen positions X_{1i}, X_{4i}, Y_{2i}, Y_{5i}, Z_{3i}, and Z_{6i}, by using, for instance, the Monte Carlo simulations or numerical relaxation methods (see Press et al., 1986, Chapter 10). To reduce the burden on the numerical calculations, the displacements of oxygen ions are assumed to be along the bond direction between nearest-neighboring manganese ions. In other words, the displacement of the oxygen ion perpendicular to the Mn–Mn bond, i.e., the buckling mode, is usually ignored. As shown later, even in this simplified treatment, several interesting results have been obtained for the spin, charge, and orbital ordering in manganites.

Rewriting Eqs. (15), (16), and (21) in terms of the displacement of oxygens from the equilibrium positions, it can be shown that

$$Q_{1i} = Q_1^{(0)} + \frac{1}{\sqrt{3}}(\Delta_{xi} + \Delta_{yi} + \Delta_{zi}) , \tag{23}$$

$$Q_{2i} = Q_2^{(0)} + \frac{1}{\sqrt{2}}(\Delta_{xi} - \Delta_{yi}) , \tag{24}$$

$$Q_{3i} = Q_3^{(0)} + \frac{1}{\sqrt{6}}(2\Delta_{zi} - \Delta_{xi} - \Delta_{yi}) , \tag{25}$$

where Δ_{ai} is given by

$$\Delta_{ai} = u_i^a - u_{i-a}^a \tag{26}$$

with u_i^a being the displacement of oxygen ion at site $\boldsymbol{i}$ from the equilibrium position along the $\boldsymbol{a}$-axis. The offset values for the distortions, $Q_1^{(0)}$, $Q_2^{(0)}$, and $Q_3^{(0)}$, are respectively given by

$$Q_1^{(0)} = \frac{1}{\sqrt{3}}(\delta L_x + \delta L_y + \delta L_z) , \tag{27}$$

$$Q_2^{(0)} = \frac{1}{\sqrt{2}}(\delta L_x - \delta L_y) , \tag{28}$$

$$Q_3^{(0)} = \frac{1}{\sqrt{6}}(2\delta L_z - \delta L_x - \delta L_y) , \tag{29}$$

where $\delta L_a = L_a - L$, the nondistorted lattice constants are L_a, and $L = (L_x + L_y + L_z)/3$. In the *cooperative* treatment, the $\{u\}$'s are directly optimized in the numerical calculations (see Allen and Perebeinos, 1999a; Hotta et al. 1999). On the other hand, in the *noncooperative* calculations, $\{Q\}$'s are treated instead of the $\{u\}$'s. The similarities and differences between those two treatments will be discussed later for some particular cases.

3.3.4. Hopping amplitudes

Although the t_{2g}-electrons are assumed to be localized, the e_g-electrons can move around the system via the oxygen $2p$ orbital.

This hopping motion of e_g-electrons is expressed as

$$H_{\rm kin} = -\sum_{ia\gamma\gamma'\sigma} t^{a}_{\gamma\gamma'} d^{\dagger}_{i\gamma\sigma} d_{i+a\gamma'\sigma} \ , \tag{30}$$

where $\boldsymbol{a}$ is the vector connecting nearest-neighbor sites and $t^{a}_{\gamma\gamma'}$ is the nearest-neighbor hopping amplitude between γ- and γ'-orbitals along the $\boldsymbol{a}$-direction.

The amplitudes are evaluated from the overlap integral between manganese and oxygen ions by following Slater and Koster (1954). The overlap integral between $d_{x^2-y^2}$- and p_x-orbitals is given by

$$E_{x,\rm a}(\ell,m,n) = (\sqrt{3}/2)\,\ell(\ell^2 - m^2)(pd\sigma) \ , \tag{31}$$

where $(pd\sigma)$ is the overlap integral between the $d\sigma$- and $p\sigma$-orbital and (ℓ,m,n) is the unit vector along the direction from manganese to oxygen ions. The overlap integral between $d_{3z^2-r^2}$- and p_x-orbitals is expressed as

$$E_{x,\rm b}(\ell,m,n) = \ell[n^2 - (\ell^2 + m^2)/2]\,(pd\sigma) \ . \tag{32}$$

Thus, the hopping amplitude between adjacent manganese ions along the x-axis via the oxygen $2p_x$-orbitals is evaluated as

$$-t^{x}_{\gamma\gamma'} = E_{x,\gamma}(1,0,0) \times E_{x,\gamma'}(-1,0,0) \ . \tag{33}$$

Note here that the minus sign is due to the definition of hopping amplitude in $H_{\rm kin}$. Then, $t^{x}_{\gamma\gamma'}$ is explicitly given by

$$t^{x}_{\rm aa} = -\sqrt{3}t^{x}_{\rm ab} = -\sqrt{3}t^{x}_{\rm ba} = 3t^{x}_{\rm bb} = 3t_0/4 \ , \tag{34}$$

where t_0 is defined by $t_0 = (pd\sigma)^2$. By using the same procedure, the hopping amplitude along the y- and z-axis are given by

$$t^{y}_{\rm aa} = \sqrt{3}t^{y}_{\rm ab} = \sqrt{3}t^{y}_{\rm ba} = 3t^{y}_{\rm bb} = 3t_0/4 \tag{35}$$

and

$$t^{z}_{\rm bb} = t_0, \quad t^{z}_{\rm aa} = t^{z}_{\rm ab} = t^{z}_{\rm ba} = 0 \ , \tag{36}$$

respectively. It should be noted that the signs in the hopping amplitudes between different orbitals are different between the x- and y-direction, which will be important when the charge-orbital ordered phase in the doped manganites is considered. Note also that in some cases, it is convenient to define $t^{x}_{\rm aa}$ as the energy scale t, given as $t = 3t_0/4$.

3.3.5. Heisenberg term

Thus far, the role of the e_g-electrons has been discussed to characterize the manganites. However, in the fully hole-doped manganites composed of Mn^{4+} ions, for instance $CaMnO_3$, it is well known that a G-type antiferromagnetic phase appears, and this property cannot be understood within the above discussion. The minimal term to reproduce this antiferromagnetic property is the Heisenberg-like coupling between localized t_{2g}-spins, given in the form

$$H_{\rm AFM} = J_{\rm AF} \sum_{\langle i,j\rangle} \boldsymbol{S}_i \cdot \boldsymbol{S}_j \ , \tag{37}$$

where J_{AF} is the AFM coupling between nearest-neighbor t_{2g} spins. The existence of this term is quite natural from the viewpoint of the super-exchange interaction, working between neighboring localized t_{2g}-electrons. As for the magnitude of J_{AF}, it is discussed later in the text.

3.3.6. Full Hamiltonian

As discussed in the previous subsections, there are five important ingredients that regulate the physics of electrons in manganites: (i) H_{kin}, the kinetic term of the e_g-electrons. (ii) H_{Hund}, the Hund coupling between the e_g-electron spin and the localized t_{2g}-spin. (iii) H_{AFM}, the AFM Heisenberg coupling between nearest-neighbor t_{2g}-spins. (iv) H_{el-ph}, the coupling between the e_g-electrons and the local distortions of the MnO_6 octahedron. (v) H_{el-el}, the Coulomb interactions among the e_g-electrons. By unifying those five terms into one, the full Hamiltonian H is defined as

$$H = H_{kin} + H_{Hund} + H_{AFM} + H_{el-ph} + H_{el-el} \,. \tag{38}$$

This expression is believed to define an appropriate starting model for manganites, but, unfortunately, it is quite difficult to solve such a Hamiltonian. In order to investigate further the properties of manganites, some simplifications are needed.

3.3.7. Free e_g-electron model

The simplest model is obtained by retaining only the kinetic term. Although this is certainly an oversimplification for describing the complex nature of manganites, it can be a starting model to study the transport properties of these compounds, particularly in the ferromagnetic region in which the static Jahn–Teller distortion does not occur and the effect of the Coulomb interaction is simply renormalized into the quasi-particle formation. In fact, some qualitative features of manganites can be addressed in the band picture, as discussed by Shiba et al. (1997) and Gor'kov and Kresin (1998). The kinetic term is rewritten in momentum space as

$$H_0 = \sum_{\boldsymbol{k}\gamma\gamma'\sigma} \varepsilon_{\boldsymbol{k}\gamma\gamma'} d^{\dagger}_{\boldsymbol{k}\gamma\sigma} d_{\boldsymbol{k}\gamma'\sigma} \,, \tag{39}$$

where $d_{\boldsymbol{k}\gamma\sigma} = (1/N)\sum_i e^{i\boldsymbol{R}_i\cdot\boldsymbol{k}} d_{i\gamma\sigma}$, $\varepsilon_{\boldsymbol{k}aa} = -(3t_0/2)(C_x + C_y)$, $\varepsilon_{\boldsymbol{k}bb} = -(t_0/2)(C_x + C_y + 4C_z)$, and $\varepsilon_{\boldsymbol{k}ab} = \varepsilon_{\boldsymbol{k}ba} = (\sqrt{3}t_0/2)(C_x - C_y)$, with $C_\mu = \cos k_\mu$ ($\mu = x$, y, and z). After the diagonalization of $\varepsilon_{\boldsymbol{k}\gamma\gamma'}$, two bands are obtained as

$$E^{\pm}_{\boldsymbol{k}} = -t_0(C_x + C_y + C_z \pm \sqrt{C_x^2 + C_y^2 + C_z^2 - C_xC_y - C_yC_z - C_zC_x}) \,. \tag{40}$$

Note that the cubic symmetry can be seen clearly in $E^{\pm}_{\boldsymbol{k}}$, although the hopping amplitudes at first sight are quite anisotropic, due to the choice of a particular basis for the d-orbitals. Other basis certainly lead to the same result. Note also that the bandwidth W is given by $W = 6t_0$.

3.3.8. One-orbital model

A simple model for manganites to illustrate the CMR effect is obtained by neglecting the electron–phonon coupling and the Coulomb interactions. Usually, an extra simplification is carried out by neglecting the orbital degrees of freedom, leading to the FM Kondo model or one-orbital double-exchange model, which will be simply referred as the "one-orbital model"

hereafter, given as (Zener, 1951b; Furukawa, 1994)

$$H_{\rm DE} = -t \sum_{\langle i,j\rangle,\sigma} (a^{\dagger}_{i\sigma} a_{j\sigma} + \text{h.c.}) - J_{\rm H} \sum_{i} \boldsymbol{s}_i \cdot \boldsymbol{S}_j + J_{\rm AF} \sum_{\langle i,j\rangle} \boldsymbol{S}_i \cdot \boldsymbol{S}_j \ , \tag{41}$$

where $a_{i\sigma}$ is the annihilation operator for an electron with spin σ at site $\boldsymbol{i}$, but without orbital index. Note that $H_{\rm DE}$ is quadratic in the electron operators, indicating that it is reduced to a one-electron problem on the background of localized t_{2g} spins. This is a clear advantage for the Monte Carlo simulations, as discussed later in detail. Neglecting the orbital degrees of freedom is clearly an oversimplification, and important phenomena such as orbital ordering cannot be obtained in this model. However, the one-orbital model is still important, since it already includes part of the essence of manganese oxides. For example, recent computational investigations have clarified that the very important phase separation tendencies and metal–insulator competition exist in this model. The result will be discussed in detail in the following subsection.

3.3.9. $J_{\rm H} = \infty$ limit

Another simplification without the loss of essential physics is to take the widely used limit $J_{\rm H} = \infty$, since in the actual material $J_{\rm H}/t$ is much larger than unity. In such a limit, the e_g-electron spin perfectly aligns along the t_{2g}-spin direction, reducing the number of degrees of freedom. Then, in order to diagonalize the Hund term, the "spinless" e_g-electron operator, $c_{i\gamma}$, is defined as

$$c_{i\gamma} = \cos(\theta_i/2) d_{i\gamma\uparrow} + \sin(\theta_i/2) \mathrm{e}^{-\mathrm{i}\phi_i} d_{i\gamma\downarrow} \ . \tag{42}$$

In terms of the c-variables, the kinetic energy acquires the simpler form

$$H_{\rm kin} = -\sum_{\boldsymbol{i}\boldsymbol{a}\gamma\gamma'} S_{\boldsymbol{i},\boldsymbol{i}+\boldsymbol{a}} t^{\boldsymbol{a}}_{\gamma\gamma'} c^{\dagger}_{\boldsymbol{i}\gamma} c_{\boldsymbol{i}+\boldsymbol{a}\gamma'} \ , \tag{43}$$

where $S_{i,j}$ is given by

$$S_{ij} = \cos(\theta_i/2)\cos(\theta_j/2) + \sin(\theta_i/2)\sin(\theta_j/2)\mathrm{e}^{-\mathrm{i}(\phi_i - \phi_j)} \ . \tag{44}$$

This factor denotes the change of hopping amplitude due to the difference in angles between t_{2g}-spins at sites $\boldsymbol{i}$ and $\boldsymbol{j}$. Note that the effective hopping in this case is a complex number (Berry phase), contrary to the real number widely used in a large number of previous investigations (for details in the case of the one-orbital model see Müller-Hartmann and Dagotto, 1996).

The limit of infinite Hund coupling reduces the number of degrees of freedom substantially since the spin index is no longer needed. In addition, the U- and J-term in the electron–electron interaction within the e_g-sector are also no longer needed. In this case, the following simplified model is obtained:

$$\begin{aligned} H^{\infty} = & -\sum_{\boldsymbol{i}\boldsymbol{a}\gamma\gamma'} S_{\boldsymbol{i},\boldsymbol{i}+\boldsymbol{a}} t^{\boldsymbol{a}}_{\gamma\gamma'} c^{\dagger}_{\boldsymbol{i}\gamma} c_{\boldsymbol{i}+\boldsymbol{a}\gamma'} + J_{\rm AF} \sum_{\langle \boldsymbol{i},\boldsymbol{j}\rangle} \boldsymbol{S}_i \cdot \boldsymbol{S}_j + U' \sum_{i} n_{i\rm a} n_{i\rm b} + V \sum_{\langle i,j\rangle} n_i n_j \\ & + E_{\rm JT} \sum_{i} [2(q_{1i} n_i + q_{2i}\tau_{xi} + q_{3i}\tau_{zi}) + \beta q^2_{1i} + q^2_{2i} + q^2_{3i}] \ , \end{aligned} \tag{45}$$

where $n_{i\gamma} = c^{\dagger}_{i\gamma} c_{i\gamma}$, $n_i = \sum_{\gamma} n_{i\gamma}$, $\tau_{xi} = c^{\dagger}_{ia} c_{ib} + c^{\dagger}_{ib} c_{ia}$, and $\tau_{zi} = c^{\dagger}_{ia} c_{ia} - c^{\dagger}_{ib} c_{ib}$.

Considering the simplified Hamiltonian H^{∞}, two other limiting models can be obtained. One is the Jahn–Teller model $H^{\infty}_{\rm JT}$, defined as $H^{\infty}_{\rm JT} = H^{\infty}$ ($U' = V = 0$), in which the Coulomb interactions are simply ignored. Another is the Coulombic model H^{∞}_{C}, defined as $H^{\infty}_{C} = H^{\infty}$ ($E_{\rm JT} = 0$), which

denotes the two-orbital double exchange model influenced by the Coulomb interactions, neglecting the phonons. Of course, the actual situation is characterized by $U' \neq 0$, $V \neq 0$, and $E_{JT} \neq 0$, but in the spirit of the adiabatic continuation, it is convenient and quite meaningful to consider the minimal models possible to describe correctly the complicated properties of manganites.

3.3.10. JT phononic and Coulombic models

Another possible simplification could have been obtained by neglecting the electron–electron interaction in the full Hamiltonian but keeping the Hund coupling finite, leading to the following purely JT-phononic model with active spin degrees of freedom:

$$H_{JT} = H_{kin} + H_{Hund} + H_{AFM} + H_{el-ph} \ . \tag{46}$$

Often in this review this Hamiltonian will be referred to as the "two-orbital" model (unless explicitly stated otherwise). To solve H_{JT}, numerical methods such as Monte Carlo techniques and the relaxation method have been employed. Qualitatively, the negligible values of the probability of double occupancy in the strong electron–phonon coupling region with large J_H justifies the neglect of H_{el-el}, since the Jahn–Teller energy is maximized when one e_g electron exists at each site. Thus, the JT-phonon-induced interaction will produce physics quite similar to that due to the on-site correlation.

It would be important to verify this last expectation by studying a multi-orbital model with only Coulombic terms, without the extra approximation of using mean-field techniques for its analysis. Of particular relevance is whether phase separation tendencies and charge ordering appear in this case, as they do in the JT-phononic model. This analysis is particularly important since, as explained before, a mixture of phononic and Coulombic interactions is expected to be needed for a proper quantitative description of manganites. For this purpose, yet another simplified model has been analyzed in the literature:

$$H_C = H_{kin} + H_{el-el} \ . \tag{47}$$

Note that the Hund coupling term between e_g electrons and t_{2g} spins is not explicitly included. The reason for this extra simplification is that the numerical complexity in the analysis of the model is drastically reduced by neglecting the localized t_{2g} spins. In the FM phase, this is an excellent approximation, but not necessarily for other magnetic arrangements. Nevertheless, the authors believe that it is important to establish with accurate numerical techniques whether the PS tendencies are already present in this simplified two-orbital models with Coulomb interactions, even if not all degrees of freedom are incorporated from the outset. Adding the $S = 3/2$ quantum localized spins to the problem would considerably increase the size of the Hilbert space of the model, making it intractable with current computational techniques.

3.3.11. Estimations of parameters

In this subsection, estimations of the couplings that appear in the models described before are provided. However, before proceeding with the details the reader must be warned that such estimations are actually quite difficult, for the simple reason that in order to compare experiments with theory reliable calculations must be carried out. Needless to say, strong coupling many-body problems are notoriously difficult and complex, and it is quite hard to find accurate calculations to

compare against experiments. Then, the numbers quoted below must be taken simply as rough estimations of orders of magnitude. The reader should consult the cited references to analyze the reliability of the estimations mentioned here. Note also that the references discussed in this subsection correspond to only a small fraction of the vast literature on the subject. Nevertheless, the "sample" cited below is representative of the currently accepted trends in manganites.

Regarding the largest energy scales, the on-site U repulsion was estimated to be 5.2 ± 0.3 and 3.5 ± 0.3 eV, for $CaMnO_3$ and $LaMnO_3$, respectively, by Park et al. (1996) using photoemission techniques. The charge-transfer energy Δ was found to be 3.0 ± 0.5 eV for $CaMnO_3$ in the same study (note that in the models described in previous sections, the oxygen ions were simply ignored). In other photoemission studies, Dessau and Shen (1999) estimated the exchange energy for flipping an e_g-electron to be 2.7 eV.

Okimoto et al. (1995) studying the optical spectra of $La_{1-x}Sr_xMnO_3$ with $x = 0.175$ estimated the value of the Hund coupling to be of the order of 2 eV, much larger than the hopping of the one-orbital model for manganites. Note that in estimations of this variety care must be taken with the actual definition of the exchange J_H, which sometimes is in front of a ferromagnetic Heisenberg interaction where classical localized spins of module 1 are used, while in other occasions quantum spins of value 3/2 are employed. Nevertheless, the main message of the Okimoto et al. paper is that J_H is larger than the hopping. A reanalysis of the Okimoto et al. results led Millis et al. (1996) to conclude that the Hund coupling is actually even larger than previously believed. The optical data of Quijada et al. (1998) and Machida et al. (1998) also suggest that the Hund coupling is larger than 1 eV. Similar conclusions were reached by Satpathy et al. (1996) using constrained LDA calculations.

The crystal-field splitting between the e_g- and t_{2g}-states was estimated to be of the order of 1 eV by Tokura (1999) (see also Yoshida, 1998). Based on the discussion in the previous subsection, it is clear that manganites are in high-spin ionic states due to their large Hund coupling.

Regarding the hopping "t", Dessau and Shen (1999) reported a value of order 1 eV, which is somewhat larger than other estimations. In fact, the results of Bocquet et al. (1992), Arima et al. (1993), and Saitoh et al. (1995) locate its magnitude between 0.2 and 0.5 eV, which is reasonable in transition metal oxides. However, note that fair comparisons between theory and experiment require calculations of, e.g., quasiparticle band dispersions, which are difficult at present. Nevertheless, it is widely accepted that the hopping is just a fraction of eV.

Dessau and Shen (1999) estimated the static Jahn–Teller energy E_{JT} as 0.25 eV. From the static Jahn–Teller energy and the hopping amplitude, it is convenient to define the dimensionless electron-phonon coupling constant λ as

$$\lambda = \sqrt{2E_{JT}/t} = g/\sqrt{k_{JT}t}\ . \tag{48}$$

By using $E_{JT} = 0.25$ eV and $t = 0.2$–0.5 eV, λ is estimated as between 1–1.6. Actually, Millis et al. (1996) concluded that λ is between 1.3 and 1.5. It can be shown that the recent studies of Allen and Perebeinos (1999b) and Perebeinos and Allen (2000) lead to $\lambda = 1.6$, in agreement with other estimations.

As for the parameter β, it is given by $\beta = k_{br}/k_{JT} = (\omega_{br}/\omega_{JT})^2$, where ω_{br} and ω_{JT} are the vibration energies for manganite breathing- and JT modes, respectively, assuming that the reduced masses for those modes are equal. From experimental results and band-calculation data (see Iliev et al., 1998), ω_{br} and ω_{JT} are estimated as ~ 700 and 500–600 cm^{-1}, respectively, leading to $\beta \approx 2$. However, in practice it has been observed that the main conclusions are basically unchanged as

long as β is larger than unity. Thus, if an explicit value for β is not provided, the reader can consider that β is simply taken to be ∞ to suppress the breathing mode distortion.

The value of J_{AF} is the smallest of the set of couplings discussed here. In units of the hopping, it is believed to be of the order of $0.1t$ (see Perring et al., 1997), namely about 200 K. Note, however, that it would be a bad approximation to simply neglect this parameter since in the limit of vanishing density of e_g-electrons, J_{AF} is crucial to induce antiferromagnetism, as it occurs in $CaMnO_3$ for instance. Its relevance, at hole densities close to 0.5 or larger, to the formation of antiferromagnetic charge-ordered states is remarked elsewhere in this review. Also in mean-field approximations by Maezono et al. (1998a) the importance of J_{AF} has been mentioned, even though in their work this coupling was estimated to be only $0.01t$.

Summarizing, it appears well established that: (i) the largest energy scales in the Mn-oxide models studied here are the Coulomb repulsions between electrons in the same ion, which is quite reasonable. (ii) The Hund coupling is between 1 and 2 eV, larger than the typical hopping amplitudes, and sufficiently large to form high-spin Mn^{4+} and Mn^{3+} ionic states. As discussed elsewhere in the review, a large J_H leads naturally to a vanishing probability of e_g-electron double occupancy of a given orbital, thus mimicking the effect of a strong on-site Coulomb repulsion. (iii) The dimensionless electron–phonon coupling constant λ is of the order of unity, showing that the electron lattice interaction is substantial and cannot be neglected. (iv) The electron hopping energy is a fraction of eV. (v) The AF-coupling among the localized spins is about a tenth of the hopping. However, as remarked elsewhere, this apparent small coupling can be quite important in the competition between FM- and AF-state.

3.3.12. Monte Carlo simulations

In this subsection the details related to the Monte Carlo calculations are provided. For simplicity, let us focus here on one-dimensional systems as an example. Generalizations to higher dimensions are straightforward. Also, as a simple example, the case of the one-orbital model will be used, with the two-orbital case left as exercise to the readers. Note that the one-orbital model H_{DE} is simply denoted by $\hat{H}$ in this subsection. Note also that β indicates the inverse temperature, i.e., $\beta = 1/T$, in this subsection.

As explained before, the Hamiltonian for the one-orbital model is quadratic in the $\{a, a^\dagger\}$ operators and thus, it corresponds to a "one-electron" problem, with a density regulated by a chemical potential μ. For the case of a chain with L sites, the base can be considered as $a^\dagger_{1,\uparrow}|0\rangle, \ldots, a^\dagger_{L,\uparrow}|0\rangle, a^\dagger_{1,\downarrow}|0\rangle, \ldots, a^\dagger_{L,\downarrow}|0\rangle$, and thus $\hat{H}$ is given by a $2L \times 2L$ matrix for a fixed configuration of the classical spins.

The partition function in the grand canonical ensemble can be written as

$$Z = \prod_i^L \left(\int_0^\pi d\theta_i \sin\theta_i \int_0^{2\pi} d\phi_i \right) Z_g(\{\theta_i, \phi_i\}) \,. \tag{49}$$

Here g denotes conduction electrons and $Z_g(\{\theta_i, \phi_i\}) = \mathrm{Tr}_g(e^{-\beta \hat{K}})$, where $\hat{K} = \hat{H} - \mu \hat{N}$ with $\hat{N}$ the number operator and the trace is taken for the mobile electrons in the e_g-orbital, which are created and destroyed by the fermionic operators $a^\dagger$ and a. It will be shown that Z_g can be calculated in terms of the eigenvalues of $\hat{K}$ denoted by ε_λ ($\lambda = 1, \ldots, 2L$). The diagonalization is performed numerically using library routines.

Since $\hat{K}$ is an hermitian operator, it can be represented in terms of a hermitian matrix which can be diagonalized by an unitary matrix U such that

$$U^{\dagger}KU = \begin{pmatrix} \varepsilon_1 & 0 & \dots & 0 \\ 0 & \varepsilon_2 & \dots & 0 \\ \vdots & \vdots & \ddots & \vdots \\ 0 & 0 & \dots & \varepsilon_{2L} \end{pmatrix}. \tag{50}$$

The base in which the matrix K is diagonal is given by the eigenvectors $u_1^{\dagger}|0\rangle, \dots, u_{2L}^{\dagger}|0\rangle$. Defining $u_m^{\dagger}u_m = \hat{n}_m$ and denoting by n_m the eigenvalues of $\hat{n}_m$, the trace can be written as

$$\mathrm{Tr}_g(\mathrm{e}^{-\beta\hat{K}}) = \sum_{n_1,\dots,n_{2L}} \langle n_1 \dots n_{2L}|\mathrm{e}^{-\beta\hat{K}}|n_1 \dots n_{2L}\rangle = \sum_{n_1,\dots,n_{2L}} \langle n_1 \dots n_{2L}|\mathrm{e}^{-\beta\sum_{\lambda=1}^{2L}\varepsilon_\lambda n_\lambda}|n_1 \dots n_{2L}\rangle\,, \tag{51}$$

since in the $\{u_m^{\dagger}|0\rangle\}$ basis, the operator $\hat{K}$ can be replaced by its eigenvalues. The exponential is now a "c" number and it is equivalent to a product of exponentials given by

$$Z_g = \sum_{n_1} \langle n_1|\mathrm{e}^{-\beta\varepsilon_1 n_1}|n_1\rangle \dots \sum_{n_{2L}} \langle n_{2L}|\mathrm{e}^{-\beta\varepsilon_{2L}n_{2L}}|n_{2L}\rangle\,, \tag{52}$$

which can be written compactly as

$$Z_g = \prod_{\lambda=1}^{2L} \mathrm{Tr}_\lambda(\mathrm{e}^{-\beta\varepsilon_\lambda n_\lambda})\,. \tag{53}$$

Since the particles are fermions, the occupation numbers are either 0 or 1, and the sum in Eq. (52) is restricted to those values,

$$Z_g = \prod_{\lambda=1}^{2L} \sum_{n=0}^{1} \mathrm{e}^{-\beta\varepsilon_\lambda n} = \prod_{\lambda=1}^{2L} (1 + \mathrm{e}^{-\beta\varepsilon_\lambda})\,. \tag{54}$$

Thus, combining Eqs. (49) and (54), Z is obtained as

$$Z = \prod_{i}^{L} \left(\int_0^{\pi} \mathrm{d}\theta_i \sin\theta_i \int_0^{2\pi} \mathrm{d}\phi_i \right) \prod_{\lambda=1}^{2L} (1 + \mathrm{e}^{-\beta\varepsilon_\lambda})\,. \tag{55}$$

Note here that the integrand is clearly positive, and thus, "sign problems" are not present. The integral over the angular variables can be performed using a classical Monte Carlo simulation. The eigenvalues must be obtained for each classical spin configuration using library subroutines. Finding the eigenvalues is the most time consuming part of the numerical simulation.

Calculation of static observables: The equal time or static observables $\hat{O}(\{a_i, a_i^{\dagger}\})$ are given by

$$\langle\hat{O}\rangle = \frac{1}{Z}\prod_{i}^{L} \left(\int_0^{\pi} \mathrm{d}\theta_i \sin\theta_i \int_0^{2\pi} \mathrm{d}\phi_i \right) \mathrm{Tr}_g(\hat{O}\mathrm{e}^{-\beta\hat{K}}) = \frac{1}{Z}\prod_{i}^{L} \left(\int_0^{\pi} \mathrm{d}\theta_i \sin\theta_i \int_0^{2\pi} \mathrm{d}\phi_i \right) Z_g\langle\tilde{O}\rangle\,, \tag{56}$$

where $\langle\tilde{O}\rangle = \mathrm{Tr}_g(\hat{O}\mathrm{e}^{-\beta\hat{K}})/Z_g$. In practice only the Green function has to be calculated, and more complicated operators are evaluated using Wick's theorem. The Green function for a given configuration of classical spins are given by $G_{i,j,\sigma,\sigma'} = \langle a_{i,\sigma}a_{j,\sigma'}^{\dagger}\rangle$.

Let us consider the case in which $\hat{O} = a_{i,\sigma} a^{\dagger}_{j,\sigma'}$, relevant for the Green function. In this case,

$$G_{i,j,\sigma,\sigma'} = \mathrm{Tr}_g(a_{i,\sigma} a^{\dagger}_{j,\sigma'} \mathrm{e}^{-\beta \hat{K}})/Z_g \ . \tag{57}$$

Changing to the base in which $\hat{K}$ is diagonal through the transformation $a^{\dagger}_{i\sigma} = \sum_{\mu=1}^{2L} u^{\dagger}_{\mu} U^{\dagger}_{\mu,i_\sigma}$, where $i_\sigma = (i,\sigma)$, it can be shown that

$$\begin{aligned}
\mathrm{Tr}_g(a_{i,\sigma} a^{\dagger}_{j,\sigma'} \mathrm{e}^{-\beta \hat{K}}) &= \sum_{\lambda=1}^{2L} \sum_{\eta=1}^{2L} U_{i_\sigma,\lambda} U^{\dagger}_{\eta,j_{\sigma'}} \mathrm{Tr}_g \left[u_\lambda u^{\dagger}_\eta \prod_{\nu=1}^{2L} \mathrm{e}^{-\beta \varepsilon_\nu n_\nu} \right] \\
&= \sum_{\lambda=1}^{2L} \sum_{\eta=1}^{2L} U_{i_\sigma,\lambda} U^{\dagger}_{\eta,j_{\sigma'}} \mathrm{Tr}_g \left[\prod_{\nu=1}^{2L} \{1 + (\mathrm{e}^{-\beta\varepsilon_\nu} - 1) n_\nu\} u_\lambda u^{\dagger}_\eta \right] \\
&= \sum_{\lambda=1}^{2L} U_{i_\sigma,\lambda} U^{\dagger}_{\lambda,j_{\sigma'}} \prod_{\nu=1}^{2L} \{1 + (\mathrm{e}^{-\beta\varepsilon_\nu} - 1) n_\nu\} (1 - n_\lambda) \\
&= \sum_{\lambda=1}^{2L} U_{i_\sigma,\lambda} U^{\dagger}_{\lambda,j_{\sigma'}} \prod_{\nu=1 (\nu \neq \lambda)}^{2L} \left(\sum_{n_\nu=0}^{1} \{1 + (\mathrm{e}^{-\beta\varepsilon_\nu} - 1) n_\nu\} \right) \\
&= \sum_{\lambda=1}^{2L} U_{i_\sigma,\lambda} U^{\dagger}_{\lambda,j_{\sigma'}} \prod_{\nu=1 (\nu \neq \lambda)}^{2L} (1 + \mathrm{e}^{-\beta\varepsilon_\nu}) \ .
\end{aligned} \tag{58}$$

Thus, the Green function is given by

$$\begin{aligned}
G_{i,j,\sigma,\sigma'} &= \sum_{\lambda=1}^{2L} U_{i_\sigma \lambda} U^{\dagger}_{\lambda j_{\sigma'}} \prod_{\nu=1 (\nu \neq \lambda)}^{2L} (1 + \mathrm{e}^{-\beta\varepsilon_\nu}) / \prod_{\nu=1}^{2L} (1 + \mathrm{e}^{-\beta\varepsilon_\nu}) \\
&= \sum_{\lambda=1}^{2L} U_{i_\sigma,\lambda} \frac{1}{1 + \mathrm{e}^{-\beta\varepsilon_\lambda}} U^{\dagger}_{\lambda,j_{\sigma'}} \ .
\end{aligned} \tag{59}$$

Let us now consider some examples. The e_g-electron number is given by

$$\langle \hat{n} \rangle = \sum_{i,\sigma} \langle a^{\dagger}_{i,\sigma} a_{i,\sigma} \rangle = 2L - \sum_{i,\sigma} G_{i,i,\sigma,\sigma} \ . \tag{60}$$

More complicated operators can be written in terms of Green functions using Wick's theorem (Mahan, 1981, p. 95) which states that

$$\langle a_{j_1,\sigma} a^{\dagger}_{j_2,\sigma} a_{j_3,\sigma} a^{\dagger}_{j_4,\sigma} \rangle = \langle a_{j_1,\sigma} a^{\dagger}_{j_2,\sigma} \rangle \langle a_{j_3,\sigma} a^{\dagger}_{j_4,\sigma} \rangle - \langle a_{j_1,\sigma} a^{\dagger}_{j_4,\sigma} \rangle \langle a_{j_3,\sigma} a^{\dagger}_{j_2,\sigma} \rangle \ . \tag{61}$$

For example, if $\hat{O} = a^{\dagger}_{j_1,\sigma} a_{j_2,\sigma} a^{\dagger}_{j_3,\sigma} a_{j_4,\sigma}$, a combination that appears in the calculation of spin and charge correlations, and using Wick's theorem in combination with the fact that $\langle a^{\dagger}_{i,\sigma} a_{j,\sigma'} \rangle = \delta_{i,j}\delta_{\sigma,\sigma'} - \langle a_{j,\sigma'} a^{\dagger}_{i,\sigma} \rangle = \delta_{i,j}\delta_{\sigma,\sigma'} - G_{j,i,\sigma',\sigma}$, it can be shown that

$$\begin{aligned}
\langle \hat{O} \rangle &= \langle a^{\dagger}_{j_1,\sigma} a_{j_2,\sigma} \rangle \langle a^{\dagger}_{j_3,\sigma} a_{j_4,\sigma} \rangle - \langle a^{\dagger}_{j_1,\sigma} a_{j_4,\sigma} \rangle \langle a^{\dagger}_{j_3,\sigma} a_{j_2,\sigma} \rangle \\
&= (\delta_{j_1,j_2} - \langle G_{j_2,j_1,\sigma,\sigma} \rangle)(\delta_{j_3,j_4} - \langle G_{j_4,j_3,\sigma,\sigma} \rangle) - (\delta_{j_1,j_4} - \langle G_{j_4,j_1,\sigma,\sigma} \rangle)(\delta_{j_3,j_2} - \langle G_{j_2,j_3,\sigma,\sigma} \rangle) \ .
\end{aligned} \tag{62}$$

Calculation of time-dependent observables: Time-dependent observables are evaluated through the time-dependent Green function which can be readily calculated numerically. The Green

function is defined as

$$G^{>}_{i,j,\sigma,\sigma}(t) = \langle a_{i,\sigma}(t) a^{\dagger}_{j,\sigma}(0) \rangle \ , \tag{63}$$

where

$$a_{i,\sigma}(t) = \mathrm{e}^{\mathrm{i}\hat{H}t} a_{i,\sigma} \mathrm{e}^{-\mathrm{i}\hat{H}t} \ . \tag{64}$$

Note that $\hat{H}$ and $\hat{K}$ can be diagonalized by the same basis of eigenvectors $\{u^{\dagger}_{m}|0\rangle\}$, and the eigenvalues of $\hat{H}$ are denoted by ρ_{λ}. Working in this basis it is possible to write $a_{i,\sigma}(t)$ in terms of $a_{i,\sigma}$ as

$$\begin{aligned} a_{i,\sigma}(t) &= \mathrm{e}^{\mathrm{i}t\sum_{v} \rho_{v} n_{v}} \sum_{\eta} U_{i_{\sigma},\eta} u_{\eta} \mathrm{e}^{-\mathrm{i}t\sum_{v} \rho_{v} n_{v}} \\ &= \sum_{v=1}^{2L} \left[\sum_{\lambda=1}^{2L} U_{i_{\sigma},\lambda} \mathrm{e}^{-\mathrm{i}t\rho_{\lambda}} U^{\dagger}_{\lambda,v} \right] a_{v} \ , \end{aligned} \tag{65}$$

where $a_{v} = a_{v,\uparrow}$ if $v \leq L$ and $a_{v} = a_{v-L,\downarrow}$ if $v > L$.

Substituting Eq. (65) in Eq. (63), the time-dependent Green function given by

$$G^{>}_{i,j,\sigma,\sigma}(t) = \sum_{v=1}^{2L} \left[\sum_{\lambda=1}^{2L} U_{i_{\sigma},\lambda} \mathrm{e}^{-\mathrm{i}t\rho_{\lambda}} U^{\dagger}_{\lambda,v} \right] \langle a_{v} a^{\dagger}_{j,\sigma} \rangle \ . \tag{66}$$

In Eqs. (57)–(59), it has been shown that $\langle a_{v} a^{\dagger}_{j,\sigma} \rangle = \sum_{\lambda=1}^{2L} U_{v,\lambda} [1/(1 + \mathrm{e}^{-\beta\varepsilon_{\lambda}})] U^{\dagger}_{\lambda,j_{\sigma}}$, where $\varepsilon_{\lambda} = \rho_{\lambda} - \mu$. Thus, replacing Eq. (59) in Eq. (66),

$$G^{>}_{i,j,\sigma,\sigma}(t) = \sum_{\lambda=1}^{2L} U_{i_{\sigma},\lambda} \frac{\mathrm{e}^{-\mathrm{i}t\rho_{\lambda}}}{1 + \mathrm{e}^{-\beta(\rho_{\lambda} - \mu)}} U^{\dagger}_{\lambda,j_{\sigma}} \ . \tag{67}$$

Now, as an example, let us calculate the spectral function $A(k,\omega)$, given by

$$A(k,\omega) = -\frac{1}{\pi} \mathrm{Im}\, G_{\mathrm{ret}}(k,\omega) \ , \tag{68}$$

where the retarded Green function $G_{\mathrm{ret}}(k,\omega)$ is given by (see Mahan, 1981, p. 135)

$$G_{\mathrm{ret}}(k,\omega) = \int_{-\infty}^{\infty} \mathrm{d}t\, \mathrm{e}^{\mathrm{i}\omega t} G_{\mathrm{ret}}(k,t) \tag{69}$$

and

$$\begin{aligned} G_{\mathrm{ret}}(k,t) &= -\mathrm{i}\theta(t) \sum_{\sigma} \langle [a_{k,\sigma}(t) a^{\dagger}_{k,\sigma}(0) + a^{\dagger}_{k,\sigma}(0) a_{k,\sigma}(t)] \rangle \\ &= -\mathrm{i}\theta(t) \sum_{\sigma} (G^{>}_{k,\sigma} + G^{<}_{k,\sigma}) \ . \end{aligned} \tag{70}$$

Note here that $G^{>}_{k,\sigma} = \langle a_{k,\sigma}(t) a^{\dagger}_{k,\sigma}(0) \rangle$ and $G^{<}_{k,\sigma} = \langle a^{\dagger}_{k,\sigma}(0) a_{k,\sigma}(t) \rangle$ are implicitly defined.

Since the measurements are performed in coordinate space, $G^{>}_{k,\sigma}$ and $G^{<}_{k,\sigma}$ must be expressed in terms of real space operators using $a_{k,\sigma} = (1/\sqrt{L})\sum_j e^{-ikj} a_{j,\sigma}$. Then

$$G^{>}_{k,\sigma} = \frac{1}{L}\sum_{j,l} e^{-ik(j-l)} \langle a_{j,\sigma}(t) a^{\dagger}_{l,\sigma}(0)\rangle$$

$$= \frac{1}{L}\sum_{j,l} e^{-ik(j-l)} G^{>}_{j,l,\sigma,\sigma} \tag{71}$$

and analogously an expression for $G^{<}_{k,\sigma}$ can be obtained. Thus, Eq. (70) becomes

$$G_{\mathrm{ret}}(k,t) = -i\theta(t)\frac{1}{L}\sum_{j,l,\sigma} [e^{ik(l-j)} G^{>}_{j,l,\sigma,\sigma} + e^{-ik(l-j)} G^{<}_{j,l,\sigma,\sigma}] \,. \tag{72}$$

Substituting Eq. (72) in Eq. (69) it can be shown that

$$G_{\mathrm{ret}}(k,\omega) = \frac{-i}{L}\int_0^{\infty} dt\, e^{i\omega t} \sum_{j,l,\sigma} [e^{ik(l-j)} G^{>}_{j,l,\sigma,\sigma} + e^{-ik(l-j)} G^{<}_{j,l,\sigma,\sigma}] \,. \tag{73}$$

The next step is to evaluate the integral. Using Eq. (67), the first term in Eq. (73) becomes

$$\frac{-i}{L}\sum_{j,l,\sigma} e^{ik(l-j)} \sum_{\lambda=1}^{2L} \frac{U_{j_\sigma,\lambda} U^{\dagger}_{\lambda,l_\sigma}}{1+e^{-\beta(\rho_\lambda-\mu)}} \int_0^{\infty} dt\, e^{i(\omega-\rho_\lambda)t} \,. \tag{74}$$

Note that the integral is equal to $\pi\delta(\omega-\rho_\lambda)$. A similar expression is obtained for the second term and finally the spectral function can be expressed in terms of the eigenvectors and eigenvalues of $\hat{H}$ as

$$A(k,\omega) = \frac{1}{L}\mathrm{Im}\left\{ i \sum_{j,l,\sigma,\lambda} \left[e^{ik(l-j)} \frac{U_{j_\sigma,\lambda} U^{\dagger}_{\lambda,l_\sigma}}{1+e^{-\beta(\rho_\lambda-\mu)}} + e^{-ik(l-j)} \frac{U_{l_\sigma,\lambda} U^{\dagger}_{\lambda,j_\sigma}}{1+e^{\beta(\rho_\lambda-\mu)}} \right] \delta(\omega-\rho_\lambda) \right\}$$

$$= \frac{1}{L}\mathrm{Im}\left\{ i \sum_{j,l,\sigma,\lambda} \left[e^{ik(j-l)} U_{l_\sigma,\lambda} U^{\dagger}_{\lambda,j_\sigma} \delta(\omega-\rho_\lambda) \left(\frac{1}{1+e^{-\beta(\rho_\lambda-\mu)}} + \frac{1}{1+e^{\beta(\rho_\lambda-\mu)}} \right) \right] \right\} . \tag{75}$$

Noticing that the sum on the final line is equal to 1, the final expression is

$$A(k,\omega) = \frac{1}{L}\mathrm{Re}\left[\sum_{j,l,\sigma,\lambda} e^{ik(j-l)} U_{l_\sigma,\lambda} U^{\dagger}_{\lambda,j_\sigma} \delta(\omega-\rho_\lambda) \right] . \tag{76}$$

Similar algebraic manipulations allow to express other dynamical observables, such as the optical conductivity and dynamical spin correlation functions, in terms of the eigenvalues and eigenvectors of the Hamiltonian matrix.

3.3.13. Mean-field approximation for H^{∞}

Even a simplified model such as H^{∞} is still difficult to be solved exactly, except for some special cases. Thus, in this subsection, the mean-field approximation (MFA) is developed for H^{∞} to attempt to grasp its essential physics. Note that even at the mean-field level, due care should be paid to the self-consistent treatment to lift the double degeneracy of the e_g-electrons. The present

analytic MFA will be developed based on the following assumptions: (i) The background t_{2g}-spin structure is fixed through the calculation by assuming that the nearest-neighbor t_{2g}-spins (not to be confused with the full state) can only be in the FM or AF configuration. (ii) The JT- and breathing-mode distortions are noncooperative. These assumptions will be discussed later in this subsection.

First, let us rewrite the electron–phonon term by applying a standard mean-field decoupling procedure. In this approximation, a given operator O is written as $O = \langle O\rangle + \delta O$, where $\delta O = O - \langle O\rangle$. In a product of operators $O_1 O_2$, terms of order $\delta O_1 \delta O_2$ are simply discarded. Applying this trick to our case, it is shown that

$$\begin{aligned} q_{1i} n_i &\approx \langle q_{1i}\rangle n_i + q_{1i}\langle n_i\rangle - \langle q_{1i}\rangle\langle n_i\rangle \,, \\ q_{2i}\tau_{xi} &\approx \langle q_{2i}\rangle\tau_{xi} + q_{2i}\langle\tau_{xi}\rangle - \langle q_{2i}\rangle\langle\tau_{xi}\rangle \,, \\ q_{3i}\tau_{zi} &\approx \langle q_{3i}\rangle\tau_{zi} + q_{3i}\langle\tau_{zi}\rangle - \langle q_{3i}\rangle\langle\tau_{zi}\rangle \,, \\ q_{\alpha i}^2 &\approx 2\langle q_{\alpha i}\rangle q_{\alpha i} - \langle q_{\alpha i}\rangle^2 \quad (\alpha = 1,2,3) \,, \end{aligned} \tag{77}$$

where the bracket denotes the average value using the mean-field Hamiltonian described below. By minimizing the phonon energy, the local distortion is determined in the MFA as

$$q_{1i} = -\langle n_i\rangle/\beta, \quad q_{2i} = -\langle\tau_{xi}\rangle, \quad q_{3i} = -\langle\tau_{zi}\rangle \,. \tag{78}$$

Thus, after straightforward algebra, the electron–phonon term in the MFA is given by

$$\begin{aligned} H_{\text{el-ph}}^{\text{MF}} = & -2\sum_i [E_{\text{br}}\langle n_i\rangle n_i + E_{\text{JT}}(\langle\tau_{xi}\rangle\tau_{xi} + \langle\tau_{zi}\rangle\tau_{zi})] \\ & + \sum_i [E_{\text{br}}\langle n_i\rangle^2 + E_{\text{JT}}(\langle\tau_{xi}\rangle^2 + \langle\tau_{zi}\rangle^2)] \,, \end{aligned} \tag{79}$$

where $E_{\text{br}} = E_{\text{JT}}/\beta$, as already explained.

Now let us turn our attention to the electron–electron interaction term. At a first glance, it appears enough to make a similar decoupling procedure for $H_{\text{el-el}}$. However, such a decoupling cannot be uniquely carried out, since it will be shown below that $H_{\text{el-el}}$ is invariant with respect to the choice of e_g-electron orbitals due to the local SU(2) symmetry in the orbital space. Thus, it is necessary to find the optimal orbital set by determining the relevant e_g-electron orbital self-consistently at each site. For this purpose, it is convenient to use the expression Eq. (18) for q_{2i} and q_{3i}. Note in the MFA that the amplitude q_i and the phase ξ_i are, respectively, determined as

$$q_i = \sqrt{\langle\tau_{xi}\rangle^2 + \langle\tau_{zi}\rangle^2}, \quad \xi_i = \pi + \tan^{-1}(\langle\tau_{xi}\rangle/\langle\tau_{zi}\rangle) \,, \tag{80}$$

where "π" is added to ξ_i in the MFA. Originally, ξ_i is defined as $\xi_i = \tan^{-1}(q_{2i}/q_{3i})$, but in the MFA, the distortions are given by Eq. (78), in which minus signs appear in front of $\langle\tau_{xi}\rangle$ and $\langle\tau_{zi}\rangle$. Thus, due to these minus signs, the additional phase π in ξ_i should appear in order to maintain consistency with the previous definition, if ξ_i is obtained with the use of $\langle\tau_{xi}\rangle$ and $\langle\tau_{zi}\rangle$ in the MFA. By using the phase ξ_i determined by this procedure, it is convenient to transform $c_{i\text{a}}$ and

$c_{i\mathrm{b}}$ into the "phase-dressed" operators, $\tilde{c}_{i\mathrm{a}}$ and $\tilde{c}_{i\mathrm{b}}$, as

$$\begin{pmatrix}\tilde{c}_{i\mathrm{a}}\\ \tilde{c}_{i\mathrm{b}}\end{pmatrix} = \mathrm{e}^{\mathrm{i}\xi_i/2}\begin{pmatrix}\cos(\xi_i/2) & \sin(\xi_i/2)\\ -\sin(\xi_i/2) & \cos(\xi_i/2)\end{pmatrix}\begin{pmatrix}c_{i\mathrm{a}}\\ c_{i\mathrm{b}}\end{pmatrix}, \tag{81}$$

where the 2×2 matrix is SU(2) symmetric. Note that if ξ_i is increased by 2π, the SU(2) matrix itself changes its sign. To keep the transformation unchanged upon a 2π-rotation in ξ_i, a phase factor $\mathrm{e}^{\mathrm{i}\xi_i/2}$ is needed. In the expression for the ground state of the single JT molecule, namely the single-site problem discussed before, this phase factor has not been added, since the electron does not hop around from site to site and the phases do not correlate with each other. Namely, it was enough to pay attention to the double valuedness of the wave function at a single site. However, in the JT crystal in which e_{g}-electrons move in the periodic array of the JT centers, the addition of this phase factor is useful to take into account the effect of the Berry phase arising from the circular motion of e_{g}-electrons around the JT center, as has been emphasized in Koizumi et al. (1998a, b). It could be possible to carry out the calculation without including explicitly this phase factor, but in that case, it is necessary to pay due attention to the inclusion of the effect of the Berry phase. The qualitative importance of this effect will be explained later in the context of the "band-insulating picture" for the CE-type phase of half-doped manganites.

Note also that the phase ξ_i determines the electron orbital set at each site. In the previous section, the single-site problem was discussed and the ground state at site $\boldsymbol{i}$ was found to be

$$|\text{“b”}\rangle = [-\sin(\xi_i/2)d^{\dagger}_{i\mathrm{a}\sigma} + \cos(\xi_i/2)d^{\dagger}_{i\mathrm{b}\sigma}]|0\rangle\,, \tag{82}$$

which is referred to as the "b"-orbital, namely the combination with the lowest energy at a given site. The excited-state or "a"-orbital is simply obtained by requesting it to be orthogonal to "b" as

$$|\text{“a”}\rangle = [\cos(\xi_i/2)d^{\dagger}_{i\mathrm{a}\sigma} + \sin(\xi_i/2)d^{\dagger}_{i\mathrm{b}\sigma}]|0\rangle\,. \tag{83}$$

For instance, at $\xi_i = 2\pi/3$, "a" and "b" denote the $d_{y^2-z^2}$- and $d_{3x^2-r^2}$-orbitals, respectively. In Table 2, the correspondence between ξ_i and the local orbital is summarized for several important values of ξ_i. In order to arrive to the results of the table, remember that the original orbitals must be normalized such that $(x^2-y^2)/\sqrt{2}$ and $(3z^2-r^2)/\sqrt{6}$ are used. Note also that overall phase factors that may affect the orbitals are not included in Table 2. Furthermore, it should be noted that $d_{3x^2-r^2}$ and $d_{3y^2-r^2}$ never appear as the local orbital set. Sometimes those were treated as an

Table 2
Phase ξ_i and the corresponding e_{g}-electron orbitals. Note that "b" corresponds to the lowest-energy orbital for $E_{\mathrm{JT}} \neq 0$

ξ_i	"a"-orbital	"b"-orbital
0	x^2-y^2	$3z^2-r^2$
$\pi/3$	$3y^2-r^2$	z^2-x^2
$2\pi/3$	y^2-z^2	$3x^2-r^2$
π	$3z^2-r^2$	x^2-y^2
$4\pi/3$	z^2-x^2	$3y^2-r^2$
$5\pi/3$	$3x^2-r^2$	y^2-z^2

orthogonal orbital set to reproduce the experimental results, but such a treatment is an approximation, since the orbital ordering is not due to the simple alternation of two arbitrary kinds of orbitals.

Using the above-described transformations, $H^{\mathrm{MF}}_{\mathrm{el-ph}}$ and $H_{\mathrm{el-el}}$ can be rewritten after some algebra as

$$H^{\mathrm{MF}}_{\mathrm{el-ph}} = \sum_i \{E_{\mathrm{br}}(-2\langle n_i\rangle\tilde{n}_i + \langle n_i\rangle^2) + E_{\mathrm{JT}}[2q_i(\tilde{n}_{i\mathrm{a}} - \tilde{n}_{i\mathrm{b}}) + q_i^2]\} \tag{84}$$

and

$$H_{\mathrm{el-el}} = U'\sum_i \tilde{n}_{i\mathrm{a}}\tilde{n}_{i\mathrm{b}} + V\sum_{\langle i,j\rangle} \tilde{n}_i\tilde{n}_j\ , \tag{85}$$

where $\tilde{n}_{i\gamma} = \tilde{c}^{\dagger}_{i\gamma}\tilde{c}_{i\gamma}$ and $\tilde{n}_i = \tilde{n}_{i\mathrm{a}} + \tilde{n}_{i\mathrm{b}}$. Note that $H_{\mathrm{el-el}}$ is invariant with respect to the choice of ξ_i. Eq. (85) can be obtained by calculating $\tilde{c}^{\dagger}_{i\mathrm{a}}\tilde{c}_{i\mathrm{a}} + \tilde{c}^{\dagger}_{i\mathrm{b}}\tilde{c}_{i\mathrm{b}}$ using Eq. (81). This immediately leads to $\tilde{n}_i = n_i$. Then, from $\tilde{n}_i^2 = n_i^2$ and recalling that $n^2_{i\gamma} = n_{i\gamma}$ and $\tilde{n}^2_{i\gamma} = \tilde{n}_{i\gamma}$ for $\gamma = \mathrm{a}$ and b, it can be shown that $\tilde{n}_{i\mathrm{a}}\tilde{n}_{i\mathrm{b}} = n_{i\mathrm{a}}n_{i\mathrm{b}}$. Now let us apply the decoupling procedure as

$$\tilde{n}_{i\mathrm{a}}\tilde{n}_{i\mathrm{b}} \approx \langle\tilde{n}_{i\mathrm{a}}\rangle\tilde{n}_{i\mathrm{b}} + \tilde{n}_{i\mathrm{a}}\langle\tilde{n}_{i\mathrm{b}}\rangle - \langle\tilde{n}_{i\mathrm{a}}\rangle\langle\tilde{n}_{i\mathrm{b}}\rangle \tag{86}$$

and use the relations $\langle\tilde{n}_{i\mathrm{a}}\rangle = (\langle n_i\rangle - q_i)/2$, $\langle\tilde{n}_{i\mathrm{b}}\rangle = (\langle n_i\rangle + q_i)/2$, which arise from $\langle\tilde{n}_{i\mathrm{a}} - \tilde{n}_{i\mathrm{b}}\rangle = -q_i$ and $\langle\tilde{n}_{i\mathrm{a}} + \tilde{n}_{i\mathrm{b}}\rangle = \langle n_i\rangle$. The former relation indicates that the modulation in the orbital density is caused by the JT distortion, while the latter denotes the local charge conservation irrespective of the choice of electron basis. Then, the electron–electron interaction term is given in the MFA as

$$H^{\mathrm{MF}}_{\mathrm{el-el}} = (U'/4)\sum_i [2\langle n_i\rangle\tilde{n}_i - \langle n_i\rangle^2 + 2q_i(\tilde{n}_{ai} - \tilde{n}_{bi}) + q_i^2] + V\sum_{ia} [\langle n_{i+a}\rangle\tilde{n}_i - (1/2)\langle n_{i+a}\rangle\langle n_i\rangle]\ , \tag{87}$$

where the vector $\boldsymbol{a}$ has the same meaning as in the hopping term H_{kin}. For instance, in two dimensions, it denotes $\boldsymbol{a} = (\pm 1, 0)$ and $(0, \pm 1)$, where the lattice constant is taken as unity for simplicity. It should be noted that the type of orbital ordering would be automatically fixed as either $x^2 - y^2$ or $3z^2 - r^2$, if the original operators c would be simply used for the Hartree–Fock approximation. However, as it was emphasized above, the $H_{\mathrm{el-el}}$ term has a rotational invariance in orbital space, and there is no reason to fix the orbital only as $x^2 - y^2$ or $3z^2 - r^2$. In order to discuss properly the orbital ordering, the local e_{g}-electron basis, i.e., the phase ξ_i should be determined self-consistently.

By combining $H^{\mathrm{MF}}_{\mathrm{el-ph}}$ with $H^{\mathrm{MF}}_{\mathrm{el-el}}$ and transforming $\tilde{c}_{i\mathrm{a}}$ and $\tilde{c}_{i\mathrm{b}}$ into the original operators $c_{i\mathrm{a}}$ and $c_{i\mathrm{b}}$, the mean-field Hamiltonian is finally obtained as

$$\begin{aligned} H^{\infty}_{\mathrm{MF}} = & -\sum_{ia\gamma\gamma'} t^{a}_{\gamma\gamma'}c^{\dagger}_{i\gamma}c_{i+a\gamma'} + J_{\mathrm{AF}}\sum_{\langle i,j\rangle} \boldsymbol{S}_i\cdot\boldsymbol{S}_j + \tilde{E}_{\mathrm{JT}}\sum_i [-2(\langle\tau_{xi}\rangle\tau_{xi} + \langle\tau_{zi}\rangle\tau_{zi}) + \langle\tau_{xi}\rangle^2 + \langle\tau_{zi}\rangle^2] \\ & + \sum_i [(\tilde{U}'/2)\langle n_i\rangle + V\sum_a \langle n_{i+a}\rangle](n_i - \langle n_i\rangle/2)\ , \end{aligned} \tag{88}$$

where the renormalized JT energy is given by

$$\tilde{E}_{\mathrm{JT}} = E_{\mathrm{JT}} + U'/4 \tag{89}$$

and the renormalized inter-orbital Coulomb interaction is expressed as

$$\tilde{U}' = U' - 4E_{\rm br} \ . \tag{90}$$

Physically, the former relation indicates that the JT energy is effectively enhanced by U'. Namely, the strong on-site Coulombic correlation plays the *same* role as that of the JT phonon, at least at the mean-field level, indicating that it is not necessary to include U' explicitly in the models, as has been emphasized by the present authors in several publications (see for instance Hotta et al., 2000). The latter equation for $\tilde{U}'$ means that the one-site inter-orbital Coulomb interaction is effectively reduced by the breathing-mode phonon, since the optical-mode phonon provides an effective attraction between electrons. The expected positive value of $\tilde{U}'$ indicates that $e_{\rm g}$-electrons dislike double occupancy at the site, since the energy loss is proportional to the average local electron number in the mean-field argument. Thus, to exploit the gain due to the static JT energy and avoid the loss due to the on-site repulsion, an $e_{\rm g}$-electron will singly occupy a given site.

Now let us briefly discuss how to solve the present mean-field Hamiltonian on the background of the fixed $t_{2\rm g}$-spin arrangement. For some fixed spin pattern, by using appropriate initial values for the local densities $\langle n_i \rangle^{(0)}$, $\langle \tau_{xi} \rangle^{(0)}$, and $\langle \tau_{zi} \rangle^{(0)}$, the mean-field Hamiltonian $H_{\rm MF}^{\infty(0)}$ is constructed, where the superscript number (j) indicates the iteration step. By diagonalizing $H_{\rm MF}^{\infty(0)}$ on finite clusters, and usually using a variety of boundary conditions depending on the problem, the improved local densities, $\langle n_i \rangle^{(1)}$, $\langle \tau_{xi} \rangle^{(1)}$, and $\langle \tau_{zi} \rangle^{(1)}$, are obtained. This procedure is simply repeated such that in the jth iteration step, the local densities $\langle n_i \rangle^{(j+1)}$, $\langle \tau_{xi} \rangle^{(j+1)}$, and $\langle \tau_{zi} \rangle^{(j+1)}$ are obtained by using the Hamiltonian $H_{\rm MF}^{\infty(j)}$. The iterations can be terminated if $|\langle n_i \rangle^{(j+1)} - \langle n_i \rangle^{(j)}| < \delta$, $|\langle \tau_{xi} \rangle^{(j)} - \langle \tau_{xi} \rangle^{(j-1)}| < \delta$, and $\langle \tau_{zi} \rangle^{(j)} - \langle \tau_{zi} \rangle^{(j-1)}| < \delta$ are satisfied, where δ is taken to be a small number to control the convergence.

As for the choice of the cluster, in order to obtain the charge and orbital ordering pattern in the insulating phase, it is usually enough to treat a finite-size cluster with periodic boundary conditions. Note that the cluster size should be large enough to reproduce the periodicity in the spin, charge, and orbital ordering under investigation. However, to consider the transition to the metallic state from the insulating phase, in principle it is necessary to treat an infinite cluster. Of course, except for very special cases, it is impossible to treat the infinite-size cluster exactly, but fortunately, in the present MFA, it is quite effective to employ the twisted-boundary condition by introducing the momentum $\boldsymbol{k}$ in the Bloch phase factor $\mathrm{e}^{\mathrm{i}\boldsymbol{k}\cdot\boldsymbol{N}}$ at the boundary, where $\boldsymbol{N} = (N_x, N_y, N_z)$, and $N_{\boldsymbol{a}}$ is the size of the cluster along the $\boldsymbol{a}$-direction. Note that if the spin directions are changed periodically, an additional phase factor appears to develop at the boundary, but this is not the case. In the present MFA, the $t_{2\rm g}$-spin pattern is fixed from the outset, and the periodicity due to the spin pattern is already taken into account in the cluster.

Finally, here comments on some of the assumptions employed in the present MFA are provided. In the first approximation for $t_{2\rm g}$-spins, their pattern is fixed throughout the mean-field calculation and the nearest-neighbor spin configuration is assumed to be only FM or AFM. Note that this assumption does not indicate only the fully FM phase or three-dimensional G-type AFM spin pattern, but it can include more complicated spin patterns such as the CE-type AFM phase. However, under this assumption, several possible phases such as the spin canted phase and the spin flux phase, in which neighboring spins are neither FM nor AFM, are neglected from the outset.

Unfortunately, this assumption for the fixed $t_{2\rm g}$ spin pattern cannot be justified without extra tests. Thus, it is unavoidable to confirm the assumption using other methods. In order to perform

this check, unbiased numerical calculations such as the Monte Carlo simulations and relaxation techniques are employed to determine the local distortions, as well as the local spin directions. Especially for a fixed electron number, the optimization technique is found to work quite well in this type of problems.

Then, our strategy to complete the mean-field calculations is as follows: (i) For some electron density and small-size cluster, the mean-field calculations are carried out for several fixed configurations of t_{2g} spins. (ii) For the same electron density in the same size of cluster as in (i), both local distortions and t_{2g}-spin directions are optimized by using an appropriate computer code. (iii) Results obtained in (i) are compared to those in (ii). If there occurs a serious disagreement between them, go back to step (i) and/or (ii) to do again the calculations by changing the initial inputs. In this retrial, by comparing the energies between cases (i) and (ii), the initial condition for the case with higher energy should be replaced with that for the lower energy. To save CPU time it is quite effective to combine analytic MFA and numerical techniques. (iv) After several iterations, if a satisfactory agreement between (i) and (ii) is obtained, the MFA on a larger-size cluster is used to improve the results in (i). Namely, by combining the MFA and the optimization technique, it is possible to reach physically important results in a rapid and reliable way.

As for the assumption made regarding the use of noncooperative phonons in the MFA, it is also checked by comparing the noncooperative mean-field results with the optimized ones for cooperative distortions. Note here that, due to the CPU and memory restrictions, the optimization technique cannot treat large-size clusters. However, this numerical technique has the clear advantage that it is easily extended to include the cooperative effect by simply changing the coordinates from $\{Q\}$ to $\{u\}$, where $\{u\}$ symbolically indicates the oxygen displacements, while $\{Q\}$ denotes the local distortions of the MnO_6 octahedron. The effect of the cooperative phonons will be discussed separately for several values of the hole density.

3.4. *Main results*: *one orbital model*

3.4.1. *Phase diagram with classical localized spins*

Although the one-orbital model for manganites is clearly incomplete to describe these compounds since, by definition, it has only one active orbital, nevertheless, it has been shown in recent calculations that it captures part of the interesting competition between ferromagnetic and antiferromagnetic phases in these compounds. For this reason, and since this model is far simpler than the more realistic two-orbital model, it is useful to study it in detail.

A fairly detailed analysis of the phase diagram of the one-orbital model has been recently presented, mainly using computational techniques. Typical results are shown in Fig. 3.4.1a–c for $D = 1,2$, and ∞ (D is spatial dimension), the first two obtained with Monte Carlo techniques at low temperature, and the third with the dynamical mean-field approximation in the large J_H limit varying temperature. There are several important features in the results which are common in all dimensions. At e_g-density $\langle n \rangle = 1.0$, the system is antiferromagnetic (although this is not clearly shown in Fig. 3.4.1). The reason is that at large Hund coupling, double occupancy in the ground state is negligible at e_g-density $\langle n \rangle = 1.0$ or lower, and at these densities it is energetically better to have nearest-neighbor spins antiparallel, gaining an energy of order t^2/J_H, rather than to align them, since in such a case the system is basically frozen due to the Pauli principle. On the other hand, at finite hole density, antiferromagnetism is replaced by the tendency of holes to polarize the

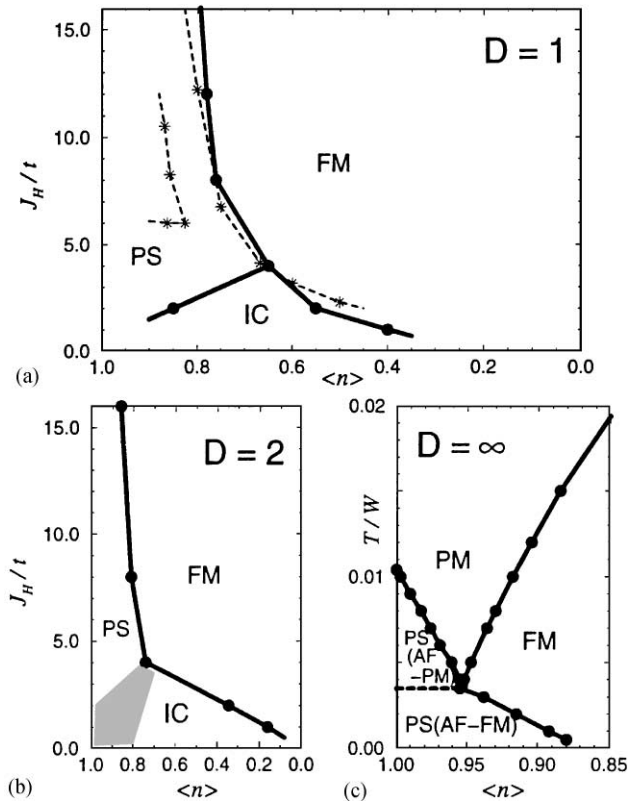

Fig. 3.4.1. Phase diagram of the one-orbital model with classical spins (and without J_{AF} coupling). (a) Results obtained with Monte Carlo methods at low temperature in 1D (Yunoki et al., 1998a; Dagotto et al., 1998). FM, PS, and IC, denote ferromagnetic, phase-separated, and spin incommensurate phases, respectively. Although not shown explicitly, the $\langle n \rangle = 1.0$ axis is antiferromagnetic. The dashed lines correspond to results obtained using quantum localized spins. For more details see Yunoki et al. (1998a) and Dagotto et al. (1998). (b) Similar to (a) but in 2D. The gray region denotes the possible location of the PS-IC transition at low Hund coupling, which is difficult to determine. Details can be found in Yunoki et al. (1998a). (c) Results obtained in the infinite dimension limit and at large Hund coupling varying the temperature (here in units of the half-width W of the density of states). Two regions with PS were identified, as well as a paramagnetic PM regime. For details see Yunoki et al. (1998a).

spin background to improve their kinetic energy, as discussed in Section 3.1. Then, a very prominent ferromagnetic phase develops in the model as shown in Fig. 3.4.1. This FM tendency appears in all dimensions of interest, and it manifests itself in the Monte Carlo simulations through the rapid growth with decreasing temperature, and/or increasing number of sites, of the zero-momentum spin–spin correlation, as shown in Fig. 3.4.2a and b reproduced from Yunoki et al. (1998a). In real space, the results correspond to spin correlations between two sites at a distance d which do not decay to a vanishing number as d grows, if there is long-range order (see results in Dagotto et al., 1998). In 1D, quantum fluctuations are expected to be so strong that long-range order cannot be achieved, but in this case the spin correlations still can decay slowly with distance following a power law. In practice, the tendency toward FM or AF is so strong even in 1D that issues of long-range order vs power-law decays are not of much importance for studying the

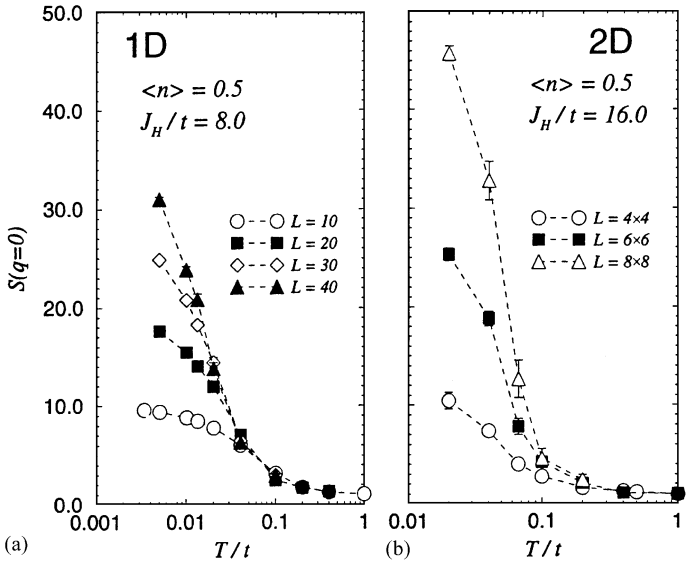

Fig. 3.4.2. Spin–spin correlations of the classical spins at zero momentum $S(\boldsymbol{q} = 0)$ vs. temperature T (units of t) obtained with the Monte Carlo technique, taken from Yunoki et al. (1998a). Density, Hund coupling, and lattice sizes are shown. (a) and (b) correspond to one and two dimensions, respectively. Closed shells and open boundary conditions were used in (a) and (b), respectively. For details see Dagotto et al. (1998).

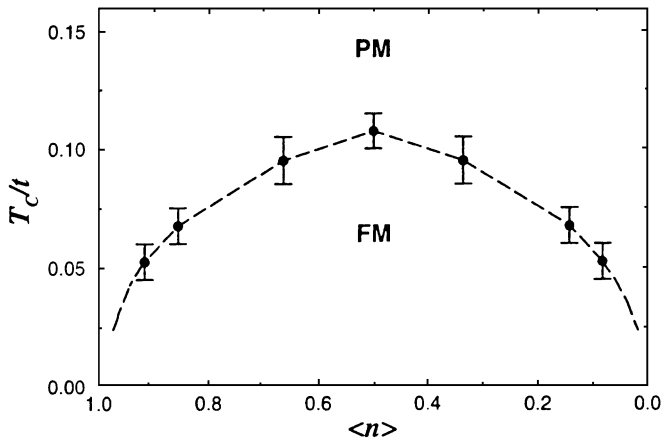

Fig. 3.4.3. Rough estimation of the Curie temperature T_C in 3D and in the limit $J_H = \infty$, as reported by Yunoki et al. (1998a). Other calculations discussed in the text produce results in reasonable agreement with these Monte Carlo simulations (see Motome and Furukawa, 1999).

dominant tendencies in the model. Nevertheless, care must be taken with these subtleties if very accurate studies are attempted in 1D.

In 3D, long-range order can be obtained at finite temperature and indeed it occurs in the one-orbital model. A rough estimation of the critical Curie temperature T_C is shown in Fig. 3.4.3 based on small 6^3 3D clusters (from Yunoki et al., 1998a). T_C is of the order of just $0.1t$, while other

estimations predicted a much higher value (Millis et al., 1995). More recent work has refined T_C, but the order of magnitude found in the first Monte Carlo simulations remains the same (see Calderon and Brey, 1998; Yi et al., 1999b; Motome and Furukawa, 1999; Held and Vollhardt, 1999). If t is about 0.2 eV, the T_C becomes of the order of 200 K, a value in reasonable agreement with experiments. However, remember that this model cannot describe orbital order properly, and thus it remains a crude approximation to manganites.

The most novel result emerging from the computational studies of the one-orbital model is the way in which the FM phase is reached by hole doping of the AF phase at $\langle n \rangle = 1.0$. As explained before, mean-field approximations by de Gennes (1960) suggested that this interpolation should proceed through a so-called "canted" state in which the spin structure remains antiferromagnetic in two directions but develops a uniform moment along the third direction. For many years this canted state was assumed to be correct, and many experiments were analyzed based on such state. However, the computational studies showed that instead of a canted state, an electronic "phase-separated" (PS) regime interpolates between the FM- and AF-phase. This PS region is very prominent in the phase diagram of Fig. 3.4.1a–c in all dimensions.

As an example of how PS is obtained from the computational work, consider Fig. 3.4.4. In the Monte Carlo simulations carried out in this context, performed in the grand-canonical ensemble, the density of mobile e_g-electrons $\langle n \rangle$ is an output of the calculation, the input being the chemical potential μ. In Fig. 3.4.4a, the density $\langle n \rangle$ vs. μ is shown for one-dimensional clusters of different sizes at low temperature and large Hund coupling, in part (b) results in two dimensions are presented, and in part (c) the limit $D = \infty$ is considered. In all cases, a clear *discontinuity* in the density appears at a particular value of μ, as in a first-order phase transition. This means that there is a finite range of densities which are simply unreachable, i.e., that they cannot be stabilized regardless of how carefully μ is tuned. If the chemical potential is fixed to the value where the discontinuity occurs, frequent tunneling events among the two limiting densities are observed (Dagotto et al., 1998). In the inset of Fig. 3.4.4a, the spin correlations are shown for the two densities at the extremes of the discontinuity, and they correspond to FM- and AF-state.

Strictly speaking, the presence of PS means that the model has a range of densities which cannot be accessed, and thus, those densities are simply *unstable*. This is clarified better using now the canonical ensemble, where the number of particles is fixed as an input and μ is an output. In this context, suppose that one attempts to stabilize a density such as $\langle n \rangle = 0.95$ (unstable in Fig. 3.4.4), by locating, say, 95 electrons into a 10×10 lattice. The ground state of such a system will not develop a uniform density, but instead two regions separated in space will be formed: a large one with approximately 67 sites and 67 electrons (density 1.0) and a smaller one with 33 sites and 28 electrons (density ~ 0.85). The last density is the lower value in the discontinuity of Fig. 3.4.4b in 2D, i.e., the first stable density after $\langle n \rangle = 1.0$ when holes are introduced. Then, whether using canonical or grand-canonical approximations, a range of densities remains unstable.

The actual spatial separation into two macroscopic regions (FM and AF in this case) leads to an energy problem. In the simulations and other mean-field approximations that produce PS, the "tail" of the Coulomb interaction was not explicitly included. In other words, the electric charge was not properly accounted for. Once this long-range Coulomb interaction is introduced into the problem, the fact that the FM- and AF-state involved in PS have different densities leads to a huge energy penalization even considering a large dielectric constant due to polarization (charge certainly cannot be accumulated in a macroscopic portion of a sample). For this reason, it is more

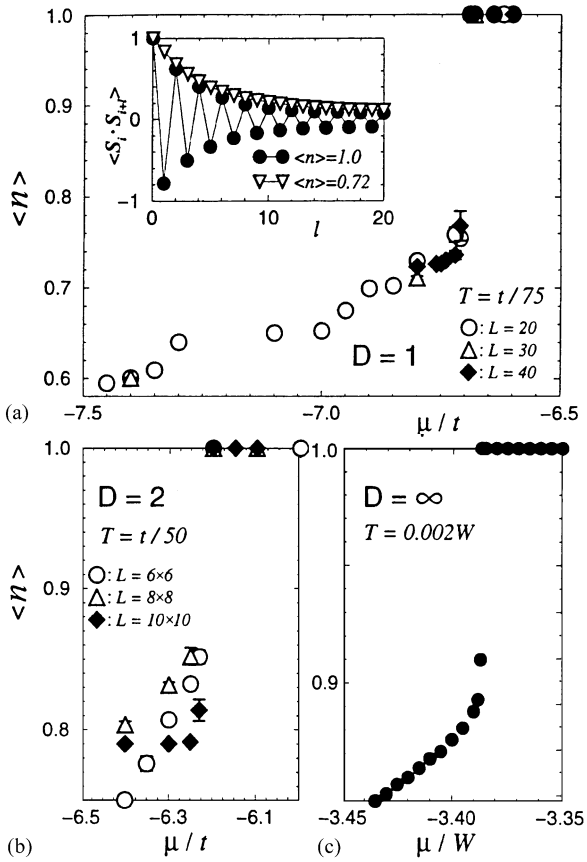

Fig. 3.4.4. Density of e_g electrons vs. chemical potential μ. The coupling is $J_H = 8t$ in (a) and (b) and $4W$ in (c) (W is the half-width of the density of states). Temperatures and lattice sizes are indicated. (a) Results in 1D with PBC. The inset contains the spin correlations at the electronic densities 1.00 and 0.72, that approximately limit the density discontinuity. (b) Same as (a) but in 2D. (c) Same as (a) but in $D = \infty$. Results reproduced from Yunoki et al. (1998a).

reasonable to expect that the PS domains will break into smaller pieces, as sketched in Fig. 3.4.5 (Moreo et al., 1999a; see also Section 3.9 and Lorenzana et al., 2000). The shape of these pieces remains to be investigated in detail since the calculations are difficult with long-range interactions (for results in 1D see below), but droplets or stripes appear as a serious possibility. This state would now be *stable*, since it would satisfy in part the tendency toward phase separation and also it will avoid a macroscopic charge accumulation. Although detailed calculations are not available, the common folklore is that the typical size of the clusters in the mixed-phase state arising from the competition PS vs. $1/r$ Coulomb will be in the *nanometer* scale, i.e., just a few lattice spacings since the Mn–Mn distance is about 4 Å. This is the electronic "phase separated" state that one usually has in mind as interpolating between FM and AF. Small clusters of FM are expected to be created in the AF background, and as the hole density grows, these clusters will increase in number and eventually overcome the AF clusters. For more details see also Section 3.9, where the effort of other authors in the context of PS is also described.

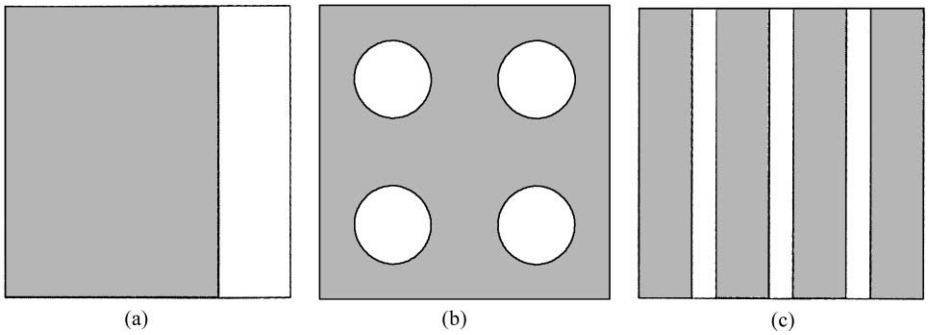

Fig. 3.4.5. Schematic representation of a macroscopic phase-separated state (a), as well as possible charge inhomogeneous states stabilized by the long-range Coulomb interaction (spherical droplets in (b), stripes in (c)). Reproduced from Moreo et al. (1999). Similar conclusions have been reached before in the context of phase separation applied to models of high-temperature superconductors.

3.4.2. Spin incommensurability and stripes

In the regime of intermediate or small J_H, the one-orbital model does not have ferromagnetism at small hole densities, which is reasonable since a large J_H was needed in the discussion of Section 3.1 to understand the stabilization of a spin polarized phase. Instead, in this regime of J_H the spin sector develops *incommensurability* (IC), namely the peak in the Fourier transform of the real space spin–spin correlations is neither at 0 (FM) nor at π (AF), but at intermediate momenta. This feature is robust and it appears both in 1D and 2D simulations, as well as with both classical and quantum spins (Yunoki et al., 1998a; Dagotto et al., 1998). An example in 2D is presented in Fig. 3.4.6a. Since a regime with IC characteristics had not been found in experiments by the time the initial Monte Carlo simulations were carried out, the spin IC regime was not given much importance, and its origin remained unclear. However, recent neutron scattering results (Adams et al., 2000; Dai et al., 2000; Kubota et al., 2000) suggest that stripes may appear in some compounds, similar to that found in the cuprates. This result induced us to further examine the numerical data obtained in the original Monte Carlo simulations. It turns out that the spin IC structure found in the 2D one-orbital model has its origin in *stripes*, as shown in Fig. 3.4.6b. These structures correspond to 1D-like regions of the 2D plane that are populated by holes, leaving undoped the area between the stripes, similar to those structures that are believed to occur in some high-temperature superconductors and (t–J)-like models (Tranquada, 1995; Dai et al., 1998; Mook, 1998; Bourges et al., 2000. See also Emery et al., 1997; Zaanen, 1998; White and Scalapino, 1998; Martins et al., 2000). In fact, the results shown in Fig. 3.4.6b are very similar to those found recently by Buhler et al. (2000) in the context of the so-called spin-fermion model for cuprates, with classical spins used for the spins (the spin-fermion model for cuprates and the one-orbital model for manganites only differ in the sign of the Hund coupling). Stripe formation with hole density close to $\langle n \rangle = 1.0$, i.e., electronic density close to 0.0, is natural near phase separation regimes. Stripes have also been identified in the more realistic case of the two-orbital model (see Section 3.5 below). A discussion of the similarities and differences between the electronic phase separation scenarios for manganites and cuprates, plus a substantial body of references, can be found in Hotta et al. (2000).

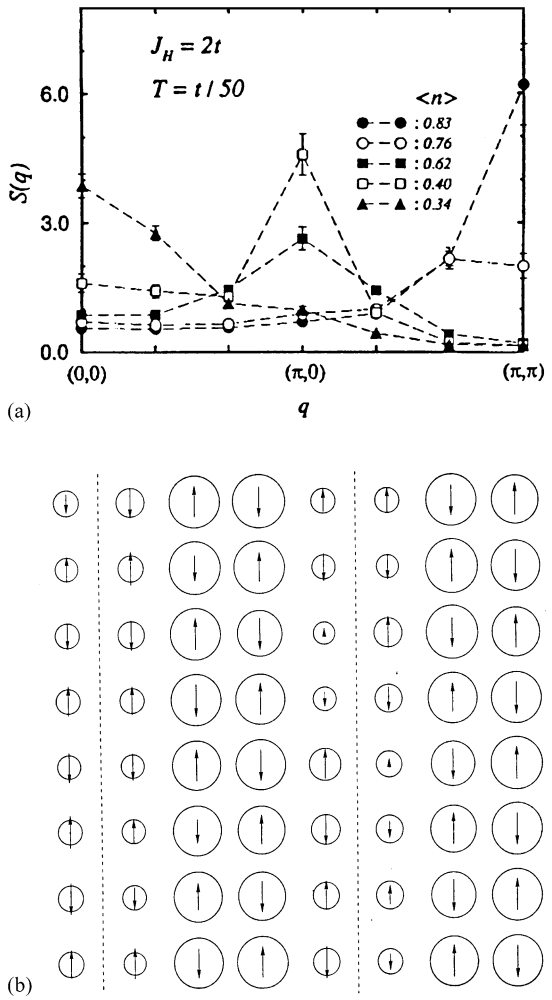

Fig. 3.4.6. (a) Spin–spin correlation $S(\boldsymbol{q})$ vs. momentum, for 2D clusters. Couplings, temperature, and densities are indicated. The cluster is 6×6. Reproduced from Dagotto et al. (1998). (b) Snapshot obtained with Monte Carlo techniques applied to the one-orbital model using an 8×8 cluster, $J_{\mathrm{H}} = 2.0$ and $\langle n \rangle = 0.75$, illustrating the existence of stripes. The area of the circles are proportional to the electronic density at each site. The arrows are proportional to the value of the z-component of the spin. Result courtesy of C. Buhler, using a program prepared by S. Yunoki (unpublished).

3.4.3. Influence of J_{AF}

The one-orbital model described in Section 3.3 included an antiferromagnetic coupling among the localized spins that is regulated by a parameter J_{AF}, which was not considered in the previous subsections. In principle, this number is the smallest of the couplings in the model according to the estimations discussed in Section 3.3, and one may naively believe that its presence is not important. However, this is incorrect as can be easily understood in the limit of $\langle n \rangle = 0.0$ ($x = 1.0$), which is realized in materials such as $CaMnO_3$. This compound is antiferromagnetic and it is widely believed that such magnetic order is precisely caused by the coupling among the localized spins. Then, J_{AF} cannot be simply neglected. In addition, the studies shown below highlight the

(unexpected) importance of this coupling in other contexts: it has been found to be crucial for the stabilization of an A-type AF phase at $\langle n \rangle = 1.0$ in the two-orbital model, and also to make stable the famous CE-phase at $\langle n \rangle = 0.5$, at least within the context of a two-orbital model with strong electron Jahn–Teller phonon coupling. Then, it is important to understand the influence of $J_{\rm AF}$ starting with the one-orbital model.

The first numerical study that included a nonzero $J_{\rm AF}$ was reported by Yunoki and Moreo (1998) (note that hereafter J' will be an alternative notation for $J_{\rm AF}$, as used sometimes in previous literature). An interesting observation emerging from their analysis is that PS occurs not only near $\langle n \rangle = 1.0$ but also near the other extreme of $\langle n \rangle = 0.0$, where again a FM–AF competition exists. In this regime, Batista et al. (2000) have shown the formation of ferromagnetic polarons upon electron doping of the $\langle n \rangle = 0.0$ AF-state. Considering several of these polarons it is likely that extended structures may form, as in a phase separated state. The 1D phase diagram at low temperature in the $(J', \langle n \rangle)$-plane is in Fig. 3.4.7. Three AF regions and two PS regions are shown, together with a FM regime at intermediate densities already discussed in previous subsections. In addition, a novel phase exists at intermediate values of J' and $\langle n \rangle$. This phase has a curious spin arrangement given by a periodically arranged pattern $\uparrow\uparrow\downarrow\downarrow$ of localized spins, namely it has an equal number of FM and AF links, and for this reason interpolates at constant density between FM and AF phases (see also Garcia et al., 2000; Aliaga et al., 2000a). This phase is a precursor in 1D of the CE-phase in 2D, as will be discussed later. Calculations of the Drude weight show that this state is insulating, as expected since it has AF links.

3.4.4. Quantum localized spins

An important issue in the context discussed in this section is whether the approximation of using classical degrees of freedom to represent the t_{2g} spins is sufficiently accurate. In principle, this spin should be $S = 3/2$, which appears large enough to justify the use of classical spins. Unfortunately, it is very difficult to study quantum spins in combination with mobile fermions, and the approximation can be explicitly tested only in a few cases. One of them is a 1D system, where the density matrix renormalization group (DMRG) method and Lanczos techniques allow for a fairly accurate characterization of the fully quantum model. The phase diagram obtained in this context by Dagotto et al. (1998) is reproduced in Fig. 3.4.8. Fortunately, the shape and even quantitative aspects of the diagram (with AF, FM, IC and PS regions) are in good agreement with those found with classical spins. The PS regime certainly appears in the study, although finite values of $J_{\rm H}$ are needed for its stabilization. The study leading to Fig. 3.4.8 was carried out in the canonical ensemble, with fixed number of particles, and the possibility of PS was analyzed by using the compressibility (κ), criterion where a $\kappa < 0$ corresponds to an unstable system, as it is well known from elementary thermodynamic considerations. κ^{-1} is proportional to the second derivative of the ground state with respect to the number of particles, which can be obtained numerically for N electrons by discretizing the derivative using the ground state energies for N, $N + 2$ and $N - 2$ particles at the fixed couplings under consideration (for details see Dagotto et al., 1998). Following this procedure, a negative compressibility was obtained, indicative of phase separation. Another method is to find μ from the ground state energies at various number of electrons, and plot density vs. μ. As in Monte Carlo simulations with classical spins, a discontinuity appears in the results in the regime of PS. It is clear that the tendency toward these unstable regimes, or mixed states after proper consideration of the $1/r$ Coulomb interaction, is very robust and independent of details in

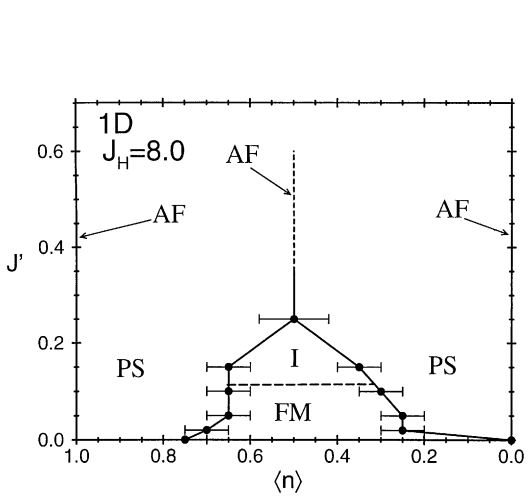

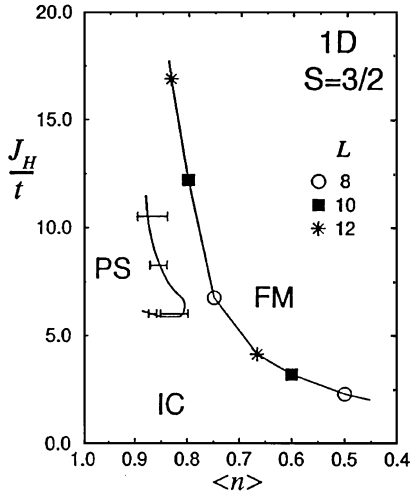

Fig. 3.4.7. Phase diagram of the one-orbital model for manganites including an antiferromagnetic Heisenberg coupling among the localized spins, here denoted by J' (while in other parts of the text it is referred to as J_{AF}). The Hund coupling is fixed to 8 and $t = 1$. Two PS regions are indicated, three AF regimes, and one FM phase. The "I" insulating phase is described in more detail in the text. Reproduced from Yunoki and Moreo (1998).

Fig. 3.4.8. Phase diagram of the one-orbital model with $S = 3/2$ localized t_{2g}-spins, obtained with the DMRG and Lanczos methods applied to the chains of finite length L indicated. The notation is as in previous figures. Results reproduced from Dagotto et al. (1998), where more details can be found.

the computational studies. Results for the much simpler case of localized $S = 1/2$ spins can also be obtained numerically. The phase diagram (Dagotto et al., 1998) is still in qualitative agreement with $S = 3/2$ and ∞, although not quantitatively. PS appears clearly in the computational studies, as well as FM and spin IC phases.

3.4.5. Influence of long-range Coulomb interactions

As already explained before, it is expected that long-range Coulomb interactions will break the electronic PS regime with two macroscopic FM and AF regions, into a stable state made out of small coexisting clusters of both phases. However, calculations are difficult in this context. One of the few attempts was carried out by Malvezzi et al. (1999) using a 1D system. On-site U and nearest-neighbor V Coulomb interactions were added to the one-orbital model. The resulting phase diagram can be found in Fig. 14 of Malvezzi et al. (1999). At $V = 0$, the effect of U is not much important, namely PS is found at both extremes of densities, and in between a charge-disordered FM-phase is present, results in good agreement with those described in previous subsections. This is reasonable since a large Hund coupling by itself suppresses double occupancy even without U added explicitly to the model.

However, when V is switched-on, the PS regime of small hole density is likely to be affected drastically due to the charge accumulation. Indeed, this regime is replaced by a charge-density wave with a peak in the spin structure factor at a momentum different from 0 and π (Malvezzi et al., 1999). Holes are spread over a few lattice spacings, rather than being close to each other as in PS. In the other extreme of many holes, the very small electronic density makes V not as important. In

between, the FM-phase persists up to large value of V, but a transition exists in the charge sector, separating a charge disordered from a charge-ordered state. Certainly more work in this interesting model is needed to fully clarify its properties, and extensions to 2D would be important, but the results thus far are sufficient to confirm that PS is rapidly destroyed by a long-range Coulomb interaction leading to nontrivial charge density waves (Malvezzi et al., 1999).

3.4.6. Tendencies toward electronic phase separation in t–J-like models for transition metal oxides

The first indications of a strong tendency toward electronic phase separation in models for manganites were actually obtained by Riera et al. (1997) using computational techniques applied to t–J-like models for Ni- and Mn-oxide. In these models, it was simply assumed that the Hund coupling was sufficiently large that the actual relevant degrees of freedom at low energy are "spins" (of value 2 and 1, for Mn- and Ni-oxide, respectively) and "holes" (with spin 3/2 and 1/2, for Mn- and Ni-oxide, respectively). The Hamiltonian at large J_H can be perturbatively deduced from the quantum one-orbital model and its form is elegant, with hole hopping which can take place with rearrangement of the spin components of "spin" and "hole". Details can be found in Riera et al. (1997). The phase diagram found with DMRG and Lanczos methods is in Fig. 3.4.9 for the special case of one dimension. The appearance of ferromagnetic and phase-separated regions is clear in this figure, and the tendency grows as the magnitude of the spin grows. In between PS and FM, regions with hole binding were identified that have not been studied in detail yet. The result in Fig. 3.4.9 has to be contrasted against those found for the standard 1D t–J model for the cuprates (see results in Dagotto, 1994) where the PS regime appears at unphysically large values of J/t, and FM was basically absent. There is a substantial *qualitative* difference between the results found for

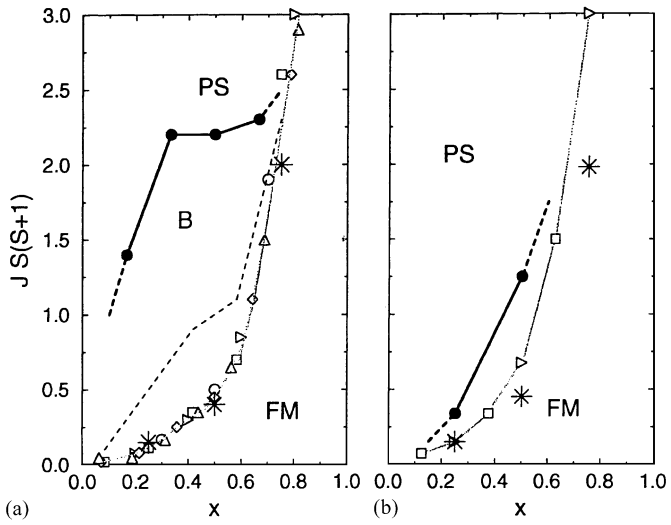

Fig. 3.4.9. Phase diagram of t–J-like models in 1D corresponding to (a) nickelates and (b) manganites. J is the coupling between Heisenberg spins at each site in the large Hund coupling limit and x is the hole density. PS, B, and FM, denote phase-separated, hole binding, and ferromagnetic phases. For the meaning of the various symbols used to find the boundaries of the phases see Riera et al. (1997). DMRG and Lanczos techniques were used for this result.

Cu-oxides and those of Ni- and Mn-oxide, mainly caused by the presence of localized spins in the last two. This suggests that cuprates do *not* share the same physics as other transition metal oxides. In particular, it is already known that cuprates are superconductors upon hole doping, while nickelates and manganites are not.

3.5. *Main results*: *two orbital model*

3.5.1. *Phase diagram at density* $x = 0.0$

The results of the previous section showed that the one-orbital model for manganites contains interesting physics, notably a FM–AF competition that has similarities with those found in experiments. However, it is clear that to explain the notorious orbital order tendency in Mn-oxides, it is crucial to use a model with two orbitals, and in Section 3.3 such a model was defined for the case where there is an electron Jahn–Teller phonon coupling and also Coulomb interactions. Under the assumption that both localized t_{2g}-spins and phonons are classical, the model without Coulombic terms can be studied fairly accurately using numerical and mean-field approximations. Results obtained with both approaches will be presented here. For the case where Coulomb terms are included, unfortunately, computational studies are difficult but mean-field approximations can still be carried out.

As in the case of one orbital, let us start with the description of the phase diagram of the two-orbital model. In this model there are more parameters than in the previous case, and more degrees of freedom, thus at present only a fraction of parameter space has been investigated. Consider first the case of e_g-density $\langle n \rangle = 1.0$, which is relatively simple to study numerically since this density is easy to stabilize in the grand canonical simulations. It corresponds to having one electron on average per site, and in this respect it must be related to the physics found in hole undoped compounds such as $LaMnO_3$. Carrying out a Monte Carlo simulation in the localized spins and phonons, and considering exactly the electrons in the absence of an explicit Coulomb repulsion (as is done for the one-orbital case), a variety of correlations have been calculated to establish the $\langle n \rangle = 1.0$ phase diagram. Typical results for the spin and orbital structure factors, $S(q)$ and $T(q)$, respectively, at the momenta of relevance are shown in Fig. 3.5.1, obtained at a large Hund coupling equal to $8t$, $J' = 0.05t$, and a small temperature, plotted as a function of the electron–phonon coupling λ. Results at dimensions 1, 2 and 3 are shown. At small λ, $S(0)$ is dominant and $T(q)$ is not active. This signals a ferromagnetic state with disordered orbitals, namely a standard ferromagnet (note, however, that Khomskii (2000a) and Maezono and Nagaosa (2000) believe that this state in experiments may have complex orbital ordering). The result with FM tendencies dominating may naively seem strange given the fact that for the one-orbital model at $\langle n \rangle = 1.0$ an AF-state was found. But here two orbitals are being considered and one electron per site is 1/2 electron per orbital. In this respect, $\langle n \rangle = 1.0$ with two orbitals should be similar to $\langle n \rangle = 0.5$ for one orbital and indeed in the last case a ferromagnetic state was observed (Section 3.4).

Results become much more interesting as λ grows beyond 1. In this case, first $T(\boldsymbol{Q})$ increases rapidly and dominates (in the spin sector still $S(0)$ dominates, i.e. the system remains ferromagnetic in the spin channel). The momentum $\boldsymbol{Q}$ corresponds to π, (π, π), and (π, π, π), in 1D, 2D, and 3D, respectively. It denotes a *staggered* orbital order, namely a given combination of the a and b original orbitals is the one mainly populated in the even sites of the cluster, while in the odd sites

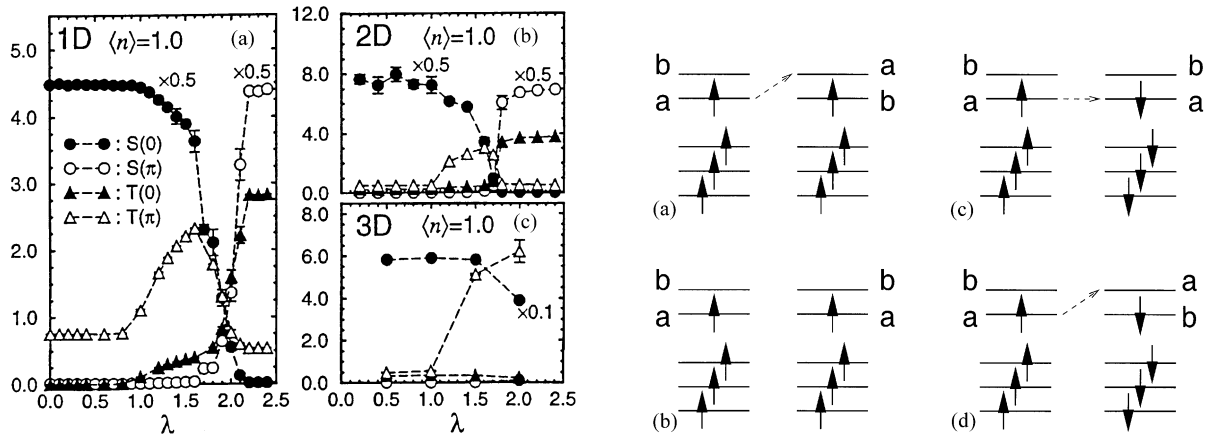

Fig. 3.5.1. (a) $T(q)$ and $S(q)$, orbital and spin structure factors vs. λ, working with the two-orbital model at $\langle n\rangle = 1.0$, low temperature, $J_H = 8$, $J' = 0.05$, and in 1D chains. The hopping set $t_{aa} = t_{bb} = 2t_{ab} = 2t_{ba}$ was used, but qualitatively the results are similar for other hoppings. (b) Same as (a) but using a 4×4 cluster and realistic hoppings (Section 3.3). (c) Same as (a) but for a 4^3 cluster and realistic hoppings, and using $J_H = \infty$. Results reproduced from Yunoki et al. (1998b), where more details can be found.

Fig. 3.5.2. Magnetic and orbital structures discussed in the text to justify the Monte Carlo results for the two-orbital model at electronic density 1.0.

another orbital combination is preferred. These populated orbitals are not necessarily only the two initial ones used in the definition of the Hamiltonian, in the same way that in a Heisenberg spin system not only spins up and down in the z-direction (the usual basis) are possible in mean value. Actually, spins can order with a mean-value pointing in any direction depending on the model and couplings, and the same occurs with the orbitals, which in this respect are like "pseudo-spins". A particular combination of the original orbitals 1 and 2 could be energetically the best in even sites and some other combination in the odd sites.

In Fig. 3.5.1, as λ increases further, a second transition was identified this time into a state which is staggered in the spin, and uniform in the orbitals. Such a state is the one in correspondence with the AF-state found in the one-orbital model, namely only one orbital matters at low energies and the spin, as a consequence, is antiferromagnetic. However, from the experimental point of view, the intermediate regime between 1.0 and 2.0 is the most relevant, since staggered orbital order is known to occur in experiments. Then, the one orbital model envisioned to work for manganites, at least close to $\langle n\rangle = 1.0$ due to the static Jahn–Teller distortion, actually does not work even there since it misses the staggered orbital order but instead assumes a uniform order. Nevertheless, the model is qualitatively interesting, as remarked upon before.

Why does orbital order occur here? This can be easily understood perturbatively in the hopping t, following Fig. 3.5.2 where a single Mn–Mn link is used and the four possibilities (spin FM or AF, orbital uniform or staggered) are considered. A hopping matrix only connecting the same orbitals, with hopping parameter t, is assumed for simplicity. The energy difference between e_g-orbitals at a given site is E_{JT}, which is a monotonous function of λ. For simplicity, in the notation let us refer to orbital uniform (staggered) as orbital "FM" ("AF"). Case (a) in Fig. 3.5.2 corresponds to spin FM and orbital AF: In this case when an electron moves from orbital a on the left to the same orbital on

the right, which is the only possible hopping by assumption, an energy of order E_{JT} is lost, but kinetic energy is gained. As in any second-order perturbative calculation the energy gain is then proportional to t^2/E_{JT}. In case (b), both spin and orbital FM, the electrons do not move and the energy gain is zero (again, the nondiagonal hoppings are assumed negligible just for simplicity). In case (c), the spin are AF but the orbitals are FM. This is like a one orbital model and the gain in energy is proportional to $t^2/(2J_H)$. Finally, in case (d) with AF in spin and orbital, both Hund and orbital splitting energies are lost in the intermediate state, and the overall gain becomes proportional to $t^2/(2J_H + E_{JT})$. As a consequence, if the Hund coupling is larger than E_{JT}, then case (a) is the best, as it occurs at intermediate E_{JT} values in Fig. 3.5.1. However, in the opposite case (orbital splitting larger than Hund coupling) case (c) has the lowest energy, a result also compatible to that found in Fig. 3.5.1. Then, the presence of orbital order can be easily understood from a perturbative estimation, quite similarly as done by Kugel and Khomskii (1974) in their pioneering work on orbital order. Recently, X-ray resonant scattering studies have confirmed the orbital order in manganites (Murakami et al., 1998a, b).

3.5.2. A-type AF at $x = 0.0$

The alert reader may have noticed that the state reported in the previous analysis at intermediate λ's is actually not quite the same state as found in experiments. It is known that the actual state has A-type AF spin order, while in the analysis of Fig. 3.5.1, such a state was not included. The intermediate λ region has FM spin in the three directions in the 3D simulations of that figure. Something else must be done in order to arrive at an A-type antiferromagnet. Recent investigations by Hotta et al. (1999) have shown that, in the context of the model with Jahn–Teller phonons, this missing ingredient is J_{AF} itself, namely by increasing this coupling from 0.05 to larger values, a transition from a FM to an A-type AF exists (the relevance of JT couplings at $\langle n \rangle = 1.0$ has also been remarked by Capone et al., 2000; see also Fratini et al., 2000). This can be visualized easily in Fig. 3.5.3 where the energy vs. J_{AF} at fixed intermediate λ and J_H is shown. Four regimes were identified: FM, A-AF, C-AF, and G-AF, states that are sketched also in that figure. The reason is simple: as J_{AF} grows, the tendency toward spin AF must grow since this coupling favors such an order. If J_{AF} is very large, then it is clear that a G-AF state must be the one that lowers the energy, in agreement with the Monte Carlo simulations. If J_{AF} is small or zero, there is no reason why spin AF will be favorable at intermediate λ and the density under consideration, and then the state is ferromagnetic to improve the electronic mobility. It should be no surprise that at intermediate J_{AF}, the dominant state is intermediate between the two extremes, with A- and C-type antiferromagnetism becoming stable in intermediate regions of parameter space.

It is interesting to note that similar results regarding the relevance of J_{AF} to stabilize the A-type order have been found by Koshibae et al. (1997) in a model with Coulomb interactions (see also Feiner and Olés, 1999). An analogous conclusion was found by Solovyev et al. (1996) and Ishihara et al. (1997a,b). Betouras and Fujimoto (1999), using bosonization techniques for the 1D one-orbital model, also emphasized the importance of J_{AF}, similarly as did Yi et al. (1999) based on Monte Carlo studies in two dimensions of the same model. The overall conclusion is that there are clear analogies between the strong Coulomb and strong Jahn–Teller coupling approaches, as discussed elsewhere in this review. Actually, in the mean-field approximation presented in Section 3.3 it was shown that the influence of the Coulombic terms can be hidden in simple redefinitions of the electron–phonon couplings (see also Benedetti and Zeyher, 1999). In our opinion, both

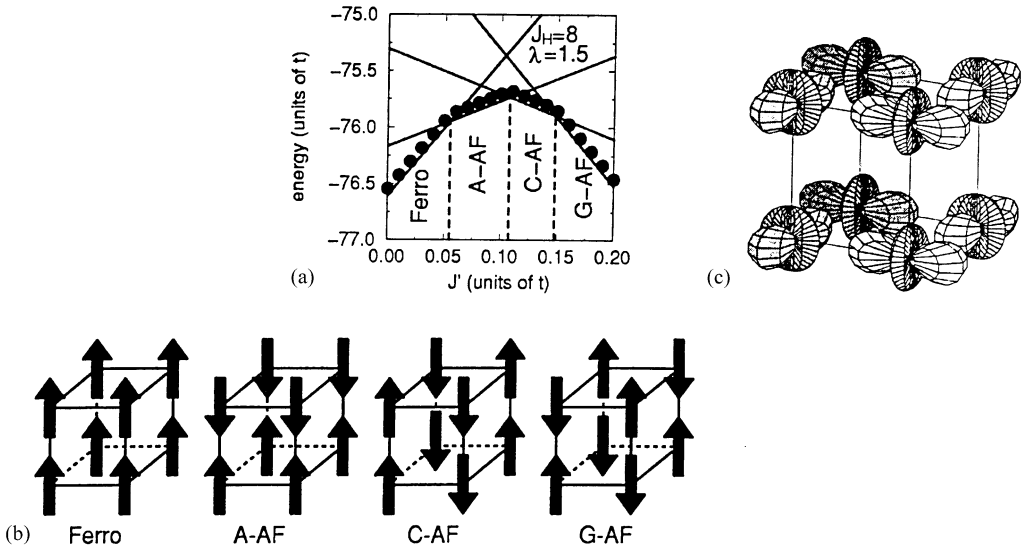

Fig. 3.5.3. (a) Total energy vs. J' on a 2^3 cluster at low temperature with $J_H = 8t$ and $\lambda = 1.5$. The results were obtained using Monte Carlo and relaxational techniques, with excellent agreement among them. (b) The four spin arrangements are also shown. (c) Orbital order corresponding to the A-type AF state. For more details the reader should consult Hotta et al. (1999).

approaches (JT and Coulomb) have strong similarities and it is not surprising that basically the same physics is obtained in both cases. Actually, Fig. 2 of Maezono et al. (1998b) showing the energy vs. J_{AF} in mean-field calculations of the Coulombic Hamiltonian without phonons is very similar to our Fig. 3.5.3, aside from overall scales. On the other hand, Mizokawa and Fujimori (1995, 1996) states that the A-type AF is stabilized only when the Jahn–Teller distortion is included, namely, the FM phase is stabilized in the purely Coulomb model, based on the unrestricted Hartree–Fock calculation for the d–p model.

The issue of what kind of orbital order is concomitant with A-type AF order is an important matter. This has been discussed at length by Hotta et al. (1999), and the final conclusion, after the introduction of perturbations caused by the experimentally known difference in lattice spacings between the three axes, is that the order shown in Fig. 3.5.3c minimizes the energy. This state has indeed been identified in recent X-ray experiments, and it is quite remarkable that such a complex pattern of spin and orbital degrees of freedom indeed emerges from mean-field and computational studies. Studies by van den Brink et al. (1999a) using purely Coulombic models arrived at similar conclusions.

3.5.3. Electronic phase separation with two orbitals

Now let us analyze the phase diagram at densities away from $\langle n \rangle = 1.0$. In the case of the one-orbital model, phase separation was very prominent in this regime. A similar situation was observed with two orbitals, as Fig. 3.5.4a–b illustrates where $\langle n \rangle$ vs. μ is shown at intermediate λ, $J_H = \infty$, and low temperature. A clear discontinuity is observed, both near $\langle n \rangle = 1.0$, as well as at

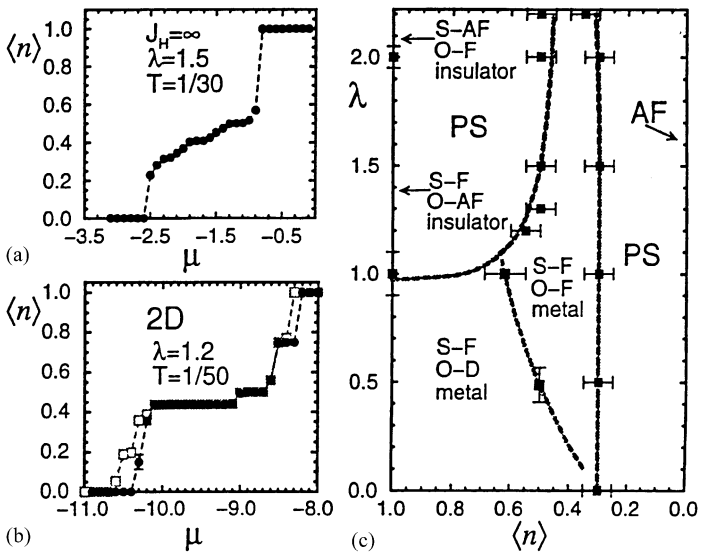

Fig. 3.5.4. (a) $\langle n\rangle$ vs. μ at the couplings and temperature indicated on a $L = 22$ site chain. The discontinuities characteristic of phase separation are clearly shown. (b) Same as (a) but in 2D at the parameters indicated. The two sets of points are obtained by increasing and decreasing μ, forming a hysteresis loop. (c) Phase diagram of the two orbitals model in 1D, $J_H = 8$, $J' = 0.05$, and using the hopping set $t_{aa} = t_{bb} = 2t_{ab} = 2t_{ba}$. The notation has been explained in the text. For more details see Yunoki et al. (1998b), from where this figure was reproduced.

low density. Measurements of spin and orbital correlations, as well as the Drude weight to distinguish between metallic and insulating behavior, have suggested the phase diagram in one dimension reproduced in Fig. 3.5.4c. There are several phases in competition. At $\langle n\rangle = 1.0$ the results were already described in the previous subsection. Away from the $\langle n\rangle = 1.0$ phases, only the spin-FM orbital-disordered survives at finite hole density, as expected due to the mapping at small λ into the one-orbital model with half the density. The other phases at $\lambda \geq 1.0$ are not stable, but electronic phase separation takes place. The $\langle n\rangle < 1.0$ extreme of the PS discontinuity is given by a spin-FM orbital-FM metallic state, which is a 1D precursor of the metallic orbitally ordered A-type state identified in some compounds precisely at densities close to 0.5. Then, the two states that compete in the $\langle n\rangle \sim 1.0$ PS regime differ in their orbital arrangement, but not in the spin sector. This is PS triggered by the *orbital* degrees of freedom, which is a novel concept. On the other hand, the PS observed at low density is very similar to that observed in the one-orbital model involving spin-FM and AF-states in competition. Finally, at $\langle n\rangle \sim 0.5$ and large λ, charge ordering takes place, but this phase will be discussed in more detail later. Overall, it is quite reassuring to observe that the stable phases in Fig. 3.5.4c all have an analog in experiments. This gives support to the models used and to the computational and mean-field techniques employed.

In addition, since all stable regions are realistic, it is natural to assume that the rest of the phase diagram, namely the PS regions, must also have an analog in experiments in the form of mixed-phase tendencies and nanometer-size cluster formation, as discussed in the case of the one-orbital model. PS is very prominent in all the models studied, as long as proper many-body techniques are employed. For instance, using accurate mean-field approximations, the PS

tendencies in 1D can also be properly reproduced (see Section 5 of Hotta, Malvezzi and Dagotto, 2000). It is also important that even in purely Coulombic cases (without JT phonons), PS has been found in 1D models in some regions of parameter space (see Hotta et al., 2000), and, thus, this phenomenon is not restricted to Jahn–Teller systems. Kagan et al. (2000) also reported phase separation near $x = 0.5$ without using JT phonons. Guerrero and Noack (2000) reported phase separation in a one-dimensional copper-oxide model with only Coulomb interactions. Varelogiannis (2000) found coexistence and competition of CO-, AF- and FM-phase in a multicomponent mean-field theory, without using a particular microscopic mechanism.

It is important to remark that plenty of work still remains to be done in establishing the phase diagram of the two-orbitals model. Studies in 2D carried out by our group suggest that the phase diagram is similar to that found in 1D, but details remain to be settled. The 3D diagram is known only in special cases. Although the experience gained in the one-orbital model suggests that all dimensions have similar phase diagrams, this issue remains to be confirmed in the two-orbital case at large λ. In addition, also note that the intermediate J_H regime has not been explored and surprises may be found there, such as the stripes described for the one-orbital case at intermediate Hund coupling. Work is in progress in this challenging area of research.

3.5.4. Charge ordering at $x = 0.5$ and the CE-state

The so-called CE-type AFM phase has been established as the ground state of half-doped perovskite manganites in the 1950s. This phase is composed of zigzag FM arrays of t_{2g}-spins, which are coupled antiferromagnetically perpendicular to the zigzag direction. Furthermore, the checkerboard-type charge ordering in the x–y plane, the charge stacking along the z-axis, and $(3x^2 - r^2/3y^2 - r^2)$ orbital ordering are associated with this phase.

Although there is little doubt that the famous CE-state of Goodenough, reviewed in Section 3.1, is indeed the ground state of $x = 0.5$ intermediate and low bandwidth manganites, only very recently such a state has received theoretical confirmation using unbiased techniques, at least within some models. In the early approach of Goodenough it was *assumed* that the charge was distributed in a checkerboard pattern, upon which spin and orbital order was found. But it would be desirable to obtain the CE-state based entirely upon a more fundamental theoretical analysis, as the true state of minimum energy of a well-defined and realistic Hamiltonian. If such a calculation can be done, as a bonus one would find out which states compete with the CE-state in parameter space, an issue very important in view of the mixed-phase tendencies of Mn-oxides, which cannot be handled within the approach of Goodenough.

One may naively believe that it is as easy as introducing a huge nearest-neighbor Coulomb repulsion V to stabilize a charge-ordered state at $x = 0.5$, upon which the reasoning of Goodenough can be applied. However, there are at least two problems with this approach. First, such a large V quite likely will destabilize the ferromagnetic charge-disordered state and others supposed to be competing with the CE-state. It may be possible to explain the CE-state with this approach, but not others also observed at $x = 0.5$ in large bandwidth Mn-oxides. Second, a large V would produce a checkerboard pattern in the *three* directions. However, experimentally it has been known for a long time (Wollan and Koehler, 1955) that the charge *stacks* along the z-axis, namely the same checkerboard pattern is repeated along z, rather than being shifted by one lattice spacing from plane to plane. A dominant Coulomb interaction V cannot be the whole story for $x = 0.5$ low-bandwidth manganese oxides.

The nontrivial task of finding a CE-state with charge stacked along the z-axis without the use of a huge nearest-neighbors repulsion has been recently performed by Yunoki et al. (2000) using the two-orbital model with strong electron Jahn–Teller phonon coupling. The calculation proceeded using an unbiased Monte Carlo simulation, and as an output of the study, the CE-state indeed emerged as the ground state in some region of coupling space. Typical results are shown in Fig. 3.5.5. In part (a) the energy at very low temperature is shown as a function of J_{AF} at fixed density $x = 0.5$, $J_H = \infty$ for simplicity, and with a robust electron–phonon coupling $\lambda = 1.5$ using the two-orbital model of Section 3.3. At small J_{AF}, a ferromagnetic phase was found to be stabilized, according to the Monte Carlo simulation. Actually, at $J_{AF} = 0.0$ it has not been possible to stabilize a partially AF-state at $x = 0.5$, namely the states are always ferromagnetic at least within the wide range of λ's investigated (but they can have charge and orbital order). On the other hand, as J_{AF} grows, a tendency to form AF links develops, as it happens at $x = 0.0$. At large J_{AF} eventually the system transitions to states that are mostly antiferromagnetic, such as the so-called "AF(2)" state of Fig. 3.5.5b (with an up–up–down–down spin pattern repeated along one axis, and AF coupling along the other axis), or directly a fully AF-state in both directions.

However, the intermediate values of J_{AF} are the most interesting ones. In this case the energy of the 2D clusters become flat as a function of J_{AF} suggesting that the state has the same number of FM and AF links, a property that the CE-state indeed has. By measuring charge correlations it was found that a checkerboard pattern is formed particularly at intermediate and large λ's, as in the CE-state. Finally, after measuring the spin and orbital correlations, it was confirmed that indeed the complex pattern of the CE-state was fully stabilized in the simulation. This occurs in a robust

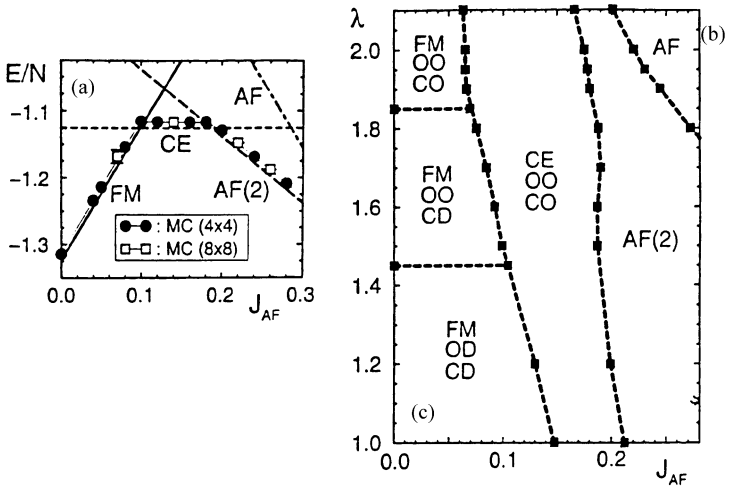

Fig. 3.5.5. (a) Monte Carlo energy per site vs. J_{AF} at density $x = 0.5$, $\lambda = 1.5$, low temperature $T = 1/100$, and $J_H = \infty$, using the two-orbital model in 2D with Jahn–Teller phonons (noncooperative ones). FM, CE, and AF states were identified measuring charge, spin, and orbital correlations. "AF(2)" denotes a state with spins $\uparrow\uparrow\downarrow\downarrow$ in one direction, and antiferromagnetically coupled in the other. The clusters used are indicated. (b) Phase diagram in the plane λ-J_{AF} at $x = 0.5$, obtained numerically using up to 8×8 clusters. All transitions are of first-order. The notation is the standard one (CD = charge disorder, CO = charge order, OO = orbital order, OD = orbital disorder). Results reproduced from Yunoki et al. (2000), where more details can be found.

portion of the λ–J_{AF} plane, as shown in Fig. 3.5.5b. The use of J_{AF} as the natural parameter to vary in order to understand the CE-state is justified based on Fig. 3.5.5b since the region of stability of the CE-phase is elongated along the λ-axis, meaning that its existence is not so much dependent on that coupling but much more on J_{AF} itself. It appears that some explicit tendency in the Hamiltonian toward the formation of AF links is necessary to form the CE-state. If this tendency is absent, a FM state if formed, while if it is too strong an AF-state appears. The $x = 0.5$ CE-state, similar to the A-type AF at $x = 0.0$, needs an intermediate value of J_{AF} for stabilization. The stability window is finite and in this respect there is no need to carry out a *fine* tuning of parameters to find the CE-phase. However, it is clear that there is a balance of AF and FM tendencies in the CE-phase that makes the state somewhat fragile.

Note that the transitions among the many states obtained when varying J_{AF} are all of *first* order, namely they correspond to crossings of levels at zero temperature. The first-order character of these transitions is a crucial ingredient of the recent scenario proposed by Moreo et al. (2000) involving mixed-phase tendencies with coexisting clusters with *equal* density, to be described in more detail below. Recently, first-order transitions have also been reported in the one-orbital model at $x = 0.5$ by Alonso et al. (2000a, b), as well as tendencies toward phase separation. Recent progress in the development of powerful techniques for manganite models (Alonso et al., 2000c; Motome and Furukawa, 2000a, b) will contribute to the clarification of these issues in the near future.

3.5.5. Charge stacking

Let us address now the issue of charge-stacking along the z-axis. For this purpose simulations using 3D clusters were carried out. The result for the energy vs. J_{AF} is shown in Fig. 3.5.6, with $J_H = \infty$ and $\lambda = 1.5$ fixed. The CE-state with charge stacking was found to be the ground state on a wide J_{AF} window. The reason that this state has lower energy than the so-called "Wigner-crystal" (WC) version of the CE-state, namely with the charge spread as much as possible, is once again the influence of J_{AF}. With a charge stacked arrangement, the links along the z-axis can all be simultaneously antiferromagnetic, thereby minimizing the energy. In the WC-state this is not possible.

It should be noted that this charge stacked CE-state is not immediately destroyed when the weak nearest-neighbor repulsion V is introduced to the model, as shown in the mean-field calculations

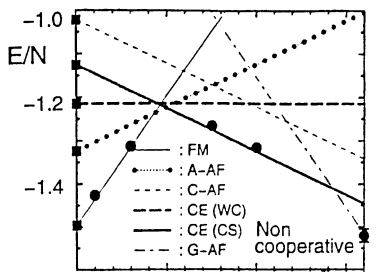

Fig. 3.5.6. Monte Carlo energy per site vs. J_{AF} obtained working on a 4^3 cube ($\lambda = 1.5$, $J_H = \infty$, $T = 1/100$). Results with both cooperative and noncooperative phonons are shown, taken from Yunoki et al. (2000). The state of relevance here is the "CE (CS)" one, which is the CE-state with charge stacking.

by Hotta et al. (2000). If V is further increased for a realistic value of J_{AF}, the ground state eventually changes from the charge stacked CE-phase to the WC version of the CE-state or the C-type AFM phase with WC charge ordering. As explained above, the stability of the charge stacked phase to the WC version of the CE-state is due to the magnetic energy difference. However, the competition between the charge-stacked CE-state and the C-type AFM phase with the WC structure is not simply understood by the effect of J_{AF}, since those two kinds of AFM phases have the same magnetic energy. In this case, the stabilization of the charge stacking originates from the difference in the geometry of the 1D FM-path, namely a zigzag-path for the CE-phase and a straight-line path for the C-type AFM state. As will be discussed later in detail, the energy for e_g-electrons in the zigzag path is lower than that in the straight-line path, and this energy difference causes the stabilization of the charge stacking. In short, the stability of the charge-stacked structure at the expense of V is supported by "the geometric energy" as well as the magnetic energy. Note that each energy gain is just a fraction of t. Thus, in the absence of other mechanisms to understand the charge stacking, another consequence of this analysis is that V actually must be substantially *smaller* than naively expected, otherwise such a charge pattern would not be stable. In fact, estimations given by Yunoki et al. (2000) suggest that the manganites must have a large dielectric function at short distances (see Arima and Tokura, 1995) to prevent the melting of the charge-stacked state.

Note also that the mean-field approximations by Hotta et al. (2000) have shown that on-site Coulomb interactions U and U' can *also* generate a 2D CE-state, in agreement with the calculations by van den Brink et al. (1999b). Then, the present authors believe that strong JT and Coulomb couplings tend to give similar results. This belief finds partial confirmation in the mean-field approximations of Hotta et al. (2000), where the similarities between a strong λ and (U, U') were investigated. Even doing the calculation with Coulombic interactions, the influence of J_{AF} is still crucial to inducing charge-stacking (note that the importance of this parameter has also been recently remarked by Mathieu et al. (2000) based on experimental results).

Many other authors carried out important work in the context of the CE-state at $x = 0.5$. For example, with the help of Hartree–Fock calculations, Mizokawa and Fujimori (1997) reported the stabilization of the CE-state at $x = 0.5$ only if Jahn–Teller distortions were incorporated into a model with Coulomb interactions. This state was found to be in competition with a uniform FM-state, as well as with an A-type AF-state with uniform orbital order. In this respect the result are very similar to those found by Yunoki et al. (2000) using Monte Carlo simulations. In addition, using a large nearest neighbor repulsion and the one-orbital model, charge ordering and a spin structure compatible with the zigzag chains of the CE-state was found by Lee and Min (1997) at $x = 0.5$. Also Jackeli et al. (1999) obtained charge-ordering at $x = 0.5$ using mean-field approximations and a large V. Charge-stacking was not investigated by those authors. The CE-state in $x = 0.5$ $Pr_{1-x}Ca_xMnO_3$ was also obtained by Anisimov et al. (1997) using LSDA + U techniques.

3.5.6. *Topological origin of the $x = 0.5$ CE-state*

The fact that λ does not play the most crucial role for the CE-state also emerges from the "topological" arguments of Hotta et al. (2000), where at least the formation of zigzag ferromagnetic chains with antiferromagnetic interchain coupling, emerges directly for $\lambda = 0$ and large J_H, as a consequence of the "band-insulator"character of those chains. Similar conclusions as those reached by Hotta et al. (2000), were independently obtained by Solovyev and Terakura (1999),

Solovyev (2000), and by van den Brink et al. (1999b). The concept of a band insulator in this context was first described in Hotta et al. (1998).

To understand the essential physics present in half-doped manganites, it is convenient to consider the complicated CE-structure in Hamiltonians simpler than those analyzed in Section 3.3. Based on the concept of "adiabatic continuation" for the introduction of the JT distortion and/or the Coulombic interactions, the following approximations will be made: (i) $H = H^{\infty}(E_{\rm JT} = U' = V = 0)$: In the first place, this simple Hamiltonian is considered based on the DE mechanism, but even in this situation, qualitative concepts can be learned for the stabilization of the zigzag AFM phase. (ii) $H = H^{\infty}(E_{\rm JT} \neq 0, U' = V = 0)$: In order to consider the charge and orbital ordering, the non-cooperative JT phonons are included in the two-orbital DE model by using the analytic MFA. In particular, the charge-stacked structure is correctly reproduced, and its origin is clarified based on a "topological" framework. (iii) $H = H^{\infty}(E_{\rm JT} \neq 0, U' \neq 0, V \neq 0)$. Here the effect of the long-range Coulomb interaction for the charge-stacked phase is discussed within the MFA. (iv) $H = H_{\rm JT}$ both for JT and non-JT phonons. Finally, to complete the above discussions, unbiased calculations for the JT model are performed using Monte Carlo simulations and the relaxation method. In this subsection, a peculiar "band-insulating" state of the CE-type is discussed in detail by focusing on the effect of the local phase ξ_i for determining the orbitals.

As is well known, the CE-type antiferromagnetic phase is composed of a bundle of spin-FM chains, each with the zigzag geometry, and with antiferromagnetic interchain coupling. Although the reason for the stabilization of this special zigzag structure should be clarified further, for the time being let us discuss what happens if this zigzag geometry is assumed, and how it compares with a straight line. To simplify the discussion, the limiting case of $J_{\rm H} = \infty$ is considered. Namely, the $e_{\rm g}$-electrons can move only along the zigzag FM path, since the hopping perpendicular to the zigzag direction vanishes due to the standard DE mechanism and the antiferromagnetism between chains, indicating that the spin degree of freedom can be effectively neglected. Thus, the problem is reduced to the analysis of the $e_{\rm g}$-electron motion along the one-dimensional zigzag chain. However, it should be emphasized that this is still a highly nontrivial system.

To solve the present one-body problem, a unit cell is defined as shown in Fig. 3.5.7, in which the hopping amplitudes change with a period of four lattice spacings, since the hopping direction changes as $\{\ldots, x, x, y, y, \ldots\}$ along the zigzag chain, with $t^{x}_{\mu\nu} = -t^{y}_{\mu\nu}$ for $\mu \neq \nu$ according to the values of the hopping amplitudes discussed before. This difference in sign, i.e., the phase change, is essential for this problem. To make this point clear, it is useful to transform the spinless $e_{\rm g}$-electron operators by using a unitary matrix as (see Koizumi et al., 1998a)

$$\begin{pmatrix} \alpha_i \\ \beta_i \end{pmatrix} = \frac{1}{\sqrt{2}} \begin{pmatrix} 1 & {\rm i} \\ 1 & -{\rm i} \end{pmatrix} \begin{pmatrix} c_{i{\rm a}} \\ c_{i{\rm b}} \end{pmatrix}. \tag{91}$$

After simple algebra, $H_{\rm kin}$ is rewritten as

$$H_{\rm kin} = -t_0/2 \sum_{i,a} \left(\alpha_i^{\dagger}\alpha_{i+a} + \beta_i^{\dagger}\beta_{i+a} + {\rm e}^{{\rm i}\phi_a}\alpha_i^{\dagger}\beta_{i+a} + {\rm e}^{-{\rm i}\phi_a}\beta_i^{\dagger}\alpha_{i+a}\right), \tag{92}$$

where the phase ϕ_a depends only on the hopping direction, and it is given by $\phi_x = -\phi$, $\phi_y = \phi$, and $\phi_z = 0$, with $\phi = \pi/3$. Note that the $e_{\rm g}$-electron picks up a phase change when it moves between different neighboring orbitals. In this expression, the effect of the change of the local phase is correctly included in the Hamiltonian.

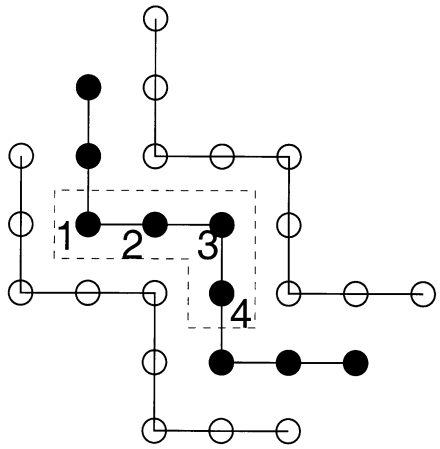

Fig. 3.5.7. The unit cell for the zigzag FM chain in the CE-type AFM phase at $x = 0.5$. Note that the hopping direction is changed periodically as $\{\ldots, x, x, y, y, \ldots\}$.

To introduce the momentum k along the zigzag chain, the Bloch's phase $e^{\pm ik}$ is added to the hopping term between adjacent sites. Then, the problem is reduced to finding the eigenvalues of an 8×8 matrix, given by

$$\hat{h}\begin{pmatrix} \psi_{\alpha 1} \\ \psi_{\beta 1} \\ \psi_{\alpha 2} \\ \psi_{\beta 2} \\ \psi_{\alpha 3} \\ \psi_{\beta 3} \\ \psi_{\alpha 4} \\ \psi_{\beta 4} \end{pmatrix} = \varepsilon_k \begin{pmatrix} \psi_{\alpha 1} \\ \psi_{\beta 1} \\ \psi_{\alpha 2} \\ \psi_{\beta 2} \\ \psi_{\alpha 3} \\ \psi_{\beta 3} \\ \psi_{\alpha 4} \\ \psi_{\beta 4} \end{pmatrix}, \tag{93}$$

where $\psi_{\alpha j}$ and $\psi_{\beta j}$ are the basis function for α- and β-electron at the j-site of the unit cell, respectively, and the Hamiltonian matrix $\hat{h}$ is given by

$$\hat{h} = -\frac{t_0}{2}\begin{pmatrix} \hat{O} & \hat{T}_k^x & \hat{O} & \hat{T}_k^{y*} \\ \hat{T}_k^{x*} & \hat{O} & \hat{T}_k^x & \hat{O} \\ \hat{O} & \hat{T}_k^{x*} & \hat{O} & \hat{T}_k^y \\ \hat{T}_k^y & \hat{O} & \hat{T}_k^{y*} & \hat{O} \end{pmatrix}. \tag{94}$$

Here $\hat{O}$ is the 2×2 matrix in which all components are zeros, and the hopping matrix $\hat{T}_k^a$ along the $\boldsymbol{a}$-direction is defined by

$$\hat{T}_k^a = e^{ik}\begin{pmatrix} 1 & e^{i\phi_a} \\ e^{-i\phi_a} & 1 \end{pmatrix}, \tag{95}$$

where note again that $-\phi_x = \phi_y = \phi = \pi/3$.

Although it is very easy to solve the present eigenvalue problem by using the computer, it is instructive to find the solution analytically. In the process of finding this solution, several important points will be clarified. First, note that there are two eigenfunctions of the 8×8 matrix which have a "localized" character, satisfying

$$\hat{h}(\psi_{\alpha 2} - e^{-i\phi}\psi_{\beta 2}) = 0 \tag{96}$$

and

$$\hat{h}(\psi_{\alpha 4} - e^{+i\phi}\psi_{\beta 4}) = 0 \, . \tag{97}$$

As easily checked by simple algebra, those localized basis functions correspond to $y^2 - z^2$ and $z^2 - x^2$ orbitals at sites 2 and 4, respectively. By orthogonality, the active orbitals are then fixed as $3x^2 - r^2$ and $3y^2 - r^2$ at sites 2 and 4, respectively. This fact suggests that if some potential acts over the e_g-electrons, the $(3x^2 - r^2/3y^2 - r^2)$-type orbital ordering immediately occurs in such a one-dimensional zigzag path due to the standard Peierls instability. This point will be discussed again later in the context of charge-orbital ordering due to the JT distortion.

To find the other extended eigenstates, it is quite natural to consider active basis functions at sites 2 and 4, given by $(\psi_{\alpha 2} + e^{-i\phi}\psi_{\beta 2})/\sqrt{2}$ and $(\psi_{\alpha 4} + e^{+i\phi}\psi_{\beta 4})/\sqrt{2}$, respectively. Then, the bonding and antibonding combinations of those basis are constructed by including appropriate phases such as

$$\Phi_1^{\pm} = (1/2)[(e^{-i\phi/2}\psi_{\alpha 4} + e^{i\phi/2}\psi_{\beta 4}) \pm (e^{i\phi/2}\psi_{\alpha 2} + e^{-i\phi/2}\psi_{\beta 2})] \, . \tag{98}$$

By acting with $\hat{h}$ over $\Phi_1^{\pm}$, it is found that two kinds of 3×3 block Hamiltonians $\tilde{h}^{\pm}$ can be constructed using new basis functions defined as

$$\Phi_2^{\pm} = (\psi_{\alpha 1} \pm \psi_{\beta 3})/\sqrt{2} \tag{99}$$

and

$$\Phi_3^{\pm} = (\psi_{\beta 1} \pm \psi_{\alpha 3})/\sqrt{2} \, . \tag{100}$$

As expected, the block Hamiltonian including the ground state is constructed using the bonding-type basis functions

$$\tilde{h}^{+}\begin{pmatrix} \Phi_1^{+} \\ \Phi_2^{+} \\ \Phi_3^{+} \end{pmatrix} = \varepsilon_k^{+}\begin{pmatrix} \Phi_1^{+} \\ \Phi_2^{+} \\ \Phi_3^{+} \end{pmatrix}, \tag{101}$$

where the 3×3 matrix $\tilde{h}^{+}$ is given by

$$\tilde{h}^{+} = -\sqrt{2}t_0\begin{pmatrix} 0 & \cos k_- & \cos k_+ \\ \cos k_- & 0 & 0 \\ \cos k_+ & 0 & 0 \end{pmatrix} \tag{102}$$

with $k_{\pm} = k \pm \phi/2$. By solving this eigenvalue problem, it can be easily shown that the eigenenergies are

$$\varepsilon_k^{+} = 0, \ \pm t_0\sqrt{2 + \cos(2k)} \, . \tag{103}$$

Note here that the momentum k is restricted to the reduced zone, $-\pi/4 \le k \le \pi/4$. As expected, the lowest-energy band has a minimum at $k = 0$, indicating that this block correctly includes the ground state of the one e_g-electron problem. At a first glance, this point appears obvious, but if the effect of the local phase is not treated correctly, an unphysical solution easily appears, as will be discussed below.

The block Hamiltonian for the antibonding sector is given by

$$\tilde{h}^- \begin{pmatrix} \Phi_1^- \\ \Phi_2^- \\ \Phi_3^- \end{pmatrix} = \varepsilon_k^- \begin{pmatrix} \Phi_1^- \\ \Phi_2^- \\ \Phi_3^- \end{pmatrix} \tag{104}$$

with

$$\tilde{h}^- = -\sqrt{2}t_0 \begin{pmatrix} 0 & \mathrm{i}\sin k_- & \mathrm{i}\sin k_+ \\ -\mathrm{i}\sin k_- & 0 & 0 \\ -\mathrm{i}\sin k_+ & 0 & 0 \end{pmatrix}. \tag{105}$$

The eigenenergies are given by

$$\varepsilon_k^- = 0, \ \pm t_0\sqrt{2-\cos(2k)}\,. \tag{106}$$

In summary, eight eigenenergies have been obtained as

$$\varepsilon_k = 0, \ \pm t_0\sqrt{2+\cos(2k)}, \ \pm t_0\sqrt{2-\cos(2k)}\,, \tag{107}$$

where the flat band $\varepsilon_k = 0$ has four-fold degeneracy. The band structure is shown in Fig. 3.5.8. The most remarkable feature is that the system is *band-insulating*, with a bandgap of value t_0 for quarter filling, i.e., $x = 0.5$. This band insulating state, without any explicit potential among the electrons moving along the zigzag chains, is caused by the phase difference between $t_{\mu v}^x$ and $t_{\mu v}^y$. Intuitively, such band-insulator originates in the presence of a standing-wave state due to the interference between two traveling waves running along the x- and y-direction. In this interference picture, the nodes of the wavefunction can exist on "the corner" of the zigzag structure, and the probability amplitude becomes larger in the "straight" segment of the path. Thus, even a weak potential can produce the charge and orbital ordering based on this band-insulating phase. Since t_0 is at least of the order of 1000 K, this band-insulating state is considered to be very robust. In fact, if some potential is included into such an insulating phase, the system maintains its "insulating" properties, and a modulation in the orbital density appears.

The problem in the zigzag one-dimensional chain provided us with a typical example to better understand the importance of the additional factor $\mathrm{e}^{\mathrm{i}\xi_i/2}$ in front of the 2×2 SU(2) unitary matrix to generate the phase dressed operator at each site. As clearly shown above, the "a" and "b" orbitals should be chosen as "a" $= y^2 - z^2$ and "b" $= 3x^2 - r^2$ at site 2, and "a" $= z^2 - x^2$ and "b" $= 3y^2 - r^2$ at site 4, respectively. Namely, $\xi_2 = 2\pi/3$ and $\xi_4 = 4\pi/3$. The reason for these choices of ξ_i is easily understood due to the fact that the orbital tends to polarize along the hopping direction to maximize the overlap. Thus, to make the Hamiltonian simple, it is useful to fix the orbitals at sites 2 and 4 as $\xi_2 = 2\pi/3$ and $\xi_4 = 4\pi/3$. Here, the phase factor $\mathrm{e}^{\mathrm{i}\xi_i/2}$ in the basis function is essential to reproduce exactly the same solution as obtained in the discussion above. As

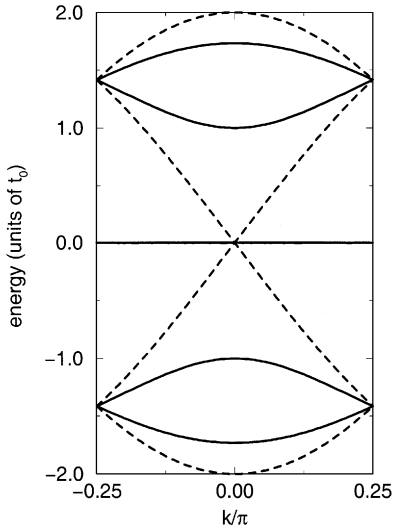

Fig. 3.5.8. Band structure for the zigzag 1D chain (solid curve) in the reduced zone $-\pi/4 \leq k \leq \pi/4$. For reference, the band structure $-2t_0 \cos k$ for the straight 1D path is also shown (broken curve). Note that the line at zero energy indicates the four-fold degenerate flat-band present for the zigzag 1D path.

already mentioned, in a single-site problem, this phase factor can be neglected, since it provides only an additional phase to the whole wave function. However, if the e_g-electron starts moving from site to site, the accumulation of the phase difference between adjacent sites does not lead just to an additional phase factor to the whole wave function. In fact, if this additional phase is accidentally neglected, the band structure will shift in momentum space as $k \to k + \pi$, indicating that the minimum of the lowest-energy band is not located at $k = 0$, but at $k = \pi$, as already pointed out by Koizumi et al. (1998b). Of course, this can be removed by the redefinition of k by including "the crystal momentum", but it is not necessary to redefine k, if the local phase factors are correctly included in the problem.

Now let us discuss the stabilization of the zigzag structure in the CE-type phase. Although it is true that the zigzag one-dimensional FM chain has a large band gap, this fact does not guarantee that this band-insulating phase is the lowest-energy state. To prove that the CE-type AFM phase composed of these zigzag FM chains is truly the ground-state, at least the following three points should be clarified: (i) Does this zigzag structure have the lowest energy compared to other zigzag paths with the same periodicity and compared with the straight one-dimensional path? (ii) Does the periodicity with four lattice spacings produce the *global* ground state? In other words, can zigzag structures with another periodicity be the global ground state? (iii) Is the energy of the zigzag AFM phase lower than that of the FM or other AFM phases? All these points have been clarified in Hotta et al. (2000), and here the essential points are discussed briefly.

The first point can be checked by directly comparing the energies for all possible zigzag structures with the periodicity of four lattice spacings. Due to translational invariance, there exist four types of zigzag states which are classified by the sequence of the hopping directions: $\{x, x, x, x\}$, $\{x, y, x, y\}$, $\{x, x, x, y\}$, and $\{x, x, y, y\}$. For quarter-filling, by an explicit calculation it has been shown that the zigzag pattern denoted by $\{x, x, y, y\}$ has the lowest energy among them (see details

in Hotta et al., 2000), but here an intuitive explanation is provided. The state characterized by $\{x,x,x,x\}$ is, of course, the one-dimensional metal with a dispersion relation simply given by $-2t_0\cos k$. Note that in this straight FM chain, the active orbital at every site is $3x^2-r^2$, since the hopping direction is restricted to be along the x-direction. As emphasized in the above discussion, a periodic change in the hopping amplitude produces a band gap, indicating that the metallic state has an energy higher than the band-insulating states. Among them, the state with the largest bandgap will be the ground state. After several calculations at quarter-filling, the zigzag state with $\{x,x,y,y\}$ was found to have the lowest energy, but without any calculation this result can be deduced based on the interference effect. As argued above, due to the interference of two traveling waves along the x- and y-direction, a standing-wave state occurs with nodes on the corner sites, and a large probability amplitude at the sites included in the straight segments. To contain two e_g-electrons in the unit cell with four lattice spacings, at least two sites in the straight segment are needed. Moreover, the nodes are distributed with equal spacing in the wave function as long as no external potential is applied. Thus, it is clear that the lowest-energy state corresponds to the zigzag structure with $\{x,x,y,y\}$.

As for the second point regarding the periodicity, it is quite difficult to carry out the direct comparison among the energies for all possible states, since there are infinite possibilities for the combinations of hopping directions. Instead, to mimic the periodic change of the phase ϕ_a in the hopping process, let us imagine a virtual situation in which a JT distortion occurs in the one-dimensional e_g-electron system, by following Koizumi et al. (1998a). To focus on the effect of the local phase, it is assumed that the amplitude of the JT distortion q_i is independent of the site index, i.e., $q_i=q$, and only the phase ξ_i is changed periodically. For simplicity, the phase is uniformly twisted with the period of M lattice spacings, namely, $\xi_j=j\times(2\pi)/M$ for $1\le j\le M$. Since the periodic change of the hopping direction is mimicked by the phase change of the JT distortion, $t^a_{\mu\nu}$ is simply taken as the unit matrix $t_0\delta_{\mu\nu}$ to avoid the double counting of the effect of the phase change. If the potential amplitude is written as $v=2qE_{\rm JT}$, the Hamiltonian for the present situation is given by

$$H=-t_0\sum_{\langle i,j\rangle}(c^\dagger_{i\mathrm{a}}c_{j\mathrm{a}}+c^\dagger_{i\mathrm{b}}c_{j\mathrm{b}}+\mathrm{h.c.})+v\sum_i\left[\sin\xi_i(c^\dagger_{i\mathrm{a}}c_{i\mathrm{b}}+c^\dagger_{i\mathrm{b}}c_{i\mathrm{a}})+\cos\xi_i(c^\dagger_{i\mathrm{a}}c_{i\mathrm{a}}-c^\dagger_{i\mathrm{b}}c_{i\mathrm{b}})\right], \tag{108}$$

where the spinless e_g-electron operator is used since the one-dimensional FM chain is considered here, and the potential term for the JT distortion is neglected since it provides only a constant energy shift in this case. By using the transformation Eq. (81), this Hamiltonian is rewritten as

$$H=-t_0\sum_{\langle i,j\rangle}\left[\mathrm{e}^{\mathrm{i}(\xi_i-\xi_j)/2}(\tilde c^\dagger_{i\mathrm{a}}\tilde c_{j\mathrm{a}}+\tilde c^\dagger_{i\mathrm{b}}\tilde c_{j\mathrm{b}})+\mathrm{h.c.}\right]+v\sum_i(\tilde c^\dagger_{i\mathrm{a}}\tilde c_{i\mathrm{a}}-\tilde c^\dagger_{i\mathrm{b}}\tilde c_{i\mathrm{b}}). \tag{109}$$

The Hamiltonian in momentum space is obtained by the Fourier transform as

$$\begin{aligned}H=&\sum_k\varepsilon_k[\cos(\pi/M)(\tilde c^\dagger_{k\mathrm{a}}\tilde c_{k\mathrm{a}}+\tilde c^\dagger_{k\mathrm{b}}\tilde c_{k\mathrm{b}})+\mathrm{i}\sin(\pi/M)(\tilde c^\dagger_{k\mathrm{a}}\tilde c_{k\mathrm{b}}-\tilde c^\dagger_{k\mathrm{b}}\tilde c_{k\mathrm{a}})]\\&+v\sum_k(\tilde c^\dagger_{k\mathrm{a}}\tilde c_{k\mathrm{a}}-\tilde c^\dagger_{k\mathrm{b}}\tilde c_{k\mathrm{b}}),\end{aligned} \tag{110}$$

where $\varepsilon_k=-2t_0\cos k$ and the periodic boundary condition (PBC) is imposed. Note that in this expression, k is the generalized quasi-momentum, redefined as $k-\pi/M\to k$, to incorporate the

additional phase π/M which appears to arise from a fictitious magnetic field (see Koizumi et al., 1998b). The eigenenergies are easily obtained by diagonalization as

$$E_k^{\pm} = \varepsilon_k \cos(\pi/M) \pm \sqrt{v^2 + \varepsilon_k^2 \sin^2(\pi/M)}$$

$$= (\tfrac{1}{2})[\varepsilon_{k+\pi/M} + \varepsilon_{k-\pi/M} \pm \sqrt{v^2 + (\varepsilon_{k+\pi/M} - \varepsilon_{k-\pi/M})^2}] \,. \tag{111}$$

Since this is just the coupling of two bands, $\varepsilon_{k+\pi/M}$ and $\varepsilon_{k-\pi/M}$, it is easily understood that the energy gain due to the opening of the bandgap is the best for the filling of $n = 2/M$. In other words, when the periodicity M is equal to $2/n$, the energy becomes the lowest among the states considered here with several possible periods. Although this is just a proof in an idealized special situation, it is believed that it captures the essence of the problem.

Here the effect of the local phase factor $e^{i\xi_i/2}$ should be again noted. If this factor is dropped, the phase π/M due to the fictitious magnetic field disappears and the eigenenergies are given by the coupling of $\varepsilon_{k+\pi+\pi/M}$ and $\varepsilon_{k+\pi-\pi/M}$, which has been also checked by the computational calculation. This "π" shift in momentum space appears at the boundary, modifying the PBC to anti-periodic BC, even if there is no intention to use APBC. Of course, this is avoidable when the momentum k is redefined as $k + \pi \to k$, as pointed out in Koizumi et al. (1998b). However, it is natural that the results for PBC are obtained in the calculation using PBC. Thus, also from this technical viewpoint, it is recommended that the phase factor $e^{i\xi_i/2}$ is added for the local rotation in the orbital space.

To show the last item of the list needed to show the stability of the CE state (see before), it is necessary to include the effect of the magnetic coupling between adjacent t_{2g}-spins. The appearance of the AFM phase with the zigzag geometry can be understood by the competition between the kinetic energy of e_g-electrons and the magnetic energy gain of t_{2g} spins based on the double-exchange mechanism. Namely, if J_{AF} is very small, for instance equal to zero, the FM phase best optimizes the kinetic energy of the e_g-electrons. On the other hand, when J_{AF} is as large as t_0, the system stabilizes a G-type AFM phase to exploit the magnetic energy of the t_{2g}-spins. For intermediate values of J_{AF}, the AFM phase with a zigzag structure can appear to take advantage at least partially of both interactions. Namely, along the FM zigzag chain with alignment of t_{2g}-spins, the e_g-electrons can move easily, optimizing the kinetic energy, and at the same time there is a magnetic energy gain due to the antiferromagnetic coupling between adjacent zigzag chains. The "window" in J_{AF} in which the zigzag AFM phase is stabilized has been found to be around $J_{AF} \approx 0.1t_0$ in Monte Carlo simulations and the mean-field approximation, as discussed elsewhere in this review.

In summary, at $x = 0.5$, the CE-type AFM phase can be stabilized even without the Coulombic and/or the JT phononic interactions, only with large Hund and finite J_{AF} couplings. Of course, those interactions are needed to reproduce the charge and orbital ordering, but as already mentioned in the above discussion, because of the special geometry of the one-dimensional zigzag FM chain, it is easy to imagine that the checkerboard-type charge ordering and $(3x^2 - r^2/3y^2 - r^2)$ orbital-ordering pattern will be stabilized. Furthermore, the charge confinement in the straight segment (sites 2 and 4 in Fig. 3.5.7), will naturally lead to charge stacking along the z-axis, with stability caused by the special geometry of the zigzag structure. Thus, the complex spin-charge-orbital structure for half-doped manganites can be understood intuitively simply from the viewpoint of its band-insulating nature.

3.5.7. Bi-stripe structure at $x > 0.5$

In the previous subsection, the discussion focused on the CE-type AFM phase at $x = 0.5$. Naively, it may be expected that similar arguments can be extended to the regime $x > 1/2$, since in the phase diagram for $La_{1-x}Ca_xMnO_3$, the AFM phase has been found at low temperatures in the region $0.50 < x \lesssim 0.88$. Then, let us try to consider the band-insulating phase for density $x = 2/3$ based on H^{∞} (as defined in Section 3.5), without both the JT phononic and Coulombic interactions, since this doping is quite important for the appearance of the bi-stripe structure, as already discussed in previous sections (see Mori et al., 1998a). Following the discussion on the periodicity of the optimal zigzag path, at $x = 2/3$ it is enough to consider the zigzag structure with $M = 6$. After several calculations for $x = 2/3$, as reported by Hotta et al. (2000), the lowest-energy state was found to be characterized by the straight path, not the zigzag one, leading to the C-type AFM phase which was also discussed in previous sections (for a visual representation of the C-type state see Fig. 4 of Kajimoto et al., 1999). At first glance, the zigzag structure, for instance the $\{x, x, x, y, y, y\}$-type path, could be the ground state for the same reason, as it occurs in the case of $x = 0.5$. However, while it is true that the state with such a zigzag structure is a band insulator, the energy gain due to the opening of the bandgap is not always the dominant effect. In fact, even in the case of $x = 0.5$, the energy of the bottom of the band for the straight path is $-2t_0$, while for the zigzag path, it is $-\sqrt{3}t_0$. For $x = 1/2$, the energy gain due to the gap opening overcomes the energy difference at the bottom of the band, leading to the band-insulating ground state. However, for $x = 2/3$ even if a band-gap opens the energy of the zigzag structure cannot be lower than that of the metallic straight-line phase. Intuitively, this point can be understood as follows: An electron can move smoothly along the one-dimensional path if it is straight. However, if the path is zigzag, "reflection" of the wave function occurs at the corner, and then a smooth movement of one electron is no longer possible. Thus, for small numbers of carriers, it is natural that the ground state is characterized by the straight path to optimize the kinetic energy of the e_g-electrons.

However, in neutron scattering experiments a spin pattern similar to the CE-type AFM phase has been suggested (Radaelli et al., 1999). In order to stabilize the zigzag AFM phase to reproduce those experiments it is necessary to include the JT distortion effectively. As discussed in Hotta et al. (2000), a variety of zigzag paths could be stabilized when the JT phonons are included. In such a case, the classification of zigzag paths is an important issue to understand the competing "bi-stripe" vs. "Wigner-crystal" structures. The former has been proposed by Mori et al. (1998b), while the latter was claimed to be stable by Radaelli et al. (1999). In the scenario by Hotta et al. (2000), the shape of the zigzag structure is characterized by the "winding number" w associated with the Berry-phase connection of an e_g-electron parallel-transported through Jahn–Teller centers, along zigzag one-dimensional paths. Namely, it is defined as

$$w = \oint \frac{d\boldsymbol{r}}{2\pi} \nabla \xi \,. \tag{112}$$

This quantity has been proven to be an integer, which is a topological invariant (see Hotta et al., 1998). Note that the integral indicates an accumulation of the phase difference along the one-dimensional FM path in the unit length M. This quantity is equal to half of the number of corners included in the unit path, which can be shown as follows. The orbital polarizes along the hopping direction, indicating that $\xi_i = 2\pi/3(4\pi/3)$ along the x-(y-)direction, as was pointed out above. This

is simply the double exchange mechanism in the orbital degree of freedom. Thus, the phase does not change in the straight segment part, indicating that $w = 0$ for the straight-line path. However, when an e_g-electron passes a corner site, the hopping direction is changed, indicating that the phase change occurs at that corner. When the same e_g-electron passes the next corner, the hopping direction is again changed. Then, the phase change in ξ_i after moving through a couple of corners should be 2π, leading to an increase of unity in w. Thus, the total winding number is equal to half of the number of corners included in the zigzag unit path. Namely, the winding number w is a good label to specify the shape of the zigzag one-dimensional FM path.

After several attempts to include effectively the JT phonons, it was found that the bi-stripe phase and the Wigner crystal phase universally appear for $w = x/(1 - x)$ and $w = 1$, respectively. Note here that the winding number for the bi-stripe structure has a remarkable dependence on x, reflecting the fact that the distance between adjacent bi-stripes changes with x. This x-dependence of the modulation vector of the lattice distortion has been observed in electron microscopy experiments (Mori et al., 1998). The corresponding zigzag paths with the charge and orbital ordering are shown in Fig. 3.5.9. In the bi-stripe structure, the charge is confined in the short straight segment as in the case of the CE-type structure at $x = 0.5$. On the other hand, in the Wigner-crystal structure, the straight segment includes two sites, indicating that the charge prefers to occupy either of these sites. Then, to minimize the JT energy and/or the Coulomb repulsion, the e_g electrons are distributed with equal spacing. The corresponding spin structure is shown in Fig. 3.5.10. A difference in the zigzag geometry can produce a significant different in the spin structure. Following the definitions for the C- and E-type AFM structures (see Wollan and Koehler (1955) and introductory section of this review), the bi-stripe and Wigner crystal structure have $C_{1-x}E_x$-type and C_xE_{1-x}-type AFM spin arrangements, respectively. Note that at $x = 1/2$, half of the plane is filled by the C-type, while another half is covered by the E-type, clearly illustrating the meaning of "CE" in the spin structure of half-doped manganites.

As for the charge structure along the z-axis for $x = 2/3$ shown in Fig. 3.5.11, a remarkable feature can be observed. Due to the confinement of charge in the short straight segment for the bi-stripe phase, the charge stacking is suggested from our topological argument. On the other hand, in the Wigner-crystal-type structure, charge is not stacked, but it is shifted by one lattice constant to avoid the Coulomb repulsion. Thus, if the charge stacking is also observed in the experiment for

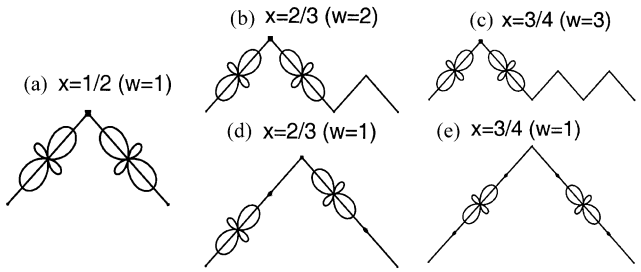

Fig. 3.5.9. (a) Path with $w = 1$ at $x = 1/2$. Charge and orbital densities are calculated in the MFA for $E_{JT} = 2t$. At each site, the orbital shape is shown with its size in proportion to the orbital density. (b) The BS-structure path with $w = 2$ at $x = 2/3$. (c) The BS-structure path with $w = 3$ at $x = 3/4$. (d) The WC-structure path with $w = 1$ at $x = 2/3$. (e) The WC-structure path with $w = 1$ at $x = 3/4$.

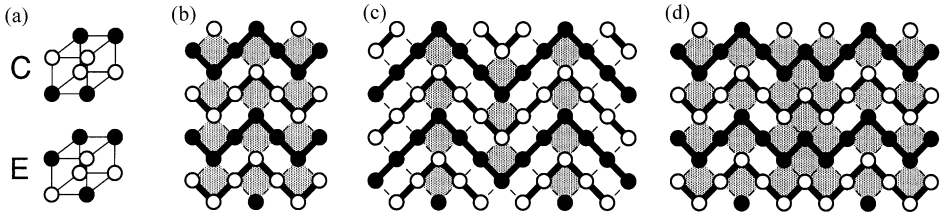

Fig. 3.5.10. (a) C- and E-type unit cell (Wollan and Koehler, 1955). (b) The spin structure in the a–b plane at $x = 1/2$. Open and solid circle denote the spin up and down, respectively. The thick line indicates the zigzag FM path. The open and shaded squares denote the C- and E-type unit cells. At $x = 1/2$, C-type unit cell occupies half of the 1D plane, clearly indicating the "CE"-type phase. (c) The spin structure at $x = 2/3$ for Wigner-crystal type phase. Note that 66% of the 2D lattice is occupied by C-type unit cell. Thus, it is called "C_2E"-type AFM phase. (d) The spin structure at $x = 2/3$ for bi-stripe-type phase. Note that 33% of the 2D lattice is occupied by C-type unit cell. Thus, it is called "CE_2"-type AFM phase.

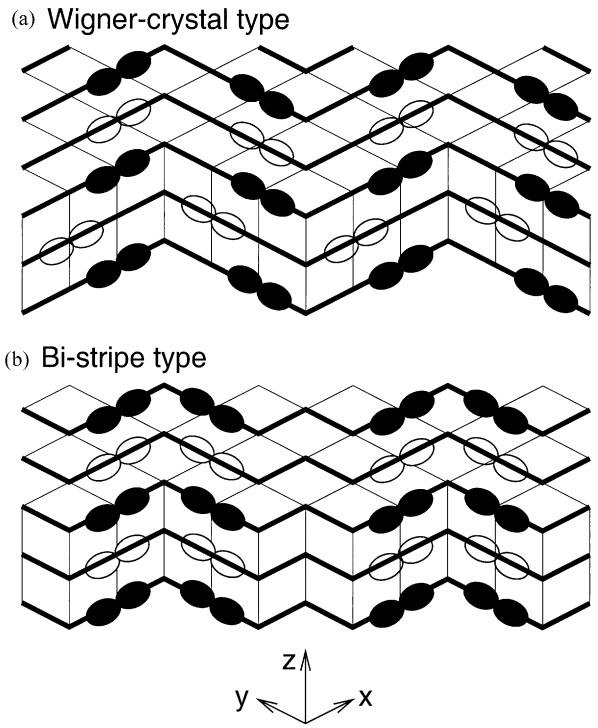

Fig. 3.5.11. Schematic figures for spin, charge, and orbital ordering for (a) WC and (b) BS structures at $x = 2/3$. The open and solid symbols indicate the spin up and down, respectively. The FM 1D path is denoted by the thick line. The empty sites denote Mn^{4+} ions, while the robes indicate the Mn^{3+} ions in which $3x^2 - r^2$ or $3y^2 - r^2$ orbitals are occupied.

$x = 2/3$, our topological scenario suggests the bi-stripe phase as the ground state in the low-temperature region. To firmly establish the final "winner" in the competition between the bi-stripe and Wigner-crystal structure at $x = 2/3$, more precise experiments, as well as quantitative calculations, will be needed in the future.

3.5.8. Charge order at $x < 0.5$

Regarding densities smaller than 0.5, the states at $x = 1/8,1/4$ and $3/8$ have received considerable attention recently (see Mizokawa et al., 1999; Korotin et al., 1999; Hotta and Dagotto, 2000). These investigations are still in a "fluid" state, and the experiments are not quite decisive yet, and for this reason, this issue will not be discussed in much detail here. However, without a doubt, it is very important to clarify the structure of charge-ordered states that may be in competition with the ferromagnetic states in the range in which the latter is stable in some compounds. "Stripes" may emerge from this picture, as recently remarked in experiments (Adams et al., 2000; Dai et al., 2000; Kubota et al., 2000. See also Vasiliu-Doloc et al., 1999) and calculations (Hotta et al., 2000c), and surely the identification of charge/orbital arrangements at $x < 0.5$ will be an important area of investigations in the very near future.

Here a typical result for this stripe-like charge ordering is shown in Fig. 3.5.12, in which the lower-energy orbital at each site is depicted, and its size is in proportion to the electron density occupying that orbital. This pattern is theoretically obtained by the relaxation technique for the optimization of oxygen positions, namely including the cooperative JT effect. At least in the strong electron–phonon coupling region, the stripe charge ordering along the *diagonal* direction in the x–y plane becomes the global ground state. Note, however, that many meta-stable states can appear very close to this ground state. Thus, the shape of the stripe is considered to fluctuate both in space and time, and in experiments it may occur that only some fragments of this stripe can be detected. It should also be emphasized that the orbital ordering occurs concomitant with this stripe charge ordering. In the electron-rich region, the same antiferro orbital-order exists as that corresponding

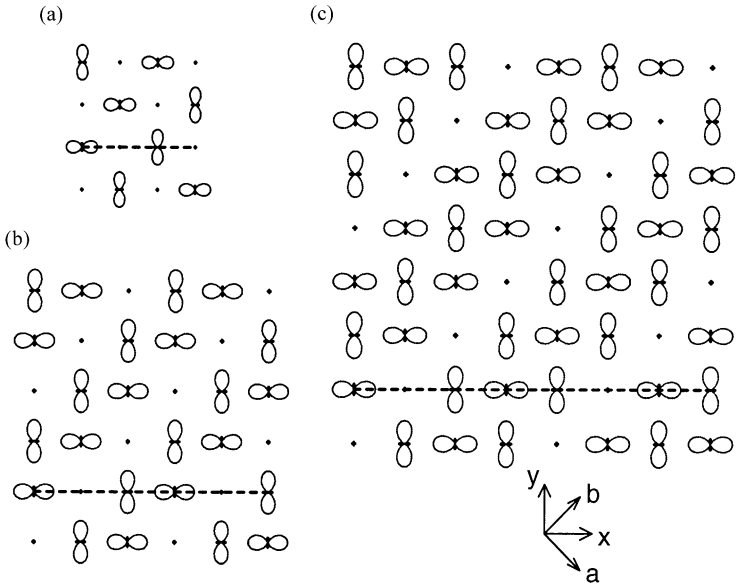

Fig. 3.5.12. Orbital densities in the FM phase for (a) $x = 1/2$, (b) $1/3$, and (c) $1/4$. The charge density in the lower-energy orbital is shown, and the size of the orbital is in proportion to this density. The broken line indicates one of the periodic paths to cover the whole 2D plane.

to $x = 0.0$. On the other hand, the pattern around the diagonal array of electron-poor sites is quite similar to the building block of the charge/orbital structure at $x = 0.5$.

If these figures are rotated by 45°, the same charge and orbital structure is found to stack along the *b*-axis. Namely, it is possible to cover the whole 2D plane by some periodic charge-orbital array along the *a*-axis (see, for instance, the broken-line path). If this periodic array is taken as the closed loop C in Eq. (112), the winding numbers are $w = 1, 2$, and 3, for $x = 1/2, 1/3$, and $1/4$, respectively. Note that in this case w is independent of the path along the *a*-axis. A relation $w = N_c/2$ holds only when the 1D FM path is fixed in the AFM spin arrangement. The results imply a general relation $w = (1 - x)/x$ for the charge-orbital stripe in the FM phase, reflecting the fact that the distance between the diagonal arrays of holes changes with x. Our topological argument predicts stable charge-orbital stripes at special doping such as $x = 1/(1 + w)$, with w an integer.

This orbital ordering can be also interpreted as providing a "π"-shift in the orbital sector, by analogy with the dynamical stripes found in cuprates (see, for instance, Buhler et al., 2000), although in copper oxides the charge/spin stripes mainly appear along the x- or y-direction. The study of the similarities and differences between stripes in manganites and cuprates is one of the most interesting open problems in the study of transition metal oxides, and considerable work is expected in the near future.

Finally, a new zigzag AFM spin configuration for $x < 0.5$ is here briefly discussed (Hotta et al., 2000c). In Fig. 3.5.13, a schematic view of this novel spin-charge-orbital structure on the 8×8 lattice at $x = 1/4$ is shown, deduced using the numerical relaxation technique applied to cooperative Jahn–Teller phonons in the strong-coupling region. This structure appears to be the global ground state, but many excited states with different spin and charge structures are also found with small excitation energy, suggesting that the AFM spin structure for $x < 0.5$ in the layered manganites is

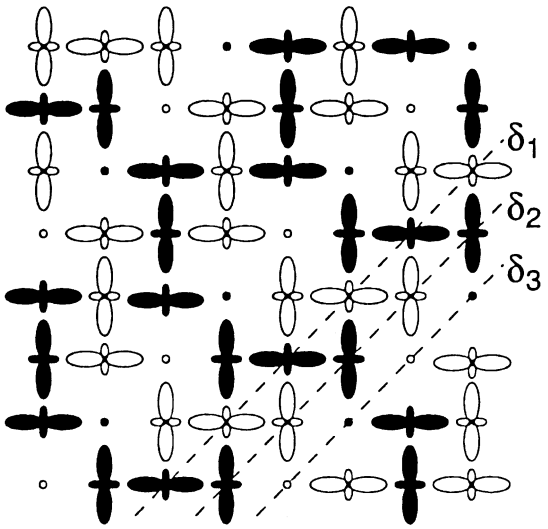

Fig. 3.5.13. Schematic representation of the spin-charge-orbital structure at $x = 1/4$ in the zigzag AFM phase at low temperature and large electron–phonon coupling. The symbol convention is the same as in Fig. 3.5.11. This figure was obtained using numerical techniques, and *cooperative* phonons, for $J_H = \infty$ and $J_{AF} = 0.1t$. For the noncooperative phonons, basically the same pattern can be obtained. Reproduced from Hotta et al. (2000c).

easily disordered due to this "quasi-degeneracy" in the ground state. This result may be related to the "spin-glass" nature of the single layer manganites reported in experiments (see Moritomo et al., 1995).

It should be noted that the charge-orbital structure is essentially the same as that in the 2D FM-phase (see Fig. 3.5.12). This suggests the following scenario for the layered manganites: When the temperature is decreased from the higher-temperature region, first charge ordering occurs due to the cooperative Jahn–Teller distortions in the FM (or paramagnetic) region. If the temperature is further decreased, the zigzag AFM spin arrangement is stabilized, adjusting itself to the orbital structure. Thus, the separation between the charge ordering temperature T_{CO} and the Néel temperature T_N occurs naturally in this context. This is not surprising, since T_{CO} is due to the electron–lattice coupling, while T_N originates in the coupling J_{AF}. However, if the electron–phonon coupling is weak, then T_{CO} becomes very low. In this case, the transition to the zigzag AFM phase may occur prior to the charge ordering. As discussed above, the e_g-electron hopping is confined to one-dimensional structures in the zigzag AFM environment. Thus, in this situation, even a weak coupling electron–phonon coupling can produce the charge-orbital ordering, as easily understood from the Peierls instability argument. Namely, just at the transition to the zigzag AFM phase, the charge-orbital ordering occurs simultaneously, indicating that $T_{CO} = T_N$. Note also that in the zigzag AFM phase, there is no essential difference in the charge-orbital structures for the non-cooperative and cooperative phonons, due to the one dimensionality of those zigzag chains.

3.6. Pseudo-gap in mixed-phase states

Recent theoretical investigations suggest that the density of states (DOS) in mixed-phase regimes of manganites may have "pseudo-gap" characteristics, namely a prominent depletion of weight at the chemical potential. This feature is similar to that extensively discussed in copper oxides. The calculations in the Mn-oxide context have been carried out using both the one- and two-orbital models, with and without disorder (see Moreo et al., 1999b; Moreo et al., 2000). Typical results are shown in Fig. 3.6.1 Part (a) contains the DOS of the one-orbital model on a 2D cluster varying the electronic density slightly below $\langle n \rangle = 1.0$, as indicated in the caption. At zero temperature, this density regime is unstable due to phase separation, but at the temperature of the simulation those densities still correspond to stable states, but with a dynamical mixture of AF and FM features (as observed, for instance, in Monte Carlo snapshots of the spin configurations). A clear minimum in the DOS at the chemical potential can be observed. Very similar results appear also in 1D simulations (Moreo et al., 1999b). Part (b) contains results for two-orbitals and a large electron–phonon coupling, this time at a fixed density and changing temperature. Clearly a pseudogap develops in the system as a precursor of the phase separation that is reached as the temperature is further reduced. Similar results have been obtained in other parts of parameter space, as long as the system is near unstable phase-separated regimes. A pseudo-gap appears also in cases where disorder is added to the system. In Fig. 3.6.1c, taken from Moreo et al. (2000), results can be found for the case where a random on-site energy is added to the one-orbital model.

A tentative explanation of this phenomenon for the case without disorder was described by Moreo et al. (1999b), and it is explained in Fig. 3.6.2. In part (a) a typical mixed-phase FM–AF state is sketched. Shown are the localized spins. In the FM regions, the e_g-electrons improve their kinetic energy, and thus they prefer to be located in those regions as shown in (b). The FM domains act as effective attractive potentials for electrons, as sketched in part (c). When other electrons are added,

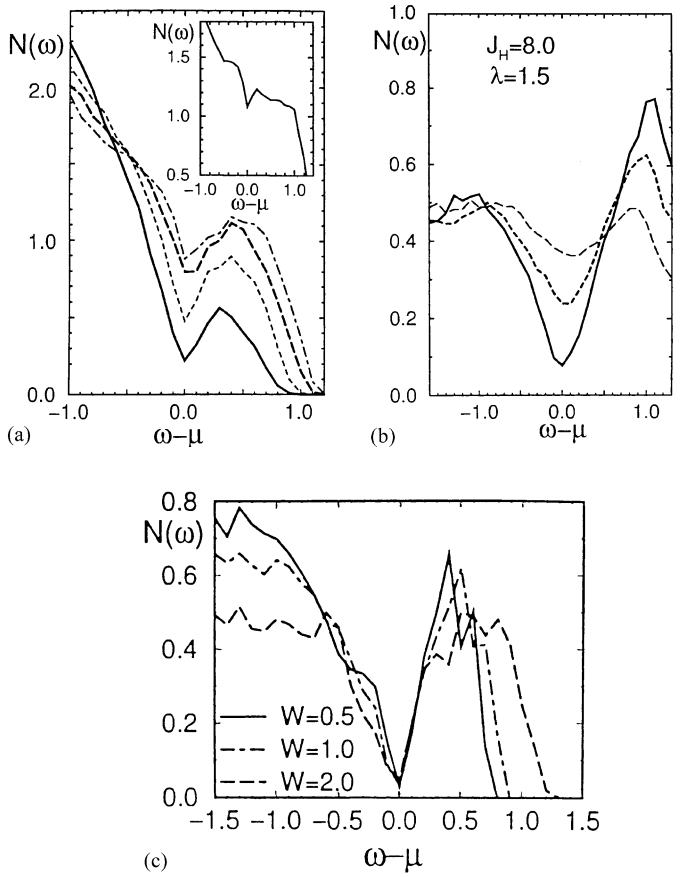

Fig. 3.6.1. (a) DOS of the one-orbital model on a 10×10 cluster at $J_H = \infty$ and temperature $T = 1/30$ (hoping $t = 1$). The four lines from the top correspond to densities 0.90, 0.92, 0.94, and 0.97. The inset has results at $\langle n \rangle = 0.86$, a marginally stable density at $T = 0$. (b) DOS of the two-orbital model on a 20-site chain, working at $\langle n \rangle = 0.7$, $J_H = 8$, and $\lambda = 1.5$. Starting from the top at ω-$\mu = 0$, the three lines represent temperatures 1/5, 1/10, and 1/20, respectively. Here the hopping along x between orbitals a is the unit of energy. Both, (a) and (b) are taken from Moreo et al. (1999b). (c) DOS using a 20-site chain of the one-orbital model at $T = 1/75$, $J_H = 8$, $\langle n \rangle = 0.87$, and at a chemical potential such that the system is phase separated in the absence of disorder. W regulates the strength of the disorder, as explained in Moreo et al. (2000) from where this figure was taken.

FM clusters are created and new occupied levels appear below the chemical potential, creating a pseudogap (part (d) of Fig. 3.6.2). The DOS is clearly nonrigid. These results are compatible with the photoemission experiments by Dessau et al. (1998) for bilayer manganites. Other features of the experiments are also reproduced such as the large width of the peaks, and the momentum independence of the results. This agreement adds to the notion pursued in this review that mixed-phase states are important to understand the behavior of manganese oxides. The reduction of the DOS at the chemical potential is also compatible with the insulating characteristics of the bilayers in the regime of the photoemission experiments. It is conceivable that the manganites present a pseudogap regime above their Curie and Néel temperatures, as rich as that found in the cuprates. More details are given in the Discussion section.

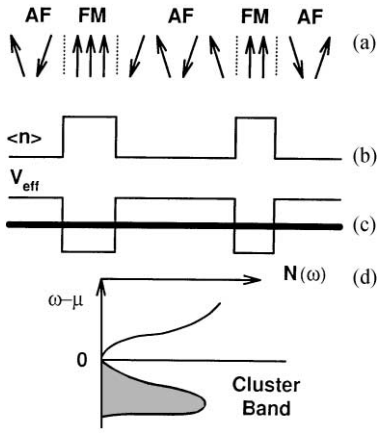

Fig. 3.6.2. Schematic explanation of pseudogap formation at low electronic density (taken from Moreo, et al., 1999b). In (a) a typical Monte Carlo configuration of localized spins is shown. In (b), the corresponding electronic density is shown. In (c), the effective potential felt by electrons is presented. A populated cluster band (thick line) is formed. In (d), the resulting DOS is shown. Figure taken from Moreo et al. (1999b).

3.7. Phase separation caused by the influence of disorder on first-order transitions

Although it is frequently stated in the literature that a variety of chemical substitutions in manganites lead to modifications in the bandwidth due to changes in the "average" A-site cation radius $\langle r_A \rangle$, this statement is only partially true. Convincing analysis of data and experiments by Rodriguez-Martinez and Attfield (1996) have shown that the disorder introduced by chemical replacements in the A-sites is also crucially important in determining the properties of manganites. For instance, Rodriguez-Martinez and Attfield (1996) found that the critical temperature T_C can be reduced by a large factor if the variance σ^2 of the ionic radii about the mean $\langle r_A \rangle$ is modified, keeping $\langle r_A \rangle$ constant. Rodriguez-Martinez and Attfield (1996) actually observed that maximum magnetoresistance effects are found in materials not only with a low value of $\langle r_A \rangle$ (small bandwidth) but also a small value of σ^2. A good example is $Pr_{1-x}Ca_xMnO_3$ since the Pr^{3+} and Ca^{2+} ions are similar in size (1.30 and 1.34 Å, respectively, according to Tomioka and Tokura (1999)).

Disorder, as described in the previous paragraph, is important for the phase separation scenario. The recent experimental results showing the existence of micrometer size coexisting clusters in $(La_{5/8-y}Pr_y)Ca_{3/8}MnO_3$ (LPCMO) by Uehara et al. (1999), to be reviewed in detail later, highlights a property of manganites that appears universal, namely the presence of intrinsic inhomogeneities in the system, even in single crystals. This issue is discussed at length in various sections of this review. In the theoretical framework described thus far, the scenario that is the closest to predicting such inhomogeneous state is the one based on electronic phase separation. However, the analysis presented before when considering the influence of long-range Coulomb interactions over a phase separated state, led us to believe that only nanometer size coexisting clusters are to be expected in this problem. Those found in LPCMO are much larger, suggesting that there must be another mechanism operative in manganites to account for their formation.

A possible explanation of the results of Uehara et al. (1999) has been recently proposed by Moreo et al. (2000), and it could be considered as a form of "disorder-induced" or "structural" phase separation, rather than electronic. The idea is based on the influence of disorder over the first-order metal–insulator (or FM–AF) transition found in models where the interactions are translationally invariant (without disorder), as it was described in Sections 3.4 and 3.5 When such a transition occurs, abruptly a metal changes into an insulator, as either concentrations or couplings are suitably changed. Unless metastable states are considered, there is no reason to assume that in the actual stable ground state of this system coexisting clusters will be found, namely the state is entirely FM or AF depending on parameters. However, different is the situation when disorder is considered into the problem. The type of disorder taken into account by Moreo et al. (2000) is based on the influence of the different ionic radius of the various elements that compose the manganites, as discussed at the beginning of this section. Depending on the environment of A-type ions (which in LPCMO involve La, Pr or Ca) a given Mn–O–Mn bond can be straight (180°) or distorted with an angle less than 180°. In the latter, the hopping across the bond under study will be less than the ideal one. For a schematic representation of this idea see Fig. 3.7.1. The random character of the distribution of A ions, leads to a concomitant random distribution of hoppings, and also random exchange between the localized spins J_{AF} since this quantity is also influenced by the angle of the Mn–O–Mn bond.

To account for this effect, Moreo et al. (2000) studied the one- and two-orbital models for manganites described before, including a small random component to both the hoppings and J_{AF}. This small component did not influence the FM- and AF-phase much away from their transition boundary, but in the vicinity of the first-order transition its influence is important. In fact, numerical studies show that the transition now becomes continuous, with FM and AF clusters in coexistence in a narrow region around the original transition point.

Typical results are shown in Fig. 3.7.2a–f, using one-dimensional clusters as an example. In the two upper frames, the energy versus J_{AF} (or J') is shown at fixed values of the other couplings such as J_H and λ, in the absence of disorder and at a fixed density $x = 0.5$. The abrupt change in the slope of the curves in (a) and (d) clearly shows that the transition is indeed first order. This is a typical result that appears recurrently in all Monte Carlo simulations of manganite models, namely FM and AF are so different that the only way to change from one to the other at low temperature is abruptly in a discontinuous transition (and spin-canted phases have not been found

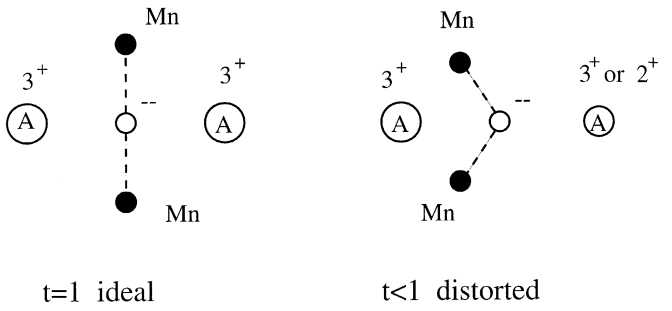

Fig. 3.7.1. Schematic representation of the influence of the A-site ionic size on the hopping amplitude "t" between two Mn ions.

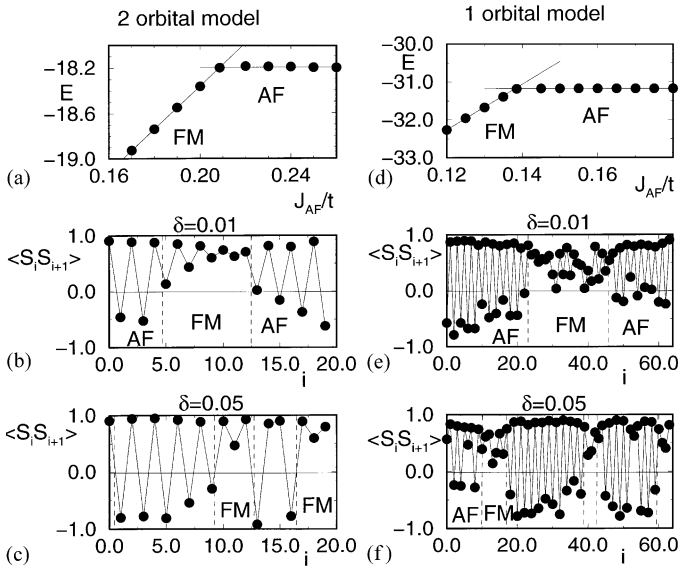

Fig. 3.7.2. Results that illustrate the generation of "giant" coexisting clusters in models for manganites (taken from Moreo et al., 2000). (a–c) are Monte Carlo results for the two-orbital model with $\langle n\rangle = 0.5$, $T = 1/100$, $J_H = \infty$, $\lambda = 1.2$, $t = 1$, PBC, and using a chain with $L = 20$ sites. (a) is the energy per site vs. J_{AF}/t for the nondisordered model, with level crossing at 0.21. (b) MC averaged nearest-neighbor t_{2g}-spins correlations vs. position along the chain (denoted by i) for one set of random hoppings t^{α}_{ab} and J_{AF} couplings (J_{AF}/t at every site is between $0.21 - \delta$ and $0.21 + \delta$ with $\delta = 0.01$). FM and AF regions are shown. For more details see Moreo et al. (2000). (c) Same as (b) but with $\delta = 0.05$. (d–f): results for the one-orbital model with $\langle n\rangle = 0.5$, $T = 1/70$, $J_H = \infty$, $t = 1$, open boundary conditions, and $L = 64$ (chain). (d) is energy per site vs. J_{AF} for the nondisordered model, showing the FM–AF states level crossing at $J_{AF} \sim 0.14$. (e) are the MC averaged nearest-neighbor t_{2g}-spin correlations vs. position for one distribution of random hoppings and t_{2g} exchanges, such that J_{AF}/t is between 0.14-δ and $0.14 + \delta$ with $\delta = 0.01$. (f) Same as (e) but with $\delta = 0.03$.

in our analysis in the absence of magnetic fields, as possible intermediate phases between FM and AF). These results are drastically changed upon the application of disorder, as shown in frames (b, c, e, and f) of Fig. 3.7.2, where the mean couplings have been fixed such that the model is located exactly at the first-order transition of the nondisordered system. In these frames, the nearest-neighbor spin correlations along the chain are shown. Clearly, this correlation is positive in some portions of the chain, while it alternates from positive to negative in others. This alternation is compatible with an AF state, with an elementary unit cell of spins in the configuration up–up–down–down, but the particular form of the AF state is not important in the following; only its competition with other ordered states, such as the FM one is significant. The important point is that there are coexisting FM and AF regions. The cluster size is regulated by the strength of the disorder, such that the smaller the disorder, the larger the cluster size. Results such as those in Fig. 3.7.2 have appeared in all simulations carried out in this context, and in dimensions larger than one (see Moreo et al., 2000). The conclusions appear independent of the particular type of AF insulating state competing with the FM-state, the details of the distribution of random numbers used, and the particular type of disorder considered which could also be in the form of a random on-site energy in some cases (Moreo et al., 2000). Note that the coexisting clusters have the *same* density, namely these are FM- and AF-phase that appear at a fixed hole concentration in the nondisordered

models, for varying couplings. Then, the problem of a large penalization due to the accumulation of charge is not present in this context.

What is the origin of such a large cluster coexistence with equal density? There are two main opposing tendencies acting in the system. On one hand, energetically it is not convenient to create FM–AF interfaces and from this perspective a fully homogeneous system is preferable. On the other hand, locally at the level of the lattice spacing the disorder in t and J_{AF} alter the couplings such that the system prefers to be either on the FM- or AF-phase, since these couplings fluctuate around the transition value. From the perspective of the disorder, the clusters should be as small as possible such that the local different tendencies can be properly accounted for. From this competition emerges the large clusters of Fig 3.7.2, namely by creating large clusters, the number of interfaces is kept small while the local tendencies toward one phase or the other are partially satisfied. "Large" here means substantially larger in size than the lattice spacing. A region where accidentally the distribution of random couplings favors the FM- or AF-state on average, will nucleate such a phase in the form of a bubble.

These simple ideas can be made more elegant using the well-known arguments by Imry and Ma (1975), which were applied originally to the random field Ising model (RFIM) (see contributions on the subject in the book of Young, 1998), namely a model with a FM Ising interaction among spins of a lattice in the presence of a magnetic field in the z-direction which changes randomly from site to site. This local field is taken from a distribution of random numbers of width $2W$. In the context of manganites it can be imagined that the spin up and down of the RFIM represent the two states in competition (metal and insulator) in the real compounds. The random field represents the local tendency to prefer either a metal or an insulator, due to the fluctuations in the disorder of the microscopic models. As a function of an external uniform magnetic field, the RFIM at zero temperature has a first-order transition at zero external field in the absence of random fields (between all spins up and all down), which turns continuous as those random fields are added, quite similar to the case described above in the FM–AF competition. Then, the RFIM captures at least part of the physics of Mn-oxides that emerged from the study of realistic Hamiltonians in the presence of disorder, as shown above. For this reason it is instructive to study this simple spin model, which can be analyzed on lattices much larger than those that can be reached with the one or two orbital models of Section 3.3. However, note that the use of the RFIM is only to guide the intuition, but it is not claimed that this model belongs to exactly the same universality class as the microscopic Hamiltonians for Mn-oxides used here. The study of universality is very complex and has not been addressed in this context yet. Nevertheless, it is expected that the RFIM will at least provide some intuition as to how real manganites behave.

Typical results are shown in Fig. 3.7.3. In part (a), the data corresponding to a simulation at low temperature on a 100×100 cluster for a fixed set of random fields is shown. The clusters are basically frozen, namely the result is representative of the ground state. The presence of coexisting clusters of spins up and down is clear. Their distribution is certainly random, and their shape fractalic, similar to that observed in experiments for LPCMO. Upon reduction of W, in frame (b) results now for a 500×500 cluster show that the typical size of the clusters grow and can easily involve a few hundred lattice spacings. When an external field is applied, a *percolation* among disconnected clusters emerges. This is a very important point, in agreement with the expectations arising from several experiments, namely percolative characteristics should appear in real manganites to the extend that the theoretical investigations presented in this section are correct. Uehara

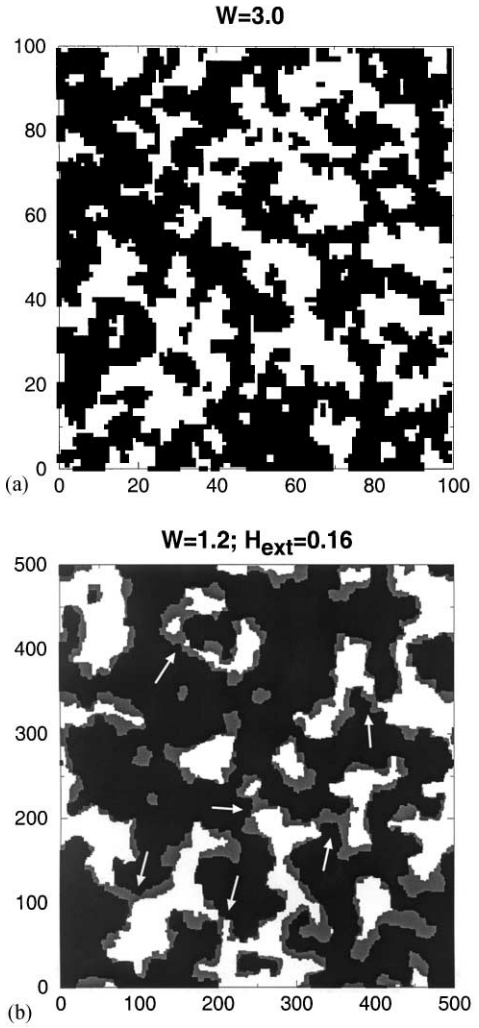

Fig. 3.7.3. Results of a Monte Carlo simulation of the random field Ising model at $T = 0.4$ ($J = 1$), with PBC, taken from Moreo et al. (2000). The dark (white) small squares represent spins up (down). At $T = 0.4$ the thermal fluctuations appear negligible, and the results shown are those of the lowest energy configuration. (a) was obtained for a random field with strength $W = 3$ taken from a box distribution $[-W, W]$, external field $H_{ext} = 0$, using a 100×100 cluster, and one set of random fields $\{h_i\}$. (b) Results using a 500×500 cluster with $W = 1.2$ and for one fixed configuration of random fields. The dark regions are spins up in the $H_{ext} = 0$ case, the grey regions are spins down at zero field that have flipped to up at $H_{ext} = 0.16$, while the white regions have spins down with and without the field. The percolative-like features of the giant clusters are apparent in the zero-field results. Special places are arrow-marked where narrow spin-down regions have flipped linking spin-up domains. For more details see Moreo et al. (2000).

et al. (1999) and other experimentalists intuitively concluded that indeed percolation is important in the study of Mn-oxides, and in the following section it will be shown that it plays a key role in rationalizing the dc resistivity of these compounds. Gor'kov and Kresin (1998) also briefly discussed a possible percolation process at low temperature.

Summarizing, phase separation can be driven by energies other than purely electronic. In fact, it can also be triggered by the influence of disorder on first-order transitions. In this case the competing clusters have the same density and for this reason can be very large. Micrometer size clusters, such as those found in the RFIM, are possible in this context, and have been observed in experiments. This result is very general, and should apply to a variety of compounds where two very different ordered states are in competition at low temperatures.

The remarkable phenomenological results of Rodriguez-Martinez and Attfield (1996) appear to be in qualitative agreement with the theoretical calculations. As explained above, Moreo et al. (2000) found that the size of the clusters induced by disorder near a transition, such as those produced by chemical substitutions in real manganites, which would be of first order in the clean limit, can be controlled by the "strength" of that disorder. In practice, this strength is monotonically related to σ^2 (in the limit $\sigma = 0$ there is no disorder). At small (but not vanishing) σ or disorder in the calculations of Moreo et al. (2000), the coexisting clusters are large. As the disorder grows, the clusters reduce their size. To the extent that the size of the coexisting clusters is directly proportional the strength of the CMR effect, then weak disorder is associated with large magnetoresistance changes with the composition, magnetic fields or pressure, a somewhat counter-intuitive result since naively strong disorder could have been expected to lead to larger modifications in the resistivity.

3.8. Resistivity of manganites in the mixed-phase regime

One of the main lessons learned from the previous analysis of models for manganites is that intrinsic inhomogeneities are very important in this context. It is likely that the real Mn-oxides in the CMR regime are in such a mixed-phase state, a conclusion that appears inevitable based on the huge recent experimental literature, to be reviewed in the next section, reporting phase separation tendencies in some form or another in these compounds. However, note that until recently estimations of the dc resistivity ρ_{dc} in such a mixed-phase regime were not available. This was unfortunate since the interesting form of the ρ_{dc} vs. temperature curves, parametric with magnetic fields, is one of the main motivations for the current huge effort in the manganite context. However, the lack of *reliable* estimations of ρ_{dc} is not accidental: it is notoriously difficult to calculate transport properties in general, and even more complicated in regions of parameter space that are expected to be microscopically inhomogeneous. Although there have been some attempts in the literature to calculate ρ_{dc}, typically a variety of approximations that are not under control have been employed. In fact, the micrometer size of some of the coexisting clusters found in experiments strongly suggest that a fully microscopic approach to the problem will likely fail since, e.g., in a computational analysis it would be very difficult to study sufficiently large clusters to account for such large scale structures. It is clear that a more phenomenological approach is needed in this context.

For all these reasons, recently Mayr et al. (2000) carried out a study of ρ_{dc} using a *random resistor network* model (see Kirkpatrick, 1973), and other approximations. This model was defined on square and cubic lattices, but with a lattice spacing much larger than the 4 Å distance between nearest-neighbor Mn ions. A schematic representation is presented in Fig. 3.8.1. Actually, the new lattice spacing is a fraction of micrometer, since the random network tries to mimic the complicated fractalic-like structure found experimentally. At each link in this sort of effective lattice, randomly

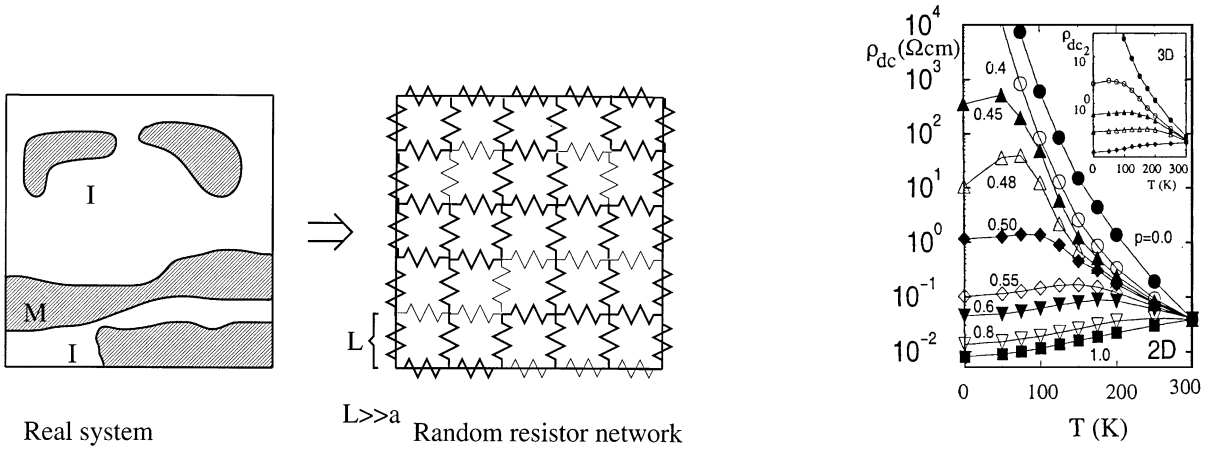

Fig. 3.8.1. Schematic representation of the random resistor network approximation. On the left is a sketch of the real system with metallic and insulating regions. On the right is the resistor network where dark (light) resistances represent the insulator (metal). "a" is the Mn–Mn lattice spacing, while L is the actual lattice spacing of the resistor network.

Fig. 3.8.2. Net resistivity ρ_{dc} of a 100×100 random resistor network cluster vs. temperature, at the indicated metallic fractions p (result taken from Mayr et al., 2000). Inset: Results for a 20^3 cluster with (from the top) $p = 0.0,0.25,0.3,0.4$ and 0.5. In both cases, averages over 40 resistance configurations were made. The $p = 1$ and 0 limits are from the experiments corresponding to LPCMO (see Uehara et al., 1999). Results on 200×200 clusters (not shown) indicate that size effects are negligible.

either a metallic or insulating resistance was located in such a way that the total fraction of metallic component was p, a number between 0 and 1.

The actual values of these resistances as a function of temperature were taken from experiments. Mayr et al. (2000) used the $\rho_{dc}(T)$ plots obtained by Uehara et al. (1999) corresponding to $(La_{5/8-y}Pr_y)Ca_{3/8}MnO_3$ (LPCMO), one of the compounds that presents the coexistence of giant FM and CO clusters at intermediate values of the Pr concentration. More specifically, using for the insulating resistances the results of LPCMO at $y = 0.42$ (after the system becomes a CO state with increasing Pr doping) and for the metallic ones the results at $y = 0.0$ (which correspond to a metallic state, at least below its Curie temperature), the results of a numerical study on a 100×100 cluster are shown in Fig. 3.8.2 (the Kirchoff equations were solved by a simple iterative procedure). It is interesting to observe that, even using such a simple phenomenological model, the results are already in reasonable agreement with the experiments, namely, (i) at large temperature insulating behavior is observed even for p as large as 0.65 (note that the classical percolation is expected to occur near $p = 0.5$; see Kirkpatrick, 1973); (ii) at small temperature a ("bad") metallic behavior appears; and (iii) a broad peak exists in between. Results in both 2D and 3D lead to similar conclusions. It is clear that the experimental results for manganites can be at least partially accounted for within the mixed-phase scenario.

The results of Fig. 3.8.2 suggest a simple qualitative picture to visualize why the resistivity in Mn-oxides has the peculiar shape it has. The relevant state in this context should be imagined as percolated, as sketched in Fig. 3.8.3a as predicted by the analysis of the previous section. Metallic filaments from one side of the sample to the other exist in the system. At low temperature,

conduction is through those filaments. Necessarily, ρ_{dc} at $T = 0$ must be large, in such a percolative regime. As temperature increases, the ρ_{dc} of the filaments grows as in any metal. However, in the other limit of large or room temperature, the resistance of the percolated metallic filament is expected to be much larger than that corresponding to one of the insulator paths. Actually, near room temperature in many experimental graphs, it can be observed that ρ_{dc} in the metallic and insulating regimes are quite similar in value, even comparing results away from the percolative region. Then, at room temperature it is more likely that conduction will occur through the insulating portions of the sample, rather than through the metallic filaments. Thus, near room temperature insulating behavior is expected. In between low and high temperatures, it is natural that ρ_{dc} will present a peak. Then, a simple "two resistances in parallel" description appears appropriate (see Fig. 3.8.3b). The insulating resistance behaves like any insulator, while the metallic one starts at $T = 0$ at a high value and then it behaves like any metal. The effective resistance shown in Fig. 3.8.3b properly reproduces the experiments at least qualitatively.

Note, however, that many experimental results suggest that ρ_{dc} has an intermediate temperature peak sharper than shown in Fig. 3.8.2. In some compounds this is quite notorious, while in others the peak is fairly broad as in Fig. 3.8.2. Nevertheless, it is important to find out alternative procedures to sharpen the ρ_{dc} peak to better mimic experiments. One possible solution to this problem is to allow for the metallic fraction p to vary with temperature. This is a reasonable assumption since it is known that the metallic portions of the sample in mixed-phase manganites originate in the ferromagnetic arrangement of spins that improves conduction. The polarization of the spins deteriorates as the temperature increases, and it is reasonable to imagine that the FM islands decrease in size as the temperature grows. Then, a pattern of FM clusters that are connected at low temperature leading to a metallic behavior may become disconnected at higher temperatures. The tendencies toward a metallic percolation decrease with increasing temperature. Such a conjecture was studied qualitatively by Mayr et al. (2000) using the random field Ising model and the one-orbital model for Mn-oxides. In both cases, indications of the disappearance of percolation with increasing temperature were indeed found. Then, assuming that p decreases with increasing temperature, approximately following the magnetization, seems a reasonable assumption.

Results with a temperature dependent p are shown in Fig. 3.8.4. The actual values of p are indicated, at least in part, in the figure. Certainly the peak is now sharper than in Fig. 3.8.2, as expected, and the results indeed resemble those found in a variety of experiments. Note that the function $p = p(T)$ has not been fine-tuned, and actually a variety of functions lead to similar conclusions as those in Fig. 3.8.4. Note also that obtaining such a result from a purely microscopic approach would have been quite difficult, although Mayr et al. (2000) showed that data taken on small clusters using the one-orbital model are at least compatible with those of the phenomenological approach. To evaluate the conductance of these clusters, the approach of Datta (1995) and Vergés (1999) were used. Also note that calculations using a cubic cluster with either metallic or insulating "hopping" (Avishai and Luck, 1992), to at least partially account for quantum effects, lead to results similar to those found in Fig. 3.8.4.

The success of the phenomenological approach described above leads to an interesting prediction. In the random resistor network, it is clear that above the peak in the resistivity, the mixed-phase character of the system remains, even with a temperature dependent metallic fraction p. Then, it is conceivable to imagine that above the Curie temperature in real manganites, a substantial fraction of the system should remain in a metallic FM-state (likely not percolated, but

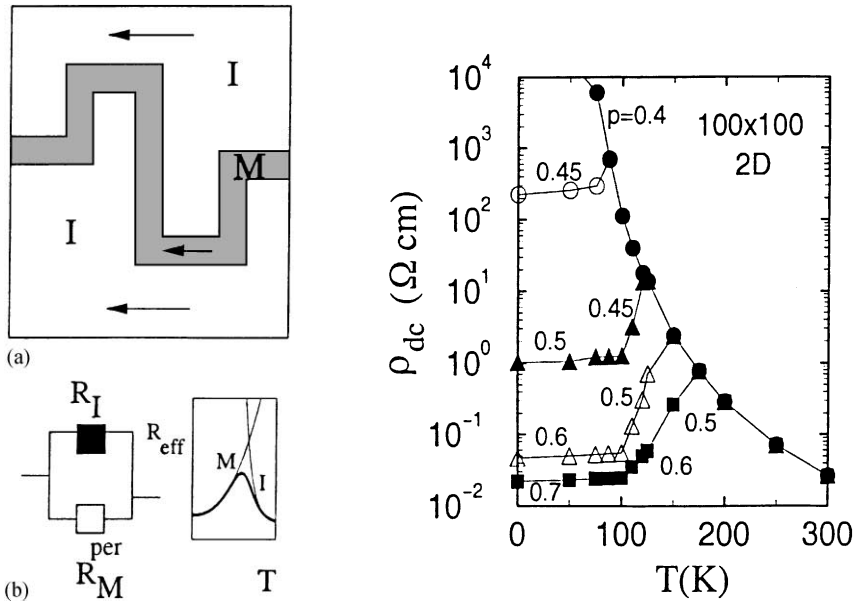

Fig. 3.8.3. (a) Schematic representation of the mixed-phase state near percolation. The arrows indicate conduction either through the insulating or metallic regions depending on temperature (see text). (b) Two resistances in parallel model for Mn-oxides. The (schematic) plot for the effective resistance $R_{\rm eff}$ vs. T arises from the parallel connection of metallic (percolative) $R_M^{\rm per}$ and insulating $R_{\rm I}$ resistances. Figure taken from Mayr et al. (2000).

Fig. 3.8.4. Net resistivity $\rho_{\rm dc}$ of the 100×100 random resistor network used in the previous figure, but with a metallic fraction p changing with T. Representative values of p are indicated. Results averaged over 40 resistance configurations are shown (taken from Mayr et al., 2000).

forming disconnected clusters). A large variety of experiments reviewed in the next section indeed suggest that having FM clusters above $T_{\rm C}$ is possible. As a consequence, this has led us to conjecture that there must exist a temperature T^* at which those clusters start forming. This defines a new temperature scale in the problem, somewhat similar to the famous pseudo-gap T^* scale of the high-temperature superconducting compounds. In fact, in mixed phase FM–AF states it is known that a pseudo-gap appears in the density of states (Sections 3.6 and 3.7; Moreo et al., 1999b, 2000), thus increasing the analogy between these two materials. In our opinion, the experimental verification that indeed such a new scale T^* exists in manganites is important to our understanding of these compounds. In fact, recent results by Kim et al. (2000) for $La_{1-x}Ca_xMnO_3$ at various densities have been interpreted as caused by small FM segments of the CE-type CO state, appearing at hole densities smaller than $x = 1/2$ and at high temperature. This result is in qualitative agreement with the theoretical analysis presented here.

The study of effective resistivities and conductances has also been carried out in the presence of magnetic fields (Mayr et al., 2000), although still mainly within a phenomenological approach. From the previous results Figs. 3.8.2–4, it is clear that in the percolative regime "small" changes in the system may lead to large changes in the resistivity. For instance, if p changes by only 5% from 0.45 to 0.5 in Fig. 3.8.4, $\rho_{\rm dc}$ is modified by two orders of magnitude! It is conceivable that small

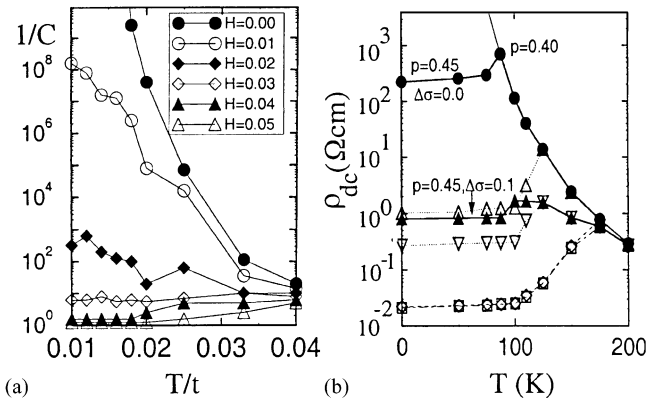

Fig. 3.8.5. (a) Inverse conductivity of the half-doped one-orbital model on a 64-site chain in the regime of coexisting clusters, with $J_H = \infty$, AF coupling among localized spins $J' = 0.14$, $t = 1$, and $\Delta = 0.03$, varying a magnetic field as indicated. The data shown corresponds to a particular disorder configuration, but results with other configurations are similar. (b) Effective resistivity of a 100×100 network of resistances. Results at $\Delta\sigma = 0.0$ (full circles, open triangles, and open squares starting at $T = 0$ with $p = 0.45$,0.5 and 0.7, respectively) are the same as found in Fig. 3.8.4. Full triangles, inverse open triangles, and diamonds, correspond to the same metallic fractions, but with a small addition to the insulating conductivity ($\Delta\sigma = 0.1$ $(\Omega\ \mathrm{cm})^{-1}$), to simulate the effect of magnetic fields (see text). Results taken from Mayr et al. (2000).

magnetic fields could induce such small changes in p, leading to substantial modifications in the resistivity. Experiments by Parisi et al. (2000) indeed show a rapid change of the fraction of the FM-phase in $La_{0.5}Ca_{0.5}MnO_3$ upon the application of magnetic fields. In addition, studies of the one-orbital model carried out in one dimension (Mayr et al., 2000) also showed that other factors may influence the large ρ_{dc} changes upon the application of external fields. For instance, in Fig. 3.8.5, the inverse conductance C^{-1} of a 64-site chain is shown in the presence of small magnetic fields (in units of the hopping), in the regime of FM–AF cluster coexistence, which is achieved by the introduction of disorder where a first-order FM–AF transition occurs, as discussed in the previous subsection. The results of Fig. 3.8.5 clearly indicate that C^{-1} can indeed change by several orders of magnitude in the presence of small fields even in a 1D system that certainly cannot have a percolation. There must be some other mechanism at work in this context. Mayr et al. (2000) believe this alternative mechanism is caused by small modifications in the conductivity of the *insulating* portions of the sample, independent of what occurs in the metallic clusters. It is possible that in an AF region, with zero conductivity at large Hund coupling due to the perfect antialignment of the nearest-neighbor t_{2g}-spins, the small fields may induce a small canting effect that leads to a nonzero conductivity. While this effect should be negligible if the AF-phases is totally dominating, it may become more important if small AF clusters separate FM ones. A sort of "valve" effect may occur, in other words magnetic fields can induce a small connection between metallic states leading to a substantial change in the resistivity. This idea can be studied qualitatively by simply altering by a small amount the conductivity of the insulating regions in the random-resistor network. Results are shown in Fig. 3.8.5b, using the same functions $p = p(T)$ employed before in Fig. 3.8.4. As anticipated, small conductivity changes lead to large resistivity modifications, comparable to those observed in experiments upon the application of magnetic fields. Although the analysis discussed above is only semi-quantitative and further studies in

magnetic fields should actively continue in this context, Mayr et al. (2000) have shown that in the percolative regime two mechanisms (described above) can lead to a large MR, leading to at least a possible framework for describing how the famous CMR effect can occur.

3.9. Related theoretical work on electronic phase separation applied to manganites

The possibility of "electronic" phase separation was already discussed by Nagaev (1967, 1968, 1972) well before it became a popular subject in the context of compounds such as the high-temperature superconductors. Its original application envisioned by Nagaev was to antiferromagnetic semiconductors, where the doping of electrons creates ferromagnetic-phase regions embedded in an AF matrix. Nagaev (1994, 1995) remarked that if the two phases have opposite charge, the Coulombic forces will break the macroscopic clusters into microscopic ones, typically of nanometer-scale size, as remarked in this review before. When the number of these FM clusters is small, the system resembles a regular array of charge sort of a Wigner crystal, as found also in the simulations of Malvezzi et al. (1999), and the system remains an insulator. However, as the density grows, a transition will be found where the clusters start overlapping, and a metal is formed. Although it may seem tempting to assign to this transition percolative properties, as Nagaev does, note that at least without incorporating disorder the clusters are regularly spaced and thus the transition does not correspond to the usual percolative ones described in textbooks and in the previous subsection where the random position of the clusters play a key role. In particular, the critical density at which regularly spaced clusters begin overlapping triggers a process that occurs in all clusters at the same time, different from the notion of a percolative filament with fractalic shape which is crucial in percolative theories. For this reason it is unclear to these authors to what extend electronic phase separation can describe percolative physics in the absence of disorder. It appears that only when randomly distributed clusters of two phases are stabilized, as described in Section 3.8, can true percolation occur.

The calculations of Nagaev (1994, 1995, 1996) have been carried out for one orbital models and usually in the limit where the hopping t of the conduction electrons is much larger than the Hund coupling (although Nagaev expects the results to qualitatively hold even in the opposite limit $J_H > t$). Also a low density of carriers was assumed, and many calculations were performed mainly for the one-electron problem (magneto polaron), and then rapidly generalized to many electrons. The formation of lattice polarons is not included in the approach of Nagaev. These parameters and assumptions are reasonable for AF semiconductors, and Nagaev (1995) argued that his results can explain a considerable body of experimental data for EuSe and EuTe. However, note that Mauger and Mills (1984, 1985) have shown that self-trapped FM polarons (ferrons) are *not* stable in three dimensions. Instead, Mauger and Mills (1984, 1985) proposed that electrons bound to donor sites induce a ferromagnetic moment, and they showed that those bound magnetic polarons can account for the FM clusters observed in EuTe. Free carriers appear "frozen" at low temperatures in these materials, and there are no ferron-like solutions of the underlying equations in the parameter range appropriate to Eu chalcogenides.

In addition, note that the manganites have a large J_H and a large density of electrons, and in principle calculations such as those described above have to be carried out for more realistic parameters, if the results can indeed apply to manganites. These calculations are difficult without the aid of computational techniques. In addition, it is clearly important to consider two orbitals to

address the orbital ordering of the manganites, the possibility of orbital phase separation, and the influence of Jahn-Teller or Coulombic interactions that lead to charge-order AF-states. Disorder also appears to play a key role in manganites.

The unstable character of the low hole-density region of the phase diagram corresponding to the one-orbital model for manganites has also been analyzed by other authors using mostly analytic approximate techniques. In fact, Arovas and Guinea (1998) found an energy convex at small hole concentration, indicative of phase separation, within a mean-field treatment of the one-orbital model using the Schwinger formalism (see also Mishra et al., 1997; Arovas et al., 1999; Guinea et al., 1999; Yi and Lee, 1999; Chattopadhyay et al., 2000; Yuan et al., 2000). Nagaev (1998) using the one-orbital model also arrived at the conclusion that the canted AF-state of the small hole density region is unstable. The same conclusion was obtained in the work of Kagan et al. (1999) where the dominance of phase separation in the small hole-density region was remarked upon, both using classical and quantum spins. Ferromagnetic polarons embedded into an AF surrounding were also discussed by those authors. Polarons in electron-doped one-orbital models where also analyzed by Batista et al. (1998). Nagai et al. (1999) using the dynamical mean-field approximation (exact in infinite dimension) studied the one-orbital model with $S = 1/2$ localized spins. Nagai et al. (1999) (see also Momoi and Kubo, 1998) identified FM-, AF-, and PM-phase. Regimes of phase separation were observed involving the AF- and PM-phase, as well as the PM and FM ones. A representative density vs. chemical potential plot is shown in Fig. 3.9.1. The results obtained by those authors are qualitatively similar to those found using the DMRG in one dimension (Dagotto et al., 1998) for $S = 1/2$ localized spins, and also similar to results obtained in higher dimensions with classical localized spins (Yunoki et al., 1998a). An AF–PM phase separation was also detected in infinite dimension calculations (Yunoki et al., 1998a), showing that not only AF–FM coexistence is possible. Calculations using (t–J)-like models, derived at large J_H starting with the one-orbital model, also reveal phase separation, as shown by Shen and Wang (1998). Overall, it can be safely concluded that using a variety of numerical and analytical techniques, convincing evidence has accumulated that the canted AF-state of deGennes (1960) is simply not stable in models believed to be realistic for manganese oxides. This state is replaced by a mixed-phase or phase-separated regime. The importance of heterogeneity in manganites was also remarked upon by von Molnar

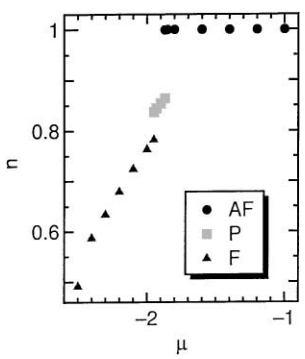

Fig. 3.9.1. Electron density vs. chemical potential in the ground state of the one-orbital model with $S = 1/2$, and a large Hund coupling. AF, P, and F, denote antiferromagnetic, paramagnetic, and ferromagnetic states, respectively. The result is taken from Nagai et al. (1999), where more details can be found.

and Coey (1998), based on an analysis of several experiments. Also Khomskii (1999) remarked upon the importance of phase-separation and percolation.

Other calculations have also shown tendencies to phase separation. For instance, Yamanaka et al. (1998) studied the one-orbital model in two and three dimensions and found phase separation between a flux and antiferromagnetic states (see also Agterberg and Yunoki, 2000). Working with the one-orbital model, computational studies by Yi and Yu (1998) arrived to the same conclusions, previously presented by Yunoki and Moreo (1998), regarding the presence of PS at both small and large hole density once the direct Heisenberg coupling among the t_{2g} spins is considered. Golosov et al. (1998), using a mean-field approximation for the one-band model, also found that the spin canted state was unstable, and indications of phase separation were reported. Schlottmann (1999) using a simple alloy-analogy model showed that the system is unstable to phase separation. Symmetry arguments discussed by Zhong and Wang (1999) also led to PS at low hole doping. In the continuum model, PS has also been found (Román and Soto, 1998).

Even for the two-orbital model, evidence has accumulated that phase separation is present, particularly at low- and high density of holes. Besides the already described robust computational evidence for the case where the orbital degree of freedom plays the key triggering role for this effect (Yunoki et al., 1998b), mean-field approximations presented by Okamoto et al. (1999) also detected phase separation involving two phases with the same spin characteristics (ferromagnetic), but differing orbital arrangement. A representative result is reproduced in Fig. 3.9.2, where the orbital states are also shown.

3.10. On-site Coulomb interactions and phase separation

What happens with phase separation when the on-site Coulomb U interaction is dominant over other interactions? This question does not have an easy answer due to the technical complications of carrying out reliable calculations with a nonzero U. In fact, the one-band Hubbard model has been studied for a long time as a model of high temperature superconductors and after more than 10 years of work it is still unclear whether it phase separates in realistic regimes of parameters. Thus, it is not surprising that similar uncertainties may arise in the context of models for manganites. As remarked before, studies of the one-dimensional one-orbital model including a nonzero U were carried out by Malvezzi et al. (1999). In this study, a region of phase separation was identified in a similar location as obtained in the Monte Carlo simulations without U (Yunoki et al., 1998). Then, certainly switching on U "slowly" starting in the phase separated regime of the one-orbital model does not alter the presence of this regime. On the other hand, Shen and Wang (1999a) claimed that if U is made larger than J_H, the model does not lead to phase separation according to their calculations (see also Gu et al., 1999). This issue is somewhat complicated by the well-known fact that pure Hubbard-like models tend to present a large compressibility near half-filling, namely the slope of the curve density vs. chemical potential is large at that density (Dagotto, 1994). This may already be indicative of at least a *tendency* to phase separation that could be triggered by small extra terms in the Hamiltonian. More recently, it has been shown that a two-orbital 1D model with a form resembling those studied in manganites (but without localized spins) indeed presents phase separation when studied using the DMRG technique (Hotta et al., 2000). This is in agreement with the results of Shen and Wang (1999b) using the two-orbital model at both large U and J_H, where it was concluded that having *both* couplings leads to a rich phase

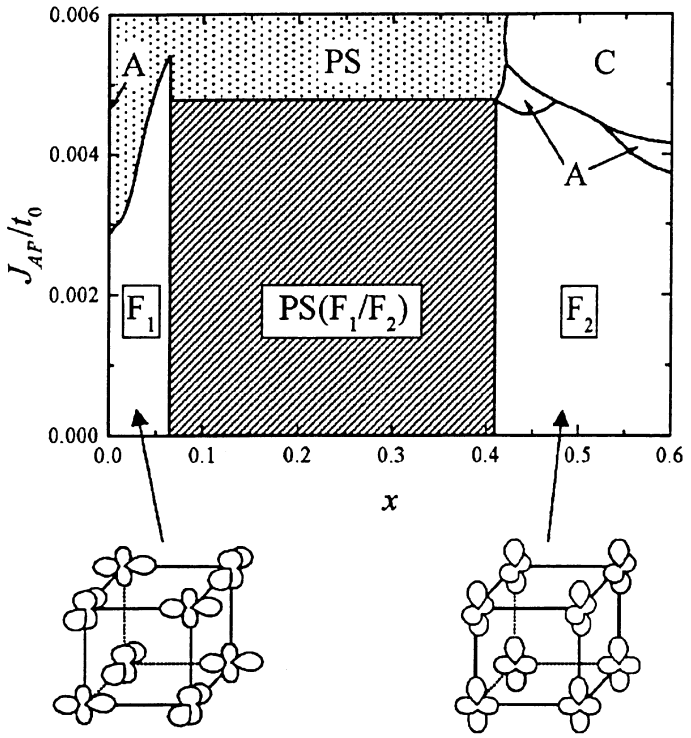

Fig. 3.9.2. Phase diagram at zero temperature in the plane of AF interaction J_{AF} and hole concentration x, using a two-orbital model with Coulomb interactions. F_1 and F_2 are the ferromagnetic phases with different types of orbital ordering (indicated). $PS(F_1/F_2)$ is the phase-separated state between the F_1 and F_2 phases. Results taken from Okamoto et al. (2000) where more details, including couplings, can be found.

diagram with phase-separated and charge-ordered states. It is likely that this conclusion is correct, namely phase separation may be weak or only incipient in the purely Coulombic models, but in order to become part of the phase diagram, the Hund coupling to localized spins may play a key role. More work is needed to clarify these issues. Finally, the reader should recall the discussion of Section 3.3, where at least within a mean-field approximation it was shown that a large electron-JT phonon coupling or large Coulombic couplings are qualitatively equivalent. This is especially true when issues such as phase separation induced by disorder are considered, in which the actual origin of the two competing phases is basically irrelevant. Note also that Motome et al. (1998) have found phase separation in a two orbital model for manganites when a combination of Coulombic and Jahn–Teller interactions is considered. Recently, Laad et al. (2000) have also investigated a model including both Coulombic and JT-phononic couplings, analyzing experiments at $x = 0.3$ $La_{1-x}Sr_xMnO_3$.

3.11. Theories based on Anderson localization

There is an alternative family of theories which relies on the possibility of electron localization induced by two effects: (1). off-diagonal disorder caused by the presence of an effective *complex*

electron hopping in the large Hund-coupling limit (see for instance Müller-Hartmann and Dagotto, 1996; Varma, 1996), and (2). non-magnetic diagonal disorder due to the different charge and sizes of the ions involved in manganese oxides, as discussed before. Calculations in this context by Sheng et al. (1997), using scaling theory and a mean-field distribution for the spin orientations (one orbital model, $J_H = \infty$), were claimed to reproduce quantitatively the magnetoresistance effect of real materials. Related calculations have been presented by Allub and Alascio (1996, 1997) and Aliaga et al. (1998). In these calculations, the electrons are localized above T_C due to strong disorder, while at low temperature the alignment of the spins reduce the spin disorder and the electrons are delocalized. In this framework, also Coey et al. (1995) argued that the e_g-electrons, while delocalized at the Mn–Mn scale, are localized at larger scales.

There are some problems with approaches based on simple Anderson localization. For example, the phases competing with ferromagnetism are in general of little importance, and the mixed-phase tendencies of manganites, which are well established from a variety of experiments as shown in Section 4, are not particularly relevant in this context. The first-order-like nature of the transitions in these compounds is also not used. Note also that recently Smolyaninova et al. (1999) have experimentally shown that the metal–insulator transition of $La_{1-x}Sr_xMnO_3$ at $x = 0.33$ is not an Anderson localization transition. In addition, the $x = 0.5$ CO state, crucial in real manganites to drive the strong CMR effect near this density, plays no important role in this context. It appears also somewhat unnatural to deal with an on-site disorder with such a large strength, typically $W \sim 12t$ (the random energies ε_i are taken from the distribution $[-W/2, W/2]$, and t is the one-orbital hopping amplitude). However, it may occur that this strong disorder is a way to effectively mimic, in a sort of coarse-grained lattice, the disorder induced by cluster formation, similar to the calculation of the resistivity in Section 3.8. For instance, Sheng et al. (1997b) noticed the relation between the $T = 0$ residual resistivity and the presence of a peak in the same quantity at T_C. However, instead of assigning the large $\rho_{dc}(T = 0)$ to the percolative process described in Section 3.8, nonmagnetic randomness was used, and naturally a large W was needed to arrive at the large resistivities that appear near percolative transitions. The authors of this review believe that theories based on electron localization ideas, although they appear at first sight not directly related to the ubiquitous clustering tendencies of real manganites, may effectively contain part of the answer to the manganite puzzle, and further work in this context should be encouraged, if possible including in the approach a description of how localization phenomena relates to the phase separation character of manganites. Steps in this direction were recently taken by Sheng et al. (1999), in which calculations with JT phonons were carried out, and phase separation tendencies somewhat similar to those reported by Yunoki et al. (1998) were observed.

4. Experimental evidence of inhomogeneities in manganites

4.1. $La_{1-x}Ca_xMnO_3$ at density $0.0 \leq x < 0.5$

The regime of intermediate and low hole densities of $La_{1-x}Ca_xMnO_3$ the former being close to the AF CE-type state at $x = 0.5$ and the latter to the antiferromagnetic A-type state at $x = 0$, is complex and interesting. In this region, the FM metallic state believed to be caused by double exchange is in competition with other states, notably AF ones, leading to the mixed-phase

tendencies that are the main motive of this review. The special density $x = 0.33$ in $La_{1-x}Ca_xMnO_3$ has received considerable experimental attention, probably caused by the peak in the Curie temperature which occurs near this hole concentration (see phase diagram in Section 2.2). For potential technological applications of manganites it is important that the FM transition temperature be as high as possible, and thus it is important to understand this particular composition. However, although this reason for focusing efforts at $x = 0.33$ is reasonable, recent experimental and theoretical work showed that it is convenient to move away from the optimal density for ferromagnetism to understand the behavior of manganites, since many of the interesting effects in these compounds are magnified as T_C decreases. Nevertheless, the information gathered at the hole density $x = 0.33$ is certainly important, and analyzed together with the results at other densities, illustrates the inhomogeneous character of manganites.

Historically, the path followed in the study of data at low and intermediate densities of LCMO is fairly clear. Earlier works focused on ideas based on polarons, objects assumed to be usually small in size, and simply represented as a local distortion of the homogeneous background caused by the presence of a hole. The use of polarons was understandable due to the absence of theoretical alternatives until a few years ago, and it may still be quite appropriate in large regions of parameter space. However, recent experimental work has shifted toward the currently more widely accepted mixed-phase picture where the ferromagnetic regions are not small isolated polarons but substantially larger clusters, at least in the important region in the vicinity of T_C (polaronic descriptions may still be realistic well above T_C). Note that the various efforts reporting polarons usually employed techniques that obtained spatially averaged information, while only recently, real-space images of the local electronic properties have been obtained that clearly illustrates the mixed-phase character of the manganite states. Below follows a summary of the main experimental results addressing mixed-phase characteristics in $La_{1-x}Ca_xMnO_3$ at densities between $x = 0.0$ and 0.5 (excluding the latter which will be analyzed separately). These results are not presented in historical order, but are mainly grouped by technique. Although the list is fairly complete, certainly it is not claimed that all reports of mixed-phase tendencies are described here as other efforts in this direction may have escaped our attention.

4.1.1. Electron microscopy

Among the most important experimental results that have convincingly shown the presence of intrinsic mixed-phase tendencies in manganites are those recently obtained by Uehara et al. (1999) in their study of $La_{5/8-y}Pr_yCa_{3/8}MnO_3$ using transport, magnetic, and electron microscopy techniques (see also Kiryukhin et al., 2000; Zuo and Tao, 2000). The results reported by those authors for the resistivity vs. temperature at several Pr compositions are reproduced in Fig. 4.1.1a. Note the rapid reduction with increasing y of the temperature at which the peak occurs, which correlates with the Curie temperature. Note also the hysteretic behavior of the resistivity, signalling the presence of first-order-like characteristics in these compounds. Another features of Fig. 4.1.1a is the presence of an abnormally large residual resistivity at low temperatures in spite of the fact that $d\rho/dT > 0$ suggests metallic behavior. The magnetoresistance factor shown in Fig. 4.1.1b is clearly large and increases rapidly as T_C is reduced. This factor is robust even at low temperatures where the resistivity is flat, namely the large MR effect does not happen exclusively at T_C.

The results of Uehara et al. (1999) have been interpreted by those authors as evidence of two-phase coexistence, involving a stable FM state at small y, and a stable CO state in the large

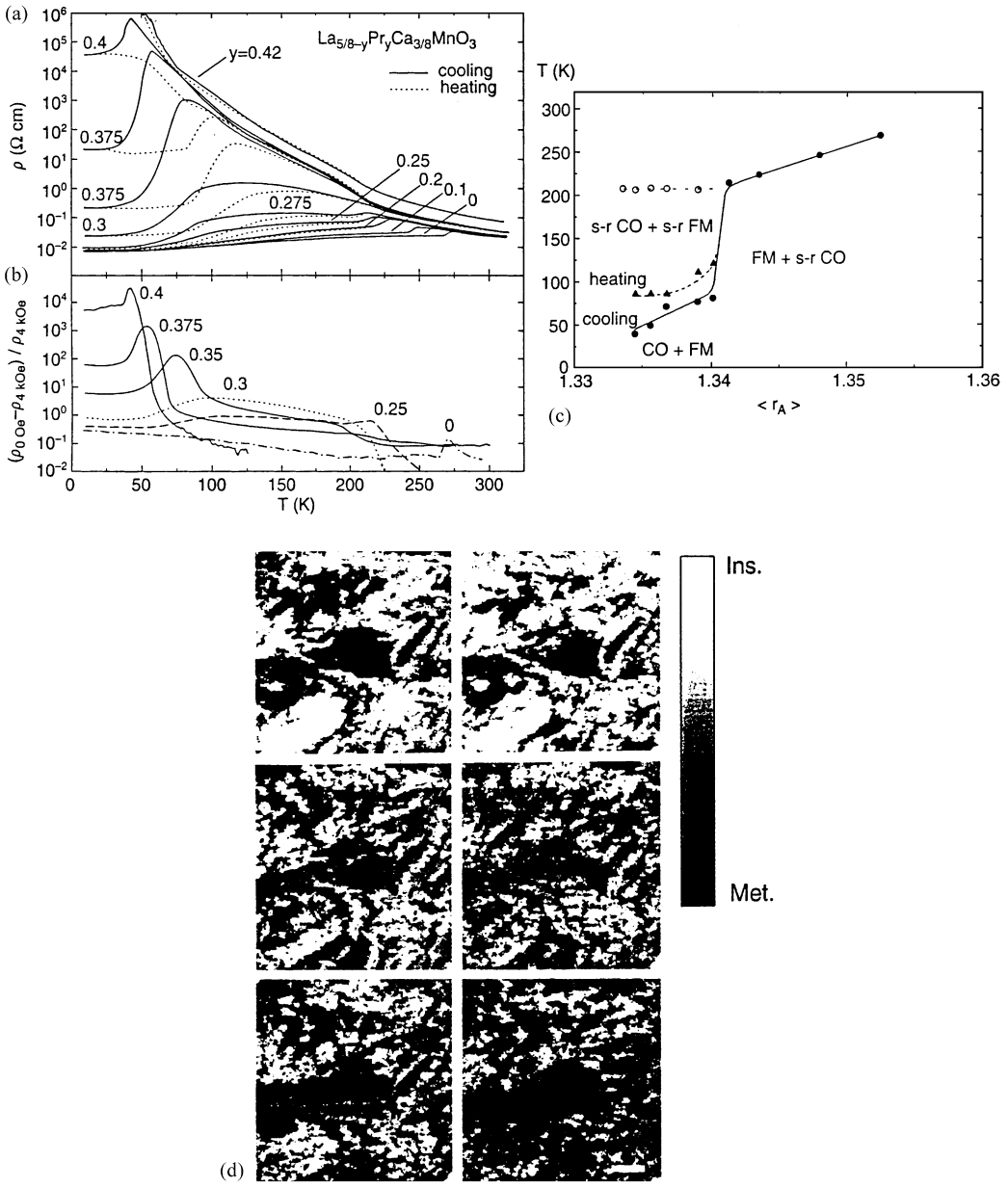

Fig. 4.1.1. Transport and magnetic properties of $La_{5/8-y}Pr_yCa_{3/8}MnO_3$ as a function of temperature and y, reproduced from Uehara et al. (1999). (a) contains the temperature dependence of the resistivity. Both cooling (solid lines) and heating (dotted lines) curves are shown. (b) Magnetoresistance of representative specimens at 4 kOe. (c) Phase diagram of $La_{5/8-y}Pr_yCa_{3/8}MnO_3$ as a function of the ionic radius of (La, Pr, Ca). T_C and T_{CO} are shown as filled circles (or triangles) and open circles, respectively. For more details, see Uehara et al. (1999) from where this figure was taken. (d) Generic spectroscopic images reported by Fäth et al. (1999) using scanning tunneling spectroscopy applied to a thin film of $La_{1-x}Ca_xMnO_3$ with x close to 0.3, and the temperature just below T_C. The size of each frame is 0.61 μm × 0.61 μm. From left to right and top to bottom the magnetic fields are 0, 0.3, 1, 3, 5, and 9 T. The light (dark) regions are insulating (metallic).

y PCMO compound. A percolative transition in the intermediate regime of compositions was proposed. The phase diagram is in Fig. 4.1.1c and it contains at low temperatures and a small range of Pr densities a phase labeled "CO + FM" which corresponds to the two-phase regime. In other regions of parameter space, short-range "s-r" FM or CO order has been observed. Uehara et al. (1999) substantiated their claims of phase separation using electron microscopy studies. Working at $y = 0.375$ and at low temperature of 20 K, coexisting domains having sizes as large as 500 nm were found. At 120 K, the clusters become nanometer in size. Note that these low-temperature large clusters appear at odds with at least one of the sources of inhomogeneities discussed in the theoretical review (electronic phase separation), since $1/r$ Coulomb interactions are expected to break large clusters into smaller ones of nanometer size. In fact, Uehara et al. (1999) remarked it is reasonable to assume that the competing phases are of the same charge density. However, the experimental results for $La_{5/8-y}Pr_yCa_{3/8}MnO_3$ are in excellent agreement with the other proposed source of mixed-phase tendencies, namely the ideas presented by Moreo et al. (2000), where first-order transitions are transformed into regions of two-phase coexistence by the intrinsic chemical disorder of the manganites (Section 3). This effect is called "disorder-induced phase separation".

4.1.2. Scanning tunneling spectroscopy

Another remarkable evidence of mixed-phase characteristics in $La_{1-x}Ca_xMnO_3$ with $x \sim 0.3$ has been recently reported by Fäth et al. (1999) using scanning tunneling spectroscopy. With this technique, a clear phase-separated state was observed below T_C using thin films. The clusters involve metallic and insulating phases, with a size that is dependent on magnetic fields. Fäth et al. (1999) believe that T_C and the associated magnetoresistance behavior is caused by a percolation process. In Fig. 4.1.1d, a generic spectroscopic image is shown. A coexistence of metallic and insulating "clouds" can be observed, with a variety of typical sizes involving tens to hundreds of nanometers. Fäth et al. (1999) remarked that it is clear that such length scales are not compatible with a picture of homogeneously distributed small polarons. The authors of this review agree with that statement.

The results of Fäth et al. (1999) suggest that small changes in the chemical composition around $La_{1-x}Ca_xMnO_3$ at $x = 0.25$ can lead to dramatic changes in transport properties. This is compatible with results by other groups. For example, Ogale et al. (1998) reported transport measurements applied to $La_{0.75}Ca_{0.25}Mn_{1-x}Fe_xO_3$, i.e., with a partial replacement of Mn by Fe, the latter being in a Fe^{3+} state. In this case, just a 4% Fe doping ($x = 0.04$) leads to an instability of the low-temperature ferromagnetic metallic phase of the $x = 0.0$ compound toward an insulating phase. The results for the resistivity vs. temperature are shown in Fig. 4.1.2. The shape of these curves is quite similar to the results observed in other compounds, such as those studied by Uehara et al. (1999), and they are suggestive of a percolative process leading eventually to a fully insulating state as x grows. Note the similarities of these curves with the theoretical calculations shown in Figs. 3.8.2 and 4.

4.1.3. Small-angle neutron scattering

Small-angle neutron scattering combined with magnetic susceptibility and volume thermal expansion measurements by De Teresa et al. (1997b) (see also Ibarra and De Teresa, 1998a) applied to $La_{1-x}Ca_xMnO_3$ with $x = 1/3$ provided evidence for small magnetic clusters of size 12 Å above T_C. Although to study their data De Teresa et al. (1997b) used the simple picture of small

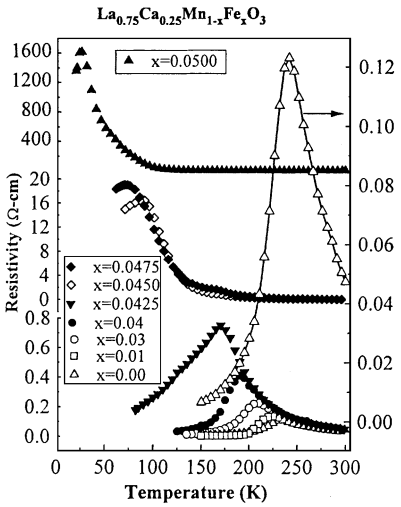

Fig. 4.1.2. Resistivity vs. temperature at several densities for $La_{0.75}Ca_{0.25}Mn_{1-x}Fe_xO_3$, taken from Ogale et al. (1998). The results for the undoped sample are shown on an expanded scale (right) still using Ω-cm as unit.

lattice/magneto polarons available by the time of their analysis, by now it is apparent that individual small polarons may not be sufficient to describe the physics of manganites near the Curie temperature. Nevertheless, leaving aside these interpretations, the very important results of De Teresa et al. (1997b) clearly experimentally showed the presence of an inhomogeneous state above T_C early in the study of manganese oxides. The coexisting clusters were found to grow in size with a magnetic field and decrease in number. Ibarra and De Teresa (1998c), have reviewed their results and concluded that electronic phase segregation in manganites emerges from their data. Even percolative characteristics were assigned by Ibarra and De Teresa (1998a) to the metal–insulator transition, in excellent agreement with theoretical calculations (Moreo et al., 2000; Mayr et al., 2000). Hints of the mixed-phase picture (involving FM clusters larger than the size of a single ferro polaron) are also contained in the comment on the De Teresa et al. results presented by Zhou and Goodenough (1998b).

Using neutron diffraction, muon-spin relaxation, and magnetic techniques, studies of $(La_{1-x}Tb_x)_{2/3}Ca_{1/3}MnO_3$ were also reported by De Teresa et al. (1996, 1997a). At low temperatures, an evolution from the FM metallic state at $x = 0$ to the antiferromagnetic insulating state at $x = 1$ was reported, involving an intermediate regime between $x = 0.33$ and 0.75 with spin-glass insulating characteristics. The phase diagram is in Fig. 4.1.3a. Static local fields randomly oriented were identified at, e.g., $x = 0.33$. No long-range ferromagnetism was found in the intermediate density regime. In view of the recent theoretical and experimental reports of giant cluster coexistence in several manganites, it is natural to conjecture the presence of similar phenomena in the studies of De Teresa et al. (1996, 1997a). In fact, the plots of resistance vs. temperature (see Fig. 4.1.3b, taken from Blasco et al., 1996) between $x = 0.0$ and 0.5 have a shape very similar to those found in other manganites that were described using percolative ideas, such as $La_{5/8-y}Pr_yCa_{3/8}MnO_3$ (Uehara et al., 1999).

Another interesting aspect of the physics of manganites that has been emphasized by Ibarra et al. (1995), Ibarra and De Teresa (1998c) and others, is the presence in the paramagnetic regime above

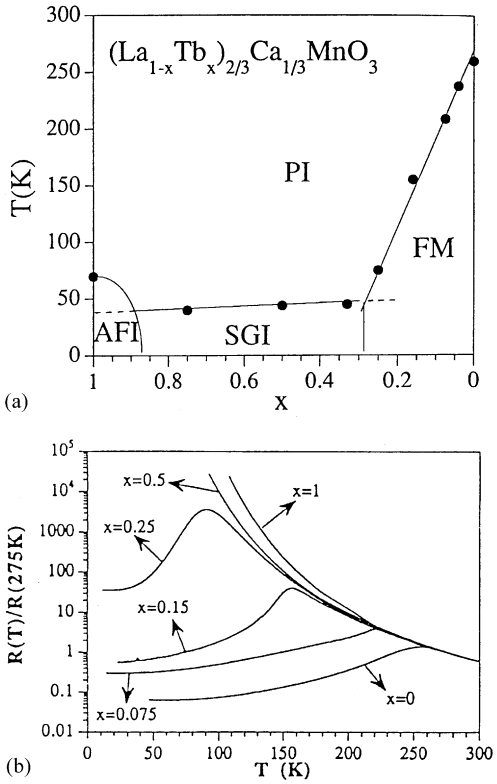

Fig. 4.1.3. (a) Electronic and magnetic phase diagram of $(La_{1-x}Tb_x)_{2/3}Ca_{1/3}MnO_3$ as a function of x, reproduced from De Teresa et al. (1997a), where more details can be found. SGI is a "spin-glass" insulating state. (b) Resistance vs. temperature corresponding to $(La_{1-x}Tb_x)_{2/3}Ca_{1/3}MnO_3$ at the densities indicated, reproduced from Blasco et al. (1996). The similarities with analogous plots for other manganites described by a percolative process are clear.

T_C of a large contribution to the volume thermal expansion that cannot be explained by the Grüneisen law. Those authors assign this extra contribution to polaron formation. Moreover, the results for the thermal expansion vs. temperature corresponding to several manganites at x approximately 0.30 can be collapsed into a universal curve (Fig. 57 of Ibarra and De Teresa, 1998c) showing that the phenomenon is common to all compounds even if they have different Curie temperatures. Above T_C, there is a coexistence of a high-volume region associated with localized carriers and a low-volume region associated with delocalized carriers. The spontaneous or field-induced metal to insulator transition is associated with a low-to-high-volume transition. From this analysis it was concluded that there are two states in close competition and that the transition should be of first order, in excellent agreement with the recent simulations of Yunoki et al. (2000).

The analysis of elastic neutron scattering experiments by Hennion et al. (1998) (see also Moussa et al., 1999) has provided very useful information on the behavior of $La_{1-x}Ca_xMnO_3$ at low values of x. While previous work by the same authors (Hennion et al., 1997) was interpreted using a description in terms of simple magnetic polarons, Hennion et al. (1998) reinterpreted their results

as arising from a liquid-like spatial distribution of magnetic *droplets*. The radius of these droplets was estimated to be 9 Å and their number was found to be substantially smaller than the number of holes (ratio droplets/holes = 1/60 for $x = 0.08$), leading to a possible picture of hole-rich droplets within a hole-poor medium, if spin polarized regions are induced by carriers. Note the use of the word droplet instead of polaron in this context: polarons are usually associated with only one carrier, while droplets can contain several. It is quite remarkable that recent analysis by the same group (Hennion et al., 1999) of the compound $La_{1-x}Sr_xMnO_3$ at $x = 0.06$ has lead to very similar results: ferromagnetic clusters were found in this "large" bandwidth manganite and the number of these clusters is larger by a factor 25 than the number of holes. Hennion et al. (1999) concluded that phase separation between hole-rich and hole-poor regions is a general feature of the low doping state of manganites. These authors believe that this phenomenon likely occurs even at higher concentrations close to the metal–insulator transition.

4.1.4. Neutron scattering

Early in the study of manganites, results of neutron scattering experiments on $La_{1-x}Ca_xMnO_3$ for a wide range of compositions were interpreted by Lynn et al. (1996, 1997) in terms of a competition between ferromagnetic metallic and paramagnetic insulating states, leading to a state consisting of two coexisting phases. The relative fraction of these two phases was believed to change as the temperature was reduced to T_C. This occurs even at the optimal composition for ferromagnetism close to $x = 1/3$. A typical result of their measurements is presented in Fig. 4.1.4a where the inelastic spectrum is shown at two temperatures and small momentum transfer, for the $x = 1/3$ compound which has a $T_C = 250$ K. The two peaks at nonzero energy are interpreted as spin waves arising from the ferromagnetic regions while the central peak is associated with the paramagnetic phase. Even at temperature as low as 200 K the two features can be observed. Fernandez-Baca et al. (1998) extended the analysis of Lynn et al. (1996) to other compounds with a similar hole concentration $x \sim 0.33$. Their conclusions are very similar, i.e., a central component near T_C is found in all the compounds studied and those authors concluded that "magnetism alone cannot explain the exotic spin dynamical properties" of manganites (Fig. 4.1.4b contains their results for $Pr_{1-x}Sr_xMnO_3$ and $Nd_{1-x}Sr_xMnO_3$ at $x \sim 0.3$). Even the compound $La_{1-x}Sr_xMnO_3$ at $x = 0.15$ and 0.30 show a similar behavior (Fig. 4.1.4c and d), in spite of the fact that Sr-based manganites are usually associated with more conventional behavior than Ca-based ones.

Overall, the neutron scattering experimental results are in good qualitative agreement with the conclusions reached by other experimental techniques, such as tunneling measurements at similar compositions which were reviewed before, and with theoretical calculations (already reviewed in Section 3). Lynn et al. (1996) also noticed the presence of irreversibilities in the transitions, and they remarked that these transitions are not of second order. These early results are also in agreement with the more recent theoretical ideas of Yunoki et al. (2000) and Moreo et al. (2000) where first-order transitions are crucial for the coexistence of giant clusters of the competing phases.

4.1.5. PDF techniques

Using pair-distribution-function (PDF) analysis of neutron powder-diffraction data, Billinge et al. (1996) studied $La_{1-x}Ca_xMnO_3$ at small and intermediate densities x. They explained their results in terms of lattice polaron formation associated with the metal–insulator transition in these materials. Below T_C, Billinge et al. (1996) believe that the polarons can be large, dynamic, and

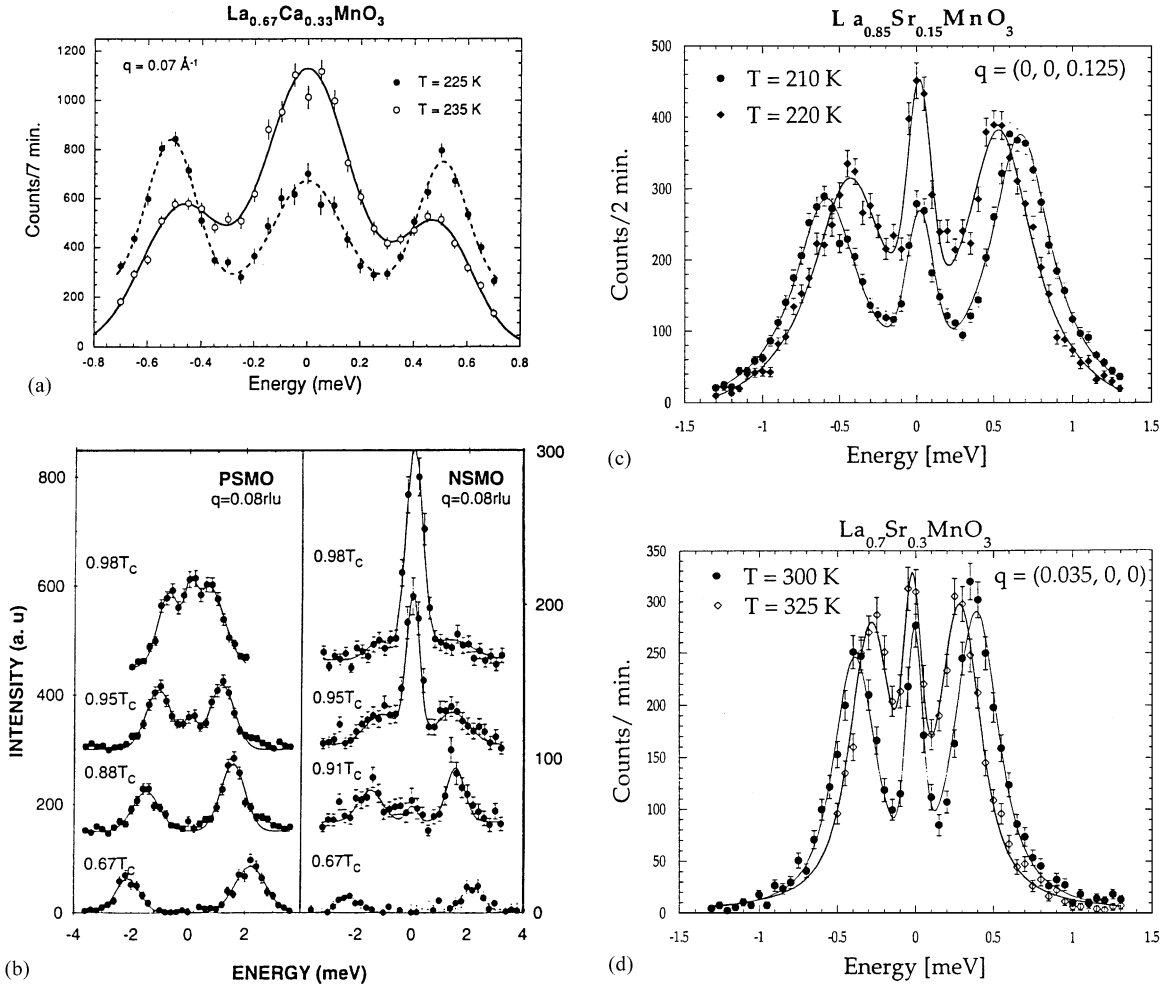

Fig. 4.1.4. (a) Inelastic spectrum at the two temperatures indicated and for $q = 0.07$ Å^{-1}, reported by Lynn et al. (1996) in their study of $La_{1-x}Ca_xMnO_3$ at $x = 0.33$. The left and right peaks are associated with spin waves in FM portions of the sample, while the central peak is attributed to paramagnetic regions. (b) Similar as (a) but for $Pr_{1-x}Sr_xMnO_3$ ($x = 0.37$) and $Nd_{1-x}Sr_xMnO_3$ ($x = 0.30$) at the temperatures and momenta indicated (reproduced from Fernandez-Baca et al., 1998). (c,d) Similar as (a) but for $La_{1-x}Sr_xMnO_3$ at the compositions, temperatures, and momenta indicated. (c) is reproduced from Vasiliu-Doloc et al. (1998a), while (d) is from Vasiliu-Doloc et al. (1998b).

spread over more than one atomic site. Note, however, that these authors use a polaronic picture due to the presence in their data of a mixture of short and long Mn–O bonds, implying distorted and undistorted MnO_6 clusters. Whether the distorted octahedra are randomly distributed, compatible with the polaronic theory, or gathered into larger structures, compatible with the phase separation theory, has not been analyzed. More recent studies by Billinge et al. (1999), using the same technique, produced the schematic phase diagram shown in Fig. 4.1.5. Note the light shaded region inside the FM-phase: in this regime Billinge et al. (1999) believe that localized and delocalized phases coexist. The white region indicates the only regime where an homogeneous FM

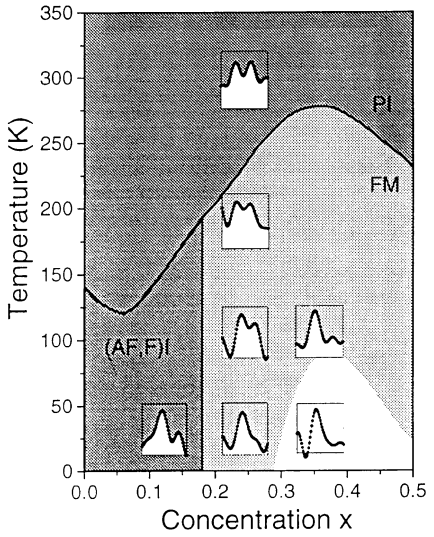

Fig. 4.1.5. Schematic phase diagram of $La_{1-x}Ca_xMnO_3$, from Billinge et al. (1999). The solid lines are transport and magnetic transitions taken from Ramirez et al. (1996). The notation is standard. The small insets are PDF peaks (for details see Billinge et al., 1999). The dark shaded regions are claim to contain fully localized polaronic phases. The light shaded region denotes coexistence of localized and delocalized phases, while the white region is a FM homogeneous phases. The boundaries between the three regimes are diffuse and continuous, and are only suggestive.

phase was found. This result is remarkable and it illustrates the fact that the simple double-exchange ideas, that lead to an homogeneous FM-state, are valid in $La_{1-x}Ca_xMnO_3$ in such a narrow region of parameter space that they are of little value to describe narrow band manganites in the important CMR regime. As remarked before, it appears that it is the *competition* between DE and the other tendencies dominant in manganites that produces the interesting magneto-transport properties of these compounds.

4.1.6. X-ray absorption, transport and magnetism

Similar conclusions as those found by Billinge et al. (1996, 1999) were reached by Booth et al. (1998a, b) using X-ray absorption measurements applied to $La_{1-x}Ca_xMnO_3$ at several hole concentrations. This technique provides information about the distribution of Mn–Mn bond lengths and the Mn–O environment. The results, obtained at several densities, favor a picture similar to that described in the previous subsection, namely there are two types of carriers: localized and delocalized. The number of delocalized holes grows exponentially with the magnetization below T_C. These results clearly show that, even in the ferromagnetic regime, there are two types of phases in competition. In agreement with such conclusions, the presence of large polarons below T_C at $x = 0.25$ was also obtained by Lanzara et al. (1998) using X-ray techniques. Near T_C those authors believe that small and large polarons coexist and a microscopic phase separation picture is suitable to describe their data.

Early work using X-ray absorption for $La_{1-x}Ca_xMnO_3$ at $x = 0.33$ by Tyson et al. (1996) showed the presence of a complex distribution of Mn–O bond lengths, with results interpreted as generated by small polarons. Hundley et al. (1995) studied the same compound using transport

techniques and, due to the observation of exponential behavior of the resistivity with the magnetization, they concluded that polaron hopping could explain their data. As remarked before, it is not surprising that early work used polaronic pictures to analyze their results, since by that time it was the main theoretical possibility available for manganites. However, Hundley et al. (1995) already noticed that the polarons could form superlattices or domains, a conjecture that later experimental work contained in this section showed to describe experiments more properly.

4.1.7. Nuclear magnetic resonance

The coexistence of FM and AF resonances in NMR data obtained for $La_{1-x}Ca_xMnO_3$ at several small hole densities was reported by Allodi et al. (1997) and Allodi et al. (1998a, b) using ceramic samples. No indications of a canted phase were observed by these authors, compatible with the conclusions of theoretical work showing that indeed the canted phase is unstable, at least within the models studied in Section 3. The NMR results showing the FM–AF coexistence contain a peak at ~ 260 MHz which corresponds to AF, and another one slightly above 300 MHz which is believed to be FM in origin, according to the analysis of Allodi et al. (1997).

A study of dynamic and static magnetic properties of $La_{1-x}Ca_xMnO_3$ in the interval between $x = 0.1$ and 0.2 by Troyanchuk (1992) also showed indications of a mixed-state consisting of ferromagnetic and antiferromagnetic clusters. Troyanchuk (1992) remarked very early on that his data was not consistent with the canted structure of deGennes (1960).

4.1.8. Muon spin relaxation

The observation of two time scales in $La_{1-x}Ca_xMnO_3$ at $x \sim 0.3$ using zero-field muon spin relaxation were explained by Heffner et al. (1999) in terms of a microscopically inhomogeneous FM phase below T_C, caused by the possible overlapping of growing polarons as the temperature is reduced. Heffner et al. (1999) concluded that a theoretical model mixing disorder and coupled JT-modes with the spin degrees of freedom may be necessary to explain their results, in agreement with the more recent theoretical calculations presented by Moreo et al. (2000) which used a mixture of disorder and strong JT correlations. Evidence for spatially inhomogeneous states using muon spin relaxation methods were also discussed by the same group in early studies (Heffner et al., 1996) where glassy spin dynamics was observed. Nonhomogeneous states for manganites were mentioned in that work as a possible alternative to the polaronic picture.

4.1.9. Photoemission

Recently, Hirai et al. (2000) applied photoemission techniques to $La_{1-x}Ca_xMnO_3$ with $x = 0.3$,0.4 and 0.5, measuring the photoabsorption and magnetic circular dichroism. Interesting systematic changes in the core level edges of Ca $2p$, O $1s$ and Mn $2p$ were observed as temperature and stoichiometry were varied. The results were interpreted in terms of a phase-separated state at room temperature, slightly above the Curie temperature. The metallic regions become larger as the temperature is reduced. These results are in excellent agreement with several other experiments describing the physics above T_C as caused by a mixed-phase state, and with the theoretical calculations reviewed in Section 3. Based on the results of Hirai et al. (2000), it is conceivable that photoemission experiments may play a role as important in manganites as they do in the cuprates.

4.1.10. Hall effect

Recent studies of the Hall constant of $La_{1-x}Ca_xMnO_3$ at $x = 0.3$ by Chun et al. (1999b) provided evidence that the picture of independent polarons believed in earlier studies to be valid in this compound above T_C is actually valid *only* for temperatures larger than $1.4T_C$ i.e. well above the region of main interest from the point of view of the CMR phenomenon. In the temperature regime between T_C and $1.4T_C$, Chun et al. (1999b) describe their results as arising from a two-phase state, with percolative characteristics at T_C. Once again, from this study it is clear that the insulating state of manganites above T_C is not a simple gas of independent lattice/spin polarons (or bipolarons, see Alexandrov and Bratkovsky, 1999). This is compatible with the phenomenological two-fluid picture of localized and itinerant carriers near T_C which was envisioned by Jaime et al. (1996, 1999) early in the study of manganites, and it is expected to apply to the $x = 0.3$ $La_{1-x}Ca_xMnO_3$ material.

4.1.11. Studies with high pressure

The properties of manganites are also very sensitive to pressure, as explained in the Introduction. As an example, consider the results of Zhou et al. (1998a) Zhou and Goodenough (1998b) obtained analyzing $(La_{0.25}Nd_{0.75})_{0.7}Ca_{0.3}MnO_3$ as a function of pressure (see also Zhou et al., 1996). This compound appears to have a tolerance factor slightly below the critical value that separates the ferromagnetic regime from the antiferromagnetic one. While Zhou and Goodenough (1998) emphasized in their work the giant isotope effect that they observed in this compound upon oxygen isotope substitution, a very interesting feature indeed, here our description of their results will mainly focus on the resistivity vs. temperature plots at various pressures shown in Fig. 4.1.6. In view of the recent experimental results observed in similar materials that are also in the region of competition between FM- and AF-state, it is natural to contrast the results of Fig. 4.1.6 with those of, e.g., Uehara et al. (1999). Both sets of data, one parametric with pressure at fixed Nd-density and the other (Fig. 4.1.1a) parametric with Pr-density at ambient pressure, are similar and also in agreement with the theoretical calculations (Moreo et al., 2000; Mayr et al., 2000). The shape of the curves Fig. 4.1.6 reveal hysteretic effects as expected in first-order transitions, flat

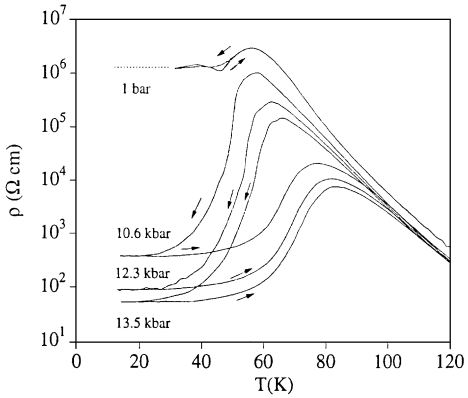

Fig. 4.1.6. Resistivity vs. temperature for $(La_{0.25}Nd_{0.75})_{0.7}Ca_{0.3}MnO_3$ reproduced from Zhou and Goodenough (1998). Pressures are indicated.

resistivities at low temperatures, a rapid change of $\rho(T=0)$ with pressure, and the typical peak in the resistivity at finite temperature that leads to CMR effects. All those features exist also in Fig. 4.1.1a.

Similar pressure effects in $(La_{0.5}Nd_{0.5})_{2/3}Ca_{1/3}MnO_3$ were reported by Ibarra et al. (1998b). Those authors concluded that, at low temperatures, insulating CO and metallic FM regions coexist, and that this is an intrinsic feature of the material. The interpretation of their results appears simple: a first-order transition smeared by the intrinsic disorder in manganites can be reached by compositional changes or by changes in the couplings induced by pressure. But the overall physics is similar. In view of this interpretation, it is natural to conjecture that the material $(La_{1-x}Nd_x)_{0.7}Ca_{0.3}MnO_3$ discussed in the previous paragraph should also contain regions with a coexistence of giant clusters of FM- and AF-phase. Zhou et al. (1998a), Zhou and Goodenough (1998b) indeed mentioned the possibility of phase segregation between hole-rich and hole-poor regions in the paramagnetic state, but the low-temperature regime may have mixed-phase properties as well. In particular, the "canted-spin ferromagnetism" below T_N reported by Zhou and Goodenough (1998) could be induced by phase coexistence.

4.1.12. Related work

Several other studies have shed light on the behavior of ferromagnetically optimally doped manganites. For instance, studies of thin films of $La_{0.67}(Ca_xSr_{1-x})_{0.33}MnO_3$ by Broussard et al. (1999a, b) showed that the value of the magnetoresistance decreases rapidly as x is reduced from 1, namely as the system moves from a low to a large bandwidth manganite at a fixed hole density of 0.33. This interesting material should indeed present a transition from a mixed-phase state near T_C for $x=1$ (all Ca), in view of the tunneling results of Fäth et al. (1999) and several others, to a more standard metal at $x=0$ (all Sr). In addition, Zhao et al. (1998) found a two component signal in the pulsed laser-excitation-induced conductance of $La_{1-x}Ca_xMnO_3$ at $x=0.3$. The results can also be interpreted as a two-phase coexistence. Recently, Wu et al. (2000) reported the presence of colossal electroresistance (CER) effects in $La_{1-x}Ca_xMnO_3$ with $x=0.3$, an interesting effect indeed, and they attributed its presence to phase separation tendencies. Kida et al. (2000a) estimated the complex dielectric constant spectrum of $La_{1-x}Ca_xMnO_3$ with $x=0.3$, concluding that the results are compatible with a mixed-phase state. Belevtsev et al. (2000) reported studies in $La_{1-x}Ca_xMnO_3$ $x=0.33$ films, where upon the application of a small dose of irradiation, large changes in the film resistivity were obtained. This is natural in a percolative regime, where small changes can lead to important modifications in transport.

Complementing the previous studies, recently Smolyaninova et al. (1999) have shown that the metal–insulator transition of $La_{1-x}Ca_xMnO_3$ at $x=0.33$ is *not* an Anderson localization transition, since scaling behavior was clearly not observed in resistivity measurements of thin films. This important study appears to rule out simple theories based on transitions driven by magnetic disorder, such as those proposed by Müller-Hartmann and Dagotto (1996), Varma (1996), and Sheng et al. (1997). A similar conclusion was reached by Li et al. (1997) through the calculation of density of states with random hopping (for a more recent density of states and localization study of the one-orbital model at $J_H=\infty$ see Cerovski et al., 1999). It was observed that this randomness was not sufficient to move the mobility edge, such that at 20% or 30% doping there was localization. It appears that both Anderson localization and the simple picture of a gas of independent small polarons are ruled out in manganites.

4.2. $La_{1-x}Ca_xMnO_3$ at $x \sim 0.5$

After a considerable experimental effort, the evidence for mixed-phase FM–CO characteristics in $La_{1-x}Ca_xMnO_3$ near $x = 0.5$ is simply overwhelming. The current theoretical explanation of experimental data at this density appears simple. According to computer simulations and mean-field approximations the FM- and CO-phase are separated by first-order transitions when models without disorder are studied. This abrupt change is due to the substantial difference between these phases that makes it difficult a smooth transition from one to the other. Intrinsic disorder caused by the slightly different ionic sizes of La and Ca can induce a smearing of the first-order transition, transforming it into a continuous transition with percolative characteristics. Coexistence of large clusters with equal density is possible, as described in the theoretical section of this review. In addition, intrinsic tendencies to electronic phase separation, which appear even without disorder, may contribute to the cluster formation.

It is important to remark that although in this review the cases of $x < 0.5$ and $x \sim 0.5$ are treated separately, it is expected that a smooth connection between the two types of mixed-phase behavior exists. Hopefully, future theoretical and experimental work will clarify how the results at, say, $x \sim 0.3$ and $x \sim 0.5$ can evolve one into the other changing the hole density.

4.2.1. Experimental evidence of inhomogeneities

Early work by Chen and Cheong (1996) and Radaelli et al. (1997) using electron and X-ray diffraction experiments found the surprising coexistence of ferromagnetism and charge ordering in a narrow temperature window of $La_{1-x}Ca_xMnO_3$. Further studies by Mori et al. (1998b) showed that the $x = 0.5$ mixture of FM and CO states arises from an inhomogeneous spatial mixture of incommensurate charge-ordered and ferromagnetic charge-disordered microdomains, with a size of 20–30 nm.

Papavassiliou et al. (1999a, b) (see also Belesi et al., 2000) observed mixed-phase tendencies in $La_{1-x}Ca_xMnO_3$ using ^{55}Mn NMR techniques. Fig. 4.2.1a shows the NMR spectra for $La_{1-x}Ca_xMnO_3$ at several densities and low temperature $T = 3.2$ K obtained by those authors. The appearance of coexisting peaks at $x = 0.1$,0.25, and 0.5 is clear from the figure, and these peaks correspond to either FM metal, FM insulator, or AF-states according to the discussion presented in Papavassiliou et al. (1999a, b). The results at $x = 0.5$ are in agreement with previous results reported by the same group (Papavassiliou et al., 1997). The revised phase diagram proposed by those authors is shown in Fig. 4.2.1b. In agreement with the conclusions of other groups, already reviewed in the previous subsection, the region in the vicinity of T_C corresponds to a mixed-phase regime. The same occurs at low temperatures in the region between the CO- and FM-state of $x = 0.5$. The coexistence of FM- and AF-phase was also observed in $La_{0.5}Ca_{0.5}MnO_3$ by Allodi et al. (1998) using similar NMR techniques. First-order characteristics in the FM–AF transition were found, including an absence of critical behavior. Their spectra is shown in Fig. 4.2.1c. As in Fig. 4.2.1a, a clear two signal spectra is observed in the vicinity of $x = 0.5$ and low temperatures. The presence of mixed-phase characteristics in NMR data was also observed by Dho et al. (1999a, b) in their studies of $La_{1-x}Ca_xMnO_3$. Their results apply mainly near the phase boundaries of the ferromagnetic regime at a fixed temperature, or near T_C at a fixed density between 0.2 and 0.5.

It can be safely concluded, overall, that the NMR results described here are in general agreement, and also in agreement with the phase separation scenario which predicts that all around the FM

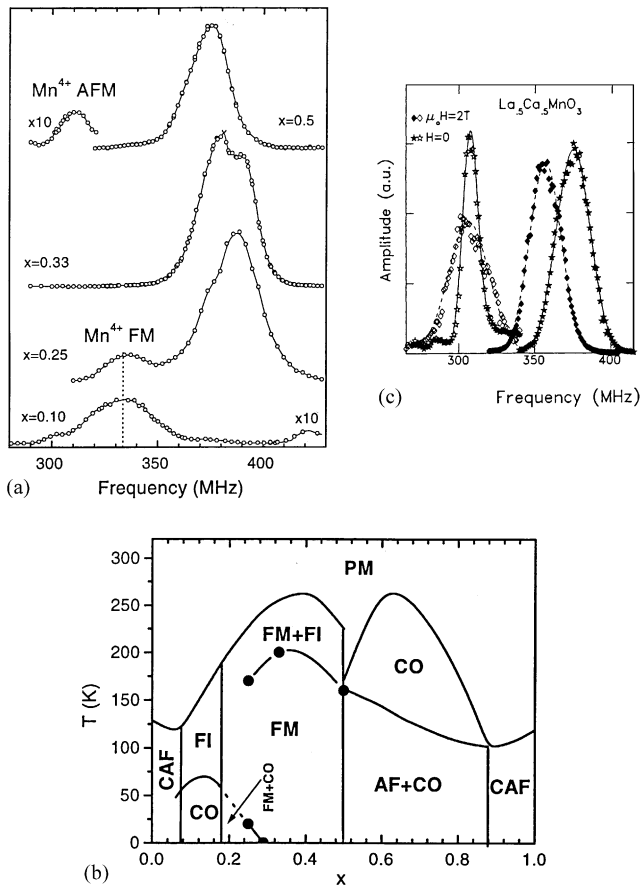

Fig. 4.2.1. (a) ^{55}Mn NMR spectra of $La_{1-x}Ca_xMnO_3$ at $T = 3.2$ K for the densities shown, reproduced from Papavassiliou et al. (1999b). Coexistence of features corresponding to two phases appear in the data. (b) Revised temperature–density phase diagram proposed by Papavassiliou et al. (1999b). The circles denote the NMR results presented in that reference. The notation is standard. (c) ^{55}Mn NMR spectra at $T = 1.3$ K of $La_{1-x}Ca_xMnO_3$ with $x = 0.5$ in zero and applied field. FM lines are marked with filled symbols, while AF ones are marked with open symbols. Figure reproduced from Allodi et al. (1998).

metallic phase in the temperature–density plane there are regions of mixed-phase characteristics due to the competition between metallic and insulating states.

Magnetization, resistivity, and specific heat data analyzed by Roy et al. (1998, 1999, 2000a, b) led to the conclusion that in a narrow region of hole densities centered at $x = 0.5$, two types of carriers coexisted: localized and free. The evidence for a rapid change from the FM to the CO phases as x was varied is clear (see Fig. 3 of Roy et al., 1998). This is compatible with the fact that La^{3+} and Ca^{2+} have a very similar ionic radius and, as a consequence, the disorder introduced by their mixing is "weak". The theoretical scenario described before (Moreo et al., 2000) suggests that, at zero temperature and for weak disorder, the density window with large cluster coexistence should be narrow (conversely in this region large cluster sizes are expected). It is also to be expected that the magnetoresistance effect for low values of magnetic fields will appear only in the same narrow

region of densities. Actually, Roy et al. (1999) showed that at $x = 0.55$, a field of 9 T is not enough to destabilize the charge-ordered state. Very recently, Roy et al. (2000a) studied, among other quantities, the resistivity vs. temperature for magnetic fields up to 9 T. The result is reproduced in Fig. 4.2.2. This figure clearly resembles results found by Uehara et al. (1999) in their study of $La_{5/8-y}Pr_yCa_{3/8}MnO_3$ (see Fig. 4.1.1a) varying the Pr concentration. In both cases, the curves are similar to those that appear in the percolative process studied by Mayr et al. (2000) (see Figs. 3.8.2 and 3.8.4). Percolation between the CO and FM states appears to occur similarly both by changing chemical compositions and also as a function of magnetic fields, a very interesting result. Phase separation in $x = 0.5$ polycrystalline samples obtained under different thermal treatments was also reported by Levy et al. (2000a). López et al. (2000) also found results compatible with FM droplets immersed in a CO background. Kallias et al. (1999) using magnetization and Mössbauer measurements also reported coexisting FM and AF components in $x = 0.5$ $La_{1-x}Ca_xMnO_3$.

It is also important to remark that experimentally it is very difficult to make reproducible $La_{1-x}Ca_xMnO_3$ samples with $x \sim 0.5$ (see for instance Roy et al., 1998, 1999, 2000a, b). Samples with the same nominal Ca content can actually present completely different behavior. This is compatible with a phase separated state at this density, which is expected to be very sensitive to small chemical changes. Another result compatible with phase separation can be found in the magnetization curves (Fig. 4.2.2), which are well below the expected saturation value for a ferromagnet, even in several Tesla fields where the magnetization is not increasing rapidly.

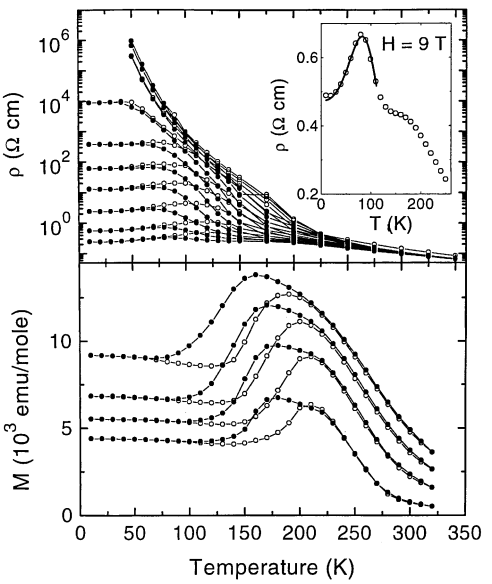

Fig. 4.2.2. Upper panel: resistivity vs. temperature on cooling (solid) and warming (open) at fields between 0 and 9 T, in steps of 1 T starting from the top. The material is $La_{0.5}Ca_{0.5}MnO_3$ and the results are reproduced from Roy et al. (2000a). Bottom panel: magnetization versus temperature for fields between 1 T and 7 T in steps of 2 T, starting from the bottom. The inset illustrates two distinct features in the resistivity associated with the coexistence of two states. For more details see Roy et al. (2000a).

Neutron powder diffraction studies by Radaelli et al. (1995) of $La_{1-x}Ca_xMnO_3$ at $x = 0.5$ revealed peak broadening effects that were explained assuming multiple phases simultaneously present in the sample. Rhyne et al. (1998) studied $La_{1-x}Ca_xMnO_3$ with $x = 0.47$ using elastic and inelastic neutron scattering. Coexisting ferromagnetic and antiferromagnetic phases were found at low temperatures. Similar conclusions were also reached by Dai et al. (1996). Further confirmation that near $x = 0.5$ in $La_{1-x}Ca_xMnO_3$ the material has mixed-phase characteristics has been recently provided by neutron powder diffraction measurements by Huang et al. (1999). Discontinuous features in the results discussed by those authors also indicate that the competing phases are likely separated by first-order transitions in the absence of intrinsic disorder, as found in the theoretical calculations (Yunoki et al., 2000). Infrared absorption studies by Calvani et al. (1998) were also described in terms of a phase separation scenario.

It is also very interesting to test materials with the hole density $x = 0.5$ but allowing for slight deviations away from the $La_{0.5}Ca_{0.5}MnO_3$ chemical composition. Among these investigations are the transport and X-ray experiments on $R_{1/2}Ca_{1/2}Mn_{0.97}Cr_{0.03}O_3$, with R = La, Nd, Sm and Eu, carried out by Moritomo et al. (1999a). Their study allowed for a systematic analysis of the charge-ordered state when the ionic radius of the rare-earth ion was changed. Due to the small presence of Cr, this material with R = La has a purely ferromagnetic state while the other rare-earths leads to a CE-type CO state. The main result obtained by Moritomo et al. (1999) is quite relevant to the subject of this review and is summarized in Fig. 4.2.3a. Moritomo et al. (1999) concluded that the region between the CO and FM phases has mixed-phase characteristics involving the two competing states. This hypothesis was confirmed by the use of electron microscopy, which showed microdomains of size 20–50 nm, a result similar to those observed by other authors in other compounds. Then, once again, mixed-phase tendencies are clear in materials with $x = 0.5$ (see also Oshima et al., 2000). Results for the Fe-doped $x = 0.5$ LCMO compound by Levy et al. (2000b) likely can be rationalized in a similar way. Other very interesting results in the context of Cr doping have been obtained by Kimura et al. (1999, 2000).

Moreover, the study of Cr-doped compounds at many Ca densities shows that this type of doping with impurities has an effect similar to that of a magnetic field, namely a small Cr percentage is enough to destabilize the CO-state into a FM-state. This result is surprising, since impurities are usually associated with a tendency to localize charge, and they are not expected to generate a metallic state. In Fig. 4.2.4a-c, the phase diagrams presented by Katsufuji et al. (1999) for three compounds are shown to illustrate this point. In $Pr_{1-x}Ca_xMnO_3$, Cr-doping destabilizes the CO-state in a wide range of densities, as a magnetic field does, while for $La_{1-x}Ca_xMnO_3$ and $Nd_{1-x}Sr_xMnO_3$, it is effective only near $x = 0.5$. The resistivity plots in Fig. 4.2.4d show that the shape of the curves are very similar to all the previous ones analyzed in this review, indicative of a percolative process.

Results similar to those of Moritomo et al. (1999) were obtained using transport techniques by Mallik et al. (1998) studying $La_{0.5}Ca_{0.5-x}Ba_xMnO_3$ with x between 0, where the sample they used is in a charge-ordered insulating state, and $x = 0.5$, where a ferromagnetic metallic compound is obtained. The resistivity vs. temperature at several compositions is shown in Fig. 4.2.3b. The results certainly resemble those obtained by Uehara et al. (1999) and other authors, especially regarding the presence of a flat resistivity in a substantial low-temperature range and a rapid variation of $\rho(T = 0)$ with Ba concentration. Mallik et al. (1998) observed that the difference in ionic sizes between Ca and Ba plays a crucial role in understanding the properties of this compound. They also found hysteretic behavior and first-order characteristics in their results, results all compatible

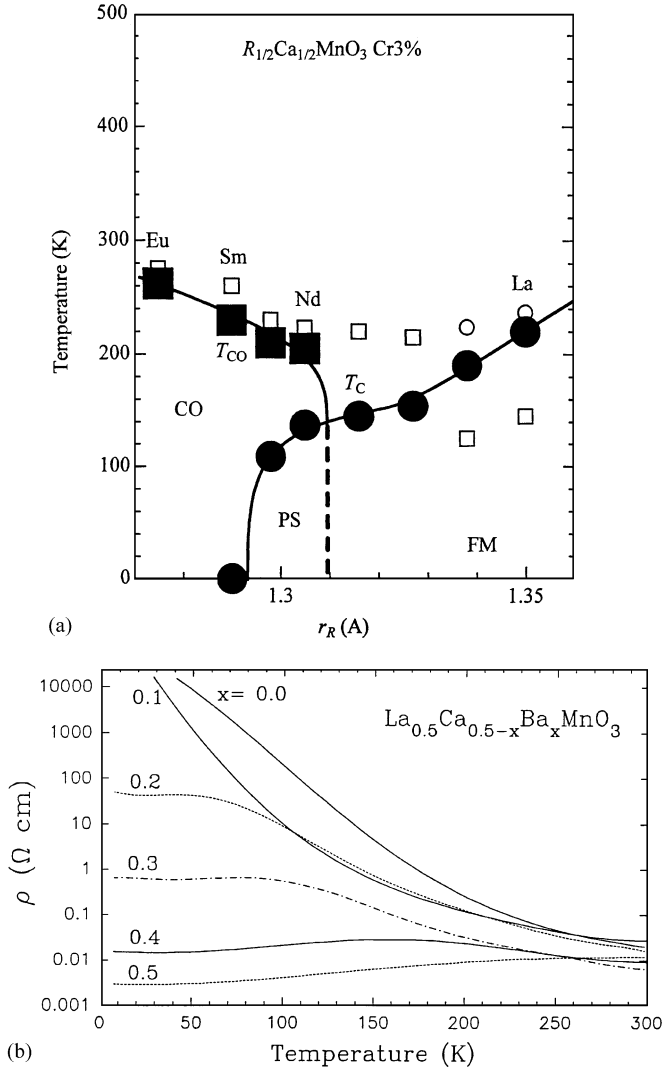

Fig. 4.2.3. (a) Phase diagram of a 3% Cr-doped manganites, $R_{1/2}Ca_{1/2}(Mn_{0.97}Cr_{0.03})O_3$, against averaged ionic radius r_R of the rare-earth ion. Closed circles and squares are Curie temperatures and critical temperatures for the charge-ordering transition, respectively. PS is the region of phase separation. Open symbols represent the data for the Cr-undoped compounds. Figure reproduced from Moritomo et al. (1999). (b) Electrical resistivity versus temperature for the compounds $La_{0.5}Ca_{0.5-x}Ba_xMnO_3$, reproduced from Mallik et al. (1998a, b).

with the theoretical scenario described before (Yunoki et al., 2000; Moreo et al., 2000). The critical concentration for percolation in Fig. 4.2.3b appears to be near $x = 0.1$, where the T_C was found to be the smallest in this compound.

Finally, it is also interesting to remark that magnetic-field-dependent optical conductivity studies by Jung et al. (1999) applied to $Nd_{1-x}Sr_xMnO_3$ at $x = 0.5$ have also found indications of a percolative transition in the melting of the charge ordered state.

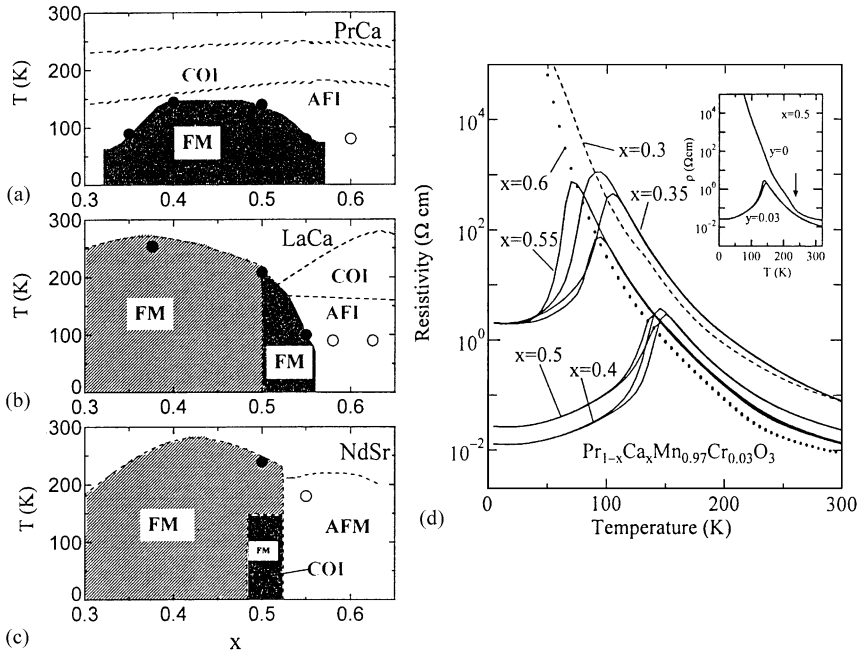

Fig. 4.2.4. Phase diagrams of (a) $Pr_{1-x}Ca_xMn_{0.97}Cr_{0.03}O_3$, (b) $La_{1-x}Ca_xMn_{0.97}Cr_{0.03}O_3$, and (c) $Nd_{1-x}Sr_xMn_{0.97}Cr_{0.03}O_3$, taken from Katsufuji et al. (1999). The grey regions are the FM phases in the absence of Cr, while the dark regions are FM metallic phases stabilized by Cr doping. The rest of the notation is standard. (d) Resistivity vs. temperature for $Pr_{1-x}Ca_xMn_{0.97}Cr_{0.03}O_3$. The inset contains results at $x = 0.5$ with ($y = 0.03$) and without ($y = 0.0$) Cr. Results taken from Katsufuji et al. (1999).

4.3. Electron-doped manganites

Neutron scattering studies of $Bi_{1-x}Ca_xMnO_3$ single crystals in the range between $x = 0.74$ and 0.82 were presented by Bao et al. (1997). It is expected that $Bi_{1-x}Ca_xMnO_3$ will have properties very similar to those of $La_{1-x}Ca_xMnO_3$ in the range of densities studied by those authors, and for this reason the analysis of a Bi-based compound is discussed in this subsection. One of the most interesting results reported by Bao et al. (1997) is the presence of ferromagnetic correlations at high temperatures, which are replaced by antiferromagnetic ones as the temperature is reduced. Fig. 4.3.1a taken from Bao et al. (1997) show the intensity of the FM and AF peaks as a function of temperature at $x = 0.82$. It is clear from the figure that in the intermediate regime, roughly between 150 and 200 K, there is a coexistence of FM and AF features, as in a mixed-phase state. In a related study, Bao et al. (1998) concluded that manganites have only two important generic states: metallic ferromagnetic and localized antiferromagnetic. This is in agreement with theoretical results, although certainly combinations such as charge-ordered ferromagnetic states are also possible at least in 2D (Yunoki et al., 2000). Subsequent studies of $Bi_{1-x}Ca_xMnO_3$ single-crystals performed by Liu et al. (1998) reported optical reflectivity results in the same compositional range (i.e. between $x = 0.74$ and 0.82). The main result of this effort is reproduced in Fig. 4.3.1b. Liu et al. (1998) concluded that in the intermediate range $T_N < T < T_{CO}$ the coexistence of a polaron-like response

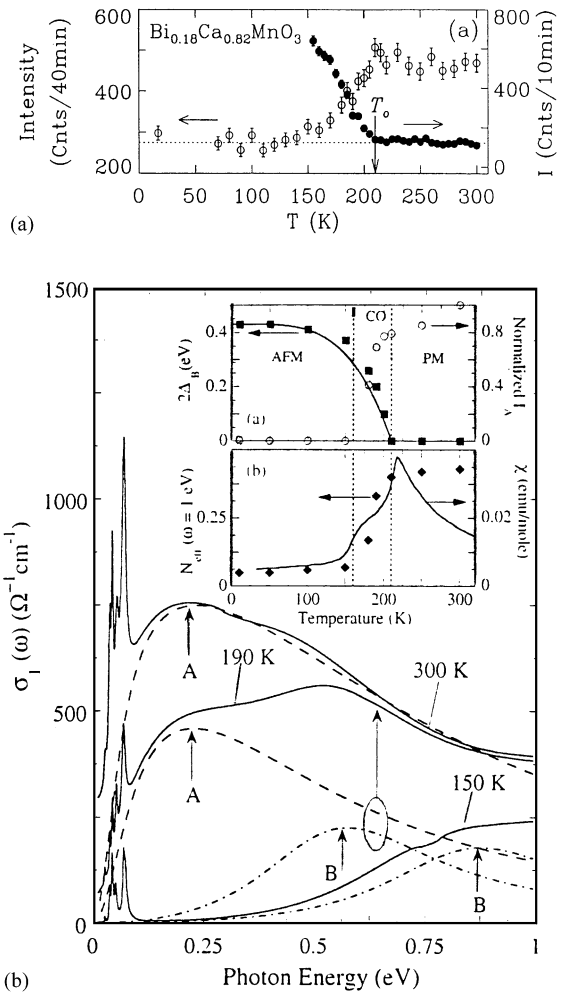

Fig. 4.3.1. (a) Neutron scattering results of Bao et al. (1997) corresponding to $Bi_{1-x}Ca_xMnO_3$ at $x = 0.82$. The solid circles correspond to the AF response, while the open circles are the FM response. The dotted line is the background. A region of FM–AF coexistence is observed. For more details the reader should consult Bao et al. (1997). (b) Real part of the optical conductivity at the three temperatures indicated, from Liu et al. (1998) where the details of the fitting results (dashed and dot–dashed lines) are explained. The upper inset contains the temperature dependence of the energy gap (filed squares) and the polaron oscillator strength (open circles). The lower inset is the effective number of carriers. Peak B evolves into a clean charge-gap as T decreases, while A corresponds to polarons.

together with a charge-gap structure signifies two-phase behavior characterized by domains of both FM and AF spin correlations. Recently, studies of $Bi_{1-x}Ca_xMnO_3$ at $x = 0.81$ and 0.82 were interpreted in terms of spin or charge "chiral" fluctuations (Yoon et al., 2000), showing that exotic physics may occur in this electron doped compound.

The range of hole densities above 0.8 for $Bi_{1-x}Ca_xMnO_3$ was analyzed by Chiba et al. (1996) using magnetic and transport techniques. They observed that large magnetoresistance effects are found even at low T_C, which is compatible with a mixed-phase state in the ferromagnetic regime,

quite different from a spin-canted state. Actually, it is important to remark that there are previous studies of the electron-doped materials (not reviewed here) that have labeled the small x region as "spin canted" due to the observation of coexisting FM and AF features. The conclusions of those papers may need revision in view of the new results described in this section.

Studies of $Ca_{1-y}Sm_yMnO_3$ by Maignan et al. (1998), using magnetic and transport techniques in the range from $y = 0.0$ to 0.12, reported results compatible with a "cluster glass" (see also Martin et al., 1999). As y increases from zero, the system rapidly becomes ferromagnetic and metallic. However, those authors remark that no true long-range order exists, and thus the FM-state is unusual. The resistivity is shown in Fig. 4.3.2a. The metallic character at $y = 0.0$ and high temperature is caused by oxygen deficiency and should not be considered as really representing the electron undoped compound, which is actually antiferromagnetic (G-type).

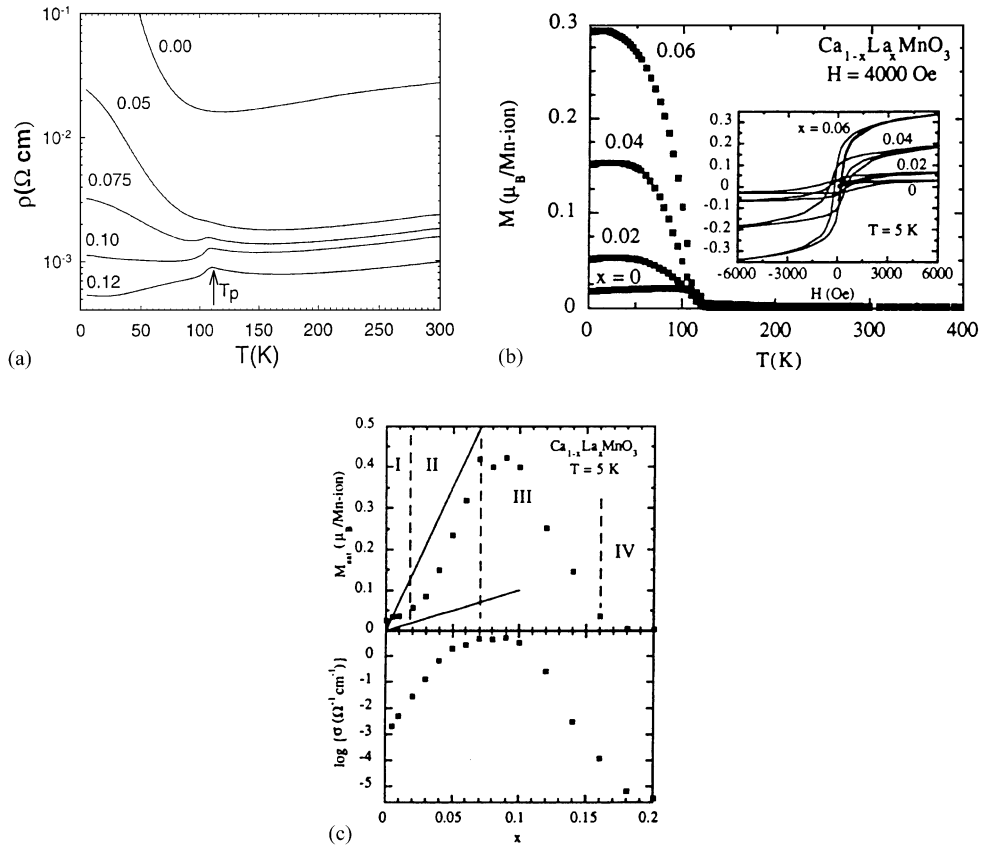

Fig. 4.3.2. (a) Temperature dependence of the resistivity of $Ca_{1-x}Sm_xMnO_3$ for several values of x (shown). For more details see Maignan et al. (1998). (b) Magnetization M vs. temperature of $Ca_{1-x}La_xMnO_3$ (x shown). In the inset M vs. the magnetic field H is plotted. (c) Upper panel: Magnetic saturation moment at 5 K vs. x. Region I is a G-type AF with local ferrimagnetism. Region II has local FM regions and G-type AF. Region III contains C- and G-type AF, as well as local FM. Region IV is a C-type AF. Lower panel: Electrical conductivity at $T = 5$ K vs. x. All the results in (b) and (c) are taken from Neumeier and Cohn (2000).

More recently, a careful and systematic study of $Ca_{1-x}La_xMnO_3$ has been carried out by Neumeier and Cohn (2000) using magnetic and transport techniques. These authors concluded that the addition of electrons to the $x = 0.0$ antiferromagnetic state promotes phase segregation. Representative magnetization vs. temperature data are shown in Fig. 4.3.2b. The saturated moment and conductivity versus density are reproduced in Fig. 4.3.2c. Neumeier and Cohn (2000) reported multiple magnetic phases emerging from the analysis of their data, and remarked that the long-accepted existence of canted AF is supplanted by phase coexistence.

In addition, recent NMR studies of $La_{1-x}Ca_xMnO_3$ for $x = 0.65$ at low temperature by Kapusta et al. (2000) reported the existence of electronic phase separation, with FM regions detected over a CO/AF background. This interesting result leads us to believe that it may be possible that the widely accepted phase diagram of $La_{1-x}Ca_xMnO_3$ may still need further revision, since a phase with coexisting FM and AF features may exist at low temperature and x around 0.65, with a shape similar to the "canted state" that appears in the phase diagram of $Pr_{1-x}Ca_xMnO_3$ and the bilayer compounds (see Figs. 2.3.1 and 4.6.1). This conjecture could be tested experimentally with NMR techniques. Results for $Ca_{1-x}Y_xMnO_3$ can be found in Aliaga et al. (2000b).

4.4. Large bandwidth manganites and inhomogeneities: the case of $La_{1-x}Sr_xMnO_3$

A compound as much scrutinized as the Ca-based manganites of the previous sections is the Sr-based $La_{1-x}Sr_xMnO_3$, which has a larger bandwidth. In spite of this property, the $La_{1-x}Sr_xMnO_3$ material presents a very complex phase diagram, especially at low Sr-density, with a behavior in many respects qualitatively similar to that of the Ca-based compound. The main experimental evidence that leads to this conclusion is reviewed below. In the other regime of large densities, the Sr-based material is metallic *both* at low and high temperatures (see phase diagram Fig. 2.1.1b) and its magnetoresistance effect is relatively small. In this density regime, studies using mainly dynamical mean-field approaches ($D = \infty$) have provided evidence that the simple double-exchange ideas are enough to understand the main properties of $La_{1-x}Sr_xMnO_3$ (Furukawa, 1994, 1995a–c, 1998), especially concerning the interplay between ferromagnetism and transport. This is a reasonable conclusion, and illustrates the fact that materials whose couplings and densities locate them in parameter space far away from insulating instabilities tend to present canonical properties. A review of the status of the theoretical approach based on the double-exchange ideas and its application to large-bandwidth manganites has been recently presented (Furukawa, 1998). Additional results for the FM Kondo model have been discussed by Zang et al. (1997), and several other authors. However, it must be kept in mind that the more canonical, and governed by double exchange, the behavior of a compound is, the smaller is the magnetoresistance effect. For this reason, in the description of experimental results for $La_{1-x}Sr_xMnO_3$ the effort is here mainly focused into the low-density regime where effects other than canonical double exchange seem to dominate in this material.

4.4.1. $La_{1-x}Sr_xMnO_3$ at low density

Among the first papers to report inhomogeneities in Sr-based manganites are those based on atomic pair-density-functional (PDF) techniques. In particular, Louca et al. (1997) studied $La_{1-x}Sr_xMnO_3$ in a wide range of densities between $x = 0.0$ and 0.4, and interpreted their results as indicative of small one-site polarons in the paramagnetic insulating phase. Those authors found

that the local atomic structure deviates significantly from the average. At lower temperatures their polarons increase in size, typically involving three sites according to their analysis. These effects were found even in the metallic phase. Based on such results, Louca et al. (1997) questioned the at-that-time prevailing homogeneous picture of the metallic state of manganites, and based their analysis mainly on a small polaron picture rather than large droplets or phase separation ideas. Nevertheless, they envisioned that increasing the density of polarons would lead to larger structures, and in more recent work (Louca and Egami, 1999) they also presented microscopic separation of charge-rich and charge-poor regions as a possible scenario to describe their results. In addition, they conjectured that the conductivity could be determined by some kind of dynamic percolative mechanism, which is the current prevailing view (see also Egami, 1996; Egami et al., 1997). The possible percolative nature of the metal–insulator transition close to $x_c = 0.16$ in $La_{1-x}Sr_xMnO_3$ was also proposed by Egami and Louca (1998). Tendencies toward a two-phase regime in low hole-density doped (La, Sr)-based manganites were also reported by Demin et al. (1999) using a variety of techniques.

Recently, Endoh et al. (1999a, 1999b) and Nojiri et al. (1999), using transport and resonant X-ray scattering, have studied in detail the region near $x \sim 1/8$ of $La_{1-x}Sr_xMnO_3$. Interesting results were observed in this regime, especially a first-order transition from a ferromagnetic metal to a ferromagnetic insulator. This ferromagnetic insulator was reported in previous work by Yamada et al. (1996) using neutron scattering techniques. Those authors interpreted their results using a state with charge ordering, which they refer to as "polaron ordering" with polarons involving only one site [note, however, that other authors could not reproduce the Yamada et al. (1996) results. See Vasiliu-Doloc et al. (1998a)]. Endoh et al. (1999a, b) reported huge changes in resistivity upon the application of a magnetic field close to the above metal–insulator transition in this compound. Regions with phase-separation characteristics were identified by Endoh et al. (1999b). The key difference between the two competing states is the orbital ordering, as revealed by the X-ray experiments. The reported phase diagram is in Fig. 4.4.1a. Similar conclusions were reached by Paraskevopoulos et al. (2000a) and previously by Zhou and Goodenough (1998b) through measurements of resistivity and thermoelectric power. The last authors reported a dynamic phase segregation into hole-rich and hole-poor phases in the region of $x = 0.12$ between the charge-ordered transition temperature and the Curie temperature. Their phase diagram resembles that of Endoh et al. (1999b) (see Fig. 4.4.1b). Overall, these experimental results are in good agreement with mean-field calculations using purely Coulombic models (Endoh et al., 1999a) and with Monte Carlo simulations using JT phonons (Yunoki et al., 1998b). In both cases, phase separation triggered by the *orbital* degree of freedom, instead of the spin, were found. It is clear once again that simple double-exchange ideas or even the proposal of small polarons are not sufficient to explain the physics of manganites, particularly in the most interesting regions of parameter space where the CMR effect occurs.

The results of Endoh et al. (1999a, b) and Nojiri et al. (1999) have characteristics similar to those of the theoretical scenario described in Section 3, namely a competition between two states which are sufficiently different to generate a first-order transition between them. The results of Moreo et al. (2000) suggest that the small ionic radii differences between La^{3+} and Sr^{2+} induces weak disorder that affects the first-order transition, inducing a narrow region of coexistence of cluster of both phases. Percolative properties are predicted in this regime based on the results of Moreo et al. (2000). It would be quite interesting to search for such properties in $x \sim 1/8$ $La_{1-x}Sr_xMnO_3$ experiments.

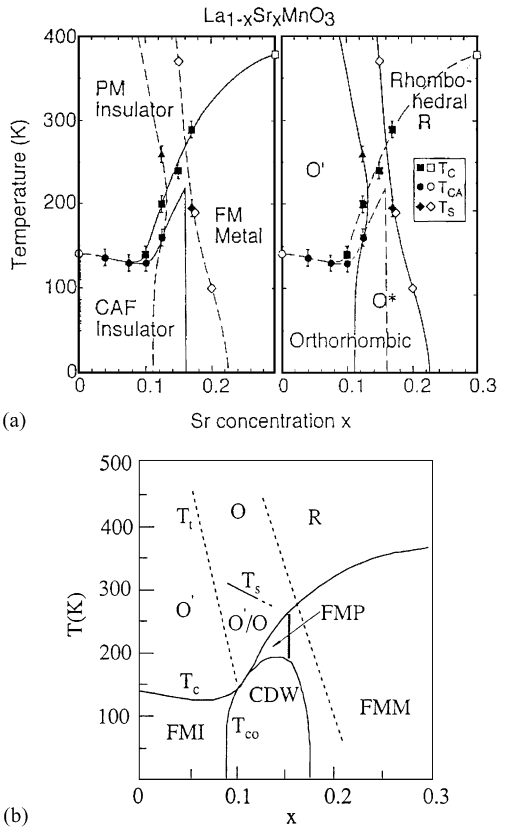

Fig. 4.4.1. (a) Magnetic and structural phase diagram of $La_{1-x}Sr_xMnO_3$ determined by neutron diffraction data, reproduced from Endoh et al. (1999a). The notation is standard. Note that at densities roughly between 0.10 and 0.15, a FM metallic phase can be identified in a narrow temperature region upon changing the temperature. (b) Phase diagram of $La_{1-x}Sr_xMnO_3$ according to Zhou and Goodenough (1998b). Most of the notation is standard. The FMP region corresponds to ferromagnetic polarons in the analysis of Zhou and Goodenough (1998b), where more details can be found.

In fact, the theoretical calculations are already in qualitative agreement with a recent experimental effort. Independent of the previously described results by Endoh et al. (1999a, b) and Nojiri et al. (1999), Kiryukhin et al. (1999) studied $x = 1/8$ $La_{1-x}Sr_xMnO_3$ using synchrotron X-ray scattering. At low temperatures, they observed an X-ray-induced transition from a charge-ordered phase to a charge-disordered state. These results are qualitatively similar to those reported by Kiryukhin et al. (1997) applied to $Pr_{1-x}Ca_xMnO_3$. Kiryukhin et al. (1999) suggest that their results can be explained within a phase-separation scenario with charge-ordered regions as large as 500 Å, sizes similar to those observed in half-doped $La_{1-x}Ca_xMnO_3$, as described before in this review (see also Baran et al., 1999). Wagner et al. (1999), using transport and magnetic techniques applied to $x = 1/8$ $La_{1-x}Sr_xMnO_3$, also found evidence of a first-order transition as a function of temperature. The possibility of phase separation was briefly mentioned in that work. Finally, the optical conductivity spectra obtained by Jung et al. (1998) in their study of $x = 1/8$ $La_{1-x}Sr_xMnO_3$ has also been explained in terms of a phase-separated picture by

comparing results with those of Yunoki et al. (1998b), which were obtained at temperatures such that dynamical clustering was present in the Monte Carlo simulations. It is interesting to remark that a large number of optical experiments have been analyzed in the near past as arising from coexisting metallic (Drude) peaks and mid-infrared bands that were usually assigned to polaronic features (see for instance Kaplan et al., 1996). In view of the novel experimental evidence pointing toward coexisting metallic and insulating clusters, even in optimal regimes for FM such as $x = 0.33$ in $La_{1-x}Ca_xMnO_3$, the previous optical conductivity may admit other interpretations perhaps replacing polarons by larger droplets. Finally, note that recent optical studies at $x = 0.175$ by Takenaka et al. (1999) have been interpreted as arising from a FM metallic phase below T_C which can have either coherent or incoherent characteristics, and a mixture of them is possible. The anomalous metallic state of Sr-doped manganites has been theoretically addressed recently by Ferrari and Rozenberg (1999) using dynamical mean-field calculations. Motome and Imada (1999) and Nakano et al. (2000) also studied this material and concluded that to reproduce the small Drude weight of experiments a mixture of strong Coulomb and electron-phonon (JT) interactions is needed.

For completeness, some remarks about related compounds are here included. For instance, $LaMnO_{3+\delta}$ was studied (see Ritter et al., 1997; Ibarra and De Teresa, 1998b) and at $\delta \sim 0.15$ a large magnetoresistance effect was observed. The magnetic and transport properties of $La_{1-\delta}MnO_3$ were analyzed by De Brion et al. (1998). In their study, they concluded that a canted state was observed, but magnetization measurements cannot distinguish between FM–AF phase separation and spin canting. In fact, recent studies by Loshkareva et al. (2000, 1999) of optical, electrical, and magnetic properties of the same compound and $x = 0.1$ $La_{1-x}Sr_xMnO_3$ were interpreted in terms of phase-separation. In addition, "cluster-glass" features were reported for this compound by Ghivelder et al. (1999). On the other hand, susceptibility, magnetization, MR and ultrasonic studies of $La_{1-x}Sr_xMnO_3$ at low doping $x < 0.1$ by Paraskevopoulos et al. (2000b) where interpreted as compatible with a canted state, rather than a phase-separated state (see also Pimenov et al., 2000; Mukhin et al., 2000). However, those authors remark that the canting does not arise from DE interactions because the carriers are localized near the Sr-ions. These trapped holes can polarize the Mn-ions in their vicinity leading to FM clusters in a PM matrix. This interesting proposal merits theoretical studies. It is safe to conclude that at very low hole density in $La_{1-x}Sr_xMnO_3$ it is still unclear what kind of state dominates the low-temperature behavior, namely whether it is homogeneous (canted) or inhomogeneous as predicted by phase-separation scenarios.

4.4.2. $La_{1-x}Sr_xMnO_3$ at intermediate density

Although some features of $La_{1-x}Sr_xMnO_3$ at intermediate densities are well described by the double-exchange ideas, experiments have revealed mixed-phase tendencies in this region if the study is carried out close to instabilities of the FM metallic phase. For instance, working at $x = 0.17$ in $La_{1-x}Sr_xMnO_3$, Darling et al. (1998) reported measurements of the elastic moduli using resonant ultrasound spectroscopy. Those authors noticed that their results suggest the existence of very small microstructures in their single crystals. Studies by Tkachuk et al. (1998) of $La_{0.83}Sr_{0.17}Mn_{0.98}Fe_{0.02}O_3$ also led to the conclusion that the paramagnetic phase contains ferromagnetic clusters. Recent ESR studies by Ivanshin et al. (2000) have also contributed interesting information to the study of $La_{1-x}Sr_xMnO_3$ at hole densities between $x = 0.00$ and

0.20. Small-angle polarized neutron scattering measurements by Viret et al. (1998) for $La_{1-x}Sr_xMnO_3$ at $x = 0.25$ indicated the presence of nanometer size inhomogeneities of magnetic origin in the vicinity of the Curie temperature. Approximately at this density occurs the metal–insulator transition above T_C, and as a consequence, mixed-phase features as observed in $La_{1-x}Ca_xMnO_3$ (which at all densities presents an insulating state above T_C) are to be expected below $x = 0.25$. Machida et al. (1998) studied the absorption spectra of thin-films of $R_{0.6}Sr_{0.4}MnO_3$ with R = Sm, $(La_{0.5}Nd_{0.5})$, $(Nd_{0.5}Sm_{0.5})$, and $(Nd_{0.25}Sm_{0.75})$. They concluded that cluster states were formed in these compounds.

4.4.3. Sr-based compounds at high-hole density: the cases of $Pr_{1-x}Sr_xMnO_3$ and $Nd_{1-x}Sr_xMnO_3$

The antiferromagnetic manganite $Pr_{1-x}Sr_xMnO_3$ at $x = 0.5$ has been recently studied using NMR techniques by Allodi et al. (1999). This material has a magnetic-field-induced transition to a ferromagnetic state and a CMR effect. The NMR results show that the transition proceeds through the nucleation of microscopic ferromagnetic domains, with percolative characteristics. Allodi et al. (1999) believe that the size of the clusters in coexistence is on the nanometer scale, to be compared with the micrometer scale found in other manganites.

Kajimoto et al. (1999) studied $Nd_{1-x}Sr_xMnO_3$ in a range of densities from $x = 0.49$ to 0.75 using neutron diffraction techniques. Four states were observed: FM metallic, CE-type insulating, A-type metallic, and a C-type AF insulator. The latter may be charge-ordered. At $x \sim 0.5$, Kajimoto et al. (1999) reported a possible mixed-phase state involving the CE- and A-type orderings. Other groups arrived at similar conclusions: Woodward et al. (1999) found coexisting macroscopic FM, A-type and CE-type phases, while Fukumoto et al. (1999) reported microscopic scale electronic phase separation in this compound. All these results are compatible with the recent theoretical work of Moreo et al. (2000) and Yunoki et al. (2000), since computer simulations of models with JT phonons at $x = 0.5$ have found first-order transitions separating the many possible states in manganites, including one between the A- and CE-type states. The addition of weak disorder would smear this sharp first-order transition into a rapid crossover. CMR effects are to be expected in this regime.

4.5. $Pr_{1-x}Ca_xMnO_3$

It is interesting to observe that the low-bandwidth compound $Pr_{1-x}Ca_xMnO_3$ with $x = 0.30$ undergoes an unusual insulator–metal transition when it is exposed to an X-ray beam. Without X-rays, the material is in a charge-ordered insulator state below 200 K. However, below 40 K, X-rays convert the insulating state into a metallic state which persists when the X-ray beam is switched off (Kiryukhin et al., 1997; Cox et al., 1998). A similar transition occurs upon the application of a magnetic field. The authors of these experiments interpreted their results as arising from a phase-segregation phenomenon induced by the X-rays, with ferromagnetic droplets coalescing into larger aggregates. Note that $x = 0.30$ is at the border between the CO-state and a FM-insulating state in this compound, and thus unusual behavior is to be expected in such a regime. Recently, transport, optical and specific heat results at $x = 0.28$ by Hemberger 2000b, Hemberger et al. (2000a) have been interpreted as a percolative metal–insulator transition induced by a magnetic field, with coexisting metallic and insulating clusters below 100 K at zero external field. Using neutron diffraction techniques applied to $x = 0.3$ PCMO, Katano et al. (2000) recently

found evidence of a phase-separated state with percolative characteristics in the metal–insulator transition induced by magnetic fields.

Recent analysis, again using X-rays, of the related material $Pr_{1-x}(Ca_{1-y}Sr_y)_xMnO_3$ showed that the metal–insulator transition present in this compound is not caused by a conventional change in the electron density, but by a change in the couplings of the system which affect the mobility of the carriers (Casa et al., 1999). It is believed that the X-rays can help connecting adjacent preformed metallic clusters which originally are separated by an insulating barrier. In other words, the picture is similar to that of the percolation process described in other manganites and also in the theoretical analysis of the influence of a magnetic field on, e.g., the random field Ising model as a toy model for cluster coexistence near first-order transitions (Moreo et al., 2000).

Studies of thermal relaxation effects by Anane et al. (1999a) applied to $Pr_{1-x}Ca_xMnO_3$ with $x = 0.33$ are also in agreement with a mixed-phase tendency and percolative characteristics description of this compound. Anane et al. (1999a) focused their effort into the hysteresis region that separates the metallic and insulating phases upon the application of a magnetic field. More recently, Anane et al. (1999b) studied the low-frequency electrical noise for the same compound, at similar temperatures and fields. Their conclusion is once again that mixed-phase behavior and percolation are characteristics of this material. More recently, Raquet et al. (2000), studying $La_{1-x}Ca_xMnO_3$ ($x = 0.33$), observed a giant and random telegraph noise in the resistance fluctuations of this compound. They attribute the origin of this effect to a dynamic mixed-phase percolative conduction process involving two phases with different conductivities and magnetizations. These important experimental results are compatible with the theoretical expectations described earlier: if it were possible to switch off the intrinsic disorder of manganites, the transition would be first order with more standard hysteresis effects (Yunoki et al., 2000; Moreo et al., 2000). But the influence of intrinsic disorder produces a distribution of critical fields which causes mixed-phase characteristics, which themselves induce colossal relaxation effects.

Oxygen isotope substitution on a material at the verge of a metal–insulator transition, such as $(La_{0.25}Pr_{0.75})_{0.7}Ca_{0.3}MnO_3$, leads to indications of phase segregation involving AF-insulating and FM-metallic phases according to neutron powder diffraction studies by Balagurov et al. (1999) (see also Babushkina et al., 1998; Voloshin et al., 2000). The results for the resistivity vs. temperature shown in those papers are quite similar to those observed in other materials where percolation seems to occur. Then, once again it is observed that near a metal–insulator transition it is easy to alter the balance by small changes in the composition.

Finally, neutron scattering studies of $Pr_{1-x}Ca_xMnO_3$ by Kajimoto et al. (1998) have shown that in the temperature regime between T_{CO} and T_N, ferromagnetic spin fluctuations have been observed. In addition, antiferromagnetic fluctuations appear to be present also in the same temperature regime (see Fig. 2 of Kajimoto et al., 1998), and thus a coexistence of FM and AF correlations exist in a finite window of temperatures. This result is similar to that observed in the same temperature window $T_N < T < T_{CO}$ for $Bi_{1-x}Ca_xMnO_3$ with large x (see Bao et al., 1997; Liu et al., 1998), and adds to the mixed-phase tendencies of these compounds. Very recently, neutron diffraction and inelastic neutron scattering results by Radaelli et al. (2000) obtained in $Pr_{1-x}Ca_xMnO_3$ ($x = 0.30$) indicated mesoscopic and microscopic phase segregation at different temperatures and magnetic fields.

4.6. Mixed-phase tendencies in bilayered manganites

Early neutron scattering experiments by Perring et al. (1997) reported the presence of long-lived antiferromagnetic clusters coexisting with ferromagnetic critical fluctuations in $La_{1.2}Sr_{1.8}Mn_2O_7$, which has a nominal hole density of $x = 0.4$. Fig. 4.6.1a contains the intensity of their signal vs. momenta. The peaks at 0.0, 1.0 and 2.0 in the horizontal axis correspond to ferromagnetism. The relatively small peak at 0.5 corresponds to an antiferromagnetic signal. In view of their results, Perring et al. (1997) concluded that a simple mean-field approach where a given typical site interacts with other typical sites cannot be valid in the bilayered material, a conclusion that the authors of this review fully agree with. Note, however, that other authors disagree with the mixed-phase interpretation of the neutron results [see Millis (1998a, b), and the reply contained in Perring et al. (1998)] and with the data itself [Osborn et al. (1998) believes that the AF signal is smaller than it appears in Fig. 4.6.1a, although they agree with the notion that FM and AF interactions are finely balanced in this compound]. Nevertheless, regardless of the actual intensities and in view of the overwhelming amount of experimental information pointing toward mixed-phase tendencies in 3D manganites, these authors believe that Perring et al. (1997) have provided reasonable evidence that bilayers could also support mixed-phase states.

Kubota et al. (1999a) studying the $x = 0.5$ bilayered manganite, concluded that here the CE-type insulating and the A-type metallic phases coexist. Battle et al. (1996a, b) and Argyriou et al. (2000) arrived at similar conclusions. This is qualitatively compatible with the Monte Carlo simulation results described in Section 3 that showed first-order transitions between many phases in the limit of a large electron–phonon coupling. In particular, in Section 3 it was shown, based on theoretical calculations, that the A- and CE-type phases are in competition, and their states cross as a function of the t_{2g} spin coupling J_{AF} (Yunoki et al., 2000). Weak disorder transforms the first-order transition into a second-order one with cluster coexistence in the vicinity of the critical point. This is an interesting detail that deserves to be reemphasized: the phenomenon of mixed-phase formation and percolation is expected to occur whenever a first-order transition separates two competing states, and whenever some sort of disorder affects the system. There is *no* need for one of the phases to be the 3D FM metallic state, which usually appears prominently in materials that show the CMR effect in manganites. This also shows that the DE mechanism is not needed to have a large magnetoresistance. This is in agreement with the conclusions of the work by Hur et al. (1998), where CMR effects for $x = 0.3$ bilayered manganites were presented even *without* long-range ferromagnetism. Hur et al. (1998) discussed the possibility of nonhomogeneous states at low temperature. Chauvet et al. (1998), using ESR techniques applied to the $x = 0.325$ bilayered system, also arrived at the conclusion that polarons or mixed-phase tendencies are possible in this compound.

Based on powder neutron-diffraction studies for bilayered manganites in a wide range of densities, Kubota et al. (1999b, c) reported the phase diagram shown in Fig. 4.6.1b (see also Hirota et al., 1998. For results at x larger than 0.5 see Ling et al., 2000). The AFM-I and -II phases are A-type AF phases with different spin periodicities along the direction perpendicular to the FM planes. The FM-I and -II phases are ferromagnetic states with the spins pointing in different directions (for more details see Kubota et al., 1999b). For our purposes, the region of main interest is the one labeled as "Canted AFM" which arises from the coexistence of AF and FM features in the neutron diffraction signal. However, as repeatedly stressed in this review, a canted state is

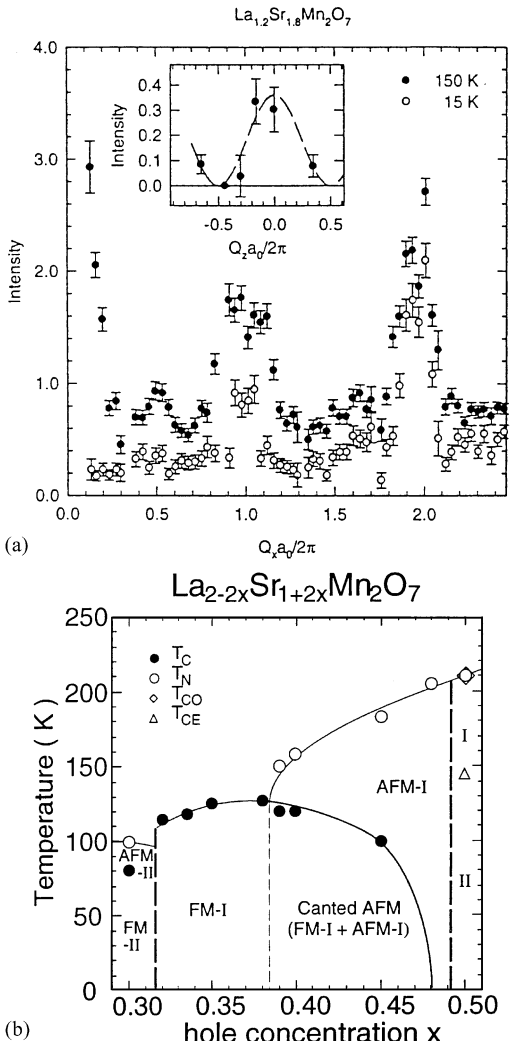

Fig. 4.6.1. (a) Intensity of neutron scattering experiments by Perring et al. (1997) performed on $La_{2-2x}Sr_{1+2x}Mn_2O_7$ with $x = 0.4$. The main figure shows the dependence with Q_x, while the inset contains a Q_z dependence (for details the reader should consult the original reference). At 150 K and 0.5 in the horizontal axis, a weak peak is observed corresponding to AF correlations, while the most dominant peaks denote ferromagnetism. (b) Magnetic phase diagram of $La_{2-2x}Sr_{1+2x}MnO_2O_7$ reproduced from Kubota et al. (1999a). Most of the notation is standard, but a more detailed explanation of the various phases can be found in the text or in the original reference. Note the prominent "Canted AFM" phase, which the authors of this review believe may have mixed-phase characteristics.

indistinguishable from a mixed FM–AF phase if the experimental techniques used average over the sample (see also Battle et al., 1999, and reply by Hirota et al., 1999). Further work, such as NMR studies, is needed to address the canted vs. mixed-phase microscopic nature of this state. Such a study would be important for clarifying these matters. Since the neutron scattering peaks observed by Kubota et al. (1999b, c) are sharp, the FM and AF clusters, if they exist, will be very

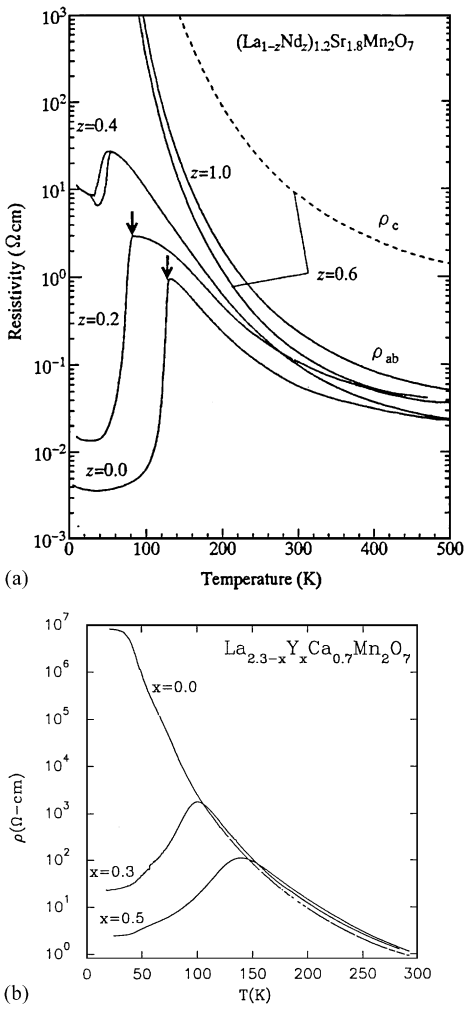

Fig. 4.6.2 . (a) In-plane resistivity component ρ_{ab} of $(La_{1-z}Nd_z)_{1.2}Sr_{1.8}Mn_2O_7$ (single crystals). The arrows indicate the Curie temperature. Reproduced from Moritomo et al. (1997). (b) Resistivity of the electron-doped manganite $La_{2.3-x}Y_xCa_{0.7}Mn_2O_7$ versus temperature for $x = 0.0$,0.3, and 0.5, reproduced from Raychaudhuri et al. (1998).

large as in other manganites that have shown a giant cluster coexistence. The resistivity vs. temperature of $x = 0.40$ and 0.45 already show features (Kubota, 1999d) somewhat similar to those that appeared in related experiments, namely dirty metallic behavior at low temperature with a $\rho(T \sim 0)$ increasing as x grows toward 0.5 (insulating phase). Very recently, Tokunaga et al. (2000) have observed with magneto-optical measurements a spatial variation of the magnetization in the region of "spin canting". Those authors produced clear images of the $x = 0.45$ bilayer compound, and also of $Pr_{1-x}Ca_xMnO_3$ at $x = 0.30$, showing domains with typical length scale exceeding one micrometer. Tokunaga et al. (2000) concluded that phase separation occurs in the region that neutron scattering experiments labeled before as spin canted, in excellent agreement with the theoretical calculations (on the other hand, above T_C Osborn et al. 1998 reported the

presence of canted-spin correlations). In addition,Zhou et al. (1998) also believe that the $x = 0.4$ compound has polaron formation that condenses into clusters as the temperature is reduced. Also Vasiliu-Doloc et al. (1999), using X-ray and neutron scattering measurements for the $x = 0.4$ bilayered manganite, concluded that there are polarons above T_C (see also Argyriou et al., 1999). More recently, Campbell et al. (2000) found indications of micro-phase separation on the $x = 0.4$ bilayer compound based on neutron scattering results. Chun et al. (2000) reported a spin-glass behavior at $x = 0.4$ which is interpreted as caused by FM–AF phase-separation tendencies.

The $x = 0.4$ low-temperature phase of double-layer manganites, which appears to be a metal according to Figs. 2.5.2 and 3, can be transformed into a charge-ordered state by chemical substitution using $(La_{1-z}Nd_z)_{1.2}Sr_{1.8}Mn_2O_7$. Data for several z's are shown in Fig. 4.6.2a. The shape of the ρ_{dc} vs. temperature curves resemble results found for other materials where clear indications of inhomogeneities were found using electron microscopy techniques. These authors believe that Fig. 4.6.2a may be indicative of a percolative transition between the FM- and CO-state at low temperature, where clusters of one phase grow in a background of the other until a percolation occurs. Moreover, recent theoretical work in this context (Moreo et al., 2000) allows for CMR effects involving two insulators, since apparently the most important feature of the compounds that present these effects is (i) a first-order-like transition between the competing phases and (ii) the presence of intrinsic disorder in the material. Thus, it is very interesting to note that in the bilayer system $Sr_{2-x}Nd_{1+x}Mn_2O_7$ with $x = 0.0$ and 0.10 a colossal MR effect has also been reported involving two insulators (Battle et al., 1996), showing that it is not necessary to have a double-exchange-induced ferromagnetic metallic phase to observe this effect, as remarked before.

Layered electron-doped compounds are also known. In fact, Raychaudhuri et al. (1998) reported transport, magnetic and specific heat studies of $La_{2.3-x}Y_xCa_{0.7}Mn_2O_7$ with $x = 0.0$,0.3, and 0.5. For $x = 0.0$ the material is a FM insulator. As x grows, a transition to a metallic state at low temperature was observed. The resistivity vs. temperature results are reproduced in Fig. 4.6.2b. The similarities with the behavior of other materials is clear. Raychaudhuri et al. (1998) concluded that the $x = 0.0$ compound may correspond to a FM–AF mixture involving unconnected ferromagnetic clusters embedded in an antiferromagnetic matrix.

Additional, although indirect, evidence for mixed-phase tendencies in bilayer compounds can be obtained from photoemission experiments. In fact, the first set of high-energy resolution angle-resolved photoemission (ARPES) measurements in the context of manganites was reported by Dessau et al. (1998) and the compound used was precisely $La_{2-2x}Sr_{1+2x}Mn_2O_7$ with $x = 0.4$ (high-resolution photoemission results for $La_{1-x}Sr_xMn\,O_3$ and $La_{1-x}Ca_xMn\,O_3$ were previously reported by Park et al., 1996. Dessau and Shen (1999) also presented results for $La_{1-x}Sr_xMnO_3$). In this experiment it was observed that the low-temperature ferromagnetic state was very different from a prototypical metal. Its resistivity is unusually high, the width of the ARPES features are anomalously broad, and they do not sharpen as they approach the Fermi momentum. Single Fermi-liquid-like quasiparticles cannot be used to describe these features. In addition, the centroids of the experimental peaks never approach closer than approximately 0.65 eV to the Fermi energy. This implies that, even in the expected "metallic" regime, the density of states at the Fermi energy is very small. Dessau et al. (1998) refers to these results as the formation of a "pseudogap" (see Fig. 4.6.3). Those authors found that the effect is present both in the FM and paramagnetic regimes, namely below and above T_C. The pseudogap affects the entire Fermi surface, i.e., there is no important momentum dependence in its value, making it unlikely that it is caused by

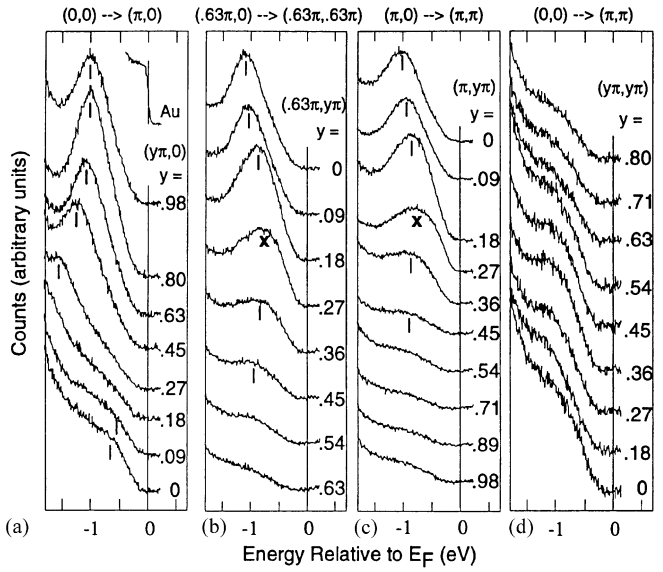

Fig. 4.6.3. Low-temperature (10 K) ARPES spectra corresponding to $(La_{1-z}Nd_z)Sr_{1.8}Mn_2O_7$ along various high symmetry directions. Results reproduced from Dessau et al. (1998).

charge, spin, or orbital ordering. Dessau et al. (1998) and Dessau and Shen (1999) argued that the origin of this pseudogap cannot simply be a Mott–Hubbard effect since the density is $x = 0.4$. The effect cannot arise from the simple DE mechanism which does not predict a pseudogap, and also cannot be caused by Anderson localization due to disorder, which is not expected to significantly affect the density of states. In other words, it is not the mobility that appears to lead to large resistivities but the lack of states at the Fermi energy. Recent photoemission studies for bilayers and $La_{1-x}Sr_xMnO_3$ with $x = 0.18$ led to similar conclusions (Saitoh et al., 1999). For theoretical results at $x = 0$ see van den Brink et al. (2000) and Yin et al. (2000).

These ARPES results are in qualitative agreement with recent calculations by Moreo et al. (1999b) and Moreo et al. (2000), described in detail elsewhere in this review, where a pseudogap in the density of states was shown to appear naturally in mixed-phase regimes, either those created by electronic phase separation or by the influence of disorder on first-order transitions that leads to giant cluster formation. In both cases the conductivity was shown to be very small in these regimes (Moreo et al., 1999b), and a pseudogap appears in the density of states. It is possible that the low temperature region of the $x = 0.4$ bilayer can be described in terms of a percolative process, and its reported "spin-canted" character is simply caused by mixing AF- and FM-phase. This rationalization also explains the large value of the resistivity even at low temperature.

The photoemission results are consistent with scanning tunneling microscopy data (Biswas et al., 1998), gathered for single crystals and thin films of hole-doped manganites. This study showed a rapid variation in the density of states for temperatures near the Curie temperature, such that below T_C a finite density of states is observed at the Fermi energy while above T_C a hard gap opens up. This result suggests that the presence of a gap or pseudogap is not just a feature of bilayers, but it appears in other manganites as well. In addition, the work of Biswas et al. (1998) suggest that the insulating behavior above T_C is caused by a depletion in the density of states, rather than by

a change in the mobility. As in the photoemission work just described, it appears that Anderson localization is not the reason for the insulating behavior, since this mechanism is not expected to induce a gap in the density of states.

4.7. Mixed-phase tendencies in single-layered manganites

Bao et al. (1996) reported the presence of macroscopic phase separation in the planar manganite $Sr_{2-x}La_xMnO_4$ in the range between $x = 0.0$ and 0.38. At $x = 0.0$ the material is a 2D AF insulator, with no carriers in the e_g-band. As x grows, carriers are introduced and they polarize the t_{2g}-spins leading to spin polaron formation, as in other compounds at low electronic density. These polarons attract each other and form macroscopic ferromagnetic regions. This result is in agreement with the theoretical discussion of Section 3 where it was found, both for one and two orbital models, that the region of small density of e_g-electrons has phase separation characteristics. The conclusions of Bao et al. (1996) are also in excellent agreement with the studies discussed in this review in the context of $La_{1-x}Ca_xMnO_3$ at large hole density concentration.

4.8. Possible mixed-phase tendencies in nonmanganite compounds

There are several other nonmanganite compounds that present a competition between FM and AF regions, states which in clean systems should be separated by first-order transitions, at least according to theoretical calculations. One of these compounds is $La_{1-y}Y_yTiO_3$. As y is varied, the average bandwidth W of the mobile electrons changes, and experiments have shown that a FM–AF transition appears (Tokura et al., 1993). This material may be a candidate for percolative FM–AF transitions, as in the manganites (see also Hays et al., 1999, for results on $La_{1-x}Sr_xTi\ O_3$ with phase-separation characteristics). Also Tb_2PdSi_3 and Dy_2PdSi_3 present properties that have been interpreted as indicative of magnetic polaron formation (Mallik et al., 1998). Large MR effects have been found in Gd_2PdSi_3 by Saha et al. (1999). In addition, simply replacing Mn by Co has been shown to lead to physics somewhat similar to that found in manganites. For instance, results obtained for $La_{1-x}Sr_xCoO_3$ using a variety of techniques have been interpreted as mixed-phase or cluster-glass states (see Caciuffo et al., 1999; Nam et al., 1999, and references therein). Also $Se_{1-x}Te_xCuO_3$ presents a FM–AF competition with spin-glass-like features (Subramanian et al., 1999), resembling the mixed-phase states discussed in this review. First-order FM–AF transitions have also been reported in $Ce\ Fe_2$-based pseudobinary systems (Manekar et al., 2000). Even results obtained in films of vinylidene fluoride with trifluoroethylene (Borca et al., 1999) have been interpreted in terms of a compressibility phase transition similar to those discussed by Moreo et al. (1999a), reviewed in Section 3. In addition, $Ni\ S_{2-x}Se_x$ also presents some characteristics similar to those of the materials described here, namely a metal–insulator transition which is expected to be of first-order, random disorder introduced by Se substitution, and an antiferromagnetic state (see Husmann et al., 1996; Matsuura et al., 2000; and references therein).

Very recently, some ruthenates have been shown to present characteristics similar to those of electron-doped $CaMnO_3$ (as discussed for example by Neumeier and Cohn, 2000), including a tendency to phase separation. Transport and magnetic results by Cao et al. (2000) indicate that in the region between $x = 0.0$ and 0.1 of $Ca_{2-x}La_xRuO_4$, the material changes rapidly from an antiferromagnetic insulator to a ferromagnetic metal. The behavior of the magnetic susceptibility

vs. temperature is shown in Fig. 4.8.1a. The shape of the M vs. H curve (Fig. 4.8.1b) is quite significant. On one hand, at finite density x there appears to be a finite moment as the field is removed, characteristic of FM samples. On the other hand, the linear behavior with H is indicative of AF behavior, namely for antiferromagnetically ordered spins the canting that occurs in the presence of a magnetic field leads to a linearly growing moment. A mixed-phase FM–AF is probably the cause of this behavior. The curve resistivity vs. temperature (also shown in Cao et al., 2000) indeed appears to have percolative characteristics, as found in many manganites. Also perovskites such as $CaFe_{1-x}Co_xO_3$ have an interesting competition between AF and FM states as x is varied. In Fig. 4.8.2 the resistivity in the range of Co densities where the transition occurs is shown, reproduced from Kawasaki et al. (1998). The similarities with other results described in this review are clear.

It is also important to mention here the large MR found in the *pyrochlore* compound $Tl_{2-x}Sc_xMn_2O_7$, although it is believed that its origin maybe different from the analogous effect

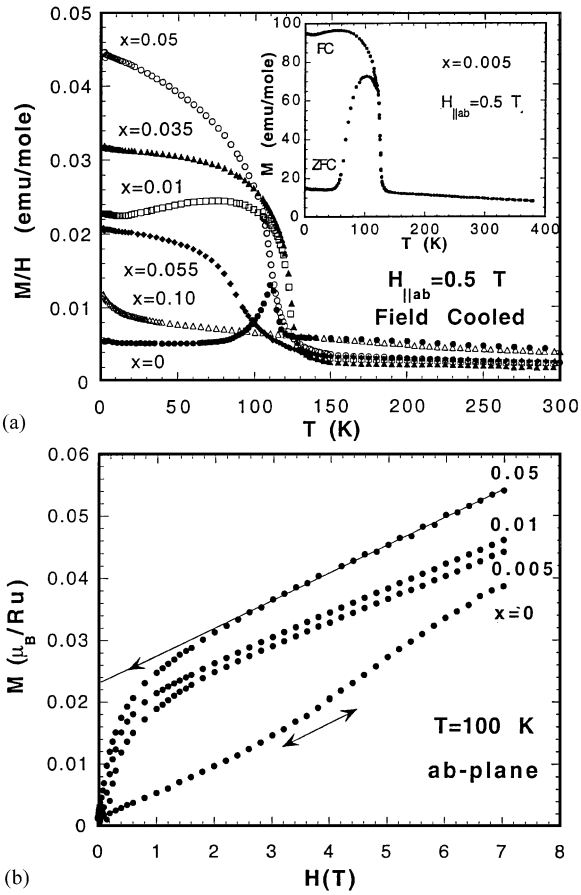

Fig. 4.8.1. (a) Magnetic susceptibility defined as M/H (M = magnetization, H = magnetic field) vs. temperature T for the densities indicated of $Ca_{2-x}La_xRuO_4$ (from Cao et al., 2000). Inset: Magnetization vs. temperature. (b) Magnetization M as a function of magnetic field for the densities indicated.

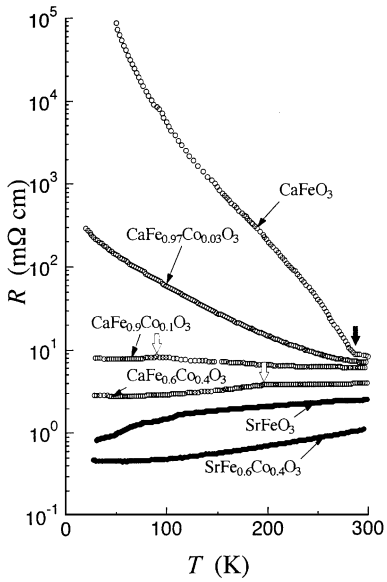

Fig. 4.8.2. Resistivity (R) vs. temperature for $SrFe_{1-x}Co_xO_3$ and $CaFe_{1-x}Co_xO_3$, reproduced from Kawasaki et al. (1998). For the meaning of the arrows the reader should consult the original reference.

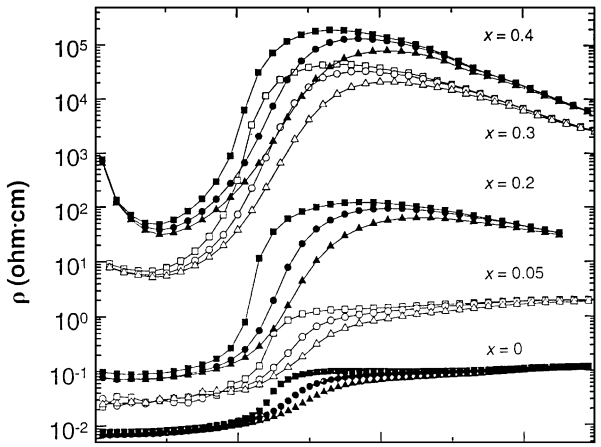

Fig. 4.8.3. Resistivity vs. temperature of $Tl_{2-x}Sc_xMn_2O_7$ for various values of x. The upper, middle, and lower curves for each x correspond to applied fields of $H = 0,3$, and 6 T, respectively. Result reproduced from Ramirez and Subramanian (1997).

found in manganites (Ramirez and Subramanian, 1997 and references therein. See also Shimakawa et al., 1996; Cheong et al., 1996). The behavior of the resistivity with temperature, parametric with the Sc concentration and magnetic fields is shown in Fig. 4.8.3. The similarities with the analogous plots for the manganites presented in previous sections is clear. More work should be devoted to clarify the possible connection between pyrochlore physics and the ideas discussed in this review.

Diluted magnetic semiconductors also present characteristics of phase-separated states. Ohno (1998) has recently reviewed part of the work in this context. The physics of magneto-polarons has also been reviewed before by Kasuya and Yanase (1968). The reader should consult these publications and others to find more references and details about this vast area of research. Diluted semiconductors have mobile carriers and localized moments in interaction. At low temperatures the spins are ferromagnetically aligned and the charge appears localized. It is believed that at these temperatures large regions of parallel spins are formed. The cluster sizes are of about 100 Å, a large number indeed (see Ohno et al., 1992). At a relatively small polaron density, their overlap will be substantial. Important experimental work in this context applied to $Eu_{1-x}Gd_xSe$ can be found in von Molnar and Methfessel (1967). The resistivity vs. temperature at several magnetic fields of EuSe is shown in Fig. 4.8.4, reproduced from Shapira et al. (1974). The similarity with results for manganites is clear.

Other compounds of this family present interesting FM–AF competitions. For instance, the phase diagram of $EuB_{6-x}C_x$ presented by Tarascon et al. (1981) contains an intermediate region labeled with a question mark between the FM and AF phases. This intermediate phase should be analyzed in more detail. Already Tarascon et al. (1981) favored an interpretation of this unusual region based on mixed-phase states. Recently, two magnetically similar but electronically inequivalent phases were detected with NMR applied to EuB_6 by Gavilano et al. (1998). Also Gavilano et al. (1995) reported a two-component NMR signal in $CeAl_3$, signalling inhomogeneities in the material. Clearly, other compounds seem to present physics very similar to that found in

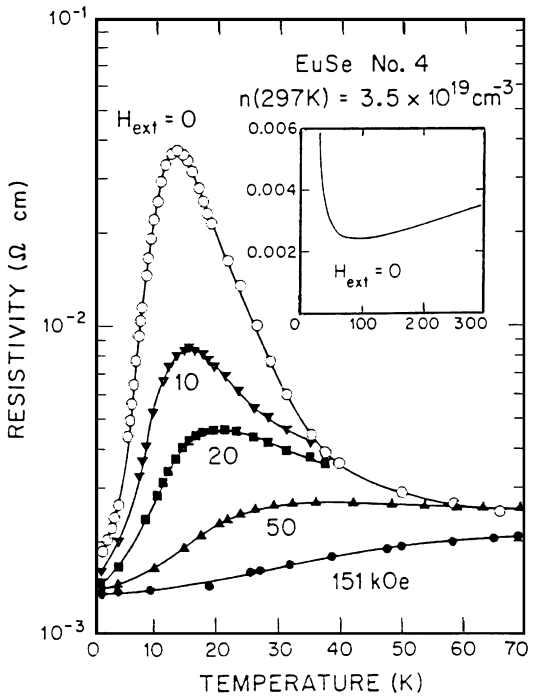

Fig. 4.8.4. Resistivity vs. temperature of EuSe for several magnetic fields. The inset contains the zero-field resistivity vs. temperature in a different scale. Results reproduced from Shapira et al. (1974).

manganites, at least regarding the FM–AF competition. The diluted magnetic semiconductors have been rationalized in the past as having physics caused by magneto-polaron formation. However, larger clusters, inhomogeneities, and percolative processes may matter in these compounds as much as in manganites. Actually, optical experiments by Yoon et al. (1998) have already shown the existence of strong similarities between manganites and EuB_6. More recently, Snow et al. (2000) presented inelastic light scattering measurements of EuO and $Eu_{1-x}La_xB_6$, as a function of doping, magnetic fields, and temperature. A variety of distinct regimes were observed, including a magnetic polaron regime above the Curie temperature and a mixed FM/AF regime at La density x larger than 0.05. These Eu-based systems do not have strong electron–lattice effects associated with Jahn–Teller modes. Then, the existence of physical properties very similar to those of manganites show that the key feature leading to such behavior is the competition between different tendencies, rather than the origin and detailed properties of those competing phases. It is clear that further experimental work should be devoted to clarify these interesting issues. The authors of this review firmly believe that mixed-phase tendencies and percolation are not only interesting properties of manganites, but should be present in a large variety of other compounds as well.

5. Discussion, open questions, and conclusions

In this review, the main results gathered in recent years in the context of theoretical studies of models for manganites have been discussed. In addition, the main experiments that have helped clarify the physics of these interesting compounds have also been reviewed. Several aspects of the problem are by now widely accepted, while others still need further work to be confirmed. Intrinsic inhomogeneities exist in models and experiments and seem to play a key role in these compounds.

Among the issues related with inhomogeneities that after a considerable effort appear well established are the following:

(1) Work carried out by several groups using a variety of techniques have shown that electronic phase separation is a dominant feature of models for manganites, particularly in the limits of small and large hole doping. This type of phase separation leads to nanometer size coexisting clusters once the long-range Coulombic repulsion is incorporated into the models.

(2) Working at constant density, the transitions between metallic (typically FM) and insulating (typically CO/AF) states are of *first* order at zero temperature. No counter-example has been found to this statement thus far.

(3) A second form of phase separation has been recently discussed. It is produced by the influence of disorder on the first-order metal–insulator transitions described in the previous item. A simple intuitive explanation is given in Fig. 5.1. If couplings are fixed such that one is exactly at the first-order transition in the absence of disorder, the system is "confused" and does not know whether to be metallic or insulating (at zero disorder). On the other hand, if the couplings are the same, but the strength of disorder is large in such a way that it becomes dominating, then tiny clusters of the two competing phases are formed with the lattice spacing as the typical length scale. For nonzero but weak disorder, an intermediate situation develops where fluctuations in the disorder pin either one phase or the other in large regions of space.

This form of phase separation is even more promising than the electronic one for explaining the physics of manganites for a variety of reasons: (i) it involves phases with the same density, thus there

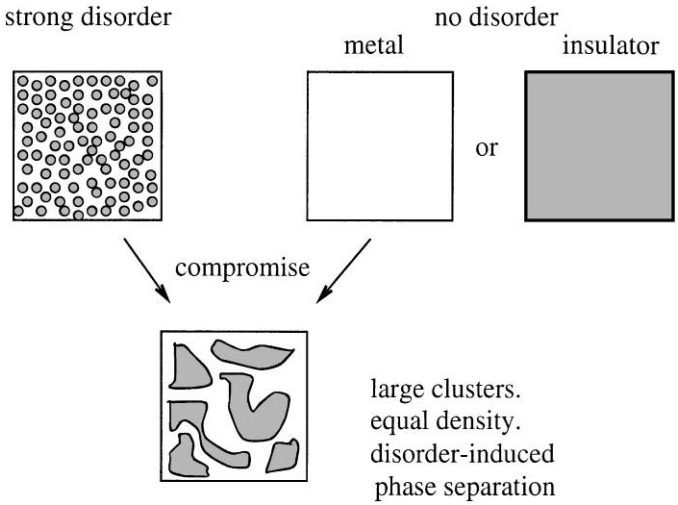

Fig. 5.1. Sketch of the competition metal–insulator in the presence of disorder, leading to equal-density coexisting large clusters in the "disorder-induced" phase separation scenario.

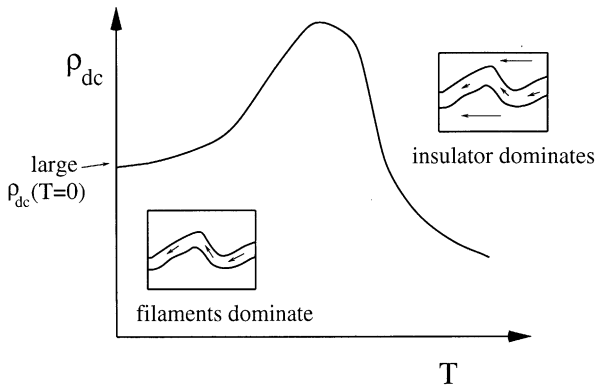

Fig. 5.2. Sketch of the expected resistivity vs. temperature in the percolative picture. For more details see text.

are no constraints on the size of the coexisting clusters which can be as large as a micrometer in scale, as found in experiments. (ii) The clusters are randomly distributed and have fractalic shapes, leading naturally to *percolative* transitions from one competing phase to the other, as couplings or densities are varied. This is in agreement with many experiments that have reported percolative features in manganites. (iii) The resistivity obtained in this context is similar to that found in experiments, as sketched in Fig. 5.2: Near the critical amount of metallic fraction for percolation, at room temperature the charge conduction can occur through the insulating regions since their resistivity at that temperature is very similar to that of the metallic state. Thus, the system behaves as an insulator. However, at low temperatures, the insulator regions have a huge resistivity and, thus, conduction is through the percolative metallic filaments which have a large intrinsic

resistivity. The system behaves as a bad metal, and $\rho_{dc}(T = 0)$ can be very large. (iv) Finally, it is expected that in a percolative regime there must be a high sensitivity to magnetic fields and other naively "small" perturbations, since tiny changes in the metallic fraction can induce large conductivity modifications. This provides the best explanation of the CMR effect of which these authors are aware.

(4) The experimental evidence for inhomogeneities in manganites is by now simply overwhelming. Dozens of groups, using a variety of techniques, have converged to such a conclusion. It is clear that homogeneous descriptions of manganites in the region of interest for the CMR effect are incorrect. These inhomogeneities appear even above the Curie temperature. In fact, the present authors believe that a new scale of temperature T^* should be introduced, as very roughly sketched in Fig. 5.3. There must be a temperature window where coexisting clusters exist above the temperatures where truly long-range order develops. Part of the clusters can be metallic, and their percolation may induce long-range order as temperature decreases. The region below T^* can be as interesting as that observed in high-temperature superconductors, at temperatures higher than the critical values. It is likely that it contains pseudogap characteristics, due to its low conductivity in low-bandwidth manganites. The search for a characterization of T^* should be pursued actively in experiments.

(5) The famous CE-state of half-doped manganites has been shown to be stable in mean-field and computational studies of models for manganites. Although such a state was postulated a long time ago, it is only recently that it has emerged from unbiased studies. The simplest view to understand the CE-state is based on a "band insulating" picture: it has been shown that in a zigzag FM chain a gap opens at $x = 0.5$, reducing the energy compared with straight chains. Thus, elegant geometrical arguments are by now available to understand the origin of the naively quite complicated CE-state of manganites. Its stabilization can be rationalized based simply on models of non-interacting spinless fermions in 1D geometries. In addition, theoretical studies have allowed one to analyze the properties of the states competing with the CE at $x = 0.5$. In order to arrive at the CE-state, the use of a strong long-range Coulomb interaction to induce the staggered charge

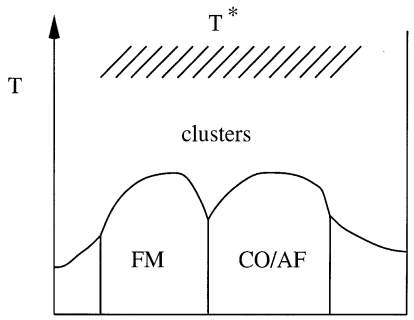

Fig. 5.3. Illustration of a conjectured new temperature scale T^* in manganites. Above the ordering temperatures T_{CO}, T_N, and T_C, a region with coexisting clusters could exist, in view of the theoretical ideas described in this review and the many experiments that are in agreement. It is possible that this region may have pseudogap characteristics, as in the high-temperature superconductors. The sketch shown here tries to roughly mimic the phase diagram of LCMO. The doping independence of T^* in the figure is just to simplify the discussion. Actually, a strong hole density dependence of T^* is possible.

pattern is not correct, since by this procedure the experimentally observed charge stacking along the z-axis could not be reproduced, and in addition the metallic regimes at $x = 0.5$ found in some manganites would not be stable. Manganese oxides are in the subtle regime where many different tendencies are in competition.

(6) Contrary to what was naively believed until recently, studies with strong electron Jahn–Teller phonon coupling or with strong on-site Coulomb interactions lead to quite similar phase diagrams. The reason is that both interactions disfavor double occupancy of a given orbital. Thus, if the goal is to understand the CMR effect, the important issue is not whether the material is Jahn–Teller or Coulomb dominated, but how the metallic and insulating phases, of whatever origin, compete. Calculations with Jahn–Teller phonons are the simplest in practice, and they have led to phase diagrams that contain most of the known phases found experimentally for manganites, such as the A-type AF insulating state at $x = 0$, the A-type AF metallic state at $x = 0.5$, the CE-state at $x = 0.5$, etc. Such an agreement theory-experiment is quite remarkable and encouraging.

(7) Also contrary to naive expectations, the smallest parameter in realistic Hamiltonians for Mn-oxides, namely "J_{AF}" between localized t_{2g} spins, plays an important role in stabilizing the experimentally observed phases of manganites, including the CE-state. Modifications of this coupling due to disorder are as important as those in the hopping amplitudes for e_g-electron movement.

In short, it appears that some of the theories proposed in early studies for manganites can already be shown to be incorrect. This includes (i) simple double-exchange ideas where the high resistivity above T_C is caused by the disordered character of the localized spins that reduce the conductivity in the e_g band. This is not enough to produce an insulating state above T_C, and does not address the notorious inhomogeneities found in experiments. It may be valid in some large-bandwidth compounds away from the region of competition between metal and insulator. (ii) Anderson localization also appears unlikely to explain the experimental data. An unphysically large value of the disorder strength is needed for this to work at high temperature, the pseudogap found in photoemission experiments cannot be rationalized in this context where the density of states is not affected by disorder, and large inhomogeneities, once again, cannot be addressed in this framework. However, note that once a percolative picture is accepted for manganites, then some sort of localization in such a fractalic environment is possible. (iii) Polaronic ideas can explain part of the experimental data at least at high temperatures, far from the Curie temperature. However, the region where CMR is maximized cannot be described by a simple gas of heavy polarons or bipolarons (see experimental results in Section 4). There is no reason in the polaronic framework for the creation of micrometer size coexisting clusters in these compounds. Actually, note that theories based on small polarons and phase separation do not differ only on subtle points if the phase separation involves microdomains. It may happen that nanometer phase separation leads to physics similar to that created by polaronic states, but certainly not when much larger clusters are formed.

As a conclusion, it is clear that the present prevailing paradigm for manganites relies on a phase-separated view of the dominant state, as suggested by dozens of experiments and also by theoretical calculations once powerful many-body techniques are used to study realistic models.

Although considerable progress has been achieved in recent years in the analysis of manganites, both in theoretical and experimental aspects, there are still a large number of issues that require

further work. Here a partial list of *open questions* is included:

(a) The phase-separation scenario needs further experimental confirmation. Are there counter-examples of compounds where CMR occurs but the system appears homogeneous?

(b) On the theory front, a phase-separated percolative state is an important challenge to our computational abilities. Is it possible to produce simple formulas with a small number of parameters that experimentalists can use in order to fit their, e.g., transport data? The large effort needed to reproduce the zero magnetic field resistivity vs. temperature results (reviewed here) suggests that this will be a hard task.

(c) It is believed that at zero temperature the metal–insulator transition is of first order and upon the introduction of disorder it becomes continuous, with percolative characteristics. A very important study that remains to be carried out is the analysis of the influence of temperature on those results. These authors believe that the generation of a "quantum critical point" (QCP) is likely in this context, and preliminary results support this view (Burgy et al., 2000). The idea is sketched in Fig. 5.4. Without disorder (part (a)), the first-order transition survives the introduction of temperature, namely in a finite temperature window the transition between the very different FM and AF states remains first order. However, introducing disorder (part (b)), a QCP can be generated since the continuous zero-temperature transition is unlikely to survive at finite temperature at fixed couplings. The presence of such QCP would be a conceptually important aspect of the competition between FM and AF phases in manganites. Experimental results showing that the generation of such QCP is possible have already been presented (Tokura, 2000).

(d) There is not much reliable theoretical work carried out in the presence of magnetic fields addressing directly the CMR effect. The reason is that calculations of resistivity are notoriously

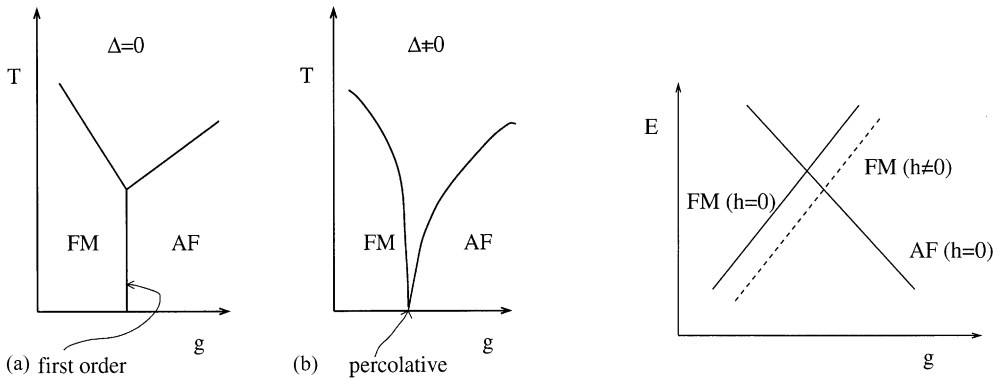

Fig. 5.4. Illustration of how a quantum critical point can be generated in models for manganites. In (a) the first-order FM–AF transition is shown as a function of temperature, without disorder ($\Delta = 0$). In (b), the expected behavior with disorder is shown. In both cases "g" is a coupling or hole density that allows the system to change from a metal to an insulator, and the disorder under discussion involves adding a random component to "g".

Fig. 5.5. Simple rationalization of the CMR effect based on a first-order transition metal–insulator. In this context CMR can only occur in a narrow window of couplings and densities. Sketched is the ground-state energy vs. a parameter "g" that causes the transition from metal to insulator (coupling or density). The FM phase is shown with and without a magnetic field "h".

difficult, and in addition, the recent developments suggest that percolative properties are important in manganites, complicating the theoretical analysis. Nevertheless, the present authors believe that a very simple view of the CMR effect could be as follows. It is known that the metallic and insulating phases are separated by first-order transitions. Then, when energy is plotted vs. the parameter "g" that transforms one phase into the other (it could be a coupling in the Hamiltonian or the hole density), a level crossing occurs at zero temperature, as sketched in Fig. 5.5. In the vicinity of the transition point, a small magnetic field can produce a rapid destabilization of the insulating phase in favor of the metallic phase. This can occur only in a small window of densities and couplings if realistic (small) magnetic fields are used. At present it is unknown how disorder, and the percolation phenomena it induces, will affect these sketchy results. In addition, there are compounds such as $Pr_{1-x}Ca_xMnO_3$ that present CMR in a large density window, suggesting that the simple picture of Fig. 5.5 can be a good starting point, but is incomplete. Thus, quantitative calculations addressing the CMR effect are still needed.

(e) Does a spin-canted phase ever appear in simple models with competing FM- and AF-phase in the absence of magnetic fields? Are the regions labeled as spin canted in some experiments truly homogeneous or mixed states?

(f) If the prediction of a phase-separated state in the CMR regime of manganites is experimentally fully confirmed, what are the differences between that state and a canonical "spin glass"? Both share complexity and complicated time dependences, but are they in the same class? Stated in more exciting terms, can the phase-separated regime of manganites be considered a "new" state of matter in any respect?

(g) Considerable progress has been achieved in understanding the $x = 0$ and 0.5 charge/orbital/spin order states of manganites. But little is known about the ordered states at intermediate densities, both in theory and experiments. Are there stripes in manganites at those intermediate hole densities as recently suggested by experimental and theoretical work?

Summarizing, the study of manganites continues challenging our understanding of transition metal oxides. While considerable progress has been achieved in recent years, much work remains to be done. In particular, a full understanding of the famous CMR effect is still lacking, although evidence is accumulating that it may be caused by intrinsic tendencies toward inhomogeneities in Mn-oxides and other compounds. Work in this challenging area of research should continue at its present fast pace.

Acknowledgements

The authors would like to thank our many collaborators that have helped us in recent years in the development of the phase separation scenario for manganites. Particularly, the key contributions of Seiji Yunoki are here acknowledged. It is remarked that a considerable portion of the subsection entitled "Monte Carlo Simulations" has been originally prepared by Seiji Yunoki. We also thank C. Buhler, J. Burgy, S. Capponi, A. Feiguin, N. Furukawa, K. Hallberg, J. Hu, H. Koizumi, A. Malvezzi, M. Mayr, D. Poilblanc, J. Riera, Y. Takada, J. A. Verges, for their help in these projects.

We are also very grateful to S. L. Cooper, T. Egami, J. P. Hill, J. Lynn, D. Mills, J. Neumeier, A. Pimenov, and P. Schiffer, for their valuable comments on early drafts of the present review.

E.D. and A.M. are supported by grant NSF-DMR-9814350, the National High Magnetic Field Laboratory (NHMFL), and the Center for Materials Research and Technology (MARTECH). T.H. has been supported by the Ministry of Education, Science, Sports, and Culture (ESSC) of Japan during his stay in the National High Magnetic Field Laboratory, Florida State University. T.H. is also supported by the Grant-in-Aid for Encouragement of Young Scientists under the contact No. 12740230 from the Ministry of ESSC.

References

Adams, C. P., Lynn, J. W., Mukovskii, Y. M., Arsenov, A. A., Shulyatev, D. A., 2000. Phys. Rev. Lett. 85, 3954.
Agterberg, D., Yunoki, S., 2000. Phys. Rev. B62, 13,816.
Akimoto, T., Maruyama, Y., Moritomo, Y., Nakamura, A., Hirota, K., Ohoyama, K., Ohashi, M., 1998. Phys. Rev. B57, R5594.
Alexandrov, A.S., Bratkovsky, A.M., 1999. Phys. Rev. Lett. 82, 141.
Aliaga, R., Allub, R., Alascio, B., 1998. Preprint, cond-mat/9804248.
Aliaga, H., Normand, B., Hallberg, K., Avignon, M., Alascio, B., 2000a. Preprint, cond-mat/0011342.
Aliaga, H., Causa, M.T., Butera, A., Alascio, B., Salva, H., Tovar, M., Vega, D., Polla, G., Leyva, G., Koning, P., 2000b. Preprint, cond-mat/0010295.
Allen, P.B., Perebeinos, V., 1999a. Phys. Rev. B60, 10,747.
Allen, P.B., Perebeinos, V., 1999b. Phys. Rev. Lett. 83, 4828.
Allodi, G., De Renzi, R., Guidi, G., Licci, F., Pieper, M.W., 1997. Phys. Rev. B56, 6036.
Allodi, G., De Renzi, R., Guidi, G., 1998a. Phys. Rev. B57, 1024.
Allodi, G., De Renzi, R., Licci, F., Pieper, M.W., 1998b. Phys. Rev. Lett. 81, 4736.
Allodi, G., De Renzi, R., Solzi, M., Kamenev, K., Balakrishnan, G., Pieper, M. W., 1999. Preprint, cond-mat/9911164.
Allub, R., Alascio, B., 1996. Solid State Commun. 99, 613.
Allub, R., Alascio, B., 1997. Phys. Rev. B55, 14,113.
Alonso, J. L., Fernández, L. A., Guinea, F., Laliena, V., Martín-Mayor, V., 2000a. Preprint, cond-mat/0003472.
Alonso, J. L., Fernández, L. A., Guinea, F., Laliena, V., Martín-Mayor, V., 2000b. Preprint, cond-mat/0007438.
Alonso, J. L., Fernández, L. A., Guinea, F., Laliena, V., Martín-Mayor, V., 2000c. Preprint, cond-mat/0007450.
Anane, A., Renard, J.P., Reversat, L., Dupas, C., Veillet, P., Viret, M., Pinsard, L., Revcolevschi, A., 1999a. Phys. Rev. B59, 77.
Anane, A., Raquet, B., von Molnar, S., Pinsard-Godart, L., Revcolevschi, A., 1999b. Preprint, cond-mat/9910204.
Anderson, P.W., Hasegawa, H., 1955. Phys. Rev. 100, 675.
Anisimov, V.I., Elfimov, I.S., Korotin, M.A., Terakura, K., 1997. Phys. Rev. B55, 15,494.
Argyriou, D.N., Bordallo, H.N., Mitchell, J.F., Jorgensen, J.D., Strouse, G.F., 1999. Phys. Rev. B60, 6200.
Argyriou, D.N., Bordallo, H.N., Campbell, B.J., Cheetham, A.K., Cox, D.E., Gardner, J.S., Hanif, K., dos Santos, A., Strouse, G.F., 2000. Phys. Rev. B61, 15,269.
Arima, T., Tokura, Y., Torrance, J.B., 1993. Phys. Rev. B48, 17006.
Arima, T., Tokura, Y., 1995. Phys. Soc. Japan 64, 2488.
Arovas, D., Guinea, F., 1998. Phys. Rev. B58, 9150.
Arovas, D., Gómez-Santos, G., Guinea, F., 1999. Phys. Rev. B59, 13,569.
Avishai, Y., Luck, J.M., 1992. Phys. Rev. B45, 1074.
Babushkina, N.A., Belova, L.M., Ozhogin, V.I., Gorbenko, O.Yu., Kaul, A.R., Bosak, A.A., Khomskii, D.I., Kugel, K.I., 1998. J. Appl. Phys. 83, 7369.
Balagurov, A.M., Pomjakushin, V.Yu., Sheptyakov, D.V., Aksenov, V.L., Babushkina, N.A., Belova, L.M., Taldenkov, A.N., Inyushkin, A.V., Fischer, P., Gutmann, M., Keller, L., Gorbenko, O.Yu., Kaul, A.R., 1999. Phys. Rev. B60, 383.
Bao, W., Chen, C.H., Carter, S.A., Cheong, S.-W., 1996. Solid State Commun. 98, 55.
Bao, W., Axe, J.D., Chen, C.H., Cheong, S.-W., 1997. Phys. Rev. Lett. 78, 543.
Bao, W., Axe, J.D., Chen, C.H., Cheong, S.-W., Schiffer, P., Roy, M., 1998. Physica B 241–243, 418.
Baran, M., Gnatchenko, S., Gorbenko, O., Kaul, A., Szymczak, R., Szymczak, H., 1999. Phys. Rev. B60, 9244.

Batista, C. D., Eroles, J. M., Avignon, M., Alascio, B., 2000. Preprint, cond-mat/0008367.
Batista, C. D., Eroles, J. M., Avignon, M., Alascio, B., 1998. Phys. Rev. B58, R14689.
Battle, P.D., Blundell, S.J., Green, M.A., Hayes, W., Honold, M., Klehe, A.K., Laskey, N.S., Millburn, J.E., Murphy, L., Rosseinsky, M.J., Samarin, N.A., Singleton, S., Sluchanko, N.A., Sullivan, S.P., Vente, J.F., 1996. J. Phys.: Condens. Matter 8, L427.
Battle, P.D., Green, M.A., Laskey, N.S., Millburn, J.E., Rosseinsky, M.J., Sullivan, S.P., Vente, J.F., 1996a. Chem. Commun. 767.
Battle, P.D., Green, M.A., Laskey, N.S., Millburn, J.E., Radaelli, P.G., Rosseinsky, M.J., Sullivan, S.P., Vente, J.F., 1996b. Phys. Rev. B54, 15,967.
Battle, P.D., Rosseinsky, M.J., Radaelli, P.G., 1999. J. Phys. Soc. Japan 68, 1462.
Belesi, M., Papavassiliou, G., Fardis, M., Kallias, G., Dimitropoulos, C., 2000. Preprint, cond-mat/0004332.
Belevtsev, B. I., Krasovitsky, V. B., Bobkov, V. V., Naugle, D. G., Rathnayaka, K. D. D., Parasiris, A., 2000. Preprint, cond-mat/0001372.
Benedetti, P., Zeyher, R., 1999. Phys. Rev. B59, 9923.
Betouras, J.J., Fujimoto, S., 1999. Phys. Rev. B59, 529.
Billinge, S.J.L., DiFrancesco, R.G., Kwei, G.H., Neumeier, J.J., Thompson, J.D., 1996. Phys. Rev. Lett. 77, 715.
Billinge, S. J. L., Proffen, Th., Petkov, V., Sarrao, J.L., Kycia, S. 1999. Preprint, cond-mat/9907329.
Biswas, A., Elizabeth, S., Raychaudhuri, A.K., Bhat, H. L., 1998. Preprint, cond-mat/9806084.
Blasco, J., Garcia, J., de Teresa, J.M., Ibarra, M.R., Algarabel, P.A., Marquina, C., 1996. J. Phys.: Condens. Matter 8, 7427.
Bocquet, A., Mizokawa, T., Saitoh, T., Namatame, H., Fujimori, A., 1992. Phys. Rev. B46, 3771.
Booth, C.H., Bridges, F., Kwei, G.H., Lawrence, J.M., Cornelius, A.L., Neumeier, J.J., 1998a. Phys. Rev. Lett. 80, 853.
Booth, C.H., Bridges, F., Kwei, G.H., Lawrence, J.M., Cornelius, A.L., Neumeier, J.J., 1998b. Phys. Rev. Lett. B 57, 10440.
Borca, C.N., Adenwalla, S., Choi, J., Sprunger, P.T., Ducharme, S., Robertson, L., Palto, S.P., Liu, J., Poulsen, M., Fridkin, V.M., You, H., Dowben, P.A., 1999. Phys. Rev. Lett. 83, 4562.
Bourges, P., et al., 2000. Science 288, 1234.
de Brion, S., Ciorcas, F., Chouteau, G., Lejay, P., Radaelli, P., Chaillout, C., 1998. Preprint, cond-mat/9803024.
Broussard, P.R., Browning, V.M., Cestone, V.C., 1999a. Preprint, cond-mat/9901189.
Broussard, P.R., Qadri, S.B., Browning, V.M., Cestone, V.C., 1999b. Preprint, cond-mat/9902020.
Buhler, C., Yunoki, S., Moreo, A., 2000. Phys. Rev. Lett. 84, 2690.
Burgy, J. et al, 2000. in preparation.
Caciuffo, R., Rinaldi, D., Barucca, G., Mira, J., Rivas, J., Senaris-Rodriguez, M.A., Radaelli, P.G., Fiorani, D., Goodenough, J.B., 1999. Phys. Rev. B59, 1068.
Calderon, M.J., Brey, L., 1998. Phys. Rev. B58, 3286.
Calderon, M., Vergés, J., Brey, L., 1999. Phys. Rev. B59, 4170.
Calvani, P., De Marzi, G., Dore, P., Lupi, S., Maselli, P., D'Amore, F., Gagliardi, S., 1998. Phys. Rev. Lett. 81, 4504.
Campbell, B.J. et al, 2000. Unpublished.
Cao, G., McCall, S., Dobrosavljevic, V., Alexander, C.S., Crow, J.E., Guertin, R.P., 2000. Phys. Rev. B61, 5053.
Capone, M., Feinberg, D., Grilli, M., 2000. Euro. Phys. J. B17, 103.
Casa, D., Kiryukhin, V., Saleh, O.A., Keimer, B., Hill, J.P., Tomioka, Y., Tokura, Y., 1999. Europhys. Lett. 47, 90.
Castellani, C., Natoli, C.R., Ranninger, J., 1978. Phys. Rev. 18, 4945.
Cerovski, V.Z., Mahanti, S.D., Kaplan, T.A., Taraphder, A., 1999. Phys. Rev. B59, 13,977.
Chattopadhyay, A., Millis, A.J., Das Sarma, S., 2000. Preprint, cond-mat/0004151.
Chauvet, O., Goglio, G., Molinie, P., Corraze, B., Brohan, L., 1998. Phys. Rev. Lett. 81, 1102.
Chen, C.H., Cheong, S.-W., 1996. Phys. Rev. Lett. 76, 4042.
Chen, Z.Y., Biswas, A., Zutić, I., Wu, T., Ogale, S.B., Orozco, A., Greene, R.L., Venkatesan, T., 2000. Preprint, cond-mat/0007353.
Cheong, S.-W., Hwang, H.Y., Batlogg, B., Rupp Jr, L.W., 1996. Solid State Commun. 98, 163.
Cheong, S.-W., Hwang, H.Y., 1999. In: Tokura, Y. (Ed.), Contribution to Colossal Magnetoresistance Oxides, Monographs in Condensed Matter Science.. Gordon & Breach, London.
Chiba, H., Kikuchi, M., Kusaba, K., Muraoka, Y., Syono, Y., 1996. Solid State Commun. 99, 499.

Chun, S.H., Salamon, M.B., Han, P.D., Lyanda-Geller, Y., Goldbart, P.M., 1999a. Preprint, cond-mat/9904332.
Chun, S.H., Salamon, M.B., Tomioka, Y., Tokura, Y., 1999b. Preprint, cond-mat/9906198.
Chun, S.H., Lyanda-Geller, Y., Salamon, M.B., Suryanarayanan, R., Dhalenne, G., Revcolevschi, A., 2000. Preprint, cond-mat/0007249.
Cieplak, M., 1978. Phys. Rev. B18, 3470.
Coey, J.M.D., Viret, M., Ranno, L., Ounadjela, K., 1995. Phys. Rev. Lett. 75, 3910.
Coey, J.M.D., Viret, M., von Molnar, S., 1998. Mixed-valence manganites. Adv. Phys., in press.
Coffey, D., Bedell, K., Trugman, S., Phys. Rev. 1990. B42, 6509.
Cox, D.E., Radaelli, P.G., Marezio, M, et al., 1998. Phys. Rev. B57, 3305.
Dagotto, E., 1994. Rev. Mod. Phys. 66, 763.
Dagotto, E., Yunoki, S., Malvezzi, A.L., Moreo, A., Hu, J., Capponi, S., Poilblanc, D., Furukawa, N., 1998. Phys. Rev. 58 B, 6414.
Dai, P., Fernandez-Baca, J.A., Chakoumakos, B.C., Cable, J.W., Nagler, S.E., Schiffer, P., Kalechofsky, N., Roy, M., Tsui, Y.-K., McGinn, P., Einloth, S., Ramirez, A.P., 1996. Preprint, unpublished.
Dai, P, et al., 1998. Phys. Rev. Lett. 80, 1738.
Dai, P., Fernandez-Baca, J.A., Wakabayashi, N., Plummer, E.W., Tomioka, Y., Tokura, Y., 2000. Phys. Rev. Lett. 85, 2553.
Darling, T.W., Migliori, A., Moshopoulos, E.G., Trugman, S.A., Neumeier, J.J., Sanao, J.L., Bishop, A.R., Thompson, J.D., 1998. Phys. Rev. B57, 5093.
Datta, S., 1995. Electronic Transport in Mesoscopic Systems.. Cambridge University Press, Cambridge.
deGennes, P.G., 1960. Phys. Rev. 118, 141.
Demin, R.V., Koroleva, L.I., Balbashov, A.M., 1999. JETP Lett. 70, 314, and references therein.
Dessau, D.S., Saitoh, T., Park, C.-H., Shen, Z.-X., Villella, P., Hamada, N., Moritomo, Y., Tokura, Y., 1998. Phys. Rev. Lett. 81, 192.
Dessau, D.S., Shen, Z.-X., 1999. In: Tokura, Y. (Ed.), Contribution to Colossal Magnetoresistance Oxides, Monographs in Condensed Matter Science. Gordon & Breach, London.
De Teresa, J.M., Ibarra, M.R., Garcia, J., Blasco, J., Ritter, C., Algarabel, P.A., Marquina, C., del Moral, A., 1996. Phys. Rev. Lett. 76, 3392.
De Teresa, J.M., Ritter, C., Ibarra, M.R., Algarabel, P.A., Garcia-Muñoz, J., Blasco, J., Garcia, J., Marquina, C., 1997a. Phys. Rev. B56, 3317.
De Teresa, J.M., Ibarra, M.R., Algarabel, P.A., Ritter, C., Marquina, C., Blasco, J., Garcia, J., del Moral, A., Arnold, Z., 1997b. Nature 386, 256.
Dho, J., Kim, I., Lee, S., Kim, K.H., Lee, H.J., Jung, J.H., Noh, T.W., 1999a. Phys. Rev. B59, 492.
Dho, J., Kim, I., Lee, S., 1999b. Preprint.
Dworin, L., Narath, A., 1970. Phys. Rev. Lett. 25, 1287.
Egami, T., 1996. J. Low Temp. Phys. 105, 791.
Egami, T., Louca, D., McQueeney, R.J., 1997. J. Supercond. 10, 323.
Egami, T., Louca, D., 1998. Proceedings of the Euroconference on "Polarons: Condensation, Pairing, Magnetism", Erice, Sicily, June, J. Supercond., to be published.
Elemans, J.B., Van Laar, B., Van Der Keen, K.R., Loopstra, B., 1971. J. Solid State Chem. 3, 238.
Emery, V., Kivelson, S.A., Zachar, O., 1997. Phys. Rev. B56, 6120.
Endoh, Y., Nojiri, H., Kaneko, K., Hirota, K., Fukuda, T., Kimura, H., Murakami, Y., Ishihara, S., Maekawa, S., Okamoto, S., Motokawa, M., 1999a. J. Mater. Sci. Eng. B 56, 1, see also Cond-mat/9812404.
Endoh, Y., Hirota, K., Ishihara, S., Okamoto, S., Murakami, Y., Nishizawa, A., Fukuda, T., Kimura, H., Nojiri, H., Kaneko, K., Maekawa, S., 1999b. Phys. Rev. Lett. 82, 4328.
Eremin, M.V., Kalinenkov, V.N., 1978. Sov. Phys. Solid State 20, 2051.
Eremin, M.V., Kalinenkov, V.N., 1981. Sov. Phys. Solid State 23, 828.
Fäth, M., Freisem, S., Menovsky, A.A., Tomioka, Y., Aarts, J., Mydosh, J.A., 1999. Science 285, 1540.
Feiner, L.F., Olés, A.M., 1999. Phys. Rev. B59, 3295.
Fernandez-Baca, J.A., Dai, P., Hwang, H.Y., Kloc, C., Cheong, S.-W., 1998. Phys. Rev. Lett. 80, 4012.
Ferrari, V., Rozenberg, M.J., 1999. Preprint, Cond-mat/9906131.

Fert, A., Campbell, I.A., 1976. J. Phys. F6, 849.
Fratini, S., Feinberg, D., Grilli, M., 2000. Preprint, cond-mat/0011419.
Frésard, R., Kotliar, G., 1997. Phys. Rev. B56, 12,909.
Fujishiro, H, et al., 1998. J. Phys. Soc. Japan. 67 1799.
Fukumoto, N., Mori, S., Yamamoto, N., Moritomo, Y., Katsufuji, T., Chen, C.H., Cheong, S-W., 1999. Phys. Rev. B60, 12,963.
Furukawa, N., 1994. J. Phys. Soc. Japan 63, 3214.
Furukawa, N., 1995a. J. Phys. Soc. Japan 64, 2734.
Furukawa, N., 1995b. J. Phys. Soc. Japan 64, 2754.
Furukawa, N., 1995c. J. Phys. Soc. Japan 64, 3164.
Furukawa, N., Moritomo, Y., Hirota, K., Endoh, Y., 1998. Preprint, cond-mat/9808076.
Furukawa, N., 1998. Preprint, cond-mat/9812066.
Garcia, D.J., Hallberg, K., Batista, C.D., Avignon, M., Alascio, B., 2000. Phys. Rev. Lett. 85, 3720.
Gavilano, J., Hunzifer, J., Ott, H.R., 1995. Phys. Rev. B52, R13106.
Gavilano, J.L., Ambrosini, B., Vonlanthen, P., Ott, H.R., Young, D.P., Fisk, Z., 1998. Phys. Rev. Lett. 81, 5648.
Gerloch, M., Slade, R.C., 1973. Ligand-Field Parameters. Cambridge, London.
Ghivelder, L., Abrego Castillo, I., Gusmao, M.A., Alonso, J.A., Cohen, L.F., 1999. Preprint, cond-mat/9904232.
Golosov, D.I., Norman, M.R., Levin, K., 1998. Preprint, cond-mat/9805238.
Goodenough, J., 1955. Phys. Rev. 100, 564.
Goodenough, J.B., 1963. Magnetism and the Chemical Bond. Interscience, New York.
Gor'kov, L.P., Kresin, V.Z., 1998. JETP Lett. 67, 985.
Griffith, J.S., 1961. The Theory of Transition-Metal Ions. Cambridge.
Gu, R.Y., Wang, Z.D., Shen, S.-Q., Xing, D.Y., 1999. Preprint, cond-mat/9905152.
Guerrero, M., Noack, R.M., 2000. Preprint, cond-mat/0004265.
Guinea, F., Gómez-Santos, G., Arovas, D.P., 1999. Preprint, cond-mat/9907184.
Harrison, W.A., 1989. Electronic Structure and The Properties of Solids. Dover Publications, New York.
Hays, C.C., Zhou, J.-S., Markert, J.T., Goodenough, J.B., 1999. Phys. Rev. B60, 10,367.
Heffner, R.H., Le, L.P., Hundley, M.F., Neumeier, J.J., Luke, G.M., Kojima, K., Nachumi, B., Uemura, Y.J., MacLaughlin, D.E., Cheong, S.-W., 1996. Phys. Rev. Lett. 77, 1869.
Heffner, R.H., Sonier, J.E., MacLaughlin, D.E., Nieuwenhuys, G.J., Ehlers, G., Mezei, F., Cheong, S.-W., Gardner, J.S., Röder, H., 1999. Cond-mat/9910064.
Held, K., Vollhardt, D., 1999. Preprint, Cond-mat/9909311.
Helman, J.S., Abeles, B., 1976. Phys. Rev. Lett. 37, 1429.
Hemberger, J., Paraskevoupolos, M., Sichelschmidt, J., Brando, M., Wehn, R., Mayr, R., Pucher, K., Lunkenheimer, P., Loidl, A., 2000a. Preprint.
Hemberger, J., 2000b. Talk given at the NATO Advanced Research Workshop, Bled, Slovenia, April.
Hennion, M., Moussa, F., Biotteau, G., Rodriguez Carvajal, J., Pinsard, L., Revcolevschi, A., 1998. Phys. Rev. Lett. 81, 1957.
Hennion, M., Moussa, F., Rodriguez Carvajal, J., Pinsard, L., Revcolevschi, A., 1997. Phys. Rev. B56, R497.
Hennion, M., Moussa, F., Biotteau, G., Rodriguez Carvajal, J., Pinsard, L., Revcolevschi, A., 1999. Preprint, cond-mat/9910361.
Hirai, Y., Frazer, B.H., Schneider, M.L., Rast, S., Onellion, M., O'Brien, W.L., Roy, S., Ignatov, A., Ali, N., 2000. Preprint.
Hirota, K., Moritomo, Y., Fujioka, H., Kubota, M., Yoshizawa, H., Endoh, Y., 1998. J. Phys. Soc. Japan 67, 3380.
Hirota, K., Moritomo, Y., Fujioka, H., Kubota, M., Yoshizawa, H., Endoh, Y., 1999. J. Phys. Soc. Japan 68, 1463.
Holstein, T., 1959. Ann. Phys. 8, 343.
Hotta, T., Takada, Y., Koizumi, H., 1998. Int. J. Mod. Phys. B12, 3437.
Hotta, T., Yunoki, S., Mayr, M., Dagotto, E., 1999. Phys. Rev. B60, R15,009.
Hotta, T., Takada, Y., Koizumi, H., Dagotto, E., 2000a. Phys. Rev. Lett. 84, 2477.
Hotta, T., Dagotto, E., 2000. Phys. Rev. B61, R11,879.
Hotta, T., Malvezzi, A., Dagotto, E., 2000b. Phys. Rev. B 62, 9432.
Hotta, T., Feiguin, A., Dagotto, E., 2000c. Preprint, cond-mat/0012098.

Huang, Q., Lynn, J.W., Erwin, R.W., Santoro, A., Dender, D.C., Smolyaninova, V.N., Ghosh, K., Greene, R.L., 1999. Preprint.
Hundley, M.F., Hawley, M., Heffner, R.H., Jia, Q.X., Neumeier, J.J., Tesmer, J., Thompson, J.D., Wu, X.D., 1995. Appl. Phys. Lett. 67, 860.
Hur, N.H., Kim, J.-T., Yoo, K.H., Park, Y.K., Park, J.-C., Chi, E.O., Kwon, Y.U., 1998. Phys. Rev. B57, 10,740.
Husmann, A., Jin, D.S., Zastavker, Y.V., Rosenbaum, T.F., Yao, X., Honig, J.M., 1996. Science 274, 1874.
Hwang, H.Y., Cheong, S.-W., Radaelli, P.G., Marezio, M., Batlogg, B., 1995a. Phys. Rev. Lett. 75, 914.
Hwang, H.Y., Palstra, T.T.M., Cheong, S.-W., Batlogg, B., 1995b. Phys. Rev. B52, 15,046.
Ibarra, M.R., Algarabel, P.A., Marquina, C., Blasco, J., Garcia, J., 1995. Phys. Rev. B75, 3541.
Ibarra, M.R., De Teresa, J.M., 1998a. J. Magn. Magn. Mater. 177–181, 846.
Ibarra, M.R., Zhao, G.-M., De Teresa, J.M., Garcia-Landa, B., Arnold, Z., Marquina, C., Algarabel, P.A., Keller, H., Ritter, C., 1998b. Phys. Rev. B57, 7446.
Ibarra, M.R., De Teresa, J.M., 1998c. In: Rao, C.N.R., Raveau, B. (Eds.), Contribution to Colossal Magnetoresistance, Charge Ordering and Related Properties of Manganese Oxides.. World Scientific, Singapore.
Iliev, M.N., Abrashev, M.V., Lee, H.-G., Sun, Y.Y., Thomsen, C., Meng, R.L., Chu, C.W., 1998. Phys. Rev. B57, 2872.
Imry, Y., Ma, S.K., 1975. Phys. Rev. Lett. 35, 1399.
Ishihara, S., Yamanaka, M., Nagaosa, N., 1997a. Phys. Rev. B56, 686.
Ishihara, S., Inoue, J., Maekawa, S., 1997b. Phys. Rev. B55, 8280.
Ivanshin, V.A., Deisenhofer, J., Krug von Nidda, H.-A., Loidl, A., Mukhin, A.A., Balbashov, A.M., Eremin, M.V., 2000. Phys. Rev. B61, 6213.
Jackeli, G., Perkins, N.B., Plakida, N.M., 1999. Preprint, cond-mat/9910391.
Jahn, H.A., Teller, E., 1937. Proc. Roy. Soc. London A 161, 220.
Jaime, M., Salamon, M.B., Rubinstein, M., Treece, R.E., Horwitz, J.S., Chrisey, D.B., 1996. Phys. Rev. B54, 11,914.
Jaime, M., Lin, P., Chun, S.H., Salamon, M.B., Dorsey, P., Rubinstein, M., 1999. Phys. Rev. B60, 1028.
Jin, S., Tiefel, T.H., McCormack, M., Fastnacht, R.A., Ramesh, R., Chen, L.H., 1994. Science 264, 413.
Jirak, Z., Krupicka, S., Simsa, Z., Dlouha, M., Vratislav, Z., 1985. J. Magn. Magn. Mater. 53, 153.
Jonker, G.H., Van Santen, J.H., 1950. Physica (Utrecht) 16, 337.
Jung, J.H., Kim, K.H., Lee, H.J., Ahn, J.S., Hur, N.J., Noh, T.W., Kim, M.S., Park, J.-G., 1999. Phys. Rev. B59, 3793.
Jung, J.H., Lee, H.J., Noh, T.W., Choi, E.J., Moritomo, Y., Wang, Y.J., Wei, X., 1998. Preprint, cond-mat/9912451.
Kagan, M.Yu., Khomskii, D.I., Mostovoy, M., 1999. Eur. Phys. J. B12, 217.
Kagan, M.Yu., Khomskii, D.I., Kugel, K.I., 2000. Preprint, cond-mat/0001245.
Kajimoto, R., Kakeshita, T., Oohara, Y., Yoshizawa, H., Tomioka, Y., Tokura, Y., 1998. Phys. Rev. B58, R11,837.
Kajimoto, R., Yoshizawa, H., Kawano, H., Kuwahara, H., Tokura, Y., Ohoyama, K., Ohashi, M., 1999. Phys. Rev. B60, 9506.
Kallias, G., Pissas, M., Devlin, E., Simopoulos, A., Niarchos, D., 1999. Phys. Rev. B59, 1272.
Kanamori, J., 1960. J. Appl. Phys. 31 (Suppl.), 14S.
Kanamori, J., 1963. Prog. Theor. Phys. 30, 275.
Kanki, T., Tanaka, H., Kawai, T., 2000. Solid State Commun. 114, 267.
Kaplan, S.G., Quijada, M., Drew, H., Tanner, D., Xiong, G., Ramesh, R., Kwon, C., Venkatesan, T., 1996. Phys. Rev. Lett. 77, 2081.
Kaplan, T., Mahanti, S., 1999. (Eds.), Physics of Manganites, Kluwer Academic/Plenum Publ., New York.
Kapusta, Cz., Riedi, P.C., Sikora, M., Ibarra, M.R., 2000. Phys. Rev. Lett. 84, 4216.
Kasuya, T., Yanase, A., 1968. Rev. Mod. Phys. 40, 684.
Katano, S., Fernandez-Baca, J.A., Yamada, Y., 2000. Physica B 276–278, 786.
Katsufuji, T., Cheong, S.-W., Mori, S., Chen, C.-H., 1999. J. Phys. Soc. Japan 68, 1090.
Kawano, H., Kajimoto, R., Yoshizawa, H., Tomioka, Y., Kuwahara, H., Tokura, Y., 1997. Phys. Rev. Lett. 78, 4253.
Kawasaki, S., Takano, M., Kanno, R., Takeda, T., Fujimori, A., 1998. J. Phys. Soc. Japan 67, 1529.
Khomskii, D., 2000a. Preprint, cond-mat/9909349.
Khomskii, D., 1999. Preprint, cond-mat/0004034.
Kida, N., Hangyo, M., Tonouchi, M., 2000a. Phys. Rev. B62, R11965.
Kida, N., Tonouchi, M., 2000b. Preprint, cond-mat/0008298.

Kim, K.H., Uehara, M., Cheong, S.-W., 2000. Preprint, cond-mat/0004467.
Kirkpatrick, S., 1973. Rev. Mod. Phys. 45, 574.
Kiryukhin, V., Casa, D., Hill, J.P., Keimer, B., Vigliante, A., Tomioka, Y., Tokura, Y., 1997. Nature 386, 813.
Kiryukhin, V., Wang, Y.J., Chou, F.C., Kastner, M.A., Birgeneau, R.J., 1999. Phys. Rev. B59, R6581.
Kiryukhin, V., Kim, B.G., Podzorov, V., Cheong, S.-W., Koo, T.Y., Hill, J.P., Moon, I., Jeong, Y.H., 2000. Preprint, cond-mat/0007295.
Koizumi, H., Hotta, T., Takada, Y., 1998a. Phys. Rev. Lett. 80, 4518.
Koizumi, H., Hotta, T., Takada, Y., 1998b. Phys. Rev. Lett. 81, 3803.
Korotin, M., Fujiwara, T., Anisimov, V., 1999. Preprint, cond-mat/9912456.
Koshibae, W., Kawamura, Y., Ishihara, S., Okamoto, S., Inoue, J., Maekawa, S., 1997. J. Phys. Soc. Japan 66, 957.
Kubo, K., Ohata, N., 1972. J. Phys. Soc. Japan 33, 21.
Kubota, M., Yoshizawa, H., Moritomo, Y., Fujioka, H., Hirota, K., Endoh, Y., 1999a. J. Phys. Soc. Japan 68, 2202.
Kubota, M., Fujioka, H., Ohoyama, K., Hirota, K., Moritomo, Y., Yoshizawa, H., Endoh, Y., 1999b. J. Phys. Chem. Solids 60, 1161.
Kubota, M., Fujioka, H., Hirota, K., Ohoyama, K., Moritomo, Y., Yoshizawa, H., Endoh, Y., 1999c. Preprint, cond-mat/9902288.
Kubota, M., 1999d. Private communication.
Kubota, M., Oohara, Y., Yoshizawa, H., Fujioka, H., Shimizu, K., Hirota, K., Moritomo, Y., Endoh, Y., 2000. Preprint.
Kuei, J., Scalettar, R.T., 1997. Phys. Rev. B55, 14,968.
Kugel, K.I., Khomskii, D.I., 1974. Sov. Phys.-JETP 37, 725.
Kusters, R.M., Singleton, J., Keen, D.A., McGreevy, R., Hayes, W., 1989. Physica B155, 362.
Kuwahara, H., Tomioka, Y., Asamitsu, A., Moritomo, Y., Tokura, Y., 1995. Science 270, 961.
Laad, M.S., Craco, L., Müller-Hartmann, E., 2000. Preprint, cond-mat/0007184.
Lanzara, A., Saini, N.L., Brunelli, M., Natali, F., Bianconi, A., Radaelli, P.G., Cheong, S.-W., 1998. Phys. Rev. Lett. 81, 878.
Larochelle, S., Mehta, A., Kameko, N., Mang, P.K., Panchula, A.F., Zhou, L., Arthur, J., Greven, M., 2000. Preprint.
Lee, J.D., Min, B.I., 1997. Phys. Rev. B55, R14,713.
Levy, P., Parisi, F., Polla, G., Vega, D., Leyva, G., Lanza, H., Freitas, R.S., Ghivelder, L., 2000a. Phys. Rev. B62, 6437.
Levy, P., Granja, L., Indelicato, E., Vega, D., Polla, G., Parisi, F., 2000b. Preprint, cond-mat/0008236.
Li, Q., Zang, J., Bishop, A.R., Soukoulis, C.M., 1997. Phys. Rev. B56, 4541.
Ling, C.D., Millburn, J.E., Mitchell, J.F., Argyriou, D.N., Linton, J., Bordallo, H.N., 2000. Preprint.
Liu, H.L., Cooper, S.L., Cheong, S.-W., 1998. Phys. Rev. Lett. 81, 4684.
Loktev, V.M., Pogorelov, Yu.G., 2000. Low Temp. Phys. 26, 171.
López, J., Lisboa-Filho, P.N., Passos, W.A.C., Ortiz, W.A., Araujo-Moreira, F.M., 2000. Preprint, cond-mat/0004460.
Lorenzana, J., Castellani, C., Di Castro, C., 2000. Preprint, cond-mat/0010092.
Loshkareva, N.N., Sukhorukov, Yu.P., Neifel'd, E.A., Arkhipov, V.E., Korolev, A.V., Gaviko, V.S., Panfilova, E.V., Dyakina, V.P., Mukovskii, Ya.M., Shulyatev, D.A., 2000. J. Exp. Theoret. Phys. 90, 389.
Loshkareva, N.N., Sukhorukov, Yu.P., Solin, N.I., Naumov, S.V., Mukovskii, Ya.M., Lobachevskaya, N.I., 1999. Proceedings of MSM'99 Moscow International Symposium on Magnetism, Moscow, June.
Louca, D., Egami, T., Brosha, E.L., Röder, H., Bishop, A.R., 1997. Phys. Rev. B56, R8475.
Louca, D., Egami, T., 1999. Phys. Rev. B59, 6193.
Lyanda-Geller, Y., Goldbart, P.M., Chun, S.H., Salamon, M.B., 1999. Preprint, cond-mat/9904331.
Lynn, J.W., Erwin, R.W., Borchers, J.A., Huang, Q., Santoro, A., Peng, J.-L., Li, Z.Y., 1996. Phys. Rev. Lett. 76, 4046.
Lynn, J.W., Erwin, R.W., Borchers, J.A., Santoro, A., Huang, Q., Peng, J.-L., Greene, R.L., 1997. J. Appl. Phys. 81, 5488.
Machida, A., Moritomo, Y., Nakamura, A., 1998. Phys. Rev. B 58, R4281.
Maezono, R., Ishihara, S., Nagaosa, N., 1998a. Phys. Rev. B 57, R13,993.
Maezono, R., Ishihara, S., Nagaosa, N., 1998b. Phys. Rev. B 58, 11,583.
Maezono, R., Nagaosa, N., 2000. Preprint.
Mahan, G.D., 1981. Many-Particle Physics, 1st Ed., Plenum Press (2nd Ed., 1990).
Maignan, A., Martin, C., Damay, F., Raveau, B., Hejtmanek, J., 1998. Phys. Rev. B 58, 2758.
Mallik, R., Sampathkumaran, E.V., Paulose, P.L., 1998a. Preprint, cond-mat/9811387.

Mallik, R., Reddy, E.S., Paulose, P.L., Majumdar, S., Sampathkumaran, E.V., 1998b. Preprint, cond-mat/9811351.
Malvezzi, A.L., Yunoki, S., Dagotto, E., 1999. Phys. Rev. B 59, 7033.
Manekar, M., Roy, S.B., Chaddah, P., 2000. Preprint, cond-mat/0005399.
Martin, C., Maignan, A., Hervieu, M., Raveau, B., 1999. Phys. Rev. B 60, 12,191.
Martins, G., Gazza, C., Xavier, J.C., Feiguin, A., Dagotto, E., 2000. Phys. Rev. Lett. 84, 5844.
Mathieu, R., Svedlindh, P., Nordblad, P., 2000. Europhys. Lett. 52, 441.
Matsumoto, G., 1970a. J. Phys. Soc. Japan 29, 606.
Matsumoto, G., 1970b. J. Phys. Soc. Japan 29, 615.
Matsuura, M., Hiraka, H., Yamada, K., Endoh, Y., 2000. J. Phys. Soc. Jpn. 69, 1503.
Mauger, A., Mills, D.L., 1984. Phys. Rev. Lett. 53, 1594.
Mauger, A., Mills, D.L., 1985. Phys. Rev. B 31, 8024.
Mayr, M., Moreo, A., Vergés, J., Arispe, J., Feiguin, A., Dagotto, E., 2000. Phys. Rev. Lett. 85 (26), in press.
Millis, A., Shraiman, B.I., Littlewood, P.B., 1995. Phys. Rev. Lett. 74, 5144.
Millis, A.J., Shraiman, B.I., Mueller, R., 1996. Phys. Rev. Lett. 77, 175.
Millis, A.J., Shraiman, B.I., Mueller, R., 1996a. Phys. Rev. B 54, 5389.
Millis, A.J., Mueller, R., Shraiman, B.I., 1996b. Phys. Rev. B 54, 5405.
Millis, A.J., 1998a. Nature 392, 147.
Millis, A.J., 1998b. Phys. Rev. Lett. 80, 4358.
Mishra, S., Satpathy, S., Aryasetiawan, F., Gunnarson, O., 1997. Phys. Rev. B 55, 2725.
Mizokawa, T., Fujimori, A., 1995. Phys. Rev. B 51, R12,880.
Mizokawa, T., Fujimori, A., 1996. Phys. Rev. B 54, 5368.
Mizokawa, T., Fujimori, A., 1997. Phys. Rev. B 56, R493.
Mizokawa, T., Khomskii, D.I., Sawatzky, D.A., 1999. Preprint, cond-mat/9912021.
Momoi, T., Kubo, K., 1998. Phys. Rev. B 58, R567.
Mook, M.K., 1998. Nature 395, 580.
Moreo, A., Yunoki, S., Dagotto, E., 1999a. Science 283, 2034.
Moreo, A., Yunoki, S., Dagotto, E., 1999b. Phys. Rev. Lett. 83, 2773.
Moreo, A., Mayr, M., Feiguin, A., Yunoki, S., Dagotto, E., 2000. Phys. Rev. Lett. 84, 5568.
Mori, S., Chen, C.H., Cheong, S.-W., 1998a. Nature 392, 473.
Mori, S., Chen, C.H., Cheong, S.-W., 1998b. Phys. Rev. Lett. 81, 3972.
Moritomo, Y., Tomioka, Y., Asamitsu, A., Tokura, Y., Matsui, Y., 1995. Phys. Rev. B 51, 3297.
Moritomo, Y., Asamitsu, A., Kuwahara, H., Tokura, Y., 1996. Nature 380, 141.
Moritomo, Y., Kuwahara, H., Tomioka, Y., Tokura, Y., 1997. Phys. Rev. B 55, 7549.
Moritomo, Y., Akimoto, T., Nakamura, A., Ohoyama, K., Ohashi, M., 1998. Phys. Rev. B 58, 5544.
Moritomo, Y., Machida, A., Mori, S., Yamamoto, N., Nakamura, A., 1999a. Phys. Rev. B 60, 9220.
Moritomo, Y., 1999b. Phys. Rev. B 60, 10,374.
Motome, Y., Nakano, H., Imada, M., 1998. Preprint, cond-mat/9811221.
Motome, Y., Imada, M., 1999. Phys. Rev. B 60, 7921.
Motome, Y., Furukawa, N., 1999. J. Phys. Soc. Japan 68, 3853.
Motome, Y., Furukawa, N., 2000a. Preprint, cond-mat/0007407.
Motome, Y., Furukawa, N., 2000b. Preprint, cond-mat/0007408.
Moussa, F., Hennion, M., Biotteau, G., Rodriguez Carvajal, J., Pinsard, L., Revcolevschi, A., 1999. Phys. Rev. B 60, 12,299.
Mukhin, A.A., Ivanov, V.Yu., Travkin, V.D., Pimenov, A., Loidl, A., Balbashov, A.M., 2000. Europhys. Lett. 49, 514.
Müller-Hartmann, E., Dagotto, E., 1996. Phys. Rev. B 54, R6819.
Murakami, Y., Kawada, H., Kawata, H., Tanaka, M., Arima, T., Moritomo, Y., Tokura, Y., 1998a. Phys. Rev. Lett. 80, 1932.
Murakami, Y., et al., 1998b. Phys. Rev. Lett. 81, 582.
Nagaev, E.L., 1967. JETP Lett. 6, 18.
Nagaev, E.L., 1968. Sov. Phys. Lett. 27, 122.
Nagaev, E.L., 1972. JETP Lett. 16, 394.
Nagaev, E.L., 1994. Phys. Stat. Sol. B 186, 9.

Nagaev, E.L., 1995. Phys.-Usp. 38, 497.
Nagaev, E.L., 1996. Phys.-Usp. 39, 781.
Nagaev, E.L., 1998. Phys. Rev. B 58, 2415.
Nagai, K., Momoi, T., Kubo, K., 1999. Preprint, cond-mat/9911091.
Nakano, H., Motome, Y., Imada, M., 2000. J. Phys. Soc. Jpn. 69, 1282.
Nam, D.N.H., Jonason, K., Nordblad, P., Khiem, N.V., Phuc, N.X., 1999. Phys. Rev. B 59, 4189.
Neumeier, J.J., Hundley, M.F., Thompson, J.D., Heffner, R.H., 1995. Phys. Rev. B 52, R7006.
Neumeier, J.J., Cohn, J.L., 2000. Phys. Rev. B 61, 14,319.
Nojiri, H., Kaneko, K., Motokawa, M., Hirota, K., Endoh, Y., Takahashi, K., 1999. Phys. Rev. B 60, 4142.
Ogale, S.B., Shreekala, R., Bathe, R., Date, S.K., Patil, S.I., Hannoyer, B., Petit, F., Marest, G., 1998. Phys. Rev. B 57, 7841.
Ohno, H., Munekata, H., Penney, T., von Molnar, S., Chang, L.L., 1992. Phys. Rev. Lett. 68, 2664.
Ohno, H., 1998. Science 281, 951.
Okamoto, S., Ishihara, S., Maekawa, S., 2000. Phys. Rev. B 61, 451.
Okimoto, Y., Katsufuji, T., Ishikawa, T., Urushibara, A., Arima, T., Tokura, Y., 1995. Phys. Rev. Lett. 75, 109.
Osborn, R., Rosenkranz, S., Argyriou, D.N., Vasiliu-Doloc, L., Lynn, J.W., Sinha, S.K., Mitchell, J.F., Gray, K.E., Bader, S.D., 1998. Phys. Rev. Lett. 81, 3964.
Oshima, H., Ishihara, Y., Nakamura, M., Miyano, K., 2000. Preprint.
Papavassiliou, G., Fardis, M., Milia, F., Simopoulos, A., Kallias, G., Pissas, M., Niarchos, D., Ioannidis, N., Dimitropoulos, C., Dolinsek, J., 1997. Phys. Rev. B 55, 15,000.
Papavassiliou, G., Fardis, M., Belesi, M., Pissas, M., Panagiotopoulos, I., Kallias, G., Niarchos, D., Dimitropoulos, C., Dolinsek, J., 1999a. Phys. Rev. B 59, 6390.
Papavassiliou, G., Fardis, M., Belesi, M., Maris, T., Kallias, G., Pissas, M., Dimitropoulos, C., Dolinsek, J., 1999b. Preprint.
Paraskevopoulos, M., Mayr, F., Hartinger, C., Pimenov, A., Hemberger, J., Lunkenheimer, P., Loidl, A., Mukhin, A.A., Ivanov, V.Yu., Balbashov, A.M., 2000a. J. Magn. Magn. Mater. 211, 118.
Paraskevopoulos, M., Mayr, F., Hemberger, J., Loidl, A., Heichele, R., Maurer, D., Müller, V., Mukhin, A.A., Balbashov, A.M., 2000b. J. Phys.: Condens. Matter 12, 3993.
Parisi, F., Levy, P., Polla, G., Vega, D., 2000. Preprint, cond-mat/0008080.
Park, J.-H., Chen, C.T., Cheong, S.-W., Bao, W., Meigs, G., Chakarian, V., Idzerda, Y.U., 1996. Phys. Rev. Lett. 76, 4215.
Perebeinos, V., Allen, P.B., 2000. Phys. Rev. Lett. 85, 5178.
Perring, T.G., Aeppli, G., Moritomo, Y., Tokura, Y., 1997. Phys. Rev. Lett. 78, 3197.
Perring, T.G., Aeppli, G., Tokura, Y., 1998. Phys. Rev. Lett. 80, 4359.
Pimenov, A., Biberacher, M., Ivannikov, D., Loidl, A., Ivanov, V.Yu., Mukhin, A.A., Balbashov, A.M., 2000. Phys. Rev. B 62, 5685.
Press, W.H., Teukolsky, S.A., Vitterling, W.T., Flannery, B.P., 1986. Numerical Recipes. Cambridge University Press, New York.
Quijada, M., Cerne, J., Simpson, J.R., Drew, H.D., Ahn, K.H., Millis, A.J., Shreekala, R., Ramesh, R., Rajeswari, M., Venkatesan, T., 1998. Phys. Rev. B 58, 16,093.
Radaelli, P.G., Cox, D.E., Marezio, M., Cheong, S.-W., Schiffer, P.E., Ramirez, A.P., 1995. Phys. Rev. Lett. 75, 4488.
Radaelli, P.G., Cox, D.E., Marezio, M., Cheong, S.-W., 1997. Phys. Rev. B 55, 3015.
Radaelli, P.G., Cox, D.E., Capogna, L., Cheong, S.-W., Marezio, M., 1999. Phys. Rev. B 59, 14,440.
Radaelli, P.G., Ibberson, R.M., Argyriou, D.N., Casalta, H., Andersen, K.H., Cheong, S.-W., Mitchell, J.F., 2000. Preprint, cond-mat/0006190.
Ramirez, A.P., Schiffer, P., Cheong, S-W., Chen, C.H., Bao, W., Palstra, T.T.M., Gammel, P.L., Bishop, D.J., Zegarski, B., 1996. Phys. Rev. Lett. 76, 3188.
Ramirez, A.P., Subramanian, M.A., 1997. Science 277, 546.
Ramirez, A.P., 1997. J. Phys.: Condens. Matter 9, 8171.
Ramos, C.A., Salva, H.R., Sanchez, R.D., Tovar, M., Rivadulla, F., Mira, J., Rivas, J., Lopez-Quintela, A.M., Hueso, L., Saint-Paul, M., Lejay, P., Tokura, Y., 2000. Preprint, Proceedings of the SCM 2000 Conference, Recife, Brazil.
Rao, C.N.R., Ganguly, P., Singh, K.K., Mohan Ram, R.A., 1988. J. Solid State Chem 72, 14.

Rao, C.N.R., Raveau, B. (Eds.), 1998. Colossal Magnetoresistance, Charge Ordering and Related Properties of Manganese Oxides. World Scientific, Singapore.
Raquet, B., Anane, A., Wirth, S., Xiong, P., von Molnár, S., 2000. Phys. Rev. Lett. 84, 4485.
Raychaudhuri, P., Mitra, C., Paramekanti, A., Pinto, R., Nigam, A.K., Dhar, S.K., 1998. J. Phys.: Condens. Matter 10, L191.
Rhyne, J.J., Kaiser, H., Luo, H., Xiao, G., Gardel, M.L., 1998. J. Appl. Phys. 83, 7339.
Riera, J., Hallberg, K., Dagotto, K., 1997. Phys. Rev. Lett. 79, 713.
Ritter, C., Ibarra, M.R., De Teresa, J.M., Algarabel, P.A., Marquina, C., Blasco, J., Garcia, J., Oseroff, S., Cheong, S.-W., 1997. Phys. Rev. B 56, 8902.
Röder, H., Zang, J., Bishop, A.R., 1996. Phys. Rev. Lett. 76, 1356.
Röder, H., Singh, R.R.P., Zang, J., 1997. Phys. Rev. B 56, 5084.
Rodriguez-Martinez, L.M., Attfield, J.P., 1996. Phys. Rev. B 54, R15,622.
Román, J.M., Soto, J., 1998. Preprint, cond-mat/9810389.
Roy, M., Mitchell, J.F., Ramirez, A.P., Schiffer, P., 1998. Phys. Rev. B 58, 5185.
Roy, M., Mitchell, J.F., Ramirez, A.P., Schiffer, P., 1999. J. Phys.: Condens. Matter 11, 4843.
Roy, M., Mitchell, J.F., Potashnik, S.J., Schiffer, P., 2000a. J. Magn. Magn. Mater. 218, 191.
Roy, M., Mitchell, J.F., Schiffer, P., 2000b. J. Appl. Phys. 87, 5831.
Saha, S.R., Sugawara, H., Matsuda, T.D., Sato, H., Mallik, R., Sampathkumaran, E.V., 1999. Phys. Rev. B 60, 12,162.
Saitoh, T., Bocquet, A., Mizokawa, T., Namatame, H., Fujimori, A., Abbate, M., Takeda, Y., Takano, M., 1995. Phys. Rev. B 51, 13,942.
Saitoh, T., Dessau, D.S., Moritomo, Y., Kimura, T., Tokura, Y., Hamada, N., Preprint, cond-mat/9911189.
Satpathy, S., Popovic, Z.S., Vukajlovic, F.R., 1996. Phys. Rev. Lett. 76, 960.
Schiffer, P., Ramirez, A.P., Bao, W., Cheong, S.-W., 1995. Phys. Rev. Lett. 75, 3336.
Schlottmann, P., 1999. Phys. Rev. B 59, 11,484.
Searle, C.W., Wang, S.T., 1969. Can. J. Phys. 47, 2703.
Shapira, Y., Foner, S., Oliveira Jr., N., 1974. Phys. Rev. B 10, 4765.
Shen, S.-Q., Wang, Z.D., 1998. Phys. Rev. B 58, R8877.
Shen, S.-Q., Wang, Z.D., 1999a. Phys. Rev. B 59, 14,484.
Shen, S.-Q., Wang, Z.D., 1999b. Preprint, cond-mat/9906126.
Sheng, L., Xing, D.Y., Sheng, D.N., Ting, C.S., 1997. Phys. Rev. Lett. 79, 1710; Phys. Rev. B 56, R7053.
Sheng, L., Sheng, D.N., Ting, C.S., 1999. Phys. Rev. B 59, 13,550.
Shiba, H., Shiina, R., Takahashi, A., 1997. J. Phys. Soc. Jpn. 66, 941.
Shimakawa, Y., Kubo, Y., Manako, T., 1996. Nature 379, 53.
Slater, J.C., Koster, G.F., 1954. Phys. Rev. 94, 1498
Smolyaninova, V.N., Xie, X.C., Zhang, F.C., Rajeswari, M., Greene, R.L., Das Sarma, S., 1999. Preprint, cond-mat/9903238.
Snow, C.S., Cooper, S.L., Young, D.P., Fisk, Z., 2000. Preprint.
Solovyev, I., Hamada, N., Terakura, K., 1996. Phys. Rev. Lett. 76, 4825.
Solovyev, I., Terakura, K., 1999. Phys. Rev. Lett. B 83, 2825.
Solovyev, I., 2000. Preprint.
Sternlieb, B.J., Hill, J.P., Wildgruber, U.C., Luke, G.M., Nachumi, B., Moritomo, Y., Tokura, Y., 1996. Phys. Rev. Lett. 76, 2169.
Subramanian, M.A., Ramirez, A.P., Marshall, W.J., 1999. Phys. Rev. Lett. 82, 1558.
Takenaka, K., Sawaki, Y., Sugai, S., 1999. Phys. Rev. B 60, 13,011.
Tang, H., Plihal, M., Mills, D.L., 1998. J. Magn. Magn. Mater. 187, 23.
Tarascon, J.M., Soubeyroux, J.L., Etourneau, J., Georges, R., Coey, J.M.D., Massenet, O., 1981. Solid State Commun. 37, 133.
Tkachuk, A., Rogacki, K., Brown, D.E., Dabrowski, B., Fedro, A.J., Kimball, C.W., Pyles, B., Xiong, X., Rosenmann, D., Dunlap, B.D., 1998. Phys. Rev. B 57, 8509.
Tokunaga, M., Tokunaga, Y., Yasugaki, M., Tamegai, T., 2000. Preprint, Physica B, submitted.

Tokura, Y., et al., 1994. J. Phys. Soc. Japan 63, 3931.
Tokura, Y., et al., 1993. Phys. Rev. Lett. 70, 2126.
Tokura, Y., 1999. Fundamental features of colossal magnetoresistive manganese oxides. In: Tokura, Y. (Ed.), Contribution to Colossal Magnetoresistance Oxides, Monographs in Condensed Matter Science. Gordon & Breach, London.
Tokura, Y., 2000. Talk given at SCM 2000 Conference, Recife, Brazil, August.
Tomioka, Y., Asamitsu, A., Moritomo, Y., Kuwahara, H., Tokura, Y., 1995. Phys. Rev. Lett. 74, 5108.
Tomioka, Y., Asamitsu, A., Kuwahara, H., Moritomo, Y., Tokura, Y., 1996. Phys. Rev. B 53, R1689.
Tomioka, Y., Asamitsu, A., Kuwahara, H., Tokura, Y., 1997. J. Phys. Soc. Japan 66, 302.
Tomioka, Y., Tokura, Y., 1999. Metal-insulator phenomena relevant to charge/orbital-ordering in perovskite-type manganese oxides. Preprint.
Tranquada, J.M., 1995. Nature 375, 561.
Troyanchuk, I.O., 1992. Sov. Phys. JETP 75, 132.
Tyson, T.A., Mustre de Leon, J., Conradson, S.R., Bishop, A.R., Neumeier, J.J., Röder, H., Zang, J., 1996. Phys. Rev. B 53, 13,985.
Uehara, M., Mori, S., Chen, C.H., Cheong, S.-W., 1999. Nature 399, 560.
Urushibara, A., Moritomo, Y., Arima, T., Asamitsu, A., Kido, G., Tokura, Y., 1995. Phys. Rev. B 51, 14,103.
Varelogiannis, G., 2000. Phys. Rev. Lett. 85, 4172.
van den Brink, J., Horsch, P., Mack, F., Oleś, A.M., 1999a. Phys. Rev. B 59, 6795.
van den Brink, J., Khaliullin, G., Khomskii, D., 1999b. Phys. Rev. Lett. 83, 5118.
van den Brink, J., Horsch, P., Olés, A.M., 2000. Phys. Rev. Lett. 85, 5174.
Varma, C., 1996. Phys. Rev. B 54, 7328.
Vasiliu-Doloc, L., Lynn, J.W., Moudden, A.H., de Leon-Guevara, A.M., Revcolevschi, A., 1998a. Phys. Rev. B 58, 14,913.
Vasiliu-Doloc, L., Lynn, J.W., Mukovskii, Y.M., Arsenov, A.A., Shulyatev, D.A., 1998b. J. Appl. Phys. 83, 7342.
Vasiliu-Doloc, L., Rosenkranz, S., Osborn, R., Sinha, S.K., Lynn, J.W., Mesot, J., Seeck, O.H., Preosti, G., Fedro, A.J., Mitchell, J.F., 1999. Phys. Rev. Lett. 83, 4393.
Venimadhav, A., Hedge, M.S., Prasad, V., Subramanyam, S.V., 2000. Cond-mat/0006388.
Vergés, J.A., 1999. Comput. Phys. Commun. 118, 71.
Viret, M., Glättli, H., Fermon, C., de Leon-Guevara, A.M., Revcolevschi, A., 1998. Europhys. Lett. 42, 301.
Voloshin, I.F., Kalinov, A.V., Savel'ev, S.V., Fisher, L.M., Babushkina, N.A., Belova, L.M., Khomskii, D.I., Kugel, K.I., 2000. JETP Letters 71, 106.
von Helmolt, R., Wecker, J., Holzapfel, B., Schultz, L., Samwer, K., 1993. Phys. Rev. Lett. 71, 2331.
von Molnar, S., Methfessel, S., 1967. J. Appl. Phys. 38, 959.
von Molnar, S., Coey, J.M.D., 1998. Curr. Opin. Solid State Mater. Sci. 3, 171–174.
Wagner, P., Gordon, I., Mangin, S., Moshchalkov, V.V., Bruynseraede, Y., 1999. Preprint, cond-mat/9908374.
White, S., Scalapino, D., 1998. Phys. Rev. Lett. 80, 1272.
Wollan, E.O., Koehler, W.C., 1955. Phys. Rev. 100, 545.
Woodward, P.M., Cox, D.E., Vogt, T., Rao, C.N.R., Cheetham, A.K., 1999. Preprint, submitted to Chem. Mater., submitted.
Wu, T., Ogale, S.B., Garrison, J.E., Nagaraj, B., Chen, Z., Greene, R.L., Ramesh, R., Venkatesan, T., Millis, A.J., 2000. Preprint.
Xiong, G.C., Li, Q., Ju, H.L., Mao, S.N., Senapati, L., Xi, X.X., Greene, R.L., Venkatesan, T., 1995. Appl. Phys. Lett. 66, 1427.
Yamada, Y., Hino, O., Nohdo, S., Kanao, R., Inami, T., Katano, S., 1996. Phys. Rev. Lett. 77, 904.
Yamanaka, M., Koshibae, W., Maekawa, S., 1998. Phys. Rev. Lett. 81, 5604.
Yi, H., Yu, J., 1998. Phys. Rev. B 58, 11,123.
Yi, H., Lee, S.-I., 1999. Phys. Rev. B 60, 6250.
Yi, H., Yu, J., Lee, S.-I., 1999a. Preprint, cond-mat/9910152.
Yi, H., Hur, N.H., Yu, J., 1999b. Preprint, cond-mat/9910153.
Yin, W.-G., Lin, H.-Q., Gong, C.-D., 2000. Preprint, cond-mat/0011433.
Yoon, S., Liu, H.L., Schollerer, G., Cooper, S.L., Han, P.D., Payne, D.A., Cheong, S.-W., Fisk, Z., 1998. Phys. Rev. B 58, 2795.

Yoon, S., Rübhausen, M., Cooper, S.L., Kim, K.H., Cheong, S.-W., 2000. Preprint, cond-mat/0003250, Oct. Phys. Rev. Lett., to appear.
Yoshida, K., 1998. Theory of Magnetism. Springer, Berlin.
Yoshizawa, H., Kawano, H., Tomioka, Y., Tokura, Y., 1995. Phys. Rev. B 52, R13,145.
Yoshizawa, H., Kawano, H., Fernandez-Baca, J.A., Kuwahara, H., Tokura, Y., 1998. Phys. Rev. B 58, R571.
Young, A.P., Ed. 1998. Spin Glasses and Random Fields. World Scientific, Singapore.
Yuan, Q., Yamamoto, T., Thalmeier, P., 2000. Preprint, cond-mat/0008296.
Yunoki, S., Hu, J., Malvezzi, A., Moreo, A., Furukawa, N., Dagotto, E., 1998a. Phys. Rev. Lett. 80, 845.
Yunoki, S., Moreo, A., Dagotto, E., 1998b. Phys. Rev. Lett. 81, 5612.
Yunoki, S., Moreo, A., 1998. Phys. Rev. B58, 6403.
Yunoki, S., Hotta, R., Dagotto, E, 2000. Phys. Rev. Lett. 84, 3714.
Zaanen, J., 1998. J. Phys. Chem. Solids 59, 1769.
Zang, J., Bishop, A.R., Röder, H., 1996. Phys. Rev. B53, R8840.
Zang, J., Trugman, S.A., Bishop, A.R., Röder, H, 1997. Phys. Rev. B56, 11,839.
Zener, C., 1951a. Phys. Rev. 81, 440.
Zener, C., 1951b. Phys. Rev. 82, 403.
Zhao, G.-M., Conder, K., Keller, H., Müller, K.A., 1996. Nature 381, 676.
Zhao, G.-M., Conder, K., Keller, H., Müller, K.A., 1999. Phys. Rev. B60, 11,914.
Zhao, G.-M., 2000. Phys. Rev. B 62, 11,639.
Zhao, Y.G., Li, J.J., Shreekala, R., Drew, H.D., Chen, C.L., Cao, W.L., Lee, C.H., Rajeswari, M., Ogale, S.B., Ramesh, R., Baskaran, G., Venkatesan, T., 1998. Phys. Rev. Lett. 81, 1310.
Zhong, F., Wang, Z.D., 1999. Phys. Rev. B60, 11,883.
Zhou, J.-S., Archibald, W., Goodenough, J.B., 1996. Nature 381, 770.
Zhou, J.-S., Goodenough, J.B., Mitchell, J.F., 1998a. Phys. Rev. B58, R579.
Zhou, J.-S., Goodenough, J.B., 1998b. Phys. Rev. Lett. 80, 2665.
Zimmermann, M.v., Hill, J.P., Gibbs, D., Blume, M., Casa, D., Keimer, B., Murakami, Y., Tomioka, Y., Tokura, Y., 1999. Phys. Rev. Lett. 83, 4872.
Zimmermann, M.v., Nelson, C.S., Hill, J.P., Gibbs, D., Blume, M., Casa, D., Keimer, B., Murakami, Y., Kao, C.-C., Venkataraman, C., Gog, T., Tomioka, Y., Tokura, Y., 2000. Preprint, cond-mat/0007231.
Zuo, J.M., Tao, J., 2000. Preprint, cond-mat/0009472.
Zvyagin, S., Saylor, C., Martins, G., Brunel, L.-C., Kamenev, K., Balakrishnan, G., Paul, D.M.K., 2000. Preprint.